Modified Cellulose Nanocrystals (CNC) for Functional Foods

by

Jiyoo Baek

A thesis
presented to the University of Waterloo
in fulfillment of the
thesis requirement for the degree of
Doctor of Philosophy
in
Chemical Engineering
(Nanotechnology)

Waterloo, Ontario, Canada, 2021

Examining Committee Membership

The following served on the Examining Committee for this thesis.

External Examiner: Professor Indrawati Oey

Professor, Dept. of Food Science,

University of Otago, Dunedin, New Zealand

Supervisor: Professor Michael Tam

Professor, Dept. of Chemical Engineering nanotechnology,

University of Waterloo

Internal Member: Professor Evelyn Yim

Professor, Dept. of Chemical Engineering,

University of Waterloo

Internal Member: Professor Valerie Ward

Professor, Dept. of Chemical Engineering,

University of Waterloo

Internal-External Member: Professor Shirley Tang

Professor, Dept. of Chemistry,

University of Waterloo

Author's Declaration

I hereby declare that I am the sole author of this thesis. This is a true copy of the thesis, including any required final revisions, as accepted by my examiners.

I understand that my thesis may be made available electronically to the public.

Abstract

In recent years, food safety has attracted increasing attention, as consumers desire a healthier lifestyle and a prolonged lifespan. The interests in food to satisfy hunger have taken a shift towards providing more functional ingredients that offer a better state of well-being while also providing satiety to the consumer. With this shift, the primary focus has been directed towards replacing conventional chemical, synthetic additives with healthier and natural ingredients. Additionally, the interest in general health care and nutritious functional foods that can improve immunity is also generating much attraction, especially with the rising desire to boost our immunity against viruses, such as COVID-19. These efforts are evident in the food industry, with companies actively looking into the development of natural emulsifiers to replace artificial or synthetic ones, which can lower the health risks while providing the same taste and state of well-being.

Cellulose nanocrystals (CNC) in food applications have attracted a great deal of interest due to their biodegradability, biocompatibility, sustainability, and abundant supply. CNC is extracted from traditional raw materials, such as cotton or wood, exposed to physical and chemical processes like homogenization and acid hydrolysis. During these steps, the cellulose plant wall experiences the following changes to its hierarchical structure: the plant wall is broken down into hemicellulose and lignin, which is further reduced to the elementary fibers. With further chemical treatment, such as with acids, sustainable rod-like nanoparticles are produced. Recently, a new trend in producing CNC from agri-food waste, such as fruit

peels, has emerged (tomato, mango, pineapple etc.). CNC is easily dispersible in water and possesses a high aspect ratio due to its rod-like structure and surface charges. This allows for facile chemical modification to tune and introduces new properties to the CNC. The modified CNC makes it a suitable material for applications in food packaging, food thickeners, and emulsion stabilizers.

Phosphorylated cellulose nanocrystals (PCNC) were prepared via acid hydrolysis using phosphoric acid, and chitosan was modified with glycidyltrimethylammonium chloride (GTMAC). The PCNC was simultaneously used as a "nanoparticle" cross-linker (similar to sodium tripolyphosphate (TPP)) and a Pickering emulsifier. The PCNC and GTMAC-Chitosan (GCh) were complexed via ionic gelation to produce GCh-PCNC nanoparticles. The nanocomplexes transformed from a rod-like to hard-sphere and random coil morphology with increasing GTMAC-Chitosan/PCNC. Pickering emulsions prepared using the GCh-PCNC complex were more stable over 3 months without coalescence or phase separation.

Vitamin C (VC) is necessary for human health. However, it is susceptible to oxidation during processing or storage. To increase its stability, VC was encapsulated via electrostatic interaction with GCh cross-linked with PCNC to form VC-GCh-PCNC nanocapsules. VC-GCh-PCNC possessed a broad-spectrum antibacterial activity with a minimum inhibition concentration (MIC) of 8-16 μg/mL. These results demonstrated that modified CNC-based

nano-formulations could preserve, protect, and control the release of active compounds with improved antioxidant and antibacterial properties for food and nutraceutical applications.

CNC was modified with ferulic acid (FA) and starch nanoparticles (SNP) to produce a new, natural emulsifier that is environment-friendly and beneficial to human health. This new approach was developed and utilized to formulate a multiple Pickering emulsion ($W_1/O/W_2$) for probiotic encapsulation. The adsorption capacity of FA on CNC was evaluated, and the highest adsorption capacity below the *pKa* of FA (4.5) was 1.91 mg FA/g of CNC and greater than 4.5. The adsorption capacity decreased to 0.03 mg FA/g of CNC. At high pH, carboxyl groups from the CNCFA-based Pickering multiple emulsions were deprotonated, inducing phase separation. The newly developed emulsifiers were used to reduce the interfacial tension between the oil and water phase to prepare stable emulsions that could be stored over a long period.

With the worldwide emergence of health challenges facing humanity and the associated immunity and intestinal health, the use of probiotics is becoming prevalent. We developed a sustainable, biocompatible, rigid, and long-lasting enteric coating system using pH-responsive natural-based materials, shellac (Sh), and cellulose nanocrystals (CNC). Yeast (*Saccharomyces cerevisiae*) was encapsulated in the ShCNC microcapsules and $CaCl_2$. We elucidated the 3D structure of ShCNCCa microcapsules using a confocal laser microscope, where a 1-1.3 μm shell consisting of shellac and CNC nanocomplex protected the yeast

resulting in high yeast viability and retention of 602.35%. During processing, storage and transport through the gastric environment, the yeasts were protected and then triggered to release in the intestinal environment of pH 7-8. Viscosity synergism and mucoadhesion analysis revealed that the microcapsules bound strongly to the mucus membrane in the presence of pancreatin.

This Ph.D. study explores new strategies to improve current functional food systems using modified CNC. In the design and development of the project, replicable methods, simple processes, and fewer chemicals are being considered. The research has contributed to the development and understanding of functional cellulose nanocrystals, which are suitable for use in the food industry.

Acknowledgements

There are no proper words to convey my deep gratitude and respect for my supervisor, Professor Michael Tam, for the continuous support of my Ph.D. study and research and his patience. At the beginning of my study, I was frustrated and disappointed in myself for my inability to handle academics and research, but Professor Tam was there all the time to help me and his students. Throughout the terms, Professor Tam continuously provided the advice I needed to help guide me in the right direction. Without his guidance, feedback, and encouragement, I would not have been able to complete the thesis.

I would like to thank my committee members, Professors Evelyn Yim, Shirley Tang, and Valerie Ward, for their insightful comments and constructive criticism on my Ph.D. research. I would also like to thank Professor Indrawati Oey for agreeing to be my external thesis examiner and agreeing to attend my thesis defence at 6.00 am in New Zealand.

My sincere thanks go to Dr. Mohankandhasamy Ramasamy and Dr. Howard Siu for their valuable discussion, advice, and support on- and off-campus.

I would like to acknowledge my lovely co-op students, my labmates, and friends; Dr. Zengqian Shi, Dr. Zhen Zhang, Dr. Jianxiang Chen, Dr. Marjan Ashrafizadeh, Dr. Debbie Wu, Dr. Juntao Tang, Dr. Nate Grishkewich, Dr. Nadeem Akhtar, Dr. Hyeonghwa Yu, Fatima Awan, Daesung Kim, Yebin Lee, Salha Alharthi, Parinaz Ataeian, Sara Xu, Chunxia Tang, Yi Wang, Iflah Shahid, Fatemah Haji, Damin Kim, and Areum Kim, for their kind help and encouragement.

I am grateful to my parents and parents-in-law for their endless love and support.
Lastly, I am very thankful to my husband, Taehee Kim, for his love, continued support, and consideration to complete this Ph.D. study. Also, to my baby Leo Kim, who, despite needing his mother's attention and care during my Ph.D. study, was always patient and loving. Thank you, and I love you, Leo.

Table of Contents

Examining Committee Membership ..... **ii**

Author's Declaration ..... **iii**

Abstract ..... **iv**

Acknowledgements ..... **viii**

List of Figures ..... **xiv**

List of Tables ..... **xxiii**

Chapter 1 Introduction **24**

1.1 Research background and motivation 24

1.2 Objectives 27

1.3 Thesis outlines 29

Chapter 2 Literature review **31**

2.1 Colloidal systems 31

2.2 Emulsion systems 32

2.2.1 Single emulsion 32

2.2.2 Multiple emulsion 32

2.3 Current status of emulsion technology 35

2.4 Mechanical emulsion process 35

2.4.1 High-speed homogenizer 35

2.4.2 Ultrasonic homogenizer 36

2.4.3 High-pressure homogenizer 37
2.5 Chemical emulsification process 38
2.5.1 Surfactant 38
2.6 Pickering emulsion 40
2.7 Types of green solid particles 44
2.7.1 Cellulose and cellulose nanocrystals 45
2.7.2 Chitosan 55
2.7.3 Shellac 61
2.8 Encapsulation system 67
2.8.1 Encapsulation of Vitamin C (L-Ascorbic acid) 68
2.8.2 Encapsulation of probiotics 75
Chapter 3 Phosphorylated-CNC/Modified-Chitosan Nanocomplexes for the Stabilization of Pickering Emulsion 82
3.1 Introduction 82
3.2 Material and Methods 86
3.2.1 Materials 86
3.2.2 Extraction and preparation of PCNC 87
3.2.3 Synthesis of GTMAC-Chitosan 88
3.2.4 Preparation of GCh-PCNC nanoparticles 89
3.2.5 Oil in water Pickering emulsion preparation 89
3.2.6 Characterization of GCh-PCNC nanoparticles 90

3.3 Results and discussion 93
3.3.1 Bleaching and delignification of hardwood pulp 93
3.3.2 FTIR spectrum of bleaching pulps 95
3.3.3 Preparation and characterization of PCNC 96
3.3.4 Quantification of GCh 99
3.3.5 Morphological studies of GCh-PCNC complexes 101
3.3.6 Pickering emulsions 104
3.4 Conclusions 106
Chapter 4 Encapsulation and Controlled Release of Vitamin C in Modified Cellulose Nanocrystals/Chitosan Nanocapsules 107
4.1 Introduction 107
4.2 Materials and methods 111
4.2.1 Materials 111
4.2.2 Preparation of VC-GCh-PCNC/VC-GCh-TPP nanocapsules 111
4.2.3 Characterization 112
4.2.4 Degradation analysis of VC 113
4.2.5 Determination of encapsulation efficiency 114
4.2.6 Cumulative VC release study 114
4.2.7 DPPH free radical scavenging activity 115
4.2.8 Drug release kinetics and mathematical models 115
4.2.9 Digestive system simulation release test 116

4.2.10 Antibacterial tests 117
4.2.11 Statistical analysis 118
4.3 Results and discussion 118
4.4 Conclusions 133
Chapter 5 Functionalized Ferulic Acid and Cellulose Nanocrystals Stabilized Smart Multiple Pickering Emulsion for Enhanced Probiotics Delivery 135
5.1 Introduction 135
5.2 Materials and Methods 138
5.2.1 Materials 138
5.2.2 Preparation of CNCFA 139
5.2.3 Preparation of SNPs 139
5.2.4 RPM test 139
5.2.5 Preparation of double Pickering emulsion 140
5.2.6 Characterization of the nanoparticles 141
5.3 Results and discussion 144
5.4 Conclusions 163
Chapter 6 A New Approach for the Encapsulation of Probiotics using Shellac and Cellulose Nanocrystals 164
6.1 Introduction 164
6.2 Experimental section 167
6.2.1 Materials 167

6.2.2 Preparation of Shellac dispersion 168
6.2.3 CO_2 test 168
6.2.4 Determination of the antisolvent effect 169
6.2.5 Preparation of Pickering emulsion 170
6.2.6 Preparation of simulated gastric (SGF) and intestinal fluid (SIF) 170
6.2.7 Material characterization 171
6.2.8 Statistical analysis 174
6.3 Results and discussion 174
6.4 Conclusions 201
Chapter 7 Conclusions and recommendation for future studies 203
7.1 Conclusions and Contributions 203
7.2 Recommendation for future studies 206
References 208

List of Figures

Fig. 1.1 The global and Canada functional foods market size from 2014 to 2025.....25

Fig. 2.1 Types of conventional emulsions (A) water in oil in water, (B) oil in water in oil emulsion (Ito *et al*., 2012; Zafeiri *et al.*, 2017), and C) schematic of W/O/W emulsion preparation: (a) an ultrasonic liquid processing and (b) high-pressure homogenization (HPH) (Ghasemi *et al.*, 2020).....33

Fig. 2.2 Schematic illustrating the synthesis, and self-assembly of PDAA copolymers, and the application of PDAA nanoparticles as a stabilizer to prepare multiple emulsions (Zhu *et al*., 2016) 34

Fig. 2.3 Effect of ultrasound on the change in mean droplet size of dispersed droplets of O/W emulsions stored at 26−30 °C: for 1.2% coconut milk protein emulsion; Sonication was applied at 20 kHz (Lad & Murthy, 2012).....37

Fig. 2.4 A schematic of High-pressure homogenizers (Hebishy *et al.*, 2015) 38

Fig. 2.5 a-c) Confocal microscope images of the barrier cross-section of mice fed with water (left), emulsifier CMC (center), and P80 (right) containing 1% water. Blue epithelium, green mucosa, red intestinal microorganism (Scale bar, 20 μm), and d) distance of closest bacteria to intestinal epithelial cells (IEC) per condition over five high-powered fields per mouse (Chassaing *et al.*, 2015).....40

Fig. 2.6 Emulsifiers play two key roles in producing commercial emulsion-based food products: They (a) facilitate emulsion formation and (b) promote emulsion stability (McClements *et al.*, 2017).....41
Fig. 2.7 Number of publications related to "Pickering emulsions" (a) and "Pickering emulsions & food," "Pickering emulsions & protein" (b) by year. Data was obtained from "Web of Science" in April 2020 (Yan *et al*., 2020).....42
Fig. 2.8 The location of a particle at the oil-water interface is determined by the contact angle, measured through the aqueous phase. When less than 90˚(left) oil-in-water emulsions are most likely formed, and when larger than 90˚(right), water-in-oil emulsions may form (Rayner *et al.*, 2014). 43
Fig. 2.9 The chemical structures of wood; Simple structures of cellulose, hemicellulose, and lignin: Major components of biomass (Akash, 2015).....45
Fig. 2.10 The three phenylpropane units, the building blocks of lignin (a) sinapyl alcohol, (b) coniferyl alcohol, (c) p-coumaryl alcohol (Chesner, 1963).....46
Fig. 2.11 Chemical structure of cellulose (Ghalia & Dahman, 2017) 47
Fig. 2.12 Disruption of cellulosic biomass by pretreatment (Kumar *et al*., 2009).....49
Fig. 2.13 Structure of conjugated chromophores (Chesner, 1963).....49
Fig. 2.14 SEM images of pinecone before and after chemical treatments (a) RPC 100X, (b) AL 500X, (c) BL 500X and (d) the ESEM image of cellulose nanofibers 100 000X (Rambabu *et al*., 2016).....51

Fig. 2.15 Reaction scheme illustrating the cellulose hydrolysis and esterification reactivity of hydroxyl groups (Sanchez-Dominguez & Rodriguez-Abreu, 2016) 52

Fig. 2.16 TGA traces of S-CNCs, P-CNCs, and H-CNCs (Camarero Espinosa *et al.*, 2013) 54

Fig. 2.17 Structure of chitin and chitosan (Younes & Rinaudo, 2015) 56

Fig. 2.18 Formation of the chitosan-tripolyphosphate complex by ionotropic gelation. (a) Schematic illustration of the chitosan-TPP complex and (b) SEM image. Bar, 200 nm (de Paz *et al.*, 2011) 58

Fig. 2.19 Synthesis route for HTCC (Mivehi *et al.*, 2008) 60

Fig. 2.20 (A): Effect of alkali-treatment time on acid value and ester value of Shellac. (blue) Acid value; (black) ester value and (B): pH-solubility profiles of native shellac and hydrolyzed Shellac after alkali treatment for different times. (diamond) Native shellac; (square) 15-min hydrolyzed shellac; (circle) 30-min hydrolyzed shellac; (cross) 60-min hydrolyzed shellac; (triangle up) 120-min hydrolyzed shellac (Limmatvapirat *et al.*, 2004). 64

Fig. 2.21 A) Chemical structure of shellac. Polyesters (a) and single esters (b) (Limmatvapirat *et al.*, 2004) and B) the generalized molecular structure of shellac (Gao *et al.*, 2018) 65

Fig. 2.22 Important applications of microencapsulation in the food industry (Iravani *et al.*, 2015) 68

Fig. 2.23 Oxidation of vitamin c (ascorbic acid) via dehydroascorbic acid as intermediate (Shanmugam *et al.*, 2010) 70

Fig. 2.24 SEM images of bovine serum albumin (BSA) hydrogel (a,b), BSA−pectin (B-P) mixture at pH 7.0 (c,d), B-P mixture at pH 4.5 (e,f), and BPH (BSA−Pectin hydrogel) at pH 4.5 (g,h)-thermal treatment (Peng *et al*., 2016) 72

Fig. 2.25 Schematic representation of the structural changes of AL-CH-NLs during storage at 4 C. (a) Fresh AL-CH-NLs prepared by chitosan (CH) and sodium alginate (AL) decorating on NLs (day 1) and (b) Loose interaction, rupture and new network formation in AL-CH-NLs after storage for 90 days (Liu *et al.,* 2017) 75

Fig. 2. 26 Flow diagram of encapsulation of bacteria by the extrusion and emulsion technique (Krasaekoopt *et al.,* 2003) 77

Fig. 3.1 Schematic for the acid hydrolysis process of kraft pulp 87

Fig. 3.2 Lengths of cellulose fibers upon bleaching and delignification treatment, (A): hardwood pulp fibers, (B): after NaOH treatment, and (C): after $NaClO_2$ treatment (Scale bar: 200 μm) 94

Fig. 3.3 The FTIR spectra of (A): original hardwood pulp, (B): bleached fibers with bleaching and delignification agents, and (C): phosphorylated cellulose nanocrystals 96

Fig. 3.4 (A): TEM image of PCNC (Scale bar: 500 nm), (B): Conductometric titration curve of PCNC, and (C): the reaction mechanism of cellulose to PCNC 98

Fig. 3.5 Conductometric titration curve to determine the degree of deacetylation of chitosan 99

Fig. 3.6 (A): Zeta-potential profiles of chitosan and GTMAC-Chitosan at different pHs, (B): digital photographs demonstrating the solubility of chitosan and GTMAC-Chitosan at different pH values, and (C): the reaction scheme of chitosan to GTMAC-Chitosan.....100

Fig. 3.7 The dependence of (A): radius of gyration (R_g), (B): hydrodynamic radius (R_h), and (C): shape factor (R_g/R_h) on the ratio of GCh and PCNC.....103

Fig. 3.8 A schematic on the microstructural evolution of the nanoscale complexes.....104

Fig. 3.9 (A): The Comparative stability of GCh-PCNC and GCh-TPP oil in water Pickering emulsion in vials and (B): fluorescence microscope image of GCh-PCNC oil in water Pickering emulsion.....106

Scheme. 4.1 Schematic illustrations describing the formations of VC-GCh-TPP and VC-GCh-PCNC nanocapsules by utilizing VC, GCh, TPP, and PCNC 112

Fig. 4.1 (A) The IR spectra of TPP (upper trace) and PCNC (lower trace); (B) Zeta potential and z-average particle sizes of VC-GCh, VC-GCh-PCNC and VC-GCh-TPP nanocapsules, and (C) TEM images of (a): VC-GCh complex (Scale bar: 500 nm) (b): VC-GCh-TPP (Scale bar: 2μm), and (c): VC-GCh-PCNC (Scale bar: 2μm) 123

Scheme. 4.2 Schematic illustrations describing the microstructure of the nanocapsules and the chemical functionality of each of the components.....124

Fig. 4.2 (A) Changes in concentration concerning the time of a 0.04 mg/mL VC solution in PBS under nitrogen gas purging, limited light exposure, and constant temperature. (B) The cumulative release profile of VC from nanocapsules through a dialysis membrane to time 127

Fig. 4.3 (A) DPPH absorption spectra, (B) DPPH free radical scavenging activity from the filtrates of nanocapsule dispersions of VC- GCh-TPP and VC-GCh-PCNC for 30 min, and (C) DPPH free radical scavenging activity from the filtrates of nanocapsule dispersions of VC- GCh-TPP and VC-GCh-PCNC for 5 days.....128

Fig. 4.4 (A): diagram of the human digestive system and (B): *In vitro* simulation of various conditions of the digestive system of VC-GCh-PCNC.....131

Fig. 4.5 Antimicrobial activity of VC- GCh-PCNC with *E. coli* and with *S. aureus*. (*MIC values of GTMAC-Chitosan for two types of bacteria were 32-64 μg/mL-data not shown) 132

Fig. 5.1 The schematic for the process of multiple Pickering emulsion (W/O/W) 141

Fig. 5.2 A) The chemical structure of FA below and above *pKa* value (pH 4.5) and B) absorbance spectra of FA, the effect of pH changes from 2 to 7.5.....146

Fig. 5.3 CNCFA dispersions containing different concentrations of FA (10-100 mg) and optical microscope images of O/W Pickering emulsions (Scale bar: 20μm).....147

Fig. 5.4 A) Particle size and zeta-potential of CNC from pH 1-9 and B) particle size and zeta-potential of CNCFA from pH 1-9.....148

Fig. 5.5 The chemical structure of CNCFA by hydrogen bonding 150

Fig. 5.6 A) Influence of pH on maximum adsorption capacity of FA on CNC, B) images of contact angles of native CNC and CNCFA, and C) schematic illustration demonstrating the *pKa* of FA.....152

Fig. 5.7 The FTIR spectra of CNC, FA, and CNCFA 153

Fig. 5.8 The TEM images of SNPs at A) & B) at pH 2 and C) at pH 7.5 and contact angle of SNPs at pH 2 155
Fig. 5.9 The free-radical scavenging activity of FA and CNCFA at pH 2 and 7.5 by DPPH assay 157
Fig. 5.10 Effect of homogenization time with a high-speed homogenizer at various speeds 158
Fig. 5.11 The optical microscope images of A) yeast, B) W/O/W Pickering emulsion at pH 4.3, C) W/O/W Pickering emulsion at pH 2, D-1 to D-3) change in the morphologies of W/O/W Pickering emulsion at 7.5 (scale bar: 20 μm).....160
Fig. 5.12 A) Optical microscope images of Pickering emulsions at pH 2 after 2 weeks and B) actual pictures of the Pickering emulsions before and after 2 weeks (scale bar: 50 μm 161
Fig. 5.13 The optical microscope images after swabbing of (A-1 and A-2) yeast at pH 2 and (B) at pH 7.5.....162
Fig. 6.1 The scheme of self-assembled apparatus for CO_2 test.....169
Fig. 6.2 A) Shellac dispersion in 5% DA at different concentrations (2.5, 5, 7.5, and 10 mg/mL), B) size and zeta-potential of 4 concentrations of shellac dispersion in 5% DA, C) zeta-potential of shellac dispersion (5 mg/mL) at various pH (2-9), and D) diameter of ShCNCCa at various pH (2-9).....176
Fig. 6.3 Photographs of Shellac solutions at different pH (2-9).....177
Fig. 6.4 Photographs of ShCNCCa complex at different pH (2-9) 177
Fig. 6.5 Schematic of the formation of ShCNCCa complex.....178

Fig. 6.6 FT-IR data of CNC, Shellac, ShCNC, and ShCNCCa.....179

Fig. 6.7 A) Proposed 3D model of the growth of particle size during anti-solvent precipitation process, B) Intensity size distribution of shellac nanoparticles in water versus particle diameter. The different colours represent the measurements at different mixing times, C) Particle size change of shellac nanoparticles in water as a function of mixing time, and D) 3D images of W/O emulsion and the corresponding fluorescence intensity profiles of shellac (green) and oil (pink) 182

Fig. 6.8 A) Control CO_2 release of yeast in varying pHs B) CO_2 release by yeast at pH 5 with and without $CaCl_2$, C) Optical and fluorescence microscopy of yeast dyed with methylene blue to determine the viability at pH 2 (Scale bar: 50 μm), D) Optical and fluorescence microscopy of the partial coverage of yeast by ShCNCCa (dyed in methylene blue) to determine the viability at pH 2 (Scale bar: 50 μm), E) Zeta-potential of yeast and yeast with 0.8% $CaCl_2$ at various pH (2-9), and F) CO_2 release of yeast at various conditions at pH 2 185

Fig. 6.9 Optical and fluorescence micrographs of encapsulation of yeast with A) Shellac B) ShCa, C) ShCNC, and E) ShCNCCa. TEM Micrographs of D) ShCa and F) ShCNCCa. Scale bar; A, B, C, and E: 50 μm, D and F: 500 nm.....188

Fig. 6.10 A) Confocal images of isolating the materials that compose the surface of the encapsulation; CNC, Shellac, oil, and merges capsule and B) Z-sequences of optical slices (*3D* image stacks) 190

Fig. 6.11 Confocal microscope images of W_{yeast}/O emulsion with ShCNCCa complex in pH 2 (pepsin) shows preventing coalescence effect (Blue; CNCCW, green; Shellac, and red; oil) 191

Fig. 6.12 2.5-dimensional image of emulsion, displaying both blue and green at the outer surface, implying that CNC and Shellac are present 191

Fig. 6.13 A) determination of complex intensity through transverse scan and thickness of the coating and B) secant along with the ark of the emulsion 193

Fig. 6.14 TEM images of W/O emulsion with ShCNCCa complex in (A) pH 2 (pepsin) and (B) pH 7.5 (pancreatin) 194

Fig. 6.15 SEM images of W_{yeast}/O emulsion with ShCNCCa complex in (A) pH 2 (pepsin) and (B) pH 7.5 (pancreatin).....195

Fig. 6.16. Confocal images of droplets with ShCNCCa at (A) pH 2 and (B) pH 7.5.....197

Fig. 6.17. CO_2 release of yeast in varying pH levels in Pickering emulsions.....198

Fig. 6.18. Shows the viscosity versus a shear rate of (A) mucin, *ShCNC and ShCNCCa*-mucin B) the same composition, but with added yeast. Each sample was subjected to a shear rate of 0.1 to 50 1/s. Rheometric data was measured using a Kinexus Ultra + rheometer via a cup (DO25 C0107 AL) and bob (DG25 L0381 SS) at 37°C.....199

List of Tables

Table 2.1 Colloidal Systems (Mollet & Grubenmann, 2008) 31

Table 2.2 Some examples of emulsion and extrusion techniques applied in microencapsulation studies. Survival under gastrointestinal is higher than 10^6cfu/mL 79

Table 4.1 Experimental conditions to simulate the digestive system 117

Table 4.2 Rate and correlation constants for both VC-GCh-PCNC and VC-GCh-TPP nanocapsules fit zero-order, first-order, and Higuchi mathematical models 129

Table 5.1 Particle size and zeta-potential of SNPs at pH 2 and 7.5 154

Table 5.2 The total number and survivability of yeasts in pH-treated Pickering emulsions 162

Table 6.1 Viscosities of 2% CNC + 0.5% Shellac + 5% Mucin and 2% CNC + 0.5% Shellac + 5% Mucin + Yeast (10 mg/mL).....201

Chapter 1

Introduction

1.1 Research background and motivation

In the past, the criteria for selecting foods were taste, appearance, nutrition, and aroma. In contrast, the choice of safe foods, such as functional/nutraceutical foods and chemical-free foods that guarantee health benefits with specific healthy ingredients, has become a significant issue due to the increased occurrence of various diseases (Burdock *et al.*, 2006). Functional foods provide essential nutrients needed for good health and guarantee the well-being of consumers. These functional foods are processed to enhance existing ingredients or add new components that are not present in the original foods (Hasler, 2002).

Recently, the functional food market, which has grown steadily with “Self-Medication,” has become more important due to the impact of the COVID-19 pandemic. "Self-medication" is the trend of taking ownership over individual health due to fatigue, stress, lack of exercise, lack of motivation, and nutritionally imbalanced eating (Díaz *et al.*, 2020). According to Grand View Research, the size of the global and Canada functional health food market in 2018 was USD 161.49 billion and USD 18.29 billion, respectively. The functional health food market size has an expected upward trend over the next five years (Grand View Research, 2019).

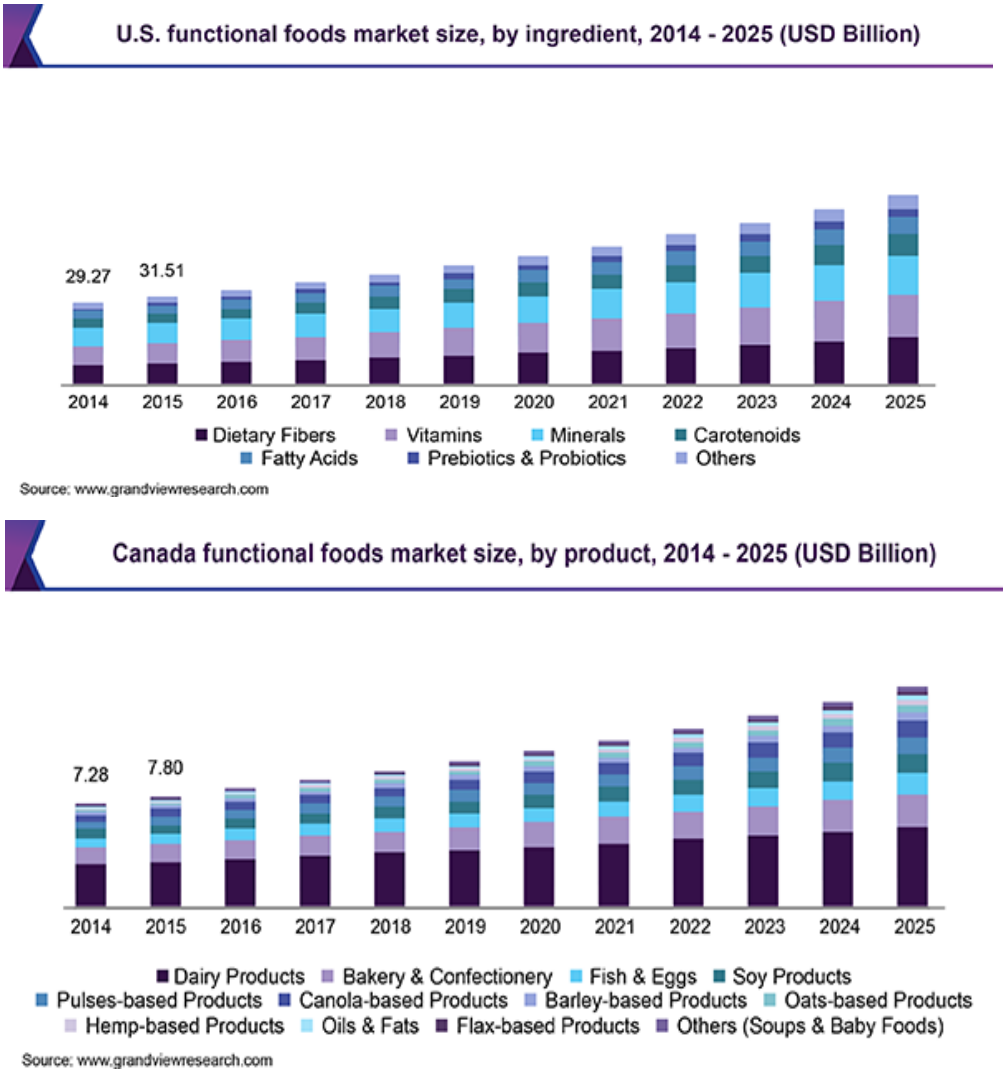

Fig. 1.1. The global and Canada functional foods market size from 2014 to 2025.

Many synthetic preservatives are used to prevent food deterioration caused by microorganisms and reduce the occurrence of food poisoning. However, consumers have increasingly become aware of the safety concerns on the consumption of synthetic additives, and they are cautiously looking for safer natural products. Moreover, synthetic surfactants in the food industry are becoming less desirable due to their potential toxicity and limitations

in stabilizing emulsions. For example, when emulsifying with low molecular weight emulsifiers, the interfacial tension decreases during the process, eventually breaking the particles. As a result of this, Pickering emulsion has recently emerged as an excellent strategy to stabilize emulsion systems in functional foods. Unlike conventional emulsions, the Pickering emulsion is attractive in food research since it's surfactant-free and can irreversibly absorb on the oil-water interface to produce safe, stable and environmentally friendly food systems. In place of synthetic surfactants, Pickering emulsions use solid particles as emulsifiers, which reduce the added health-risks, while providing the same emulsifying characteristics. Among the functional foods reported recently are enteric-coated foods designed to protect functional materials, such as nutrients and probiotics. These enteric-coated foods protect these functional materials throughout their passage in the gastrointestinal tract and allow the release at the desired targeted site. This, in turn, maximizes the viability of the nutrients, providing greater health benefits and a state of well-being, as envisioned. Among various enteric coating formulations, capsules, pellets, and tablets are coated for protection in the stomach and delivery to the small intestine, where the constituents can be absorbed and passed through the enteric epithelial lining into the systemic circulation (Krause & Müller, 2001; Xiong *et al.*, 2020). Likewise, the enteric coating is pH and enzyme-dependent as they degrade in environments with high intestinal pH; moreover, colonic enzymes that break down the core formulations will accelerate the release of the active compounds (Fude *et al*., 2007). Some example of enteric coating materials is cellulose acetate phthalate (CAP), hydroxypropyl methylcellulose acetate succinate (HPMCAS),

hydroxypropyl methylcellulose phthalate (HPMCP), polyvinyl acetate phthalate (PVAP), methacrylic acid copolymers, Shellac, waxes, plastics and plant fibers (Ghube *et al.*, 2020). In general, the cellulosic compounds are dissolved in a solvent mixture, including an organic solvent, to form an enteric coating material for food applications. However, there is a disadvantage where residual organic solvents can cause environmental and safety concerns. Moreover, cellulosic compounds lack plasticity, resulting in a non-uniform surface and cracking during long-term storage; hence the addition of a plasticizer often solves this problem. Therefore, a food-grade plasticizer needs to be incorporated into the enteric composition. (Cha *et al.*, 2016).

This Ph.D. study aims to develop food-grade emulsifiers and plasticizers from natural resources and to elucidate the relationship between chemical compositions and physical properties and how they impact the characteristics of food emulsions.

1.2 Objectives

Recently, numerous studies have focused on investigating the capability of a ‘clean label’ coating material to preserve and prolong the shelf life of food materials. The main material for the four chapters (chapter 3-6), natural biomaterial and biodegradable cellulose nanocrystals (CNC), has been fully utilized owing to their unique characteristics. It formulated into a suitable delivery system to improve their functionality, stability in emulsion, and applicability to meet consumer’s perceptions when applied in functional food

or nutraceutical formulations. This Ph.D. study describes the recent state-of-the-art formulation of colloidal delivery systems to preserve food products by producing an enteric coating with a Pickering emulsion system and encapsulation of nutrients (vitamins) or probiotics.

The specific goals of this Ph.D. are as follows:

1. Development of nanocomposite including both CNC and chitosan to replace synthetic cross-linker and to achieve stable emulsifiers. The CNC would show an excellent percolating network by electrostatic interaction and hydrogen bonding within chitosan polymer matrices.
2. Study of the influence of the active substance loaded nanocomposite on their release profile, antimicrobial and antioxidant effect.
3. Innovative non-chemical surface modification of CNC via hydrogen bonding and hydrophobic interaction with natural sources for the enteric coating system.
4. Comparison of emulsion stability and functional material encapsulation efficiency of the with and without CNC in Complex.

A fundamental theory behind the formulation methods, including the utilization of various sustainable material compositions and their effects on physicochemical and physiological properties of functional foods, including solubility and adsorption in the mucus membrane, is discussed. Finally, some useful insights on selecting an optimal formulation methodology, simple experimental techniques, and green chemistry principles are discussed. Additionally, this thesis defines the best approaches in selecting materials for encapsulating active

compounds that will offer health benefits without compromising their nutritional characteristics.

1.3 Thesis outlines

Chapter 1 provides a brief introduction, where the objectives and the thesis outlines are described. Chapter 2 presents a thorough review of the various topics relevant to the Ph.D. research. In Chapter 3, the development and study of phosphorylated-CNC/modified-chitosan nanocomplexes to stabilize Pickering emulsions are described. Cellulose nanocrystals (CNC) are sustainable nanomaterials with high tensile strength, stiffness, and surface functional groups suitable for various modifications. This chapter reports on the phosphorylated cellulose nanocrystals (PCNC) prepared via acid hydrolysis with phosphoric acid to decorate phosphate groups on the surface of CNC. Also, chitosan was modified with glycidyltrimethylammonium chloride (GTMAC) to improve its solubility. GTMAC-Chitosan (GCh) and phosphorylated cellulose nanocrystals (PCNC) were complexed via ionic gelation to produce GCh-PCNC nanoparticles under mild sonication. Chapter 4 discusses the controlled release of Vitamin C from modified cellulose nanocrystal/chitosan nanocapsules for functional food applications. Vitamin C (VC), widely used in food, pharmaceutical and cosmetic products, is susceptible to degradation, and thus new formulations are necessary to maintain its stability. To address this challenge, VC encapsulation was achieved via electrostatic interaction with glycidyltrimethylammonium chloride (GTMAC)-chitosan (GCh), followed by cross-linking with phosphorylated-

cellulose nanocrystals (PCNC) to form VC-GCh-PCNC nanocapsules. The particle size, surface charge, degradation, encapsulation efficiency, cumulative release, free-radical scavenging assay, and antibacterial test were quantified. Additionally, a simulated human gastrointestinal environment was used to assess the efficacy of the encapsulated VC under physiological conditions. Chapter 5 describes the modification of cellulose nanocrystals (CNC) with ferulic acid (FA) and starch nanoparticles (SNP) to produce a new, natural emulsifier that is environment-friendly and safe for human consumption. This new system is developed and utilized to formulate a multiple Pickering emulsion ($W_1/O/W_2$) for probiotic encapsulation. Physicochemical properties of CNCFA were studied by surface charge, contact angle, TEM, UV-vis, DPPH assay, and CO_2 production analysis. A sustainable, biocompatible, and long-lasting enteric coating system using pH-responsive natural-based materials, Shellac, and cellulose nanocrystals (CNC) are described in Chapter 6. This system could be applied in food, cosmetics, and pharmaceuticals. Yeast (*Saccharomyces cerevisiae*) was used as a probiotic model and was encapsulated in the Shellac-CNC (ShCNC) microcapsules with $CaCl_2$ (ShCNCCa). Chapter 7 summarizes the key conclusions and recommendations for further studies.

Chapter 2

Literature review

2.1 Colloidal systems

Colloids refer to a substance (molecular phase) dispersed within another substance or solution (continuous phase). The fine and intermediate particles of a colloid possess diameters ranging from 1 to 1000 nm (Mollet & Grubenmann, 2008). The Tyndall effect is one of the most common phenomena in colloids, where colloidal particles scatter the incident light (Brinker & Scherer, 2013), and this is often used to distinguish colloidal from the dissolved solution (Hunter, 2001).

Table 2.1 Colloidal Systems (Mollet & Grubenmann, 2008)

Examples	Class	Disperse Phase	Continuous Phase
Fog, Spray, Vapor, Tobacco smoke, Aerosol sprays	Liquid or solid aerosols	Liquid or solid	gas
Milk, butter, mayonnaise	Emulsions	liquid	liquid
Inorganic colloids	Sols or colloidal suspensions	solid	liquid
Clay, mud, toothpaste	Slurry	solid	liquid
Pearls, pigmented plastics	Solid dispersions	solid	solid
foam	Liquid foams	gas	liquid
Foamed plastics	Solid foams	gas	Solid

The colloidal system can be divided into 8 classes according to the combination of the dispersed substance and the dispersing medium (Table 2.1), such as liquid aerosols, solid aerosols, liquid foams, emulsions, sols, solid foams, gels, and solid sols. In terms of foods, these colloidal systems can also be classified into sols, gels, emulsions, and foams, where their structure, texture, and sensory property in the mouth can vary.

2.2 Emulsion systems

2.2.1 Single emulsion

An emulsion is one example of a colloid system with at least two immiscible liquids, such as oil and water, with one dispersing in the other (Chappat, 1994). Emulsions are divided into two types: (a) Oil in water emulsion (O/W) and (b) Water in Oil Emulsion (W/O), and they are used in a variety of applications, such as foods, pharmaceuticals, and cosmetics. Some examples of emulsions in foods are mayonnaise, milk, salad dressing, butter and margarine (Bai *et al*., 2017).

2.2.2 Multiple emulsion

When a W/O emulsion is emulsified in water, a W/O/W emulsion can be produced. This type of emulsion is often referred to as a multiple or double emulsion. Recently, various multiple emulsions are being developed, such as W/O/W and O/W/O, depending on whether the oil phase or the water phase is present as the continuous phase (Fig. 2.1) (Sapei *et al*., 2012). W/O/W emulsions are the preferred choice over O/W/O type emulsions for many

applications due to their solubility limitations. Typically, they are used as a drug delivery system (DDS), encapsulation of vitamins and minerals, encapsulation and release of active compounds and reduction of total fat content (Zafeiri *et al*., 2017). A general W/O/W emulsion can be produced in two steps. First, a stable W/O emulsion is prepared under high shear, which is then re-dispersed in an aqueous solution containing a hydrophilic emulsifier at a lower shear condition. When a high shear is applied in the second step, coalescence can occur due to the collision of water droplets and the rupture of the oil phase (Morais *et al*., 2010). However, in recent years, one-step, multi-emulsion has been successfully applied to emulsify and prepare various types of emulsions.

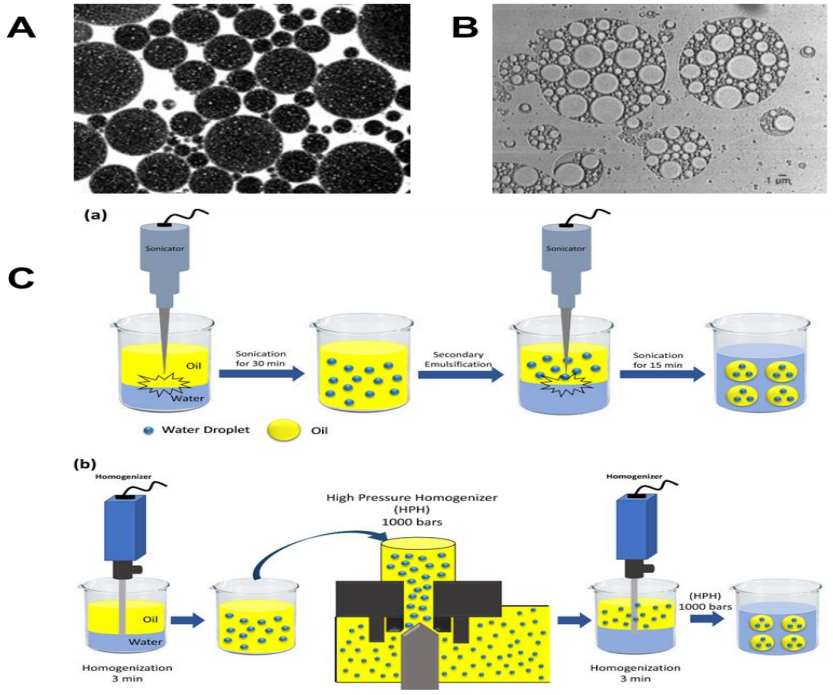

Fig. 2.1 Types of conventional emulsions (A) water in oil in water and (B) oil in water in oil emulsion (Ito *et al*., 2012; Zafeiri *et al*., 2017), and C) schematic of W/O/W emulsion preparation: (a) ultrasonic liquid processing and (b) high-pressure homogenization (HPH) (Ghasemi *et al*., 2020).

For example, Zhu *et al*. (2016) used an amphiphilic random copolymer, poly (dodecyl acrylate-co-acrylic acid) (PDAA) nanoparticle, as a stabilizer to prepare multiple emulsion via a one-step self-assembly process. Nanoparticles with hydrophobic and hydrophilic segments were absorbed in the oil-water interface, reducing the interfacial tension resulting in improved stability (Fig. 2.2). Usually, the one-step formation of multiple emulsions is produced by phase inversion induced by the volume fraction of the oil. During the emulsification, the continuous phase is dispersed as droplets and stabilized by the surfactant. When the droplets reach the critical packing, an inversion occurs to produce multiple emulsions. This process is controlled by key parameters, such as the speed of addition of the internal phase and mechanical stirring (Thakur *et al*., 2008).

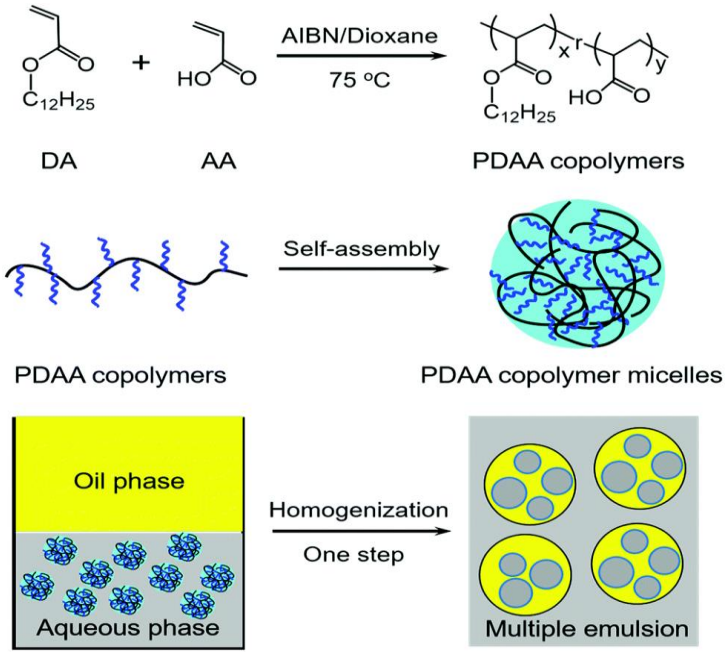

Fig. 2.2 Schematic illustrating the synthesis and self-assembly of poly(dodecyl acrylate-co-acrylic acid) (PDAA) copolymers and the application of PDAA nanoparticles as a stabilizer to prepare multiple emulsions (Zhu *et al*., 2016).

2.3 Current status of emulsion technology

Emulsions can be produced in two ways: (1) physical methods (mechanical) and (2) chemical methods (interfacial chemistry) (Karbstein & Schubert, 1995; Zafeiri *et al.*, 2017). Chemical methods are dependent on the balance of hydrophilicity-hydrophobicity (HLB value) of the emulsifier and the concentration of the emulsifier (Sanchez-Dominguez & Rodriguez-Abreu, 2016). The physical method utilizes an emulsifying device with high shear or high-pressure capabilities. A homo-mixer, such as a high-speed or ultrasonic homogenizer, is used to prepare small particles, while a microfluidizer can be used to produce nano- and microemulsions. Often, the combination of the two methods is used to prepare these emulsions.

2.4 Mechanical emulsion process

2.4.1 High-speed homogenizer

High-speed homogenizers consisting of a rotor and stator are the most common equipment for the homogenization and emulsification of oil-water mixture. In principle, the sample passes through the rotor and stator that produce a high shear force. The sample is forcefully drawn into the rotor and stator and then dispersed horizontally or vertically at high pressure (Urban *et al*., 2006). The size of the particles depends on the gap between the rotor and the stator, the stirring time and rotational speed. As Albert *et al*. (2019) stated, this high-speed homogenizer has its advantages and disadvantages. First, the advantage is that it is easy, convenient, requires short emulsification time and has a low operating cost. It is also possible

to adjust the rotor and stator depending on the type of sample, desired particle size, and viscosity. However, if the stator and rotor gap is too close, the shear rate may be too high, and the sample may break down, deform or aggregate (Albert *et al*., 2019).

2.4.2 Ultrasonic homogenizer

It is known that sound produces vibrations of varying frequencies, and the human audible frequency is between 16 to 20000 Hz. Usually, the standard ultrasonic homogenizer uses a frequency of 20-100 kHz (Hansuld *et al*., 2009). The ultrasonic homogenizer consists of 3 parts: the generator, transducer, and probe. Firstly, the generator's ultrasonic power supply converts 50-60 Hz of electrical energy into 20 kHz of electrical energy. This high-frequency electrical energy is converted into mechanical vibration energy by the piezoelectric transducer in the converter. The oscillation energy of the converter is amplified by the probe connected to the converter and generates a vibration wave in the liquid. When the vibration wave is at negative pressure, millions of microbubbles are generated. When the vibration wave is again at a positive pressure, these bubbles are cavitated, and a significant amount of energy is released in a shearing action. When bubbles are imploded, ultra-high pressure (500 bar) and ultra-high temperature together with shock waves occur (Hansuld *et al*., 2009). Moreover, the Ultrasonic probe is more effective than a bath in reducing particle size due to the concentration of the cavitation bubbles adjacent to the probe (Lad & Murthy, 2012). The amplitude of the oscillator embedded in the ultrasonic bath is fixed, the intensity is weak and not constant (Fig. 2.3).

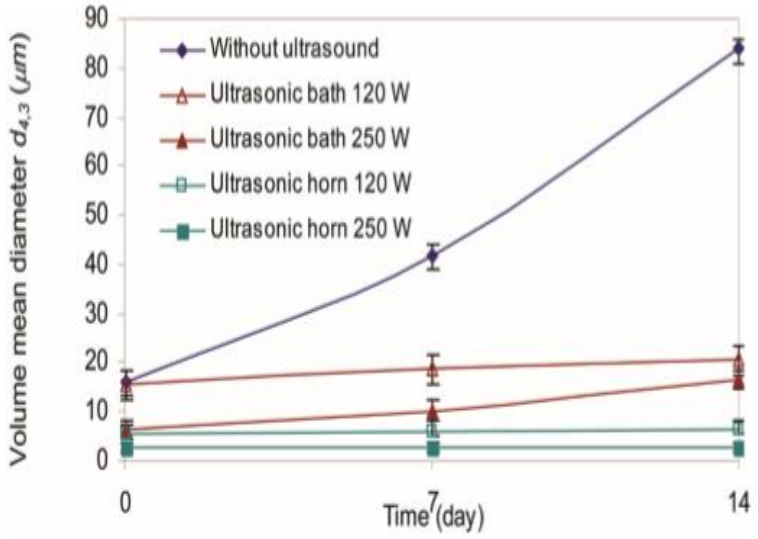

Fig. 2.3 Effect of ultrasound on the change in mean droplet size of dispersed droplets of O/W emulsions stored at 26−30 °C: for 1.2% coconut milk protein emulsion; Sonication was applied at 20 kHz (Lad & Murthy, 2012).

2.4.3 High-pressure homogenizer

High-pressure homogenization is a widely used process in the emulsification, dispersion and mixing of various formulations in the food, pharmaceutical, and biotechnological industries. This method produces nano-sized particles and uniformly dispersed particles via three processes: collision, shear force induced by velocity gradient and cavitation arising from the abrupt pressure reduction. High-pressure homogenization is used to finely grind rough emulsions or lumps of matter to make it more stable. In the case of dairy food products, it enhances product safety, improves product life and taste. The homogenization process produces fine particles by cavitation and through the application of turbulent shear as the

fluid passes through a small gap at high pressure generated by the plunger action (Fig. 2.4) (Hebishy *et al.*, 2015).

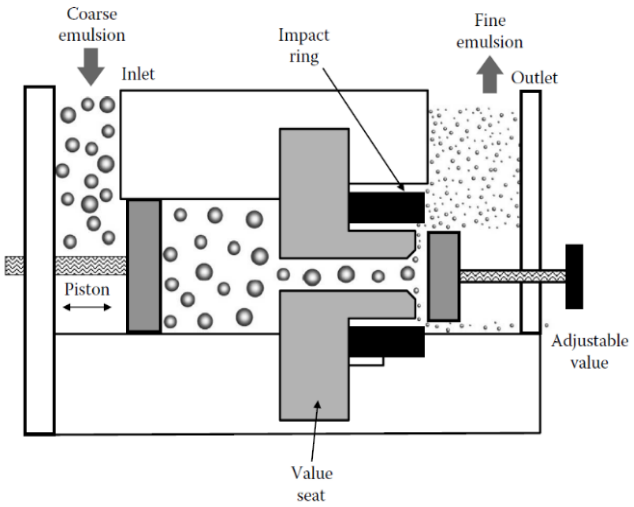

Fig. 2.4 A schematic of High-pressure homogenizers (Hebishy *et al.*, 2015).

2.5 Chemical emulsification process

2.5.1 Surfactant

Since emulsions are thermodynamically unstable, destabilization may occur resulting from various physical processes, such as creaming, sedimentation, Ostwald ripening, flocculation, and coalescence. To prevent the destabilization of the emulsion, a third component is needed. A surface-active agent (surfactant) is an amphipathic compound having both hydrophilic and hydrophobic properties. It is adsorbed onto the interface to lower the interfacial free energy, which significantly alters the characteristic of the interface resulting in the formation of an emulsion. Surfactants are used in many industrial sectors, such as agriculture, food, cosmetics, and pharmaceuticals. The hydrophilic-lipophilic balance (HLB) (emulsifiers with

HLB values of 3-6 are lipophilic and suit for W/O emulsions and of 8-18 are hydrophilic and best suit for O/W emulsions) is a common index used to evaluate and assess the performance of the surfactants (Manoharan *et al.*, 2010). A higher HLB value corresponds to a more hydrophilic surfactant system. Surfactants are classified into anionic surfactant, a cationic surfactant, nonionic surfactant, and zwitterionic surfactant, and often they may depend on the pH. It has been reported that a mixture of two or more emulsifiers when preparing an emulsion produces a more stable emulsion than when each of them is used alone.

As most surfactants are produced by chemical synthesis, they cause environmental and toxicological problems. Chassaing *et al*. (2015) reported that the two common emulsifiers (carboxymethylcellulose, polysorbate-80) used in food formulations induced mild inflammation in the intestine and obesity/metabolic syndrome at low concentrations (1 % w/v or v/v, respectively) in 12 weeks study on mice (Fig. 2.5). Usually, the normal intestine is protected from various harmful bacteria by the mucosal membrane, covering the intestinal surface and preventing harmful bacteria from accessing the small intestine epithelial cells. However, mice fed with water containing the emulsifier had a thinner mucosal layer on the intestine compared to the control. It has been confirmed that emulsifiers change the composition of intestinal bacteria and help bacteria pass through the epithelial cells. In addition, ingestion of emulsifiers seriously changes the composition of the gut microbiota, thereby promoting inflammation and creating a cancer-prone environment (Chassaing *et al*., 2015).

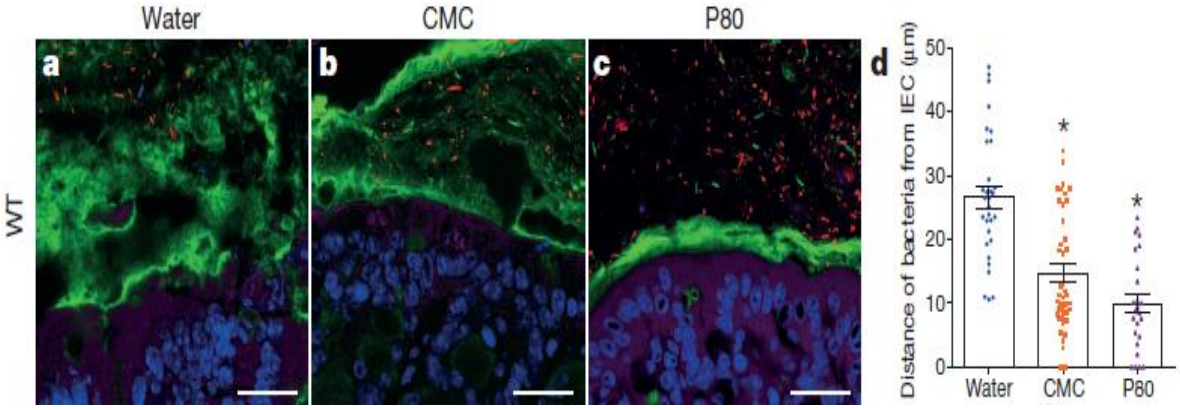

Fig. 2.5 a-c) Confocal microscope images of the barrier cross-section of mice fed with water (left), emulsifier CMC (center), and P80 (right) containing 1% water. Blue epithelium, green mucosa, red intestinal microorganism (Scale bar, 20 μm), and d) distance of closest bacteria to intestinal epithelial cells (IEC) per condition over five high-powered fields per mouse (Chassaing *et al.*, 2015).

2.6 Pickering emulsion

Surfactants used in the food industry are generally referred to as emulsifiers. Ideally, an emulsifier should rapidly adsorb to the oil-water interface, reducing the interfacial tension and prevent droplet coalescence during homogenization (Fig. 2.6). These food emulsifiers affect the viscosity and texture of the food by changing the uniformity and stability in various foods. The most common emulsifiers used in the food industry are small molecular weight surfactants (SMWS), phospholipids, macromolecular polymer, and amphiphilic biopolymers. Food emulsifiers are classified into natural emulsifiers, such as lecithin and saponin and synthetic emulsifiers, by a chemical reaction between fatty acid and glycerol,

such as glycerin fatty acid esters, sorbitan fatty acid esters and sucrose fatty acid esters. Some emulsifiers, including glycerin fatty acid esters, are generally not recognized as safe

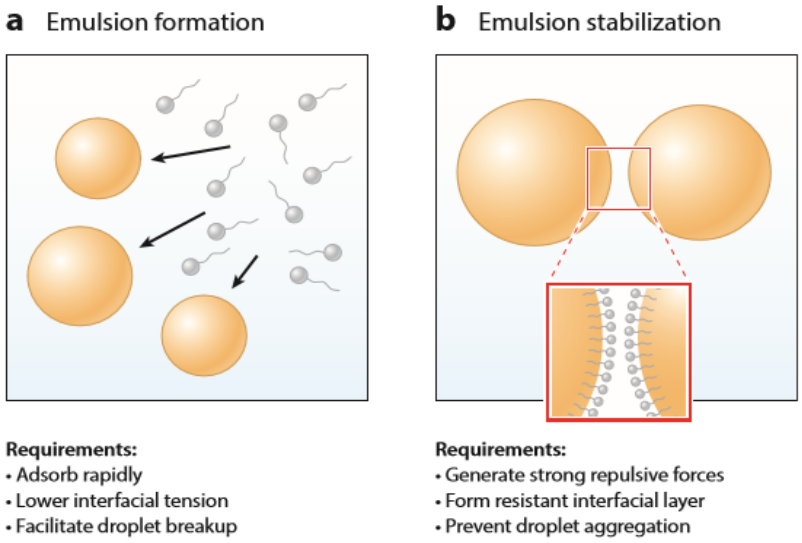

(Chiarappa *et al*., 2017).

Fig. 2.6 Emulsifiers play two key roles in producing commercial emulsion-based food products: They (a) facilitate emulsion formation and (b) promote emulsion stability (McClements *et al.*, 2017).

However, synthetic surfactants in the food industry are becoming less desirable due to their potential toxicity and clean labelling requirements by consumers. In addition, natural emulsifiers have limitations in their ability to stabilize emulsions. For example, when emulsifying with low molecular weight emulsifiers, the interfacial tension decreases during the process, which eventually breaks the particles. At this time, the low molecular weight emulsifier rapidly adsorbs at the interface at the early stages with some unoccupied regions at the interface. Therefore, there is increasing interest in using surface-active colloidal

particles for emulsion stabilization (Yan *et al*., 2020). Pickering emulsions stabilized with solid particles emerged under the concept of "emulsifier free" or "surfactant-free," and research on food Pickering emulsion is showing an increasing trend (Fig. 2.7).

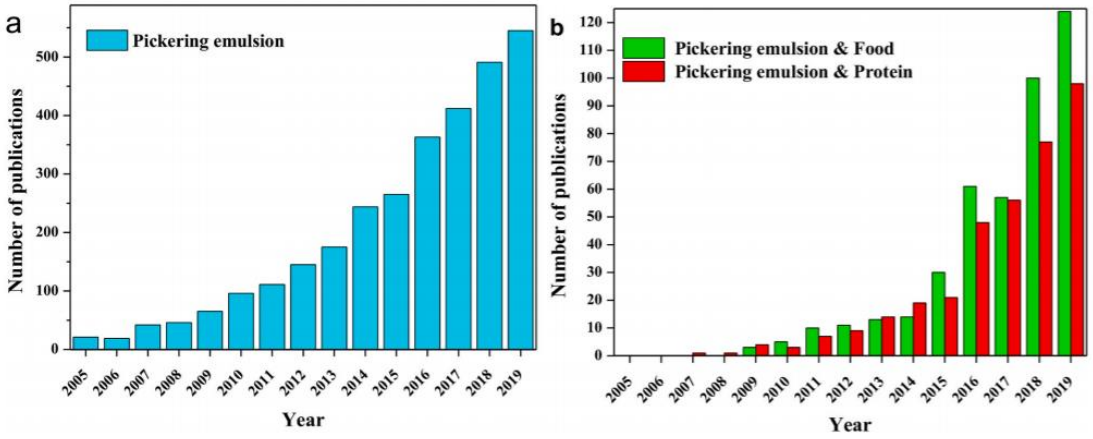

Fig. 2.7 Number of publications related to “Pickering emulsions” (a) and “Pickering emulsions & food,” “Pickering emulsions & protein” (b) by year. Data were obtained from the “Web of Science” in April 2020 (Yan *et al*., 2020).

Pickering emulsions are stabilized by adsorbing nano- or micro-sized solid particles at the oil-water interface to prevent coalescence of the emulsion droplets. The unique properties of Pickering emulsions are due to their large interfacial adsorption energies. The main difference from the regular emulsions is that the solid particles irreversibly adsorb at the interface (Fujisawa *et al*., 2017). The particles must have a wettability number which is measured by a three-phase contact angle (θ) that has sufficient interface adsorption capacities (Chen *et al*., 2020) and are selected by emulsion types (Ortiz *et al*., 2020) (Fig. 2.8).

Hydrophilic particles have a contact angle, measured at the waterside of the interface, smaller than 90° and a large part of the particle surface is present on the waterside. In addition, the oil-treated silica particles have a contact angle greater than 90°, and a large part of the particle surface is present on the oil side (Rayner *et al.*, 2014). Therefore, hydrophilic particles tend to form an O/W emulsion, and lipophilic particles tend to form a W/O emulsion.

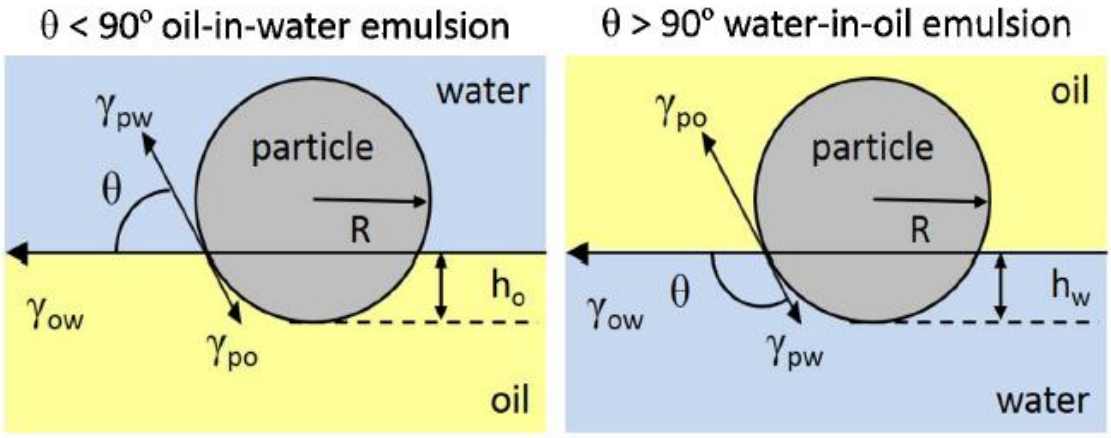

Fig. 2.8 The location of a particle at the oil-water interface is determined by the contact angle, measured through the aqueous phase. When less than 90°(left) oil-in-water emulsions are most likely formed, and when larger than 90°(right), water-in-oil emulsions may form (Rayner *et al.*, 2014).

As mentioned above, a solid particle with a contact angle close to 90° forms the most stable emulsion with the highest irreversible adsorption at the interface between water and oil. The reason can be explained as follows. When spherical particles with radius are adsorbed at the interface of two fluids (e.g., oil and water), the attachment energy can be described by the equations below.

The energy of adsorption E represents the energy required to remove a particle of radius r from an oil and water interface with an interfacial tension $\gamma_{ow.}$ Equations (2.1) and (2.2) describe the adsorption energy to the interface when the particles exist in the water or oil phase in the initial state, respectively. The wettability of particles at the fluid interface can be characterized by the three-phase contact angle (θ_c) at the three-phase (particle-oil-water) interface. For example, when a particle of 1 mm with the property of neutral wetting (θ_c=90°) is adsorbed at the oil-water interface, its energy is approximately ~10^8 k_BT, which corresponds to a very large energy barrier. Here, k_BT is the thermal energy of one particle, k_B is the Boltzmann's constant, and T is the temperature. The intensity of the adsorption energy indicates particles adsorbed to the interface are irreversible, and the particles cannot be spontaneously desorbed from the interface unless a significant amount of energy is supplied (Binks & Fletcher, 2001; Binks, 2002).

$$\Delta E_{IW} = -\pi\alpha^2\gamma_{ow}(1-\cos\theta c)^2 \quad (2.1)$$

$$\Delta E_{Io} = -\pi\alpha^2\gamma_{ow}(1+\cos\theta c)^2 \quad (2.2)$$

2.7 Types of green solid particles

To date, there have been several examples of 1) food grade Pickering emulsion stabilizations; polysaccharide, protein, lipid particles and 2) inorganic particles; silica, calcium carbonate (Albert *et al*., 2019).

2.7.1 Cellulose and cellulose nanocrystals

One of the most significant green materials that are gaining increasing attention is cellulosic materials, which are predominantly used in paper, textiles, and clothing (Brinchi *et al*., 2013). Cellulose is the most abundant natural organic compound that comprises the basic structure of plant cell walls. Also, it is well-known that cellulose occupies up to 50% of all plant material. Wood is composed largely of three natural polymers, cellulose, hemicellulose and lignin (Grishkewich *et al*., 2017), and the molecular structure of each is shown in Fig. 2.9.

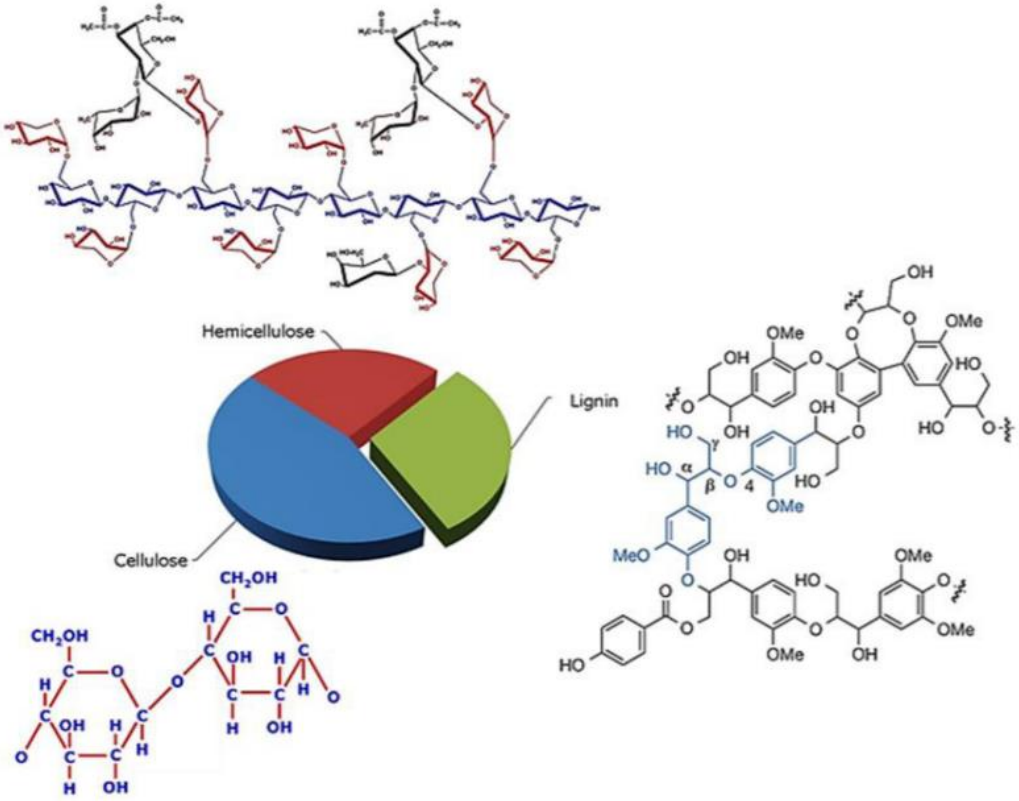

Fig. 2.9 The chemical structures of wood; Simple structures of cellulose, hemicellulose, and lignin: Major components of biomass (Akash, 2015).

Cellulose, which consists of both crystalline and amorphous regions, has a higher specific elastic modulus than steel. It has been utilized in various aspects of human life because of its excellent physical properties. For instance, paper is a representative product using cellulose and has been utilized by humans throughout human civilization. On the other hand, hemicellulose is an amorphous polymer composed of pentose, arabinose, mannose, galactose hexose, and xylose (Vishtal & Kraslawski, 2011). It differs from cellulose in that it has a branched structure with a small number of monomers and a relatively smaller molecular weight. On the other hand, lignin differs from the other two polymers in that the aromatic monomers of phenyl propane are covalently linked by carbon-carbon or aryl-ether bonds (Kumar *et al*., 2009). Lignin is composed of three types of monolignols, such as sinapyl alcohol, coniferyl alcohol, and coumaryl alcohol, depending on the species (Fig. 2.10) (Chesner, 1963). In the pulp and paper industry, lignin is a waste resource removed to produce white pulp fibers. Recently, lignin extracted from woody biomass is being used to produce bioethanol (Pérez *et al.*, 2002; Strassberger *et al.*, 2014).

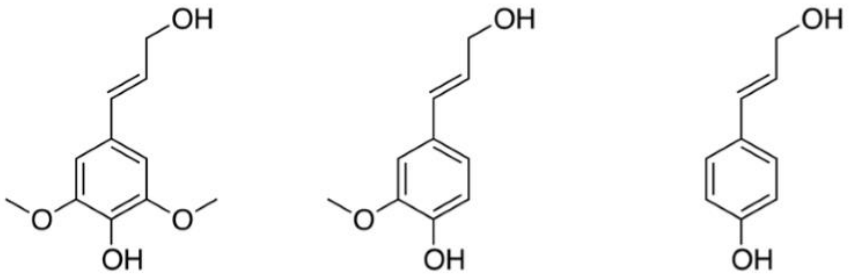

Fig. 2.10 The three phenylpropane units, the building blocks of lignin (a) sinapyl alcohol, (b) coniferyl alcohol, (c) *p*-coumaryl alcohol (Chesner, 1963).

Cellulose is a linear long-chained polymer consisting of disaccharide anhydrous-D-glucopyranose unit (Monteagudo-Mera *et al*.) units linked by 1-4 glucosidic bonds. Cellulose can be regarded as a condensation polymer. The AGU units are connected through the hydroxyl group attached to the C-1 atom of one glucose molecule and the hydroxyl group attached to the C-4 atom of another glucose molecule (Fig. 2.11). The molecular formula of an anhydrous glucose unit is $C_6H_{10}O_5$, and thus the molecular formula of cellulose can be specified as $(C_6H_{10}O_5)_n$ (Ifuku *et al.*, 2007)

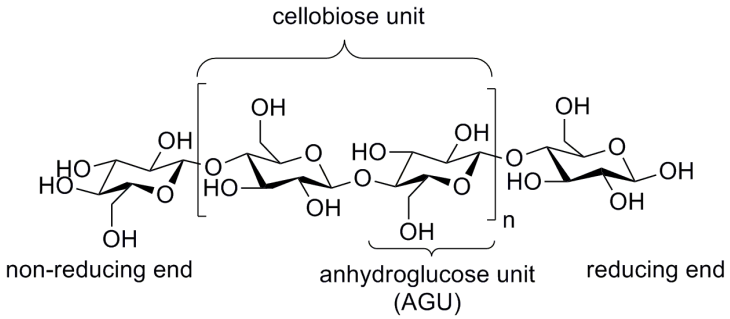

Fig. 2.11 Chemical structure of cellulose (Ghalia & Dahman, 2017).

In addition, cellulose derivatives or microcrystalline cellulose (MCC) are used in a wide range of industries, such as pharmaceuticals, food, and cosmetics (Park *et al*., 2004). Recently, cellulose nanocrystals, whose size is much smaller than MCC, can be derived from via chemical and mechanical treatment of cellulose. Nanocellulose possesses different particle size distributions, degrees of branching, crystallinity, crystal structures and surface chemistry properties depending on the source of raw materials (Brinchi *et al.*, 2013; Moxley & Zhang, 2007).

Additionally, CNCs can be produced from bacteria, such as *Acetobacter xylinum* (Sun *et al*., 2005). However, this process has several disadvantages, e.g., a bacterial culture is costly, and it is difficult to produce large quantities of nanocellulose due to the low yields of the process. Therefore, most of the nanocellulose is derived from the top-down processing of wood pulp and agriculture biomass. Nanocellulose can be divided into cellulose nanofibril (CNF) and cellulose nanocrystal (CNC), depending on the method of extractions. Cellulose nanofibers are usually produced via the mechanical treatment of pulp fibers, and they have a width of 5 to 100 nm and a length of several microns. On the other hand, cellulose nanocrystals are rod-shaped nanocrystals with a diameter (width) of 2 to 20 nm and a length of 100 to 250 nm. They are derived from chemical treatments, such as alkali pre-treatment followed by acid hydrolysis. Cellulose nanocrystals possess some desirable properties, such as a high tensile modulus, similar to steel or Kevlar (100 to 160 GPa), low density (0.8 to 1.5 g /cm^3) and a large specific surface area (~250 m^2/g) (Grishkewich *et al*., 2017). According to Brinchi *et al*. (2013), the beneficial properties of CNCs make them attractive for applications in the packaging and paper industry, filtration devices, artificial skin, and cosmetics (Brinchi *et al*., 2013).

2.7.1.1 Alkali process

Alkali pretreatment has been more effective in dissolving lignin and hemicellulose (Fig. 2.12), and without pre-bleaching, the dark colour of lignin is produced during kraft cooking.

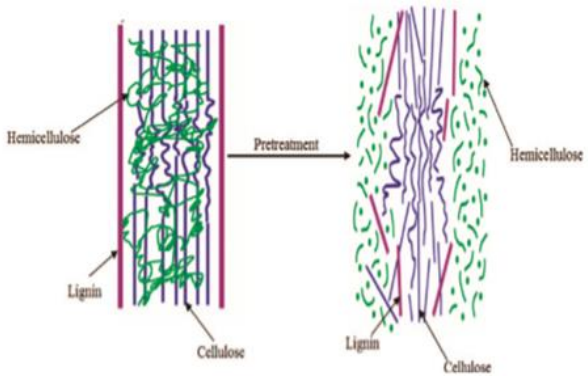

Fig. 2.12 Disruption of cellulosic biomass by pretreatment (Kumar *et al*., 2009).

Chromophores comprising benzene rings, carbon-carbon double bonds, and carbon-oxygen double bonds induce colour changes by light absorption and oxidation. As shown in Fig. 2.13, three chromophore compounds (ortho-quinone, coniferyl aldehyde and α-carbonyl) comprise the bulk of the chromophore mixtures.

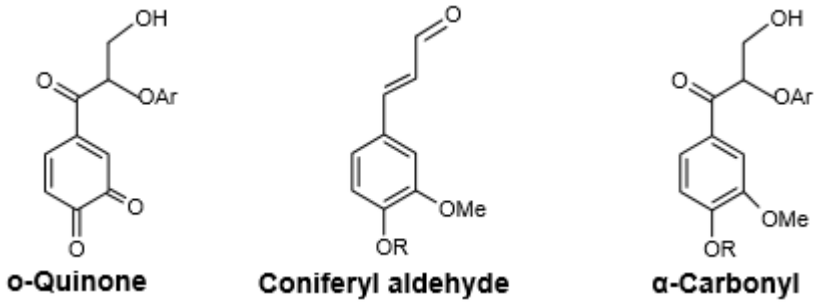

Fig. 2.13 Structure of conjugated chromophores (Chesner, 1963).

Torok & Dransfield (2017) reported that this conjugated structure is formed when an organic compound with a high carbon number is exposed to heat in the absence of oxygen (Torok & Dransfield, 2017). Therefore, the problem can be solved by adding bleaching agents, such as

hydrogen peroxide, sodium chlorite, sodium hypochlorite and chlorine dioxide (Rambabu *et al*., 2016). In addition, when sodium hydroxide is used, the swelling of cellulose chains can lead to a reduction in crystallinity and an increase in the surface area. The alkali process is usually performed at a lower temperature than the acid process and has reaction times ranging from hrs to days.

Sodium chlorite has an advantage due to its negligible harmful effects and low ash contents generated under acidic conditions. Furthermore, sodium chlorite does not attack cellulose like in a normal bleaching system (Jiang & Hsieh, 2015). Rambabu *et al*. (2016) reported on the production of nanocellulosic fibers by chemical and mechanical pinecone processing. The optimized concentration of sodium hydroxide (4 wt%) and acidified sodium chlorite (5 wt%) greatly improved the cellulose content (about 89%) in the produced fibers. Fig. 2.14 shows the SEM images of pinecone before and after chemical treatment, where the original pinecone has a rough surface (Fig. 2.14a) and the alkaline treated cellulosic fiber existed as bundles (Fig. 2.14b). After the treatment with acidified sodium chlorite, individual cellulosic fibers were obtained (Fig. 2.14c), and this treatment is highly effective in removing lignin. Fig. 2.14d is an ESEM image of nanocellulose used in supermass collider (Rambabu *et al*., 2016).

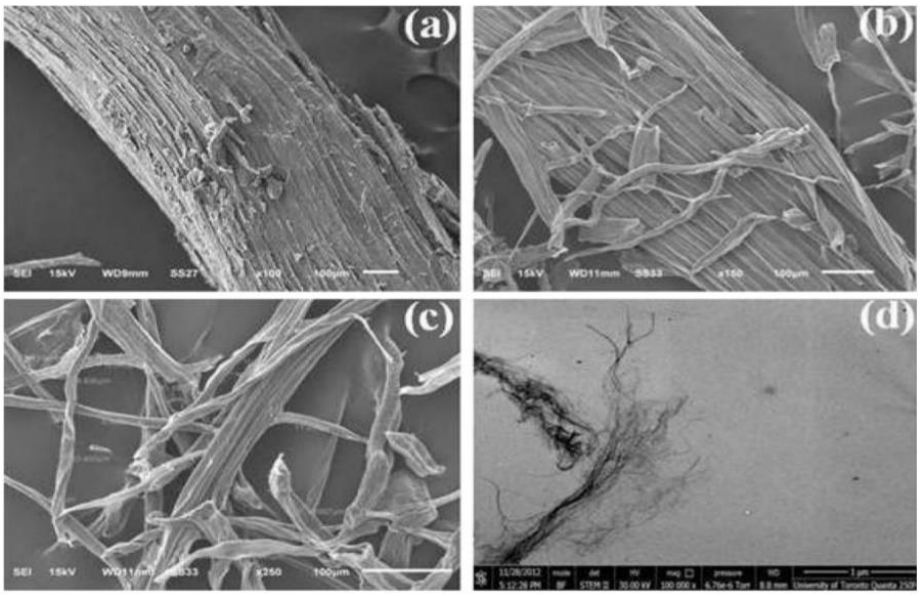

Fig. 2.14 SEM images of pinecone before and after chemical treatments (a) RPC 100X, (b) AL 500X, (c) BL 500X and (d) the ESEM image of cellulose nanofibers 100 000X (Rambabu *et al*., 2016).

Jiang & Hsieh *et al.* (2015) isolated pure cellulose from tomato peel powder and extracted nanocellulose through acid hydrolysis. Pure cellulose was separated from the tomato peel powder with acidified sodium chlorite, and then potassium hydroxide (Rosenzweig *et al.*, 2013) was used as the bleaching agent. As a result, alkaline bleach removes more mass (49.8%) than sodium chlorite (26.1%), suggesting that the tomato peel contains more hemicellulose than lignin. Therefore, the acidified $NaClO_2$/KOH treatment yielded 13.1%, whereas the NaOH/H_2O_2 treatment resulted in 10.2-11.3% cellulose after removing the hemicellulose protein (Jiang & Hsieh, 2015).

2.7.1.2 Acid hydrolysis

Cellulose is composed of crystalline and amorphous regions. When an acid is added to the cellulose fiber, hydronium ions (H_3O^+) penetrate the amorphous regions where the chains are accessible, compared to the denser crystalline regions where hydronium ions promote the hydrolysis of glycosidic bonds (Fig. 2.15).

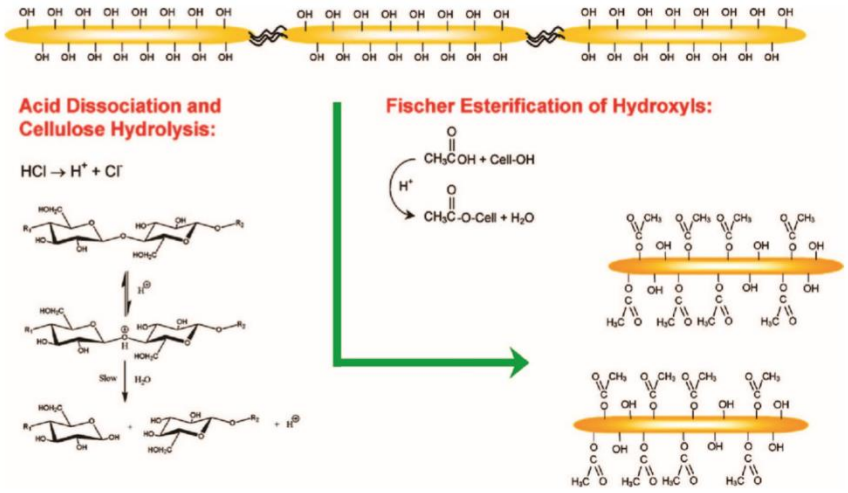

Fig. 2.15 Reaction scheme illustrating the cellulose hydrolysis and esterification reactivity of hydroxyl groups (Sanchez-Dominguez & Rodriguez-Abreu, 2016).

As a result, the amorphous regions are gradually removed, leaving behind the crystalline region. These nanoparticles have been termed cellulose nanocrystals in North America and cellulose whiskers in Europe. In most cases, strong acids, such as hydrochloric acid (HCl), sulfuric acid (H_2SO_4), phosphoric acid (H_3PO_4), hydrobromic acid (HBr), and nitric acid (HNO_3) are used to produce the cellulose nanocrystals, with sulfuric acid being the most popular (Grishkewich *et al*., 2017; Habibi *et al*., 2010; Peng *et al*., 2011; Rodrıguez-Chong *et al*., 2004). Cellulose nanocrystals prepared using sulfuric acid are very stable due to the large amounts of negative charges on the surface of CNC. When sulfuric acid is added to

cellulosic fibers, some hydroxyl groups on the surface of the cellulose nanocrystals undergo esterification with sulfuric acid and transform into negatively charged sulphate ester groups ($-SO_3^-$). The structure and physical properties of cellulose nanocrystals depend on the species and the concentration of the acid used in the acid hydrolysis process, such as hydrolysis temperature and reaction time (Limmatvapirat *et al.*, 2005). When the acid concentration is too high or is heated for a long time, the cellulose decomposes completely into the monosaccharide molecules.

On the other hand, when the acid concentration is too low or hydrolysis time is too short, the amorphous regions are not completely removed (Habibi & Dufresne, 2008). Therefore, studies have been conducted to determine the optimal conditions to prepare pure cellulose nanocrystals, which were 63.5-65 wt% (Bondeson *et al*., 2006; Cao *et al.*, 2008; Fortunati *et al*., 2012). At this condition, the size of the cellulose nanocrystals does not change considerably. When a higher acid concentration is used, the length and diameter of the cellulose nanocrystals are greatly reduced. The hydrolyzed suspension must be washed several times and centrifuged to remove residual chemicals and acids in the suspensions. This procedure is usually performed until the pH becomes neutral. If the cellulose nanocrystals are not completely dispersed, agglomerates are formed, which can be effectively dispersed using an ultrasonicator or a homogenizer. The well-dispersed suspensions should be kept in the refrigerator with a few drops of chloroform added to avoid aggregation. According to Camarero Espinosa *et al*. (2013), hydrochloric acid hydrolyzed cellulose (H-CNC) displays

a poor dispersion, while the sulphated groups on cellulose (S-CNC) can degrade at high temperatures, limiting the study of thermal stability. To address this problem, acidic hydrolysis of cellulose was carried out by mixing the two acids, which showed high heat stability and low dispersibility. Surprisingly, there are not many studies on phosphoric acid hydrolysis, and only a few groups have reported on the phosphorylation of cellulose to enhance their thermal stability and biocompatibility. Camarero Espinosa *et al*. (2013) reported on the acid-hydrolysis of cotton using phosphoric acid and compared the properties of S-CNC and H-CNC to identify the optimal conditions for heat and dispersibility (Camarero Espinosa *et al*., 2013).

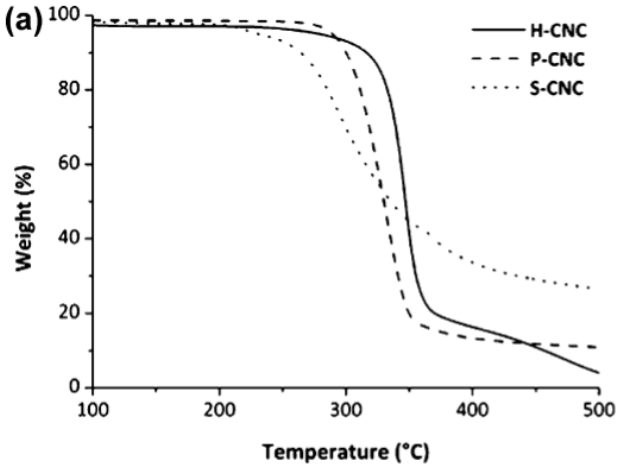

Fig. 2.16 TGA traces of S-CNCs, P-CNCs, and H-CNCs (Camarero Espinosa *et al*., 2013).

As a result, P-CNC showed dispersibility in various solvents in the following order (H_2O> DMSO> DMF> THF), which is similar to S-CNC. The decomposition onset temperature of both P-CNC and H-CNC was 220 ^oC as determined from the TGA analysis, while the onset

decomposition temperature for S-CNC was 150 ^{o}C (Fig. 2.16). The shear storage moduli (E') of P-CNC (21.6 ± 0.5 MPa) was higher than S-CNC (21.1 ± 0.6 MPa) and H-CNC (17.6 ± 2.0 MPa).

2.7.2 Chitosan

The causes of food poisoning in food are very diverse, such as bacterial food poisoning, which is mainly caused by contamination and deterioration due to poor handling of food. This is detected in various foods, such as meat, canned foods, fish, and shellfish. Many synthetic preservatives are used to prevent food deterioration caused by microorganisms and prevent the occurrence of food poisoning. However, consumers have increasingly become aware of the safety concerns on the consumption of synthetic additives, and they are increasingly looking for safer natural products. One such natural polymer is chitosan, which is obtained through the deacetylation of chitin (Fig. 2.17). Chitosan is the second most abundant natural polysaccharide on the planet, and it is extracted from the exoskeleton of crabs, shrimp, and fungi of crustaceans. The relative proportions of glucosamine and acetyl glucosamine vary depending on the degree of acetylation of chitosan. Thus the properties of chitosan can be controlled (Younes & Rinaudo, 2015). These include biocompatibility, biodegradability, and antibacterial properties.

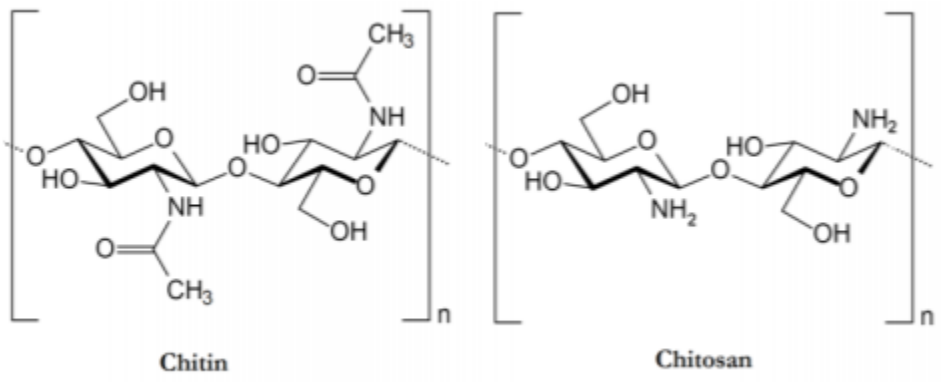

Fig. 2.17 Structure of chitin and chitosan (Younes & Rinaudo, 2015).

Above all, chitosan is known to be almost non-toxic to animals and humans. In animal experiments on mice, the lethal dose of 50% of the test animals, or LD50, was found to be as low as 16g/kg. In addition, the toxicity of chitosan has been reported to be DD (%) dependent. Chitosan with a DD above 35% has low toxicity, while less than 35% DD (e.g. chitin) has been reported to cause dose-dependent toxicity (Decarlo *et al*., 2014). On the other hand, the M_w of chitosan did not affect toxicity. As for the antibacterial property, Liu *et al*. (2013) studied the effect of chitosan on *E. coli* and concluded that low molecular weight chitosan effectively controls the growth of *E. coli* (Liu *et al*., 2013). Since the surface of the bacterial cell membrane is negatively charged, the $-NH_3^+$ the positive charge of chitosan is electrostatically attracted to the surface of the cell membrane, and often the cell membrane is disrupted, resulting in the death of the bacteria. However, its application is limited due to its poor solubility in water and organic solvents. The acid dissociation constant of chitosan (pK_a of 6.5) was determined by the degree of deacetylation, ionization strength and charge

neutralization of the amine groups. Therefore, chitosan is positively charged and dissolves in an acidic solution, and the charge density depends on pH. Chitosan has a structure similar to cellulose, one type of polysaccharide and has an amino group at the C-2 position of the glucose unit. Due to its structural characteristics, not only does chitosan find applications in wastewater treatment, but it can also be used in food additives, coatings, artificial skin materials, inhibitors, drug delivery systems, and gene delivery systems.

Chitosan is often used in nanoparticle manufacturing as it is biocompatible and biodegradable. The preparation of the nanoparticle can be performed by utilizing the physical interactions between the polymer chains, such as electrostatic forces, hydrophobic associations, or hydrogen bonds (Mivehi *et al*., 2008; Wang *et al*., 2017). As shown in Fig. 2.18. chitosan-TPP nanoparticles are prepared by ionic gelation polyvalent anion sodium tripolyphosphate (TPP) with positively charged chitosan.

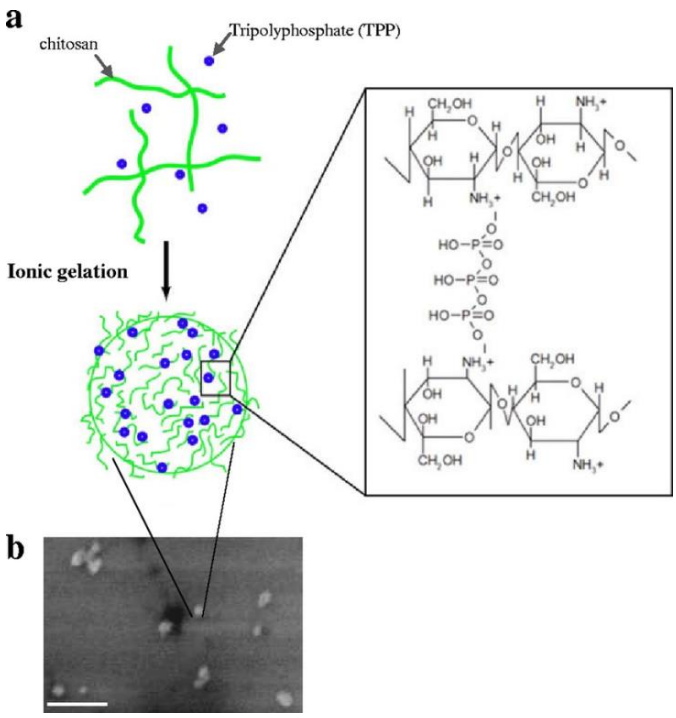

Fig. 2.18 Formation of the chitosan-tripolyphosphate complex by ionotropic gelation. (a) Schematic illustration of the chitosan-TPP complex and (b) SEM image. Bar, 200 nm (de Paz *et al*., 2011).

According to Jonassen *et al*. (2012), chitosan-TPP nanoparticles were evaluated for improving the drug delivery of small and large molecular weight drugs, and the concentration of chitosan, ratio of TPP to chitosan, the molecular weight of chitosan and ionic strength of the medium were evaluated (Jonassen *et al*., 2012). In addition, Wang *et al*. (2017) postulated that chitosan-TPP encapsulation is metastable and is driven by external conditions, such as pH and ionic strength (Wang *et al*., 2017). Therefore, new anionic cross-like agents are needed to stabilize chitosan-based nanocapsules.

2.7.2.1 Glycidyltrumethylammonium chloride (GTMAC)-Chitosan

Recently, interest in chitin and chitosan, which are animal polysaccharides, has been increasing due to the emphasis on the non-toxicity of antimicrobial agents. Chitosan is a substance derived from the deacetylation of chitin extracted from the exoskeleton of crabs and shrimps. Its structure is similar to that of cellulose. N-acetyl-2 amino-2-deoxy-D-glucose (glucosamine) is a form where the hydroxyl group at the C-2 position of cellulose is replaced with an amine group. Chitosan is superior to chitin because it can be dissolved by the protonation of amine groups at the C-2 position in a dilute acidic solution.

In the field of food additives, studies on the addition of chitosan oligosaccharides to foods to inhibit the growth of microorganisms, prevent the decay of meat, and prolong the shelf life of fruits and vegetables have been reported. The antimicrobial properties of chitosan stem from the amine groups at the C-2 position protonated in acidic conditions. The cationic chitosan interacts with the cytoplasm of an anion-bearing microorganism and inhibits the activity of the microorganism. However, in neutral and alkaline solutions, it is difficult to dissolve chitosan, which limits its ability to formulate with various polymers. In a basic environment, the chitosan precipitates and the amine groups are deprotonated, resulting in a decrease in the antimicrobial activity (Lim & Hudson, 2004). Therefore, modification is necessary to improve the solubility of chitosan and broaden its applications. In general, a compound having a quaternary ammonium salt is generally water-soluble. It has been reported that a quaternary ammonium salt can be introduced to chitosan to produce a water-

soluble chitosan derivative (Alipour *et al*., 2009). Compounds having quaternary ammonium are widely used as antimicrobial processing agents. When quaternary ammonium salts are introduced to chitosan, it imparts water solubility and antimicrobial characteristics to the polymer (Liu *et al*., 2013).

N-[(2-hydroxy-3-trimethylammonium) propyl] chitosan chloride (HTCC), a water-soluble chitosan derivative with various degrees of substitution (Mivehi *et al*., 2008), was synthesized by reacting chitosan with GTMAC, a quaternary ammonium compound with a glycidyl group. The reaction formula of chitosan and GTMAC is shown in Fig. 2.19.

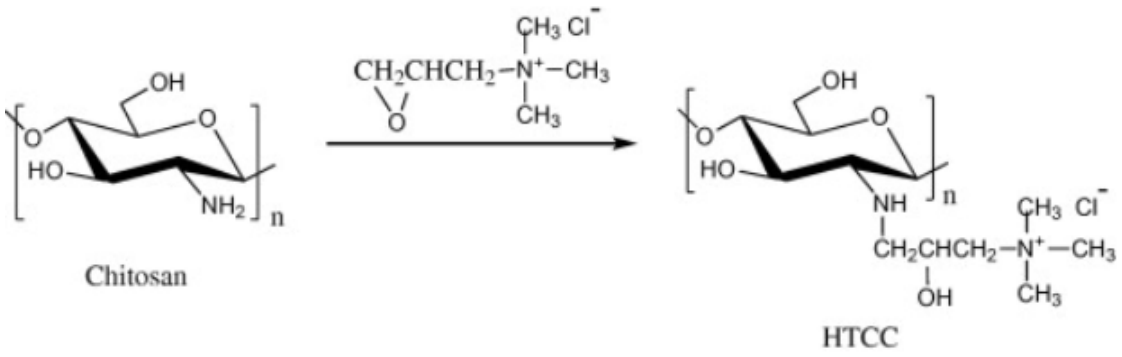

Fig. 2.19 Synthesis route for HTCC (Mivehi *et al*., 2008).

Generally, epoxy groups readily react with amine groups under neutral or acidic conditions. Therefore, a reaction between GTMAC and amine groups of chitosan can be readily implemented. HTCC, having a quaternary ammonium group at the C-2 position of chitosan, could be prepared by opening the epoxy group of GTMAC using a catalyst and then reacted with the amine groups of chitosan.

2.7.3 Shellac

Shellac is a natural resinous polymer that has been approved by the FDA (U.S. Food and Drug Administration) since the 1930s and is generally recognized as safe (GRAS). It is used worldwide as a coating agent for pharmaceuticals (tablets), confectionery, vegetables and fruit because it has not only an excellent film-forming (Hagenmaier & Shaw, 1991) but also prevents odours, gas excretion, moisture evaporation, oxidation, absorption, and it can control release rate (Chauhan *et al.*, 2015; Muhammad *et al*., 2020; Pearnchob *et al.*, 2003). Nevertheless, shellac as a coating material is still limited due to its fragile properties (Bar & Bianco-Peled, 2020; Tang *et al.*, 2019). Shellac has a weak surface and is easily scratched, but it can be easily repaired by adding a new layer of shellac coat, which will bind to the shellac compounds. Therefore, many studies have been conducted to increase the stability by combining shellac and other materials (alginate, gelatin, cellulose, chitosan, protein, etc.) in order to reduce the existing shellac coating disadvantages and improve its mechanical properties. In general, shellac is produced on trees by the female lac bug (*Kerria lacca*, *Laccifer lasca* or *Coccus lasca*) in east India, Thailand, China, Burma, and Myanmar (Farag & Leopold, 2009; Hagenmaier & Shaw, 1991; Hamad *et al*., 2012; Limmatvapirat *et al*., 2004; McGuire & Hagenmaier, 1996). *Kerria lacca* secretes shellac to form a sticklac (tube-like cocoon structure) that is intertwined onto the branches of the tree. In terms of traditional purification methods, raw shellac is removed from the branches, including bark shavings, lac bugs, and larvae. Natural shellac is sun-dried or heated via fire on a tube; the heat causes the shellac to melt and drain out of the tube, leaving behind the impurities. The melted shellac is

then pressed through a roller to form a thin sheet and flakes before distributed for production (Das & Jacob, 2011).

2.7.3.1 Bleached and dewaxed shellac

Currently, many types or grades of shellac are commercially available; their properties and colour will depend on the raw material, the insect strain, host tree purification method and processing parameters (Hamad *et al*., 2012). Most commercial shellacs are dewaxed and decolorized by a highly refined process and utilized in edible applications, such as confectioner's glaze, by forming coating and polishing.

The method of purification is by dissolving the stick lac, a resinous secretion of lac bug, in an alkaline solution and then adding bleach, sodium hypochlorite or hydrogen peroxide to break and remove the colours, which are laccaic and erythrolaccin from the lac. However, using hydrogen peroxide, high temperature and large amounts of residual rinses are required. After the bleaching step, diluted sulfuric acid is added to the bleached shellac, which is then precipitated and dried. However, this process reduces the molecular weight of the carboxyl and hydroxyl groups (Saengsod *et al.*, 2019). Finally, the wax in bleached shellac is removed by filtration to get wax-free bleached shellac (less than 0.5% wax content).

2.7.3.2 Solubility of Shellac

Shellac has been known not to dissolve in water due to its carboxyl groups (Penning, 1996);

it is solubilized in an aqueous alkali solution (the *pKa* value of Shellac is 6.9–8) due to the deprotonation of carboxylic acid, allowing the Shellac to be soluble in aqueous solvents, such as sodium hydroxide, ammonia, sodium carbonate (Limmatvapirat *et al*., 2004; Limmatvapirat *et al*., 2005; Qussi & Suess, 2005). Additionally, Shellac is completely soluble in methanol, ethanol and it partially dissolves in ethyl acetate, chloroform and ether (Cagil, 2020). Farag & Leopold (2009) prepared shellac films from an aqueous shellac solution with 1% ammonium bicarbonate solution at 50 °C; then, free ammonia is removed at 65 °C. The evaporated water is continuously replaced, and this process is repeated until the pH is constant at between 7.3 and 7.9. An alternative shellac solution was prepared by adding finely milled Shellac using a cutter mill into a bicarbonate solution at 40 °C; the dispersion is then heated between 60 and 70 °C with stirring until the Shellac is completely dissolved (Al-Gousous *et al*., 2015). Sodium shellac was formed by dissolving Shellac in sodium carbonate in a 2:1 molar ratio (Gao *et al*., 2018). Sun *et al*., (2017) used 80% aqueous ethanol (v/v) and 0.1 M phosphate buffer saline (PBS) to dissolve completely under stirring at 600 rpm at room temperature for 2h. (Sun *et al*., 2017). To prepare a coating mixture of aloe gel and Shellac, dewaxed and bleached Shellac were dissolved in 0.5% ammonium hydroxide at 95 °C and then mixed with oleic acid as an emulsifier at 95 °C and 3,000 rpm using a high-speed homogenizer. A composite coating was obtained by mixing the shellac coating and aloe gel in equal proportions (Chauhan *et al*., 2015). Kong *et al*. (2017) conducted other experiments to dissolve Shellac with an aqueous (Shellac and ethanol/water mixture). When the concentration of water was more than 22.5 volume %, its solubility

decreased. With the slight addition of Na_2CO_3, the solubility of Shellac could be increased in higher water contents (Kong *et al*., 2017). Limmatvapirat *et al.* (2004) conducted partial hydrolysis tests to increase the solubility of shellac using 2% sodium hydroxide. After hydrolysis, the acid value (AV) was increased by extending the hydrolysis time. In contrast, free carboxyl and hydroxyl groups increased from the cleavage of the ester bond led to a reduction in the ester value (Limmatvapirat, *et al*., 2007; Limmatvapirat *et al*., 2005). This result corresponded to the findings of Cagil (2020), who stated that wax-shellac and aged Shellac have the lowest acid value content.

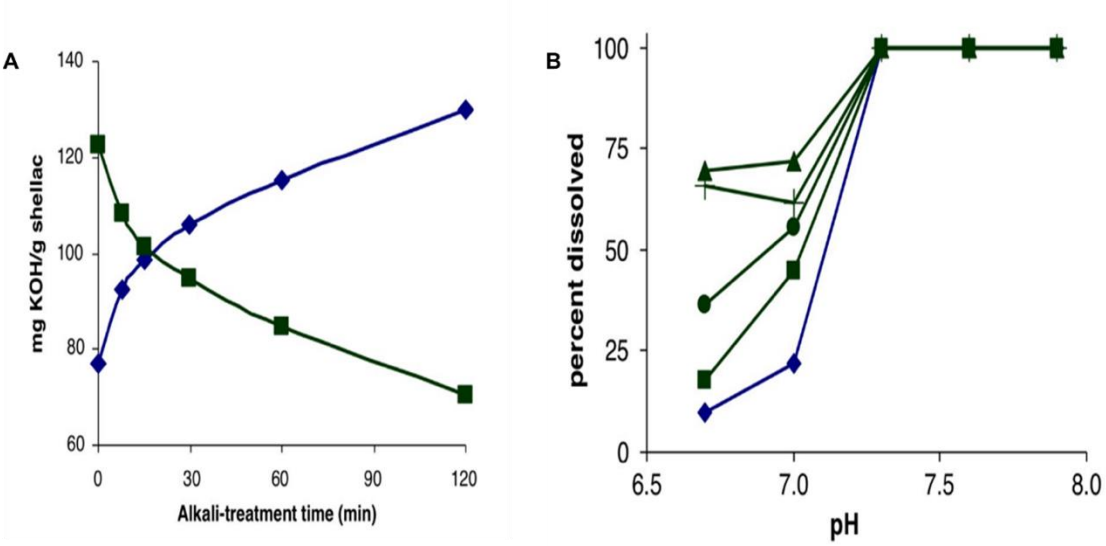

Fig. 2.20 (A): Effect of alkali-treatment time on acid value and ester value of Shellac. (blue) Acid value; (black) ester value and (B): pH-solubility profiles of native shellac and hydrolyzed Shellac after alkali treatment for different times. (diamond) Native shellac; (square) 15-min hydrolyzed shellac; (circle) 30-min hydrolyzed shellac; (cross) 60-min hydrolyzed shellac; (triangle up) 120-min hydrolyzed shellac (Limmatvapirat *et al.*, 2004).

2.7.3.3 Enteric coating and delivery

Shellac consists of 70-82% of fatty esters, 8-14% of free fatty alcohols, 1-4% of acids and 1-6% of hydrocarbons (Yılmaz, *et al.*, 2020). Shellac is structurally composed of esters and polyesters of polyhydroxy and polycarboxylic acids. The carboxylic acid is composed of four different acids, aleuritic (35%), jalaric (25%), shellolic (8%), and butolic (8%); they are connected by ester linkages into a hard resin by chemical degradation (Muhammad *et al*., 2020).

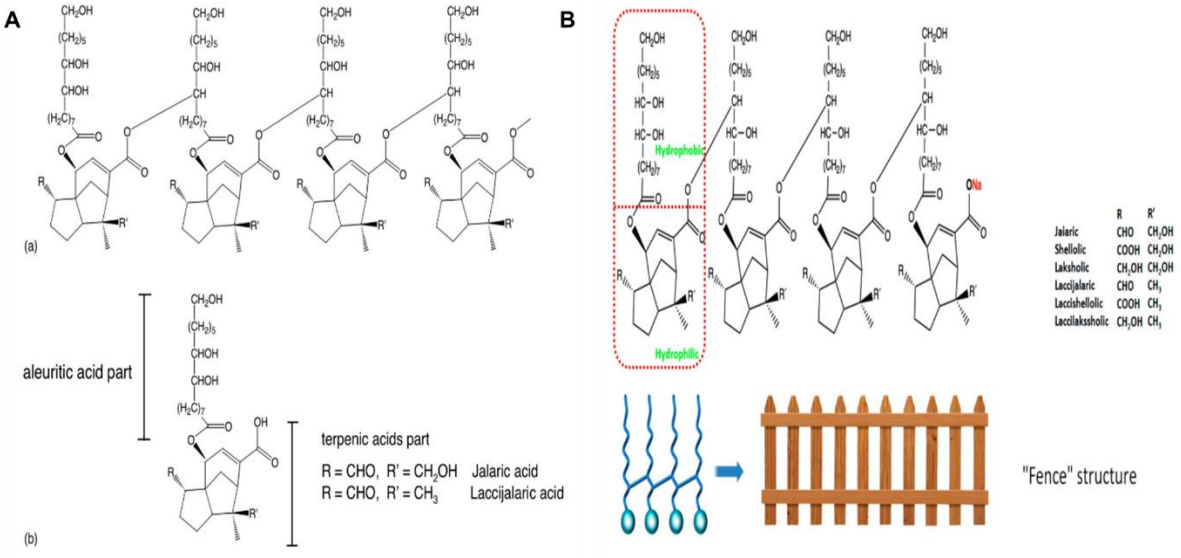

Fig. 2.21 A) Chemical structure of shellac. Polyesters (a) and single esters (b) (Limmatvapirat *et al*., 2004) and B) the generalized molecular structure of shellac (Gao *et al.*, 2018).

These acidic functional groups are essential to prepare enteric coatings because the acidic groups are protonated to make shellac insoluble in the stomach environment. Carboxylic acids are also deprotonated to carboxylate moieties, causing shellac to dissolve in the

intestine. An example of a carrier product in an enteric coating is probiotics, which are healthy bacteria widely claimed to be beneficial to humans. When probiotics are consumed, most of their activity is lost in the stomach, which is acidic with a pH of less than 3. The pH of the digestive tract changes from acidic, neutral to slightly alkaline as the probiotics reach the intestine, encountering various digestive enzymes. Probiotics are also affected by digestive enzymes and bile acids, which results in a reduced survival rate (Teoh *et al*., 2011). However, when shellac-based enteric-coated probiotics prepared by hot-melt extrusion process maintained the safe passage through the stomach, the coating will begin to degrade in the intestine. Enteric shellac capsules showed less than 5% degradation when kept for 24 h at pH 1.2 and 6.8, and complete degradation was observed only after 10-11 h in an environment of pH 7.4 (Gately & Kennedy, 2017). The released probiotics adsorb and grow in the intestinal mucosa. The adhesion of probiotics to the intestinal mucosa can play a protective role against intestinal pathogens through competition for host cell-binding sites, while probiotic adhesion increases the chances of interacting with the host, resulting in temporary colonization; thus, it can increase the time for probiotics to exert beneficial effects in the gut (Monteagudo-Mera *et al.*, 2019).

Recently, various experiments have been conducted to develop long-lasting enteric coating materials for active ingredient delivery to the mucous membranes by combining shellac with various sustainable material compositions (e.g., cellulose nanocrystals and alginate). Tang *et al.* (2019) prepared a drug encapsulated bilayer film using shellac, esterified cellulose

nanocrystals, and polyethylene glycol (PEG) as a plasticizer buccal drug delivery since solely shellac film are breakable. To examine mucoadhesive properties of the bilayer films, porcine buccal mucosal tissue from a pig was used for *in vitro* evaluation of mucosal adhesions. The prepared film was measured by mucoadhesion using a Texture Analyzer. The mucosal tissue was fixed and wetted with simulated saliva (SSF), and the film was contacted with the mucosa with force applied for 300 seconds. Then the probe was removed from the mucous membrane at a rate of 1 mm/s. As a result, the mixture of shellac and ECNC increased the swelling properties, mechanical strength, mucoadhesive properties and high drug release compared to shellac film. This is because ECNC, shellac and PEG possess many hydrogen bonding groups, such as carboxyl and hydroxyl groups, forming strong network structures and increasing adhesion strength to biological mucosa (Tang *et al*., 2019).

2.8 Encapsulation system

The encapsulation system refers to the whole process of wrapping one material with another coating material, and the size of the manufactured particles ranges from a few nanometers (nm) to a few millimetres (mm). This system provides space to encapsulate desired materials and protect the encapsulated materials from environmental conditions, such as pH or UV radiation. Encapsulation can be functionalized to mask unpleasant flavours/odours, impart stimuli-responsiveness, control targeted release, sustained and burst release (Fig. 2.22). The encapsulation of probiotics, vitamin C, insulin and other active ingredients have been used in daily life (Iravani *et al.*, 2015).

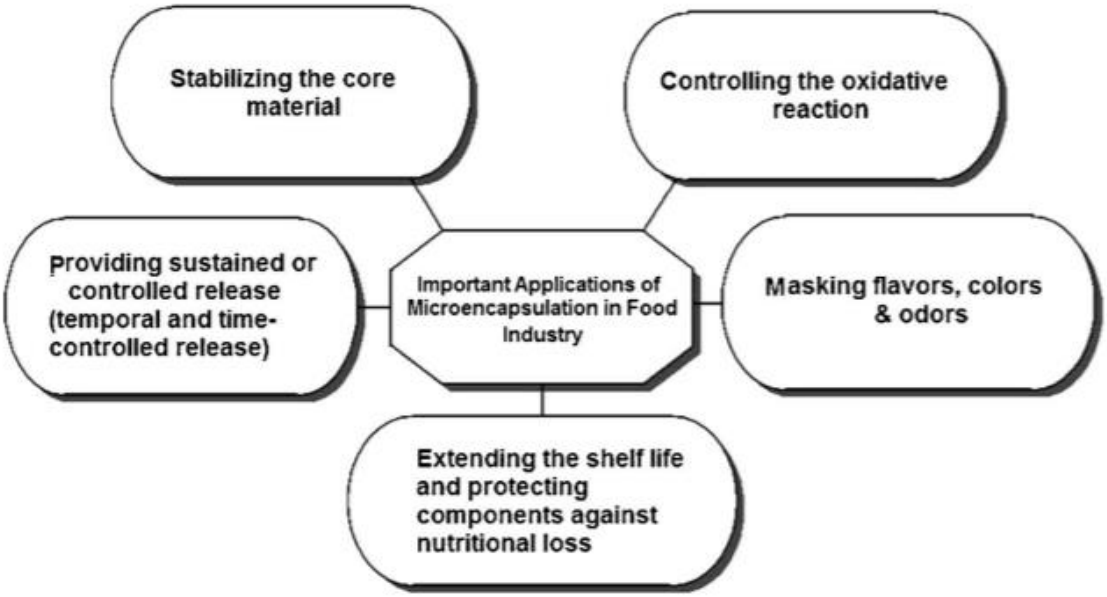

Fig. 2.22 Important applications of microencapsulation in the food industry (Iravani *et al.*, 2015).

2.8.1 Encapsulation of Vitamin C (L-Ascorbic acid)

Vitamin C, commonly referred to as L-ascorbic acid or water-soluble vitamin, is added to food as a functional food supplement. Consumption of Vitamin C is necessary for human health since humans cannot synthesize Vitamin C in their body due to the lack of gluconolactone oxidase (Uluata *et al.*, 2015). It is reported that regular intake of Vitamin C can reduce the risk of cancer, kidney, scurvy (Nemet & Monnier, 2011) and heart disease. In addition, it is a nutrient essential for collagen synthesis to manufacture healthy blood vessels, various organs, and muscles, thereby enhancing the immune system. It has strong antioxidant activity with a strong reducing action to eradicate harmful free radicals and active oxygen in

the body. However, excessive intake of Vitamin C can lead to urinary stones, diarrhea, and gastric convulsions. However, Vitamin C is unstable and will easily decompose upon exposure to air, oxygen, heat, and light. Although Vitamin C is readily soluble in an aqueous solution, much of the Vitamin C is not stable, resulting in degradation due to rapid oxidation. The oxidation process of Vitamin C is described in Fig. 2.23. Vitamin C plays a role in maintaining the redox process. L-ascorbic acid (reduced form) is oxidized to dehydro-L-ascorbic acid (oxidized form) without any Vitamin C function loss. Dehydro-L-ascorbic acid comprises 60 to 80% (HeK, 1982) of L-ascorbic acid is oxidized to 2,3-diketo-L-gulonic acid (Shanmugam *et al.*, 2010). The conversion of L-ascorbic acid to dehydro-L-ascorbic acid is reversible. However, the oxidation of dehydro-L-ascorbic acid to 2,3-diketo-L-gulonic acid is irreversible. When Vitamin C is oxidized to 2,3-diketogluconic acid (DKG), its activity is lost. Nyman *et al.* (2008) reported that when Vitamin C and sodium benzoate (benzoate salt) (a preservative added to foods to minimize decay and deterioration) are present together in a beverage, Vitamin C is oxidized by a metal catalyst, such as copper (Ushikubo & Cunha) and iron (Fe) present in the product to reduce oxygen (O_2) to form superoxide anion radical ($O_2^{-\cdot}$), generating hydrogen peroxide (H_2O_2). Also, sodium benzoate produces benzene by hydroxyl radicals formed from hydrogen peroxide and oxygen (Verbeyst *et al.*, 2013).

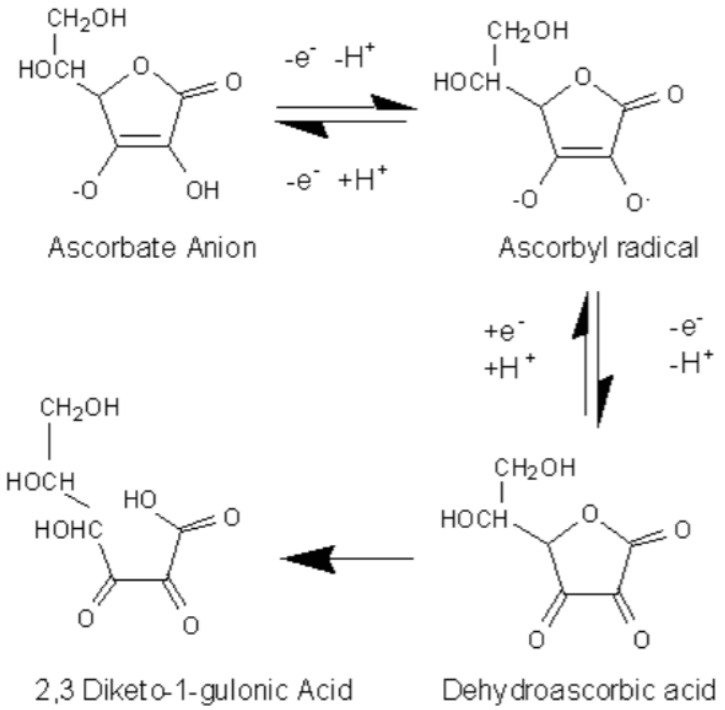

Fig. 2.23 Oxidation of vitamin c (ascorbic acid) via dehydroascorbic acid as intermediate (Shanmugam *et al.*, 2010).

Due to the instability of Vitamin C in food products, only a small proportion of Vitamin C is effective in medicines, foods, and cosmetics. Many studies aim to address the chemical instability of Vitamin C through encapsulation methods, such as spray drying, micro-emulsion, double-emulsion, and liposome, were conducted and reported. Micro or nanoencapsulation is an advanced technology that protects the degradation of sensitive compounds from temperature, humidity, and microorganisms. However, Peng *et al.* (2016) recently explained that these technologies have various challenges, such as organic solvents used in liposomes, synthetic polymers as the shell material, and high temperatures used in

nano-and micro-encapsulation, which are all factors that affect the functionality of the systems (Peng *et al*., 2016). Therefore, a new self-assembled hydrogel system with a three-dimensional and porous network structure was developed using natural biopolymers consisting of bovine serum albumin (BSA) and pectin. Compared to the encapsulation efficiency of Vitamin C within liposomes (48.30%) and chitosan-cyclodextrin nanoparticles (15.70%), BSA-Pectin-Vitamin C hydrogel possessed the highest encapsulation efficiency (65.31%), which are summarized in Fig. 2.24 (a-g) (Peng *et al*., 2016). From the results, BSA hydrogel (a and b) possessed a loose network structure, and BSA-Pectin mixture (c and d) displayed a smooth silk structure at pH 7.0. When the BSA-Pectin mixture was adjusted to a pH of 4.5, a dense structure was observed due to the formation of β-sheet-rich fibrils. Finally, in BSA-Pectin hydrogel (g and h), a solid ordered three-dimensional network structure associated with hydrogen and disulfide bonds was evident when the heat was applied (Fig. 2.24 (e and f); Zhou *et al*., 2014).

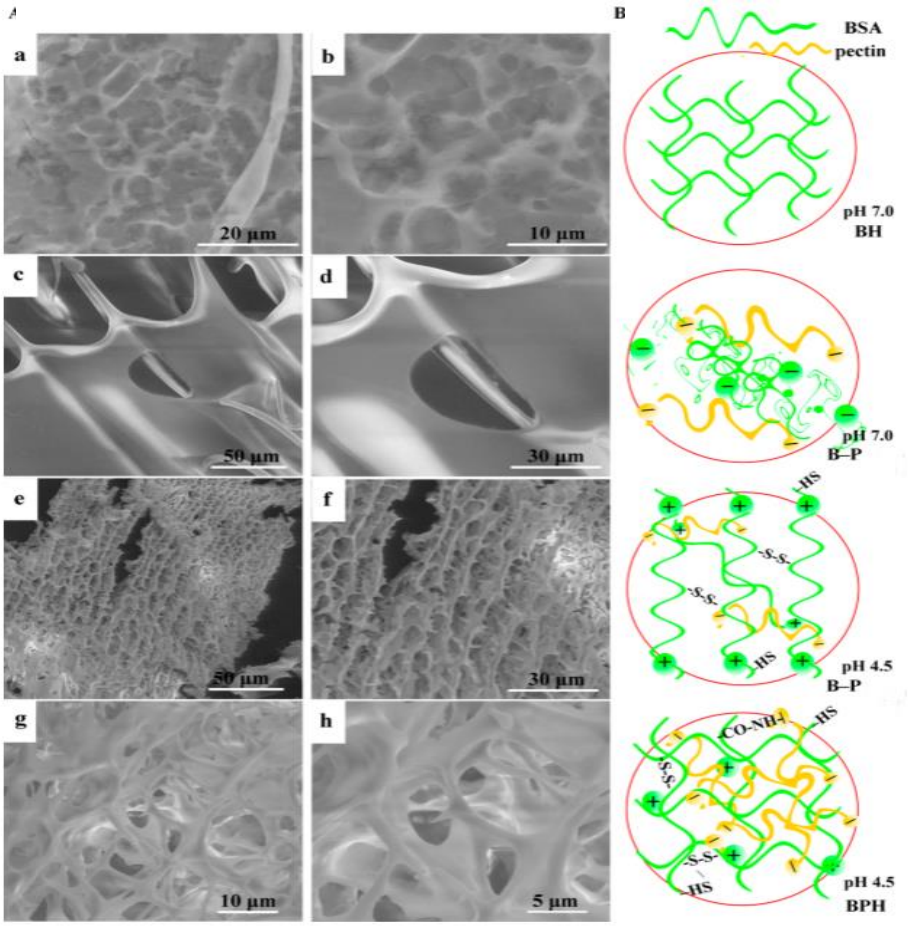

Figure 2.24 SEM images of bovine serum albumin (BSA) hydrogel (a,b), BSA−pectin (B-P) mixture at pH 7.0 (c,d), B-P mixture at pH 4.5 (e,f), and BPH (BSA−Pectin hydrogel) at pH 4.5 (g,h)-thermal treatment (Peng *et al*., 2016).

However, it seemed that there were restrictions on the application due to changes in the structure associated with pH and heat. Chitosan is widely used as a coating agent that increases the stability and absorption rate and controls the release rate. Recently, many ionic gelation methods formed capsules in a short time through a rapid crosslinking reaction

between polyvalent cationic chitosan and a crosslinking agent with a counter ion, TPP. Chitosan oligosaccharides (CSos) were grafted onto CNC through a peptidic coupling reaction and used to encapsulate Vitamin C using TPP for vitamin C delivery. Low molecular weight chitosan is known to have better water solubility and higher antioxidant properties, thereby preventing the oxidation of vitamin C. The encapsulation efficiency (EE%) and drug loading (DL%) of vitamin C were higher (E: 91.0 ± 1.0% and D: 28.6±2.7%) at pH 5 compared to pH 3 (E: 71.6% ± 6.8% and D: 38.4±2.5%) because, at pH 5 (above *pKa* 4.2), VC is deprotonated, possessing negative charge that strongly bound to positively charged CNC-CSos that encapsulated the vitamin C within the complex. In addition, *in vitro* release of vitamin C showed a sustained release of up to 3 weeks in the CNC-CSos complex. Using the DPPH method, CNC-CSOS showed higher antioxidant rate constants compared to physical mixtures that exhibited synergistic activity. The incorporated vitamin C in the CNC-nano-complex could be used for topical cosmetic applications (Akhlaghi *et al.*, 2015). In another vitamin C encapsulation study, VC and folic acid (FA) loaded liposomes (VCFA-Lip), and chitosan-coated liposomes (CS-VCFA-Lip) were prepared to improve their stability. Technically, positively charged chitosan can interact with negatively charged liposomes due to electrostatic interactions. It has also been reported that chitosan affects the stability of loaded drugs, reducing the leakage of encapsulated drugs. Initially, VCFA-Lip was prepared with soybean phosphatidylcholine (PC), cholesterol (CHOL), Tween 80, VC and FA and dissolved in ethanol. After that, the solution was injected into the phosphate buffer, and ethanol was removed. For both drugs, the encapsulation efficiency (EE%) of CS-

VCFA-Lip coated with chitosan was much higher than VCFA-Lip. The reason is that, as chitosan is coated on the surface of the liposome, and it could improve the EE (%) by filling the gap of the hydrophobic bilayer via hydrogen bonding and electrostatic interaction. In addition, the antioxidant activity of CS-VCFA-Lip was higher than VCFA-Lip, because chitosan has antioxidant power and maintains the initial antioxidant activity of VCFA-Lip in the system (Jiao *et al*., 2018). Therefore, it was confirmed that CS-VCFA-Lip could be used as a variety of functional food materials, such as the food and cosmetics industry, as a high antioxidant effect and functional material carrier (Jiao *et al*., 2018). Similar to the above study, Liu *et al.* (2017) described the layer-by-layer (LbL) electrostatic deposition technology, highlighting the disadvantages of the conventional liposomes; easily oxidizing, long-term instability, and double-layer damage due to hydrolysis of phospholipid membranes. This is an effective strategy for stabilizing liposomes by coating a polymer on the surface and states that it can better resist environmental stresses than non-coated nanoliposomes. The multilayered liposomes were prepared with sodium alginate, chitosan, and nanoliposome (AL-CH-NLs), including vitamin C. At day 1, the particle size of fresh NL and multilayered liposomes were about 58 nm and 297 nm, respectively, and this increment of thickness is due to the binding of the polymers to the NL via electrostatic interactions. After 90 days, the particle size of multilayered vitamin C nanoliposomes gradually increased to about 2578 nm. The possible reasons are due to the AL and CH layers dissociated from the surface and formed networks between polymers through polymer bridging (Fig. 2.25). However, the degree of oxidation and vitamin C release from multilayer liposomes was lower than the

conventional NL, which means that multilayer shellac minimized lipid oxidation and initial burst release.

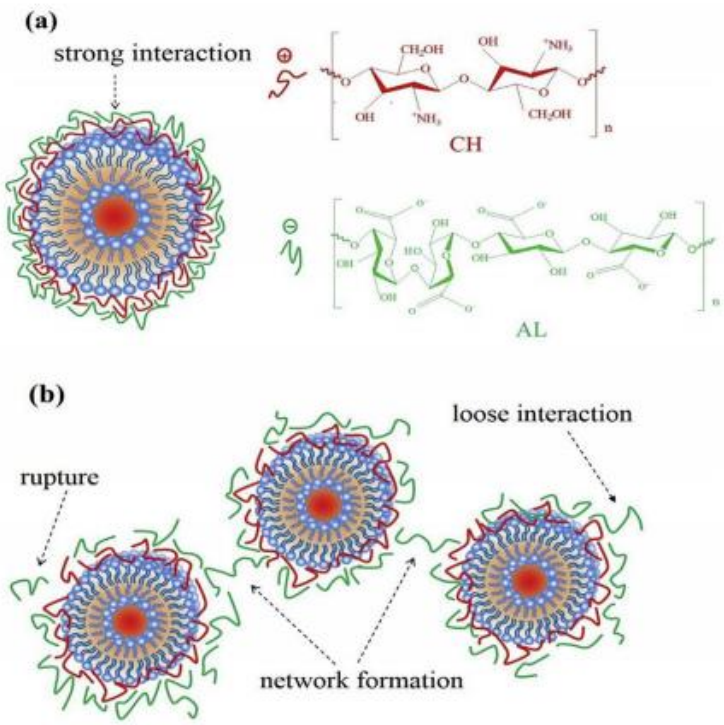

Fig. 2.25 Schematic representation of the structural changes of AL-CH-NLs during storage at 4 C. (a) Fresh AL-CH-NLs prepared by chitosan (CH) and sodium alginate (AL) decorating on NLs (day 1) and (b) Loose interaction, rupture and new network formation in AL-CH-NLs after storage for 90 days (Liu *et al.*, 2017).

2.8.2 Encapsulation of probiotics

Probiotics come from the Greek word "for life," and the World Health Organization (WHO) defines probiotics as "live microorganisms (bacteria or yeasts) which when administered in adequate amounts confer a health benefit to the host." (FAO/WHO, 2001). Probiotics

effectively inhibit harmful bacteria by secreting antibacterial bacteriocin, lactic acid, organic acid, blood cholesterol, intestinal settlement of harmful bacteria, and enhancing immune activity and anti-cancer effects. However, probiotics must survive by withstanding the gastric acid secreted from the stomach, bile from the gallbladder, and various digestive enzymes from the small intestine. A relatively large amount is recommended to have a beneficial health effect of probiotics, typically 10^6-10^7 CFU/g per day. However, adding probiotic cells directly to foods resulting in a significant reduction in cell viability during storage and passage through the intestinal tract. Therefore, during storage and digestion, these probiotics may have reduced viability below the recommended levels to achieve health benefits. Thus, probiotics must be encapsulated with another protective material, where encapsulation protects probiotic cells from external environmental factors and promotes bacterial viability during processing, storage and digestion. Moreover, encapsulation may also improve probiotic efficiency by controlling the release of probiotics at the right site of action in the intestine.

Among the various encapsulation processes (e.g. spray drying, emulsion, extrusion, adhesion to starch) (Rokka & Rantamäki, 2010), extrusion and emulsification methods are known to have excellent survival rates of 85-90% of probiotics in gastric acid and bile conditions compared to other methods (Krasaekoopt *et al.*, 2003) (Fig. 2.26). Both techniques avoid high-temperature processes during processing. By doing so, a high survival rate of probiotics is achieved. In the extrusion method, hydrocolloid materials are mainly used, such as

alginate, carrageenan, gelatin, and chitosan, as a coating material. Simply, the hydrocolloid solution is mixed with probiotics and passes through a syringe (lab scale) or extruder (pilot scale), drop it into a gelling solution containing a multivalent cation (e.g., $CaCl_2$) to prepare a hard capsule. This method is a simple and low-cost and high retention of cells. However, it has been pointed out that the size of the capsule is limited by the diameter of the nozzle, and it is challenging to scale up the process.

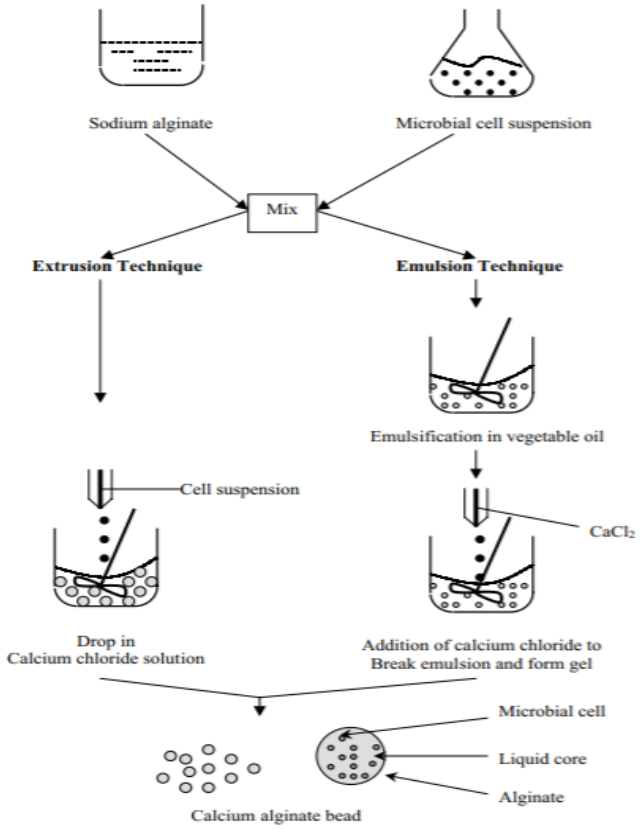

Fig. 2.26 Flow diagram of encapsulation of bacteria by the extrusion and emulsion technique (Krasaekoopt *et al.*, 2003).

In terms of emulsification technique, a hydrocolloid solution containing probiotics is mixed with a continuous phase, such as oils (e.g., vegetable, soybean, sunflower, canola or corn oil) containing emulsifier like Tween 80 to increase the stability of emulsion using a high-speed homogenizer to form a W/O emulsion. Once the gelling solution is added under slow stirring, hardened microcapsules are formed and are recovered via centrifugation (Rokka & Rantamäki, 2010).

Usually, polysaccharides such as alginate, starch, gum Arabic, gellan, xanthan, and whey protein are commonly used in microencapsulation of probiotics due to their biocompatibility and non-toxicity. However, Zanjani *et al*. (2014) reported that although sodium alginate is suitable for encapsulation, the gel possessed porosity and showed sensitivity to extreme pH, which could compromise the protection of the probiotics. Thus, multilayer coating via electrostatic interactions was introduced to improve the stability of microorganisms (Zanjani *et al*., 2014), and some examples of the encapsulating materials are summarized in Table 2.2

Table 2.2 Some examples of emulsion and extrusion techniques applied in microencapsulation studies. Survival under gastrointestinal is higher than 10^6cfu/mL.

	Encapsulating materials	Probiotic microorganisms	Reference
Emulsion techniques	κ-Carrageenan/locust bean gum	*Bifidobacterium longum*	(Maitrot *et al.*, 1997)
	2 % alginate, 5 % glycerol, 0.26 % xanthan gum +0.8 % chitosan	*Lactobacillus bulgaricus KFRI 673*	(Lee *et al*., 2004)
	1 % Alginate, glycerol + preservatives in micro porous glass (MGP) membrane	*Lactobacillus casei YIT 9018*	(Song *et al*., 2003)
	- 2 % alginate +2 % corn starch - 1 % Xanthan +0.5 % gellan	*Lactobacillus reuteri*	(Muthukumarasamy *et al*., 2006)
	32 % Oil, 20 % caseinate, 20 % fructo-oligosaccharides, 20 % glucose syrup or starch (MicroMAX)	*Bifidobacterium infantis*	(Crittenden *et al.*, 2006)
	Alginate/starch	*Bifidobacterium infantis*	(Sultana *et al*., 2000)
	13 % gelatin, 1.25 mM genipin +1 % alginate	*Bifidobacterium adolescentis 15703 T*	(Annan *et al*., 2008)
	4 % sodium alginate +2 % starch	*Lactobacillus acidophilus LA1*	(Sabikhi *et al*., 2010)
	1 % gum Arabic, gellan gum or mesquite seed gum	*Lactobacillus sp.*	(Yáñez-Fernández *et al*., 2008)
Extrusion Techniques	1.5 % alginate +0.1 % poly-L-lysine & 0.1 % alginate	*Bifidobacterium longum*	(Martoni *et al.*, 2008)
	2–4 % sodium alginate	*Bifidobacterium longum KCTC 3128* *Bifidobacterium longum HLC 3742*	(Lee and Heo, 2000)
	2 % Alginate, 1 % gellan, 0.86 % peptides, 0.2 % fructo-oligosaccharides	*Bifidobacterium bifidum*	(Chen *et al*., 2007)
	Gellan/xanthan	*Bifidobacterium infantis*	(Sun and Griffiths, 2000)
	Alginate/starch	*Bifidobacterium lactis*	(Talwalkar and Kailasapathy, 2003)
	- 2 % alginate +0.05 % poly-L-lysine	*Lactobacillus acidophilus 547 Lactobacillus casei 01*	(Krasaekoopt *et al*., 2004)

Interestingly, recent studies have shown that shellac can be a promising coating material for the encapsulation of nutrients and probiotics due to its stability in simulated gastric conditions and its non-toxicity (Farag & Leopold, 2011). However, similar to alginate, there are issues with the use of shellac, such as the formation of a porous membrane that limits its application in the conventional enteric-coated system. To improve the properties of shellac coatings, the incorporation of plasticizers or polymers can be considered. Stummer *et al*. (2010) showed that incorporating these plasticizers and water-soluble polymers improved the release profile in the simulated intestinal environment while maintaining its stability in the gastric environment. They further reported the improvement of the enteric properties of shellac and developed probiotic formulations with plasticizers, such as glycerol and water-soluble polymers, such as sodium alginate (Stummer *et al*., 2010). The bacterial microorganisms used in this study were *Bifidobacteria, Lactobacilli and Enterococci*. They found out that coatings containing shellac and plasticizer showed excellent resistance to the simulated stomach environment in the gastric phase. Coatings of shellac containing 5% glycerol or 5% sodium alginate or up to 20% (w/w) polyvinylpyrrolidone showed the greatest release of microorganisms in the simulated intestinal environment. Schell and Beerman (2014) investigated a probiotic encapsulation of *Lactobacillus reuteri*, with sweet whey, which is a waste product from cheese and a shellac coating. This study aimed to enhance bacteria survival by improving the resistance against gastric pH conditions. This encapsulation technique involved a two-step fluidized bed granulation process. A sweet whey encapsulation containing *Lactobacillus reuteri* was granulated and fluidized into a slurry, then sprayed onto

the powder for granulation, followed by a spray coating aqueous shellac. Compared to the unencapsulated bacteria control, major findings showed that encapsulation of *Lactobacillus reuteri* through a two-step fluidized bed granulation process improved the resistance to acidic pH (Schell & Beermann, 2014).

We found that functional foods provide the necessary human nutrients with specific healthy ingredients through the literature review. Also, they prevent nutrition-related diseases and increase the physical health of consumers. The sustainable material, CNC, showed attractive physicochemical properties via acid hydrolysis with various acids that impart various types of functional groups to the CNCs. Depending on the applications, they could be used as emulsifiers and preservatives. However, synthetic additives in food are still common because of the cost and stability, even though synthetic emulsifiers are known to promote colon cancer and gut inflammation. Recently, consumers desire clean labels or natural-based preservatives instead of synthetic ones. Thus strong scientific evidence to support functional materials in food application must be found. My Ph.D. study seeks to develop, design and understand simple processes based on natural resources instead of synthetic materials. By applying 3 concepts (microencapsulation system + Pickering emulsification method + sustained nanomaterials) via different approaches, we could achieve our goal to encapsulate the bioactive substances that possess the desired functionalities, such as antioxidants and antibacterial property. The following chapters will address each of the objectives of the functionalized sustainable nanomaterials.

Chapter 3

Phosphorylated-CNC/Modified-Chitosan Nanocomplexes for the Stabilization of Pickering Emulsion

The material in this chapter was published in Baek, J., Wahid-Pedro, F., Kim, K., Kim, K., & Tam, K. C. (2019). Phosphorylated-CNC/modified-chitosan nanocomplexes for the stabilization of Pickering emulsions. Carbohydrate polymers, 206, 520-527.

3.1 Introduction

As environmental and health concerns become more acute, the demand for products formulated with environmentally friendly and biocompatible substances has increased (Park *et al*., 2004). In cosmetics, health care, and food applications, the use of biopolymers that are not associated with synthetically derived ingredients has attracted increasing attention, and it will become increasingly relevant due to the enormous benefits of formulating food systems with naturally derived ingredients. Among the category of natural polymers, cellulose accounts for the largest proportion of organic matter on earth (Habibi, Lucia, & Rojas, 2010; Grishkewich *et al*., 2017). Since cellulose is a material derived from wood, cotton, recycled paper, sugarcane bagasse, wheat straw, bamboo, and living organisms (Ashori, 2006; Dagnon *et al*., 2013; Credou & Berthelot, 2014), it is renewable and is a natural carbon sink. Nano-sized cellulosic materials, such as cellulose nanocrystals (CNC), possess several advantages due to their nano size. Thus they can be used as reinforcing agents in nanocomposites,

polymeric emulsifier in oil-water emulsion and other applications that enhance the properties and performance over conventional systems.

Various strong acids have been used to produce cellulose nanocrystals, with sulfuric acid being the most common. The reason being that CNC produced from sulfuric acid possesses negative charges, and they are stable and readily dispersible in water (Bondeson*et al*., 2006; Abitbol *et al*., 2013). However, in food applications, CNC prepared with sulfuric acid hydrolysis (S-CNC) may not be suitable for human consumption as reported by Deshpande (2002), where hydrochloric or sulfuric acid is rarely used as an acidulating substance in foods. Therefore, it is desirable to perform hydrolysis of cellulose fibers using a weak acid, such as phosphoric acid, which is not harmful and can be used in food processing. Surprisingly, there are not many studies on phosphoric acid hydrolyzed CNC (PCNC), and only a few groups have reported on the phosphorylation of cellulose to enhance their thermal stability and biocompatibility. A recent report on PCNC extracted from cotton possessed a surface charge density of 44 ± 2 mmol/kg (Vanderfleet *et al*., 2018). Higher phosphate contents were achieved for hydrolysis in water and molten urea, where the phosphate content values were found to be 435.21 ± 7.2 and 1038 ± 9.9 mmol/kg, respectively (Kokol *et al*., 2015).

Due to the safety concerns in the consumption of synthetic additives in food products, there is an incentive to find naturally derived raw materials and used them in food formulations. One such natural polymer is chitosan, which is the second most abundant natural

polysaccharide. Chitosan is produced by the deacetylation of chitin extracted from shells of crabs and shrimps (Hamed *et al*., 2016; Zou *et al*., 2016), and whose structure is similar to that of cellulose. In neutral and alkaline solutions, chitosan is not soluble due to the deprotonation of the primary amine groups, which limits its application, where neutral and basic conditions are commonly encountered. Therefore, modification of chitosan is necessary to improve its solubility and broadens its potential applications. By introducing quaternary ammonium salts to the chitosan enhances its water solubility and antimicrobial characteristics. (Qin *et al.*, 2004; Yin *et al*., 2017). The glycidyltrimethylammonium chloride (GTMAC)-Chitosan, a water-soluble chitosan derivative of various degrees of substitution, was synthesized by reacting chitosan with GTMAC, a quaternary ammonium compound with a glycidyl group. Generally, epoxy groups readily react with amine groups under neutral or acidic conditions. Therefore, a reaction between GTMAC and amine groups of chitosan can be readily implemented. GTMAC-Chitosan, having a quaternary ammonium group at the C-2 position of chitosan, could be prepared by opening the epoxy group of GTMAC using a catalyst and then reacted with the amine groups of chitosan.

Pickering emulsions are stabilized by adsorbing nanoparticles at the oil-water interface to prevent coalescence of the emulsion droplets. The unique properties of the Pickering emulsions are due to the large interfacial adsorption energies of the particles. The main difference between Pickering emulsions and regular emulsions is that the solid particles irreversibly adsorb at the interface (Fujisawa *et al*., 2017). Hydrophilic particles tend to form

an O/W emulsion, and lipophilic particles tend to form a W/O emulsion due to the contact angle at the oil-water interface of the solid particles. In the case of using a hydrophilic surfactant, the area of the head portion of the surfactant is larger than that of the tail portion, so the orientation of the interfacial membrane is bent toward the oil to form an oil-in-water (O/W) emulsion. Hydrophilic particles have a contact angle, measured at the waterside of the interface, smaller than 90° and a large part of the particle surface is present on the waterside. For example, oil-treated solid particles have contact angles greater than 90°, with a large part of the particle surface being present on the oil side (Rayner *et al.*, 2014).

According to Jonassen *et al*. (2012), most chitosan-TPP nanoparticles were designed to improve the drug delivery of small and large molecular weight drugs, where the effect of chitosan concentration, its molecular weight, the ratio of TPP to chitosan, and ionic strength of the medium was examined. However, Wang *et al.* (2017) postulated that chitosan-TPP encapsulation is metastable, and it is controlled by external conditions, such as pH and ionic strength. In addition, TPP is known to interact with skin and mucous membranes. Therefore, alternative anionic cross-linking agents are being sought to stabilize chitosan-based nanocapsules. Thus, the objective of this study is to develop a PCNC that is eco-friendly and safe for the human body, with the added advantage of functioning as a new cross-linking agent for chitosan. The dynamic morphology of PCNC and GTMAC-Chitosan were elucidated with dynamic light scattering (DLS) and static light scattering (SLS) at different phosphate contents and amounts of GTMAC to develop a new emulsifier for food applications.

3.2 Material and Methods

3.2.1 Materials

Low to medium molecular weight chitosan (M_w = 50 – 190 kDa) and phosphoric acid were purchased from Sigma-Aldrich (St. Louis, MO, U.S.A.). Phosphorylated cellulose nanocrystals were produced from hardwood kraft pulp (Suzano Inc.). Glycidyltrimethylammonium chloride, acetic acid, L-ascorbic acid, sodium chlorite, hydrochloric acid, sodium hydroxide, and rhodamine B were also purchased from Sigma-Aldrich (St. Louis, MO, U.S.A.) and used as received. The extra virgin olive oil was purchased in the local market.

3.2.2 Extraction and preparation of PCNC

The process of producing cellulose nanocrystals was divided into three steps: (1) removal of hemicellulose and lignin via treatment in alkali media, (2) removal of amorphous cellulose domains by acid hydrolysis, and (3) purification of pristine cellulose nanocrystals via ultrafiltration and dialysis.

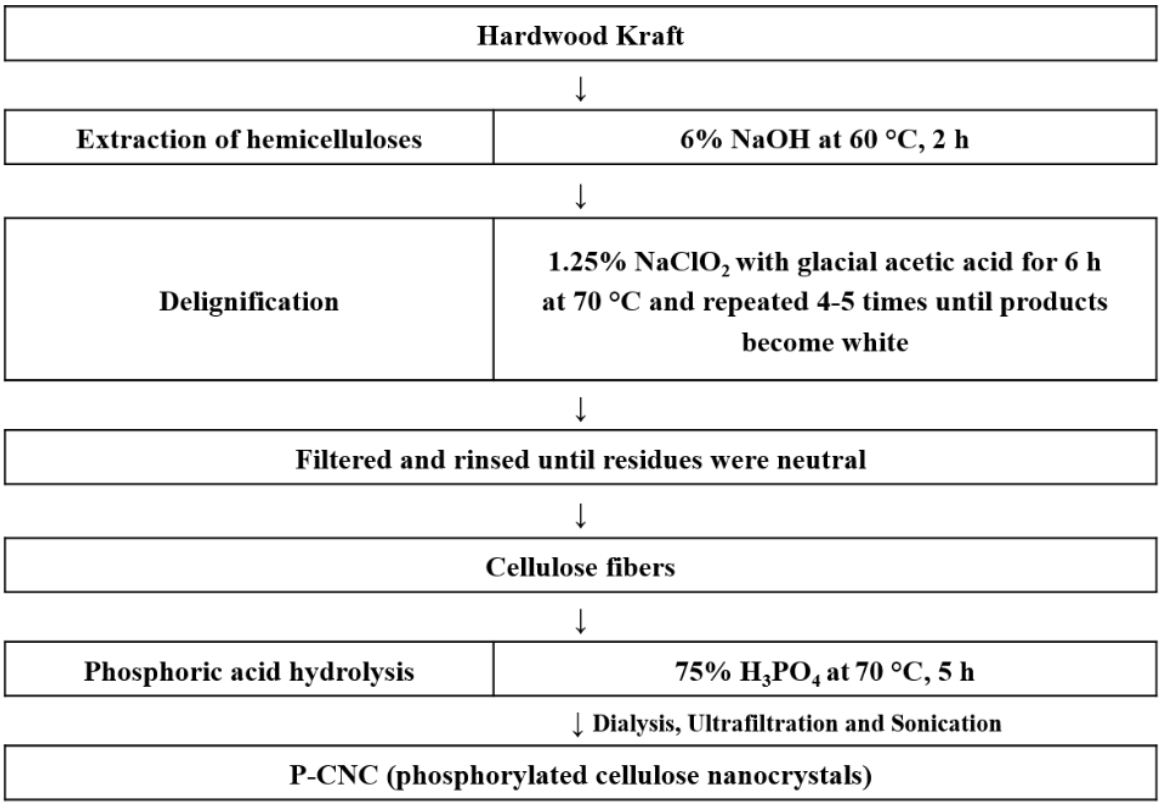

Fig. 3.1 Schematic for the acid hydrolysis process of kraft pulp.

First, cellulose nanocrystals were extracted from hardwood kraft pulp following the procedures described in the TAPPI protocol with slight modification (Zhang *et al.*, 2013; Rosli *et al*., 2013). Briefly, a suspension was prepared by adding 5 g of hardwood kraft pulp

to 300 mL of 6% NaOH solution and placed on a hot plate at 60 °C and 360 rpm for 2 h to dissociate the hemicellulose. It was then filtered via ultrafiltration and placed in a dialysis tube. To remove the lignin structures in pulp, 5 mL of sodium chlorite aqueous solution (1.25 wt%, $NaClO_2$) and 1 mL of acetic acid (CH_3COOH) were added to the filtered sample dispersed in DI water. The pulp suspension was maintained at 70 °C and stirred at 400 rpm for 1 h. The same amount of sodium chlorite and acetic acid was added at intervals of 1 h and repeated five times, followed by washing via ultrafiltration and dialysis. Upon the treatments, lengths of the cellulose fibers were observed by an optical microscope (Nikon Elipse Ti-S, Nikon Instruments Inc., USA) equipped with a CCD camera (QImaging Retiga 2000R). After dialysis, 3 g of the filtered sample was placed in a round-bottom flask, and the solution was treated with 75 wt% phosphoric acids at 70 °C for 5 h. Finally, the reaction was terminated by adding distilled water, and the unreacted chemicals were removed by ultrafiltration and dialysis.

3.2.3 Synthesis of GTMAC-Chitosan

Chitosan (0.1 wt%) was dissolved in 1 wt% acetic acid solution and heated to 50 °C on a hot plate, and GTMAC (0.06 wt%) was added to the chitosan solution and kept stirring for 12 h. The GTMAC-Chitosan (GCh) was washed with acetone (acetone: sample = 3:1) three times to remove unreacted GTMAC. The resulting solution was then filtered to recover the white precipitates of GCh, and they were resuspended in deionized water (2 mg/mL) for further processing.

3.2.4 Preparation of GCh-PCNC nanoparticles

GCh-PCNC nanoparticles were prepared according to a modified procedure of Wang *et al*. (2017) based on the ionic gelation of GCh and PCNC. To ensure uniform distribution and to prevent particle aggregation, both GCh and PCNC solutions were sonicated for 20 min using Misonix Sonicator XL-2000 Series (QSonica LLC., Newtown, CT) prior to mixing. To optimize the particle size and morphology, the concentration of GCh, PCNC, and mass ratio of GCh to PCNC were investigated. GCh-PCNC nanoparticles were prepared by the dropwise addition of PCNC solution (0.4 wt%) into the GCh solution (0.2 wt%). The mixture was sonicated with a Misonix sonicator with an output power of about 16 watts and sonicating frequency of 22.5 kHz in an ice bath for 50 seconds after the addition of one drop of PCNC solution. After the complete addition of PCNC into the GCh solution, the mixture was stirred for 5 min at room temperature to complete the reaction, and the resulting suspension was subjected to further analysis.

3.2.5 Oil in water Pickering emulsion preparation

To uniformly disperse the emulsions, both GCh and PCNC samples were dyed with rhodamine B (0.05 mg/mL), and they were placed separately in a dialysis tube. Samples were collected out and performed ionic gelation to form the nanocomplexes. Finally, olive oil was added to the aqueous phase containing GCh-PCNC nanoparticles in a 3:7 and sonicated for 3 min. The Pickering emulsions were examined by fluorescence microscopy (Nikon Eclipse Ti–S, Nikon Instruments Inc., USA) to identify the dyed nanocomplexes. The prepared

Pickering emulsions were then stored at 25 °C and used for further testing within 3 months.

3.2.6 Characterization of GCh-PCNC nanoparticles

3.2.6.1 Fourier transform infrared (FTIR) spectroscopy

FTIR spectroscopy measurements on the original hardwood pulp, bleached/delignification pulp and PCNC were performed using a Bruker Tensor 27 FTIR spectrometer (Bruker, Billerica, MA, USA). This was done to confirm the reduction of lignin and hemicellulose and the addition of phosphate groups onto the cellulose nanocrystals. The samples were freeze-dried and pressed into potassium bromide (KBr) pellets. Spectra of each sample were recorded as the average of 32 scans at 4 cm^{-1} resolution at 25 °C, using KBr-pellets as blank.

3.2.6.2 Light scattering analysis

The size and morphology of the nanoparticles were determined by light scattering analysis using a Brookhaven BI-200SM instrument apparatus equipped with a He-Ne laser operating at λ= 636 nm (Brookhaven, NY, USA). The samples were first filtered using a 0.8 µm membrane filter to remove any dust and large aggregates in the solution. The size of the nanoparticles was determined using dynamic light scattering (DLS), measured at a temperature of 25 °C and scattering angles ranging from 60° to 150°. The hydrodynamic radii were then calculated from the translation diffusion coefficient based on Stokes-Einstein as shown in Equation (3.1).

$$D = \frac{k_B T}{6\pi\eta r} \quad (3.1)$$

where D is the diffusion constant; k_B is Boltzmann's constant; T is the absolute temperature; η is the dynamic viscosity; r is the radius of the spherical particle.

Static light scattering (SLS) experiments were performed by measuring the average scattered light intensity at angles ranging from 30° to 155°. The same samples used for DLS were investigated after diluting with deionized water by a factor of 10, and the radius of gyration was determined. The particle shape factor that describes the morphology of the nanoparticles was determined according to Equation (3.2):

$$SP = \frac{R_g}{R_h} \quad (3.2)$$

where SP is the shape factor, R_g is the radius of gyration (nm), and R_h is the hydrodynamic radius (nm).

3.2.6.3 Transmission electron microscopy

The size and morphology of the nanoparticles were evaluated using a transmission electron microscope (Philips CM10 electron microscope, acceleration voltage of 60 kV). A droplet of the sample suspension (0.05%) was placed on a carbon-coated copper grid and left for 10 min, after which the excess liquid was removed using a small piece of filter paper and left to dry overnight before TEM analysis.

3.2.6.4 Zeta-potential measurements

A zeta-potential analyzer (Nanosizer ZS, Malvern co., UK) was used to measure the surface

charge of the PCNC and GCh to elucidate their dispersion characteristics. The sample, kept at 25 °C, was diluted with distilled water, and 1 mL was withdrawn and used to fill the measuring cell (folded capillary cell, Malvern).

3.2.6.5 Conductometric titration

PCNC:

150 mg of PCNC was dispersed in 25 mL of water, and 10 mL of 5 mM HCl and the sample was sonicated for 20 min. It was then titrated with 5 mM NaOH, and the number of phosphate groups was determined from Equation (3.3) as shown below (Camarero Espinosa *et al.*, 2013).

$$[HPO_4^{2-}]\left(\frac{\text{mmol}}{\text{kg}}\right) = \frac{C_{NaOH}\left(\frac{\text{mol}}{\text{L}}\right) \times (V_{NaOH,f} - V_{NaOH,i})\ (\text{L})}{W_{CNC}\ (\text{g})} \times 10^6 \quad (3.3)$$

Chitosan:

50 mg of Chitosan was dissolved in the mixture of 45 mL water and 5 mL 0.1M HCl. The sample was sonicated for 20 min and then titrated with 0.1 M NaOH. Equation (3.4) was used to calculate the concentration of amine groups: (Raymond *et al.*, 1993; Dos Santos *et al.*, 2009).

$$[NH_3^+]\left(\frac{\text{mmol}}{\text{kg}}\right) = \frac{C_{NaOH}\left(\frac{\text{mol}}{\text{L}}\right) \times (V_{NaOH,f} - V_{NaOH,i})\ (\text{L})}{W_{Ch}\ (\text{g})} \times 10^6 \quad (3.4)$$

The determination of the degree of deacetylation is by equation (3.5): (Crofton *et al.*, 2016).

$$\%DD = \frac{C_{NaOH}\left(\frac{mol}{L}\right) \times (V_{NaOH,f} - V_{NaOH,i})(L) \times 161.16 \frac{g}{mol}}{W_{Ch}\,(g)} \times 100 \quad (3.5)$$

GTMAC-Chitosan:

20 mg of GTMAC-Chitosan was dispersed in 50 mL of water and sonicated for 20 min. The sample was titrated with 0.01 M $AgNO_3$ solution, and the degree of quaternization of chitosan (DQ) is described by Equation (3.6) (Li *et al.*, 2004).

$$DQ = \frac{C \times V}{CV + \left[\frac{W - C \times V \times M_2}{M_1}\right]} \quad (3.6)$$

Where C is the concentration of $AgNO_3$ (mol/L), V is the volume of $AgNO_3$ (L), W is the weight of GTMAC-Chitosan (g), M_1 is the molecular weight of chitosan (161 g/mol), and M_2 is the molecular weight of GTMAC-Chitosan (314 g/mol).

3.3 Results and discussion

3.3.1 Bleaching and delignification of hardwood pulp

In the preliminary experiments, we observed that the pulp slurry turned from white to dark brown to black colour during the acid hydrolysis (data not shown). This colour change indicated the occurrence of chemical reactions, such as oxidation of hemicellulose, lignin and other extractive compounds. The appearance of the brown colour in the solution was caused by chromophores comprising of benzene rings, carbon-carbon double bonds, carbon-oxygen double bond quinones, and free radicals (Falkehag *et al.*, 1966; Cheng *et al.*, 2017). Three chromophores (ortho-quinone, coniferyl aldehyde and α-carbonyl) comprise the bulk

of the chromophore mixtures (Sun & Hou, 2018). The colour-causing chromophores can be removed by adding bleaching agents, such as hydrogen peroxide and sodium chlorite. After pre-bleaching, whiteness, crystallinity, flame retardant, and mechanical strength will be improved (Shahzad, 2012). Sodium chlorite, which is not dangerous and the low ash contents generated under acidic conditions, does not attack cellulose like a normal bleaching agent. Moreover, the alkali pre-treatment using sodium hydroxide (Fig. 3.1) can remove and degrade lignin and hemicellulose. Therefore, CNCs were extracted by chemical methods via alkali and bleaching treatments followed by acid hydrolysis. The hardwood fibers were treated with 6% NaOH to remove the hemicellulose. Upon the addition of sodium chlorite solution, chlorine dioxide, which is a bleaching agent, is formed according to Equation (3.7).

$$4CH_3COOH + 5NaClO_2 \longrightarrow 4ClO_2 + 2H_2O + 4CH_3COONa + NaCl \quad (3.7)$$

Upon treatment, the lengths of cellulose fibers appeared shorter as determined by optical microscopy as shown in Fig. 3.2.

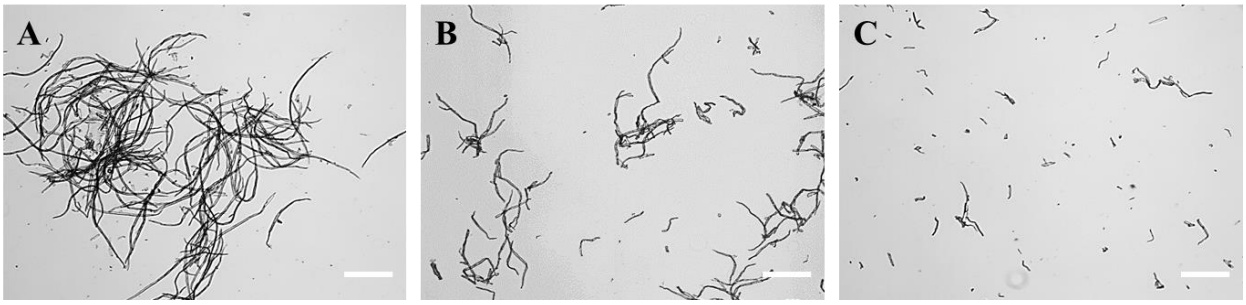

Fig 3.2 Lengths of cellulose fibers upon bleaching and delignification treatment, (A): hardwood pulp fibers, (B): after NaOH treatment, and (C): after $NaClO_2$ treatment (Scale bar: 200 μm).

3.3.2 FTIR spectrum of bleaching pulps

Fig. 3.3 (A and B) shows the changes in structural and functional groups of hemicellulose and lignin before and after alkaline pretreatment, respectively. The interpretation of the chemical bonds corresponding to the peak positions are as follows; the absorption peak at 3400-3300 cm^{-1} was due to the stretching of the OH group; 2900-2800 cm^{-1} is the result of C-H stretching in hemicellulose and cellulose. The peak at 1731 cm^{-1} is attributed to C=O, the acetyl group of hemicellulose present in the wood, and the ester group of the carboxylic group in the p-coumaric acid and ferulic acid of lignin. With the removal of lignin and hemicellulose by NaOH and $NaClO_2$/ CH_3COOH, the content of lignin and hemicellulose in the pulp decreased (Jungnikl *et al*., 2008; Reddy *et al*., 2012; Zhang *et al*., 2013; Mtibe *et al*., 2015; Ilyas *et al*., 2017). The main peaks before and after pretreatment were glucomannan peaks in the wavelength range of 850-870 cm^{-1} and lignin-related peaks in the wavelength range of 1227 cm^{-1} (Ilyas *et al*., 2017) and 1266-1270 cm^{-1}. The suppression of the peak at 1480-1510 cm^{-1}, attributed to the stretching of C-O of the aryl group present in lignin suggested that lignin and lignocellulose were removed. To confirm the esterification of CNC through successful phosphoric acid hydrolysis, the FTIR spectrum of PCNC was obtained (Fig. 3.3C). The phosphate groups were dominantly featured in the PCNC spectrum and showing the presence of the P-OH with peaks found at 1000–1034, 1163–1170 and 1223–1236 cm^{-1}, and a peak at 1164 cm^{-1} attributed to P=O bands (Loutfy *et al*., 2016).

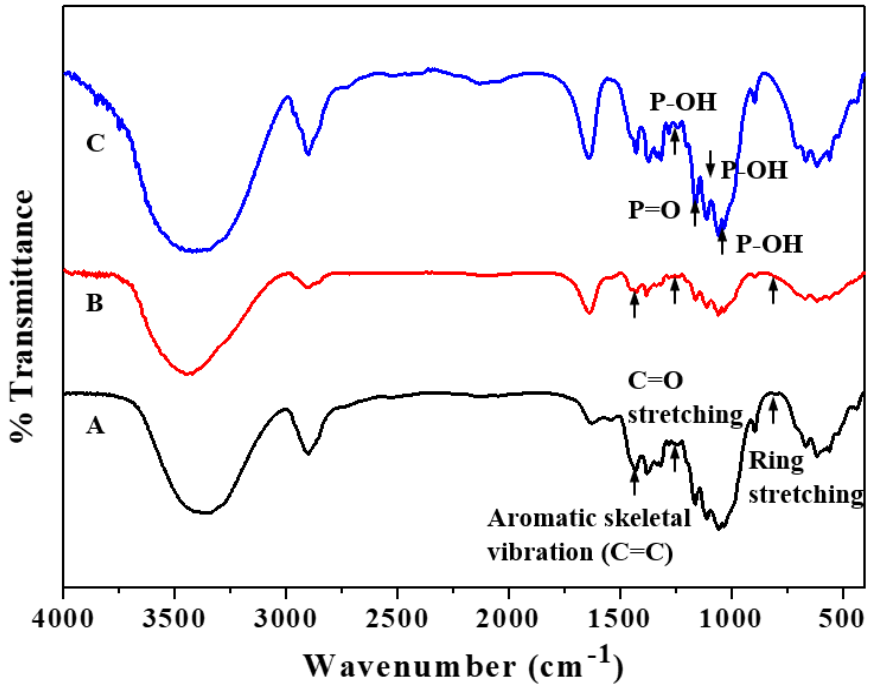

Fig. 3.3 The FTIR spectra of (A): original hardwood pulp, (B): bleached fibers with bleaching and delignification agents, and (C): phosphorylated cellulose nanocrystals.

3.3.3 Preparation and characterization of PCNC

The optimum condition for acid hydrolysis was determined to be 75% phosphoric acid at a temperature of 70 °C. As shown in Fig. 3.4A, under these conditions, the average length of CNC was determined by TEM to be approximately 200 nm. As reaction time and acid/pulp ratio were increased, the average nanocrystal length decreased.

Cellulose is composed of crystalline and amorphous domains. When an acid is added to the cellulose fibers, hydronium ions (H_3O^+) penetrate the amorphous domains where the chains are accessible compared to the denser crystalline regions, and the hydronium ions promote

the hydrolysis of glycosidic bonds (Habibi *et al*., 2010; Chen *et al*., 2017). As a result, the amorphous regions were gradually removed, leaving behind the crystalline domain in the form of CNC. The structure and physical properties of the CNC depend on the species as well as the concentration of the acid, temperature, and reaction time. In high acid concentration and long reaction time, the cellulose decomposes completely into the monosaccharide molecules. On the other hand, when the concentration of the acid is too low, or it is hydrolyzed for a very short time, the amorphous regions are not all completely removed. While hydroxyl groups on the glucose unit of cellulose were substituted by phosphorus-containing groups via an ester bond, PCNC was produced. The concentration of phosphate on the modified CNC was determined by titration, as shown in Fig. 3.4B. HCl was first added to the PCNC suspension to lower the pH, and the phosphorus groups on the PCNC were titrated with NaOH, and phosphorus content of about 200 mmol/kg of cellulose was observed. Comparing PCNC with S-CNC, which contains a sulphate ester group, S-CNC has a zeta potential of about -43 mV, whereas PCNC with the phosphate group has a zeta potential of about -26 mV.

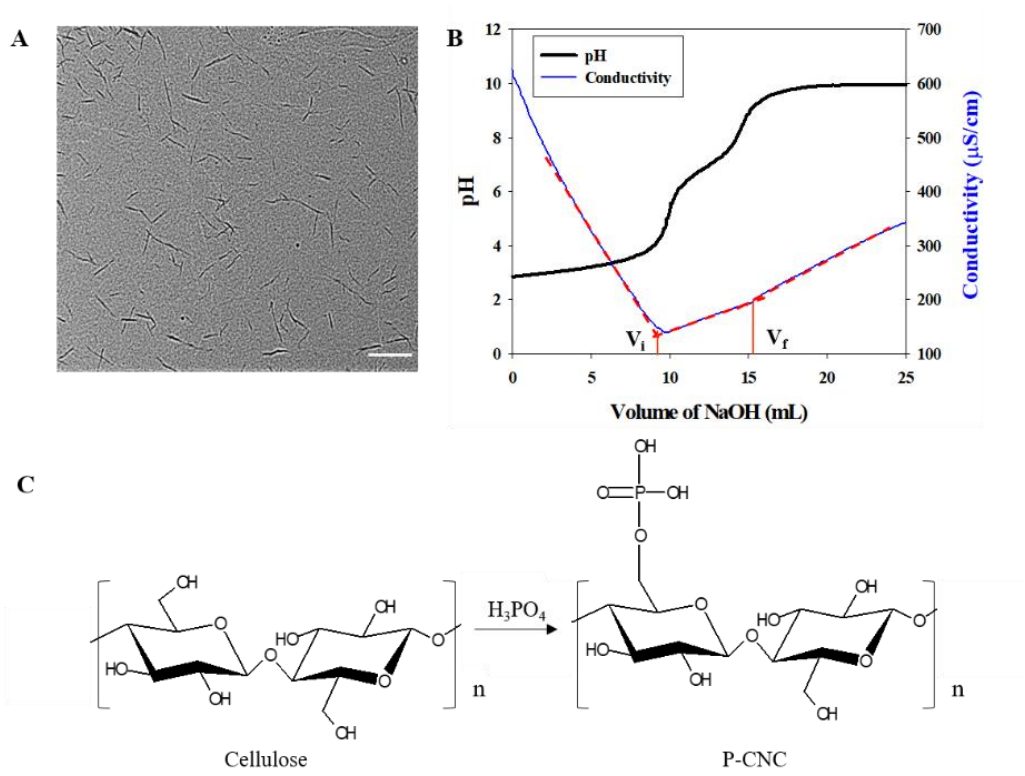

Fig. 3.4 (A): TEM image of PCNC (Scale bar: 500 nm), (B): Conductometric titration curve of PCNC, and (C): the reaction mechanism of cellulose to PCNC.

3.3.4 Quantification of GCh

The proportions of glucosamine and acetyl glucosamine vary depending on the degree of acetylation of chitosan. The degree of acetylation of chitosan used in this experiment was 84%, which is consistent with the range (75-85%) provided by Sigma Aldrich (Fig. 3.5).

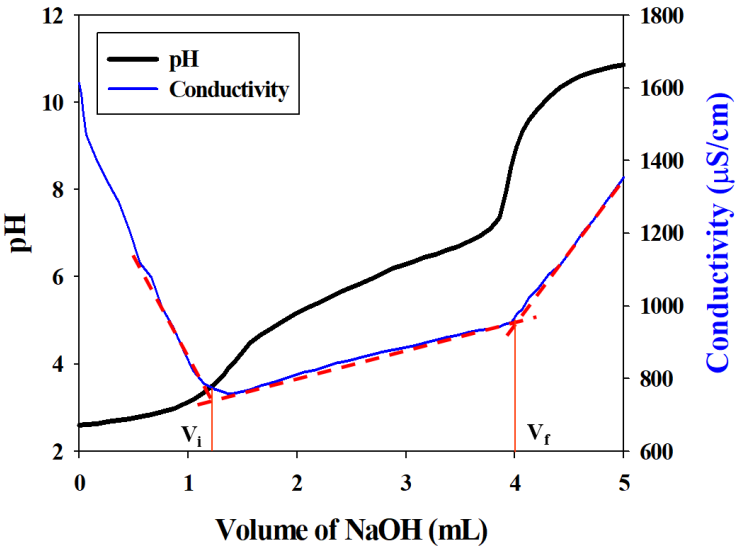

Fig. 3.5 Conductometric titration curve to determine the degree of deacetylation of chitosan.

Zeta-potential of chitosan and GTMAC-Chitosan at different pH values are shown in Fig. 3.6A. Both Chitosan and GTMAC-Chitosan showed similar positive charges at pH between 2-6 due to the protonation of primary amine groups. At pH greater than 6, the zeta-potential of chitosan decreased to the isoelectric point (Siepmann & Siepmann, 2013), and from pH 7.5, it remained slightly negative. On the other hand, the zeta-potential of GTMAC-Chitosan decreased slightly to an asymptotic value of about +15 mV. In basic conditions, chitosan was

not soluble, while GTMAC-Chitosan displayed good solubility at all pH values, as shown in Fig. 3.6B. Thus, highly soluble chitosan could be prepared by grafting GTMAC onto its polymer backbone.

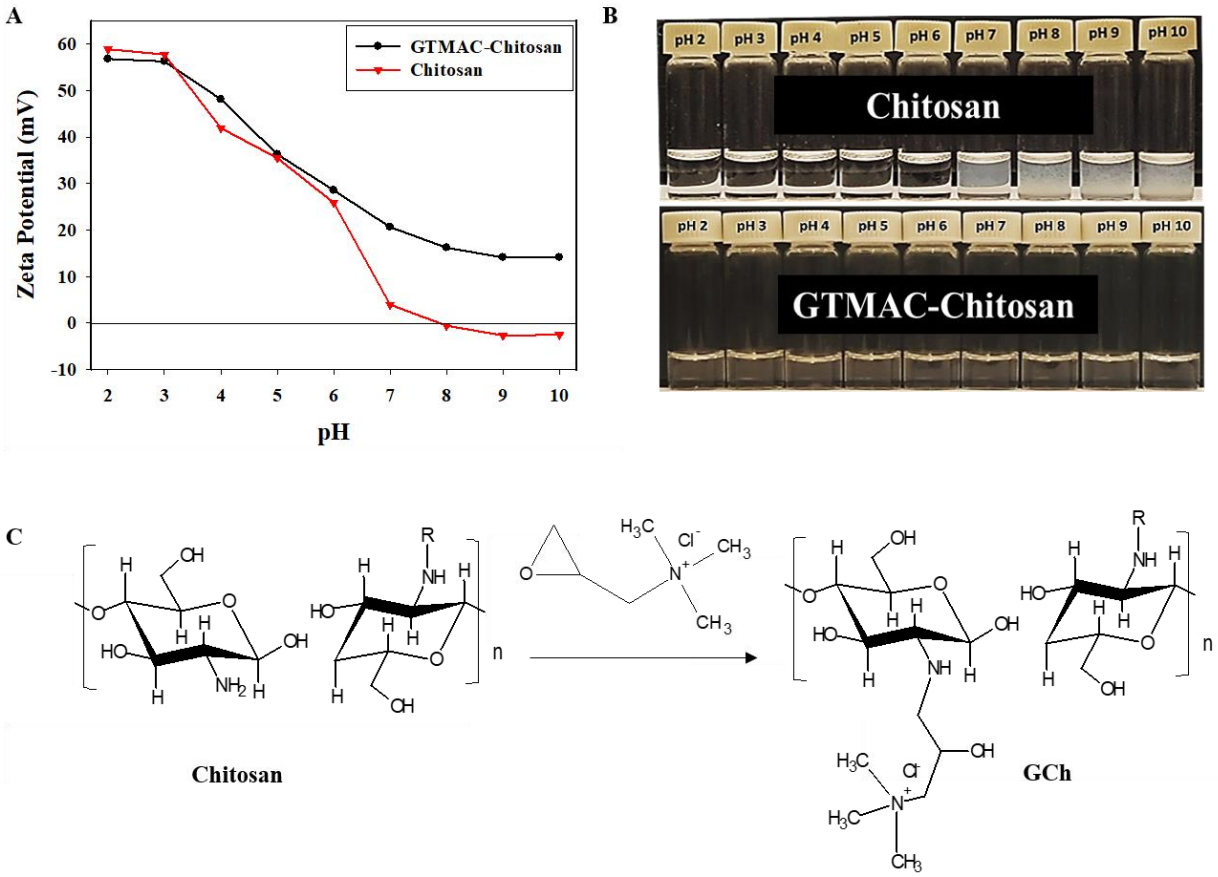

Fig. 3.6 (A): Zeta-potential profiles of chitosan and GTMAC-Chitosan at different pHs, (B): digital photographs demonstrating the solubility of chitosan and GTMAC-Chitosan at different pH values, and (C): the reaction scheme of chitosan to GTMAC-Chitosan.

Generally, epoxide groups readily react with primary amines under acidic and neutral conditions. Therefore a reaction between GTMAC and amine groups on chitosan could be

readily implemented. GTMAC-Chitosan, having a quaternary ammonium group at the C-2 position of chitosan, could be prepared using a catalyst (Cho *et al*., 2006; Zou *et al.*, 2015). The degree of quaternization (DQ) of chitosan was calculated by measuring the content of Cl^- ions of the quaternized chitosan via conductometric titration with $AgNO_3$. DQ is dependent on the reaction time, reaction temperature, and the molar ratio of GTMAC to the amino groups on chitosan (Ahmed & Mondal, 2017). In this study, quaternization of chitosan was successfully performed, yielding a DQ of 48% with amine content around 1850 mmol/kg.

3.3.5 Morphological studies of GCh-PCNC complexes

Morphology of GCh-PCNC nanoparticles with different concentration ratios was analyzed and, the most stable form can be found and utilized to prepare Pickering emulsions. Before determining the structure of the nanocomplexes of GCh-PCNC, the radius of gyration (average distance of the particle from the center of mass) and hydrodynamic radius were analyzed by SLS and DLS, respectively. At low content of GCh, R_g remained constant, and it increased with increasing $[NH_3^+]/[HPO_4^{2-}]$ (Fig. 3.7A). On the other hand, R_h increased and then became relatively constant at large values of $[NH_3^+]/[HPO_4^{2-}]$ (Fig. 3.7B). By analyzing R_g (Fig. 3.7A) and R_h (Fig. 3.7B), the morphology of nanoparticles could be elucidated from the shape factor, R_g/R_h. This trend corresponds to the interaction between PCNC and GCh, where the nanocomplexes undergo a morphological evolution with increasing GCh/PCNC content (Fig. 3.7C). Theoretically, the calculated shape factor value

of ~0.774 (3.7(b)) corresponds to a uniform hard-sphere, and 1.0-1.3 (3.7(c)) for a hyperbranched polymer cluster or a soft sphere (Barthel *et al*., 2014), 1.5-1.8 (3.7(d)) for a flexible random coil chain, and >2 (3.7(a)) for a rigid rod (Zhang *et al*. 2000; Niu *et al*., 2001).

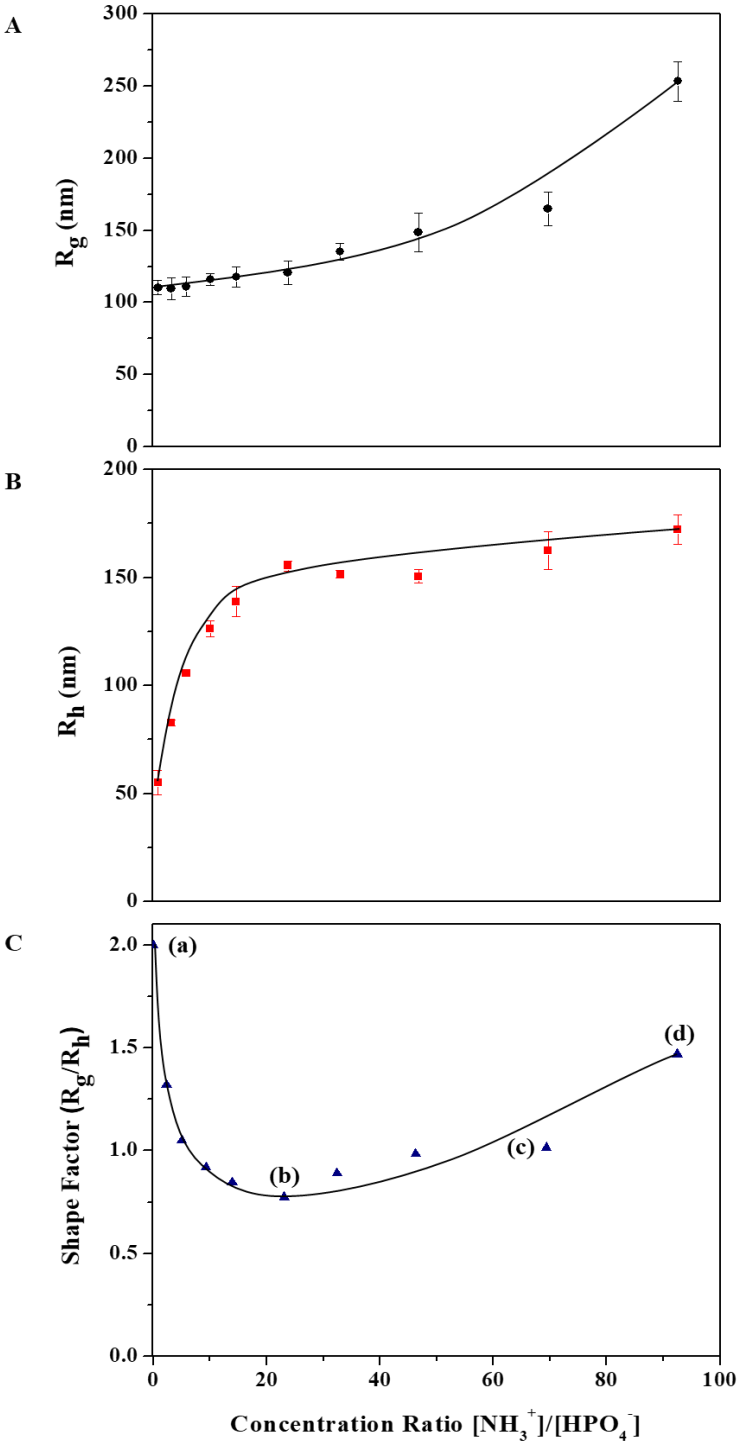

Fig. 3.7 The dependence of (A): radius of gyration (R_g), (B): hydrodynamic radius (R_h), and (C): shape factor (R_g/R_h) on the ratio of GCh and PCNC.

In the absence of GCh, PCNC displayed a rod-like structure with R_g/R_h greater than 2 (Fig. 3.7C(a) and Fig. 3.8(a)). With increasing GCh content, the morphology of the complex transformed from a rod-like structure to a hard-sphere at $[NH_3^+/HPO_4^{2-}]$ of approximately 23 (Fig. 3.7C (b) and Fig. 3.8(b)). In Fig. 3.7C(c) and Fig. 3.8(c), the hyperbranched polymers with a spherical shape were observed because of the insufficient PCNC, and GCh could no longer be complexed with PCNC. Further addition of GCh promoted the complexation and aggregation, resulting in the formation of aggregated random coils whose R_g/R_h is approximately 1.5 (Fig. 3.7C(d) and Fig. 3.8(d)). Therefore, based on these observations, the optimal mass ratio to produce a hard-sphere was determined to be 2.5:1.

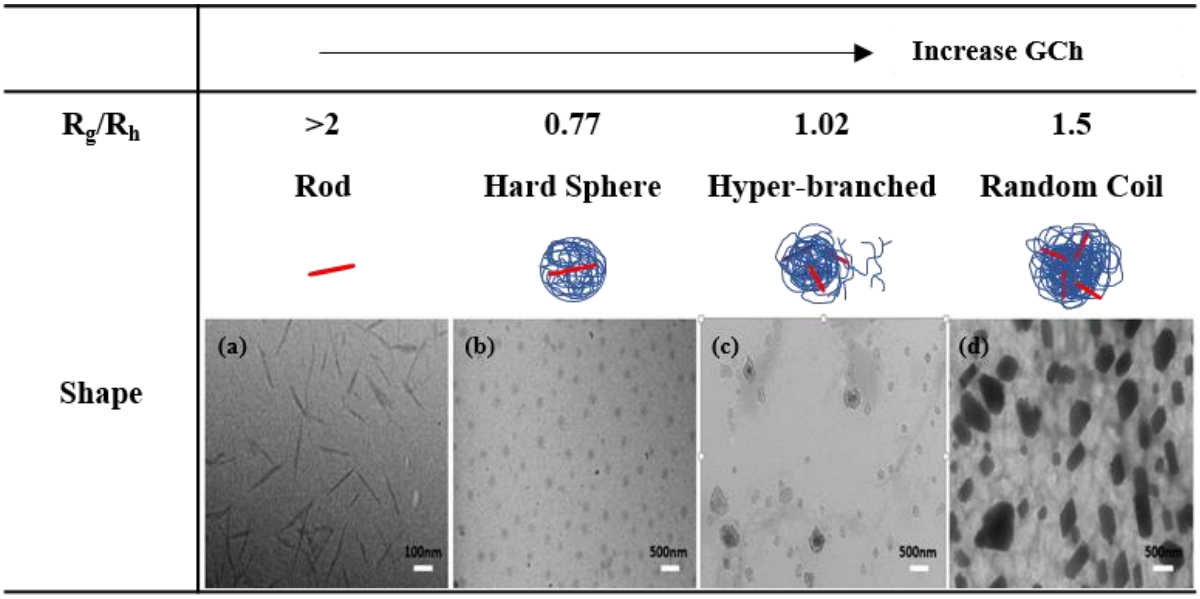

Fig. 3.8 A schematic on the microstructural evolution of the nanoscale complexes.

3.3.6 Pickering emulsions

As described previously, TPP was used to prepare spherical chitosan beads by rapid ionic gelation of the polyvalent anion sodium tripolyphosphate (TPP) with positively charged

chitosan. The phosphorus groups on the CNC imparted a zeta potential of -26 mV to PCNC, which is similar to the value of -31 mV for TPP. Therefore, PCNC was used as a crosslinking agent in the production of nanoparticles. Also, in this study, GCh-TPP and GCh-PCNC nanoparticles were used to replace conventional emulsifiers to stabilize Pickering emulsions in order to improve their storage stability (Fig. 3.9). The stability of GCh-TPP and GCh-PCNC nanoparticles were compared at the same optimal mass ratio (2.5:1), and their respective emulsions were evaluated. Based on the evaluations, the Pickering emulsions containing GCh-PCNC emulsifiers formed droplets of about 3-5 µm, and they remained stable even after 3 months (Fig. 3.9A). The emulsions did not exhibit any creaming, coalescence, or separation. According to Julius *et al*. (2014), the solid particles were densely packed at the oil-water interfacial as monolayers that remained stable for one year without coalescence. In contrast, the GCh-TPP emulsion creamed after 1 h and completely separated after 2 days (Fig. 3.9A). The Pickering emulsion prepared with GCh-PCNC (red rings) nanoparticles remained stable for a long time without phase separation due to irreversible adsorption of chitosan nanoparticles at the oil/water interface. The Pickering emulsion could be stored for a long time without coalescence (Fig. 3.9B).

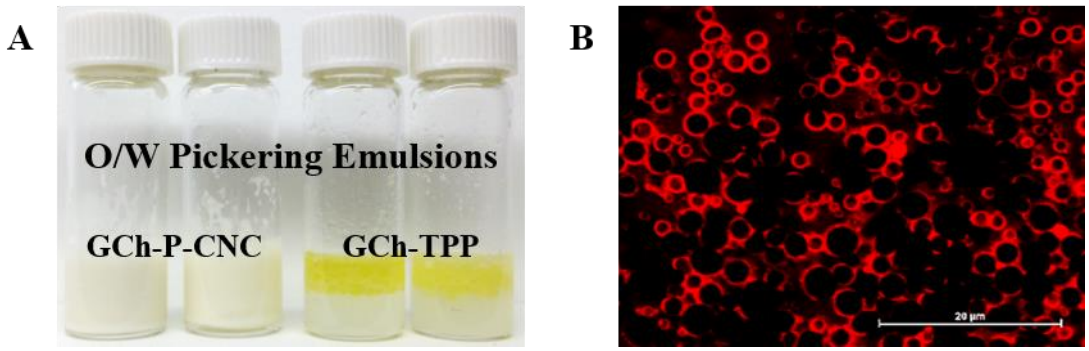

Fig. 3.9 (A): The Comparative stability of GCh-PCNC and GCh-TPP oil in water Pickering emulsion in vials and (B): fluorescence microscope image of GCh-PCNC oil in water Pickering emulsion.

3.4 Conclusions

Chitosan, a natural polymer, has been widely used as a biomaterial in drug delivery systems due to its low toxicity and antibacterial properties. Modified chitosan was complexed with PCNC to prepare nanocomplexes that could be used for functional food applications. The complexation of GCh and PCNC resulted in the formation of nanoscale complexes with an average diameter of 300-350 nm, and a hard-sphere morphology was produced at $[NH_3^+/HPO_4^{2-}]$ of approximately 23. The GCh-PCNC complexes yielded very stable Pickering emulsions compared to emulsion prepared from the GCh-TPP system. These novel nanostructures provide a new approach to stabilize emulsion for functional food formulation.

Chapter 4

Encapsulation and Controlled Release of Vitamin C in Modified Cellulose Nanocrystals/Chitosan Nanocapsules

The material in this chapter was published in Baek, J., Ramasamy, M., Willis, N. C., Kim, D., Anderson, W. A., & Tam, K. C. (2021). Encapsulation and Controlled Release of Vitamin C in Modified Cellulose Nanocrystal/Chitosan Nanocapsules. Current Research in Food Science.

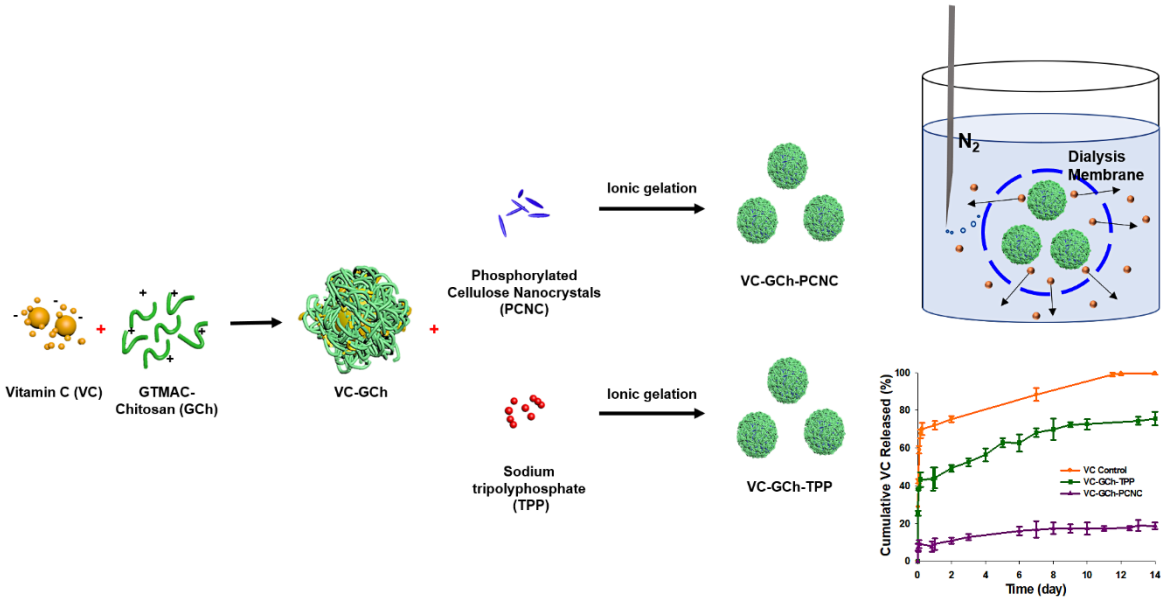

4.1 Introduction

Vitamin C (VC), commonly known as L-ascorbic acid, is a water-soluble vitamin that helps construct the biological systems by various physiological functions, such as hydroxylation reactions in collagen synthesis, growth, and repair of skin and connective tissues (A. Bendich

et al., 1986; Naidu, 2003; Sauberlich, 1994). VC is an antioxidant necessary for preventing damage to essential macromolecules in the body by scavenging harmful free radicals caused by environmental pollution and possibly infectious organisms (Bendich *et al.*, 1986; BodannesChan, 1979). Because of its antioxidant potency, VC is quickly oxidized to dehydroascorbic acid (DHA) and hydrolyzes at alkaline pH to form an irreversible 2,3-L-diketogulonate (Simpson & Ortwerth, 2000). Therefore, encapsulating VC with desirable nanoparticle systems can protect the active compound degradation from external environments, including light, maintaining stability and enhances the shelf-life of the vitamin-based products.

Increased consumer awareness of potentially harmful synthetic preservatives and the need for biodegradable and sustainable materials has led to research into natural alternatives, notably chitosan biopolymers and cellulose nanocrystals. Chitosan (Ch) is the second most abundant natural polymer, making it ideal for biomedical and food applications (Akhlaghi *et al.*, 2015; Kumar, 2000). Because of mucoadhesive, the Ch delivery system can transport bioactive agents with a longer residence time in the gastrointestinal tract with improved bioavailability (Jiménez-Fernández *et al.*, 2014). In an acidic environment, Ch protonates for efficient binding to anionic compounds (Rinaudo, 2006; Wang *et al.*, 2017). However, Ch has low solubility above the pH of 6.5, which limits its application. Therefore, it is imperative to modify Ch for extended applications over a wide pH range.

There are several reports on the synthesis of water-soluble Ch-compounds (Lim & Hudson, 2003; Liu *et al.*, 2011), and modifying Ch with quaternary ammonium groups has been shown to significantly improve the aqueous solubility of Ch. Moreover, the GTMAC could be conjugated to Ch by reacting with the epoxide rings yielding a cationic GCh that could electrostatically bind to VC due to the presence of quaternary ammonium groups. Furthermore, GTMAC has been shown to possess better antimicrobial properties, which could preserve the nanocapsules and VC from degradation (He *et al.*, 2018). Henceforth, glycidyl trimethylammonium chloride (GTMAC) was conjugated to Ch to enhance the solubility, attachment and preserve the negatively charged VC.

Cellulose nanocrystals (CNC) are extracted via sulfuric acid hydrolysis to produce sulphated-CNCs (SCNC). However, such a system may not be suitable for biomedical or food applications since sulphated materials are rarely used as a food acidulant. On the other hand, phosphoric acid is considered the most common inorganic food acidulant (Deshpande, 2002), a safer and healthier hydrolyzing acid for functionalizing CNC. Therefore, cellulose fibers were hydrolyzed using phosphoric acid to isolate the crystalline regions of phosphorylated cellulose nanocrystals (PCNC) (Camarero Espinosa *et al.*, 2013; Vanderfleet *et al.*, 2018).

Sodium tripolyphosphate (TPP) is often used as a cross-linking agent to prepare chitosan-TPP complexes. These complexes are metastable, as well as having low mechanical strength, and therefore, they have limited applications as delivery systems (Alishahi *et al.*, 2011; de

Britto *et al.*, 2012; Katouzian & Jafari, 2016). To address this shortcoming, PCNC was adopted as a novel cross-linking agent for GCh to produce VC encapsulated nanocapsules (VC-GCh-PCNC) via ionic gelation. Wang *et al.* (2017) used both TPP and SCNCs as cross-linking agents to encapsulate hydrophilic anthocyanins. They confirmed that chitosan-SCNCs yielded more stable capsules, where the external pH modulated the active molecule release (Wang *et al.*, 2017).

Desai and Park also showed that TPP cross-linked chitosan microspheres displayed almost 100% cumulative VC release in approximately 6 h (Desai & Park, 2005). A better carrier system with a higher encapsulation efficiency and sustained release rate, which also shields the active ingredient (especially VC) from degradation (Ashrafizadeh *et al.*, 2020), is needed. Ideally, GCh-PCNC nanocapsules could provide a better encapsulation, prolonged-release rate and enhanced stability than existing carrier systems.

Based on this rationale, the objective of the present study was to produce a better carrier system with a higher encapsulation efficiency and sustained release VC using GCh-PCNC nanocomplex. The VC nanocapsules characteristics, such as particle size, degradation, encapsulation efficiency, cumulative release, simulated release, and release kinetics, were analyzed and elucidated. Additionally, we investigated the nanocapsule's antioxidant activity and antibacterial behaviour.

4.2 Materials and methods

4.2.1 Materials

Vitamin C (L-ascorbic acid), low to medium molecular weight chitosan (M_w = 50-190 kDa), phosphoric acid, glycidyl trimethylammonium chloride, acetic acid, sodium acetate trihydrate, PBS buffer, hydrochloric acid, and sodium hydroxide were purchased from Sigma-Aldrich (St. Louis, MO, U.S.A.) and used as received.

4.2.2 Preparation of VC-GCh-PCNC/VC-GCh-TPP nanocapsules

PCNC and GCh were prepared based on the previously reported protocol with minor modifications (Baek *et al.*, 2019). Initially, suspensions of GCh (2 mg/mL) and PCNC (4 mg/mL) and a solution of TPP (0.9 mg/mL) were prepared in Milli-Q water. The concentrations of TPP and PCNC were selected based on the phosphate ion concentrations. GCh and PCNC suspensions were sonicated in a light-protected environment for 10 min (Misonix Sonicator XL-2000 Series, QSonica LLC) to produce a stable dispersion. Under nitrogen purging, 0.5 mL of VC solution was added to 10 mL of GCh, and the suspension was ultra-sonicated for 5 min. A 2 mL of PCNC or TPP was added using a Harvard Apparatus syringe pump into the VC-GCh dispersion every 50 s with continuous ultra-sonication to obtain VC-GCh-PCNC/VC-GCh-TPP nanocapsules as shown in Scheme 4.1. The prepared samples were stored in the dark at 4 °C and utilized for further examinations.

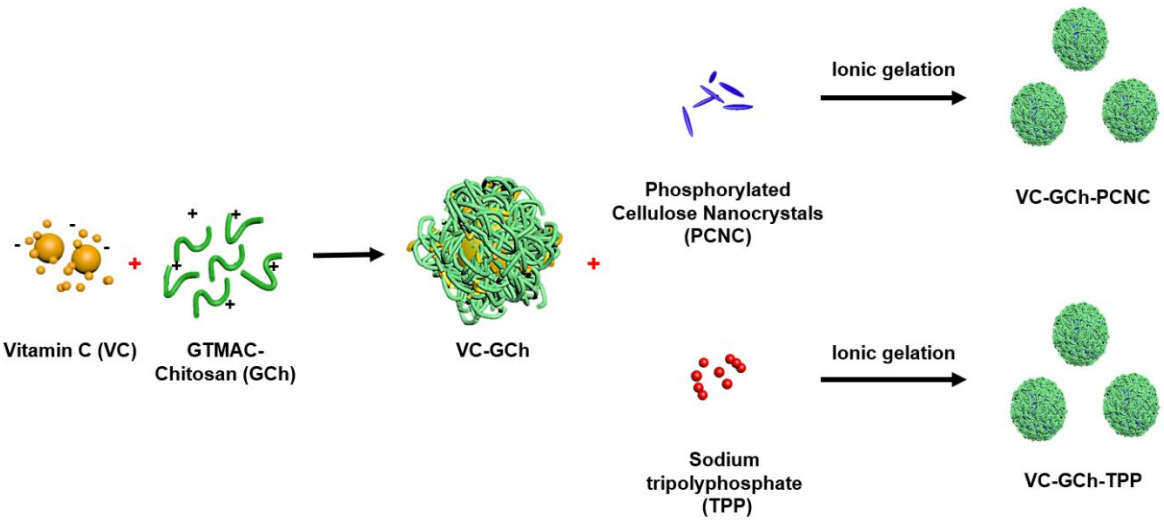

Scheme. 4.1 Schematic illustrations are describing the formations of VC-GCh-TPP and VC-GCh-PCNC nanocapsules by utilizing VC, GCh, TPP, and PCNC.

4.2.3 Characterization

4.2.3.1 FTIR

TPP and PCNC were analyzed using the FTIR spectrophotometer (Bruker Tensor 27 FTIR spectrometer, Billerica, MA, USA) to confirm the presence of phosphate groups. Freeze-dried samples were ground in a mortar and compressed with potassium bromide (KBr) to form pellets. FTIR spectra of each sample were recorded between 4000 cm^{-1} and 400 cm^{-1} with a resolution of 4 cm^{-1} and 32 scans.

4.2.3.2 Characterization of the nanocapsules

The particle size and zeta potential of VC-GCh, VC-GCh-PCNC and VC-GCh-TPP were determined using a Malvern Zetasizer Nano ZS instrument (Nanosizer ZS, Malvern, UK). All the experiments were carried out in triplicate.

4.2.3.3 Morphology

The morphology of VC-GCh, VC-GCh-TPP, and VC-GCh-TPP was evaluated using a transmission electron microscope (TEM, Philips CM10 electron microscope, an acceleration voltage of 60 kV). The sample was placed on a 200-mesh carbon-coated copper grid and air-dried before analysis.

4.2.4 Degradation analysis of VC

Degradation reaction upon storage or processing is the main problem of nutritional quality loss. To determine the optimal conditions to perform further experiments in which minimal VC degradation test has been conducted. VC solution, equivalent to the concentration in the nanocapsules used in other studies, was prepared using phosphate-buffered saline (PBS, pH 7.4) in the rubber-stoppered round bottom flask. Nitrogen purging and sample withdrawal were facilitated through the inlet and outlet needles. The flask was covered with aluminum foil and left to stir at 250 rpm at room temperature. For comparison, another flask with the same experimental setup was used but without nitrogen purging and cover. At designated time intervals, 1 mL aliquot of the solution was withdrawn and analyzed at 265 nm using a

UV-Visible spectrophotometer (Cary 100 Bio UV-Vis spectrophotometer with quartz cuvettes). The concentration of VC was determined from the calibration curve.

4.2.5 Determination of encapsulation efficiency

An encapsulation efficiency (EE, %) was performed on VC-GCh-PCNC and VC-GCh-TPP nanocapsules. At first, 1 mL of the sample dispersion was filtered by a stainless-steel syringe filter holder (Millipore and 1 Whatman 13mm) using a 25 nm pore size membrane (Durapore membrane filter PVDF 0.025 μm, Sigma-Aldrich, St. Louis, MO, U.S.A.). The VC content in the filtrate was measured using the Cary 100 Bio UV-Vis spectrophotometer. The encapsulated VC concentration was determined from a standard VC calibration curve and used to determine the EE from Eq. (4.1) (Akhlaghi *et al.*, 2015).

$$EE\ (\%) = \frac{[VC]_{total} - [VC]_{filtrate}}{[VC]_{total}} \times 100\% \qquad (4.1)$$

where VC_{total} is the absorbance of the control and $VC_{filtrate}$ is the absorbance of the unbound VC.

4.2.6 Cumulative VC release study

The cumulative release of VC from VC-GCh-PCNC or VC-GCh-TPP was performed based on the modified method of Desai & Park (2005). Ten mL of the nanocapsule dispersions was placed separately in a dialysis bag, submerged in 25 mL of PBS (at pH 7.4 and 25 °C) on a stirrer-plate with continuous nitrogen purging and under controlled light exposure. The dialysate was collected at predetermined time intervals (0-72 h, and up to 14 days), and the

VC release was analyzed using the Cary 100 Bio UV-Vis spectrophotometer. A control test with a similar experimental condition was also performed for the VC solution. This cumulative release study was conducted in triplicate, and the average values were reported.

4.2.7 DPPH free radical scavenging activity

A colorimetric 2,2-diphenyl-1-picrylhydrazyl (DPPH) assay was used to measure the free radical scavenging activity of VC, VC-GCh-PCNC and VC-GCh-TPP. The method was adapted with slight modification based on the reported assay (Wang *et al.*, 2017). DPPH is reduced when it reacts with an antioxidant reagent, causing a colour change from violet to yellow. Initially, the DPPH solution (0.025 mg/mL) was prepared in pure methanol and protected from light using an aluminum foil. The nanocapsule suspensions were filtered through a 25 nm pore size membrane, and 0.15 mL of the filtrate was stirred with 1 mL DPPH solution in the dark for 30 min and 5 days. Finally, the absorbance was measured using the Cary 100 Bio UV-Vis spectrophotometer. The encapsulated VC concentration was determined from a standard VC calibration curve. The scavenging activity was calculated using Eq. (4.2):

$$SA\% = \frac{A_{control} - A_{sample}}{A_{control}} \times 100\% \qquad (4.2)$$

where $A_{control}$ is the absorbance of the control and A_{sample} is the absorbance of the free VC.

4.2.8 Drug release kinetics and mathematical models

The different mathematical models have been used to determine the kinetics of drug release

from the delivery systems, such as zero order, first order, and Higuchi model (Starychova *et al.*, 2014; Zandi, 2017). These dissolution models are necessary to study the release mechanism of drugs, as it mathematically describes the release profiles, in our case VC.

The three models are shown in Eq 4.3, 4.4, and 4.5 (Azevedo *et al.*, 2014; Siepmann, 2013), where M_t is the amount of active ingredient eluted at time t, M_0 is the initial amount of VC in the solution (in most of the cases, M_0=0) (Larsen *et al.*, 2013; Rosenzweig *et al.*, 2013)

Various Kinetic Release Models

Zero-order equation: $M_0 - M_t = K_0 t$ (4.3)

First-order equation: $\log M_0 - \log M_t = K_1 t/2.303$ (4.4)

Higuchi equation: $M_0 - M_t = K_H t^{1/2}$ (4.5)

* K_0 is the zero-order release constant.
* K_1 is the first-order release constant.
* K_H is the Higuchi dissolution constant.

4.2.9 Digestive system simulation release test

A released study was conducted in a simulated digestive system by modifying the pH of the environment based on conditions shown in Table 1 (Li *et al.*, 2020). To mimic the gastrointestinal tract, the pH of the system was altered by replacing the buffer solution at specified time intervals using acetic acid-sodium acetate buffers of pH 2 and 5 and a PBS buffer of pH 7.4. The release test was performed in the dark with continuous nitrogen purging and stirring with a magnetic stirrer at the physiological temperature (37 °C).

Table 4.1 Experimental conditions to simulate the digestive system.

Digestive Region	**pH**	**Time** (h)
Upper Stomach	5	1
Lower Stomach	2	3
Duodenum	7.4	1
Small Intestine	5	3

4.2.10 Antibacterial tests

Escherichia coli (E. coli) and *Staphylococcus aureus* (*S. aureus)* were used as the model for Gram-negative and Gram-positive bacteria. Each strain was streaked from -80 °C glycerol stock on Lauria-Bertani agar (LBA) plates and kept overnight at 37 °C. Fully grown, a single colony was inoculated in fresh LB medium in an Erlenmeyer flask and incubated on a shaking incubator (250 r/min) for 16 h at 37 °C. Phenotypic assays were performed using overnight cultures after re-inoculating bacteria in LB broth at 0.05 initial turbidity at optical density 600 nm. The effects of VC-GCh-PCNC on both bacteria were evaluated using the standard broth dilution method. In brief, different concentrations of the dried nanoparticles (128, 64, 32, 16, 8, 4, 2, 1 μg/mL) were dispersed in sterile LB broth and sonicated. Subsequently, the turbidity of bacterial suspension (10^5 CFU/mL) was adjusted, co-inoculated and incubated in a shaking incubator for 24 h. After that, each of the bacteria-nanocapsule suspensions was serially diluted to achieve 10^8 to 10^3 CFU/mL. The samples were vortexed for 5 s, and 100 μL of the suspension was spread on the agar plate and incubated for 24 h at 37 °C. Finally,

the MIC was determined according to the lowest concentration that inhibited the maximum visible growth of microbes (Shi *et al.*, 2015).

4.2.11 Statistical analysis

All experiments were performed as three independent preparation, and the results are expressed as means with error bars of ± standard deviations.

4.3 Results and discussion

The loading of active ingredients, such as vitamins or drugs, in the nanoparticulate system, can be prepared with surface charge interaction mechanisms (de Britto *et al.*, 2012). The active ingredients, either physically entrapped (incubation) or adsorbed (incorporation) on the surface of polymer matrices to create the particles (Radtchenko *et al.*, 2002). Polysaccharide nanoparticles displayed enhanced loading efficiencies, slow/sustained release, including chitosan nanoparticles (Lazaridou *et al.*, 2020). GCh is soluble in a neutral pH medium, which ensures that the chemical degradation of the vitamin does not occur during the nanoparticle formation. The preparation, loading, and release of VC in the GCh nanocapsules will be discussed subsequently.

The FTIR was conducted to compare the two cross-linking agents and confirm the functional groups on TPP and phosphoric acid hydrolysis for preparing the PCNC. The spectra of both TPP, PCNC are shown in Fig. 4.1A. The spectrum (*enlarged view*) of TPP possesses peaks

at 1210-1218 cm^{-1} which are associated with the stretching vibration of P=O. The band at 1130-1156 cm^{-1} is assigned symmetrical and asymmetric stretching vibration of PO_2, and the peak at 1090-1094 cm^{-1} is attributed to the symmetrical and asymmetric stretching vibration of PO_3. The asymmetric peak presents at 888-892 cm^{-1} is a result of P-O-P stretching (Martins *et al.*, 2012). To prove the esterification of CNC through successful phosphoric acid hydrolysis, the IR spectrum of PCNC was also determined. As similarly found in the IR spectrum of TPP, phosphate groups were dominantly featured in the PCNC IR spectrum, revealing the presence of P-OH stretching with peaks at 1000-1034 and 1223-1236 cm^{-1}, a peak at 1164 cm^{-1} is attributed to P=O bands, and peak at between 464 and 452 cm^{-1} attributed to the HO-P=O band (Loutfy *et al.*, 2016).

In our previous study (Baek *et al.*, 2019), we observed that the shape of the nanocomplexes changed from a rod-like to hard-sphere and random coil morphology as the GCh/PCNC ratios were increased. This microstructure is considered to be optimal for the preparation of the VC encapsulation system (Geng *et al.*, 2015). The negatively charged PCNC interacted with the positively charged GCh via electrostatic interaction at all pHs, resulting in the retention of VC over a prolonged period. CNC is known to be a strong reinforcing agent for the polymer matrix (Geng *et al.*, 2015). Sampath *et al.* (2017) reported strong inter-and intramolecular interactions, resulting from hydrogen bonding between hydroxyl and amino groups on chitosan and hydroxyl groups on CNC (Sampath *et al.*, 2017). As a result, the complexation of PCNC and chitosan significantly increased the mechanical properties of the nanocomplex.

Poor mechanical strength leads to low drug loading capacity and burst release of the drug, whereas high mechanical strength produced a sustained drug release due to strong interaction between drug and matrix (Xu *et al.,* 2020).

Lin *et al*. (2016) developed a double membrane hydrogel with anionic alginate and cationic CNC (CCNC) via electrostatic interactions and drugs were encapsulated within the membranes of the hydrogel. By adding CCNC, enhanced mechanical properties, robust hydrogel and sustained drug release were observed. This CCNC provided the "nano-obstruction/locking effect" in the hydrogel, and it could be applied in the drug delivery system for prolonged drug release (Lin *et al*., 2016). TPP is an ionic cross-linker, having three phosphate groups (triple-negative charges), and it has been used as a cross-linking agent for chitosan. Since chitosan has NH_2 and OH groups which are easily protonated to NH_3^+ (below its pK_a), which could bind to the negative phosphate groups. It has been reported that the conventional Ch-TPP complex is a metastable system with poor mechanical and is highly pH-dependent. As the pK_a of chitosan is 6.5, thus at pH of 3.4, 5.5, and 6, 100%, 90% and 40% of amino groups are protonated, respectively (Bayat *et al.*, 2008; Karimi *et al.*, 2013). Additionally, Wei *et al.* (2020) reported that when the TPP content was lower than 0.04%, a burst release of theophylline (TH) in TH/Ch-TPP particles was observed within 2 h while at 0.04% of TPP content, 90% of TH was slowly released within 5 h (Wei *et al.*, 2020). In comparison, our PCNC containing nanocapsules showed prolonged VC release. Hence, they are considered to be a better delivery system.

Fig. 4.1B shows the size and zeta potential of the GCh nanocapsules loaded with VC and cross-linked using TPP or PCNC. The larger particle size of 620 nm was obtained by electrostatically binds with negatively charged VC and highly positive GCh. However, VC's high affinity towards GCh neutralized the cationic charges on the GCh, which reduced the stability of the complex and might induce the aggregation of the system (Fig. 4.1Ca). This tendency of aggregation may be addressed using other strategies to prepare a stable nanoparticulate system. The alternative methodologies of incorporating TPP or PCNC yielded highly stable nanocapsule formation with zeta potential values of about -31 mV and -26 mV, respectively. Eyley & Thielemans (2014) stated that the acid hydrolysis of CNC using sulfuric or phosphoric acid imparted negative charge to the CNC from the decoration of sulfate or phosphate groups on the surface of CNC. If the phosphate groups on the CNC surface are insufficient, it has the tendency to aggregate (Eyley & Thielemans, 2014). The alternative methodologies of incorporating TPP or PCNCs provide the nanocapsule formation with the zeta potential values of about -30 mV, which is considered highly stable. VC-GCh possessed a zeta potential (ZP) of ~+9 mV, which decreased to ~ -30mV when the VC-GCh was complexed with TPP and PCNC. The average particle diameter of 450 ± 8 and 428 ± 6 nm was recorded for VC-GCh-PCNC and VC-GCh-TPP nanocapsules. Consequently, both nanocapsules yielded 0.05 as the average PDI confirmed the uniform size distribution of the nanocapsules without aggregations. Wang *et al*. (2017) reported that anthocyanins, which are blueberry extracts, were added were formed microcapsules by CNC and TPP cross-linking agents, respectively. The anthocyanins could be presented in all parts

of the entire microcapsule, such as on the capsule surface, core, and matrix. In their prepared Ch-CNC microcapsules, anthocyanins were found on the core and the surface whereas, anthocyanins were found on the surface of the Ch-TPP microcapsules. The anthocyanins could not be encapsulated in the core due to the weaker matrix with larger space within the matrix. Besides, the sizes of their Ch-CNC and Ch-TPP microcapsules were 265–969 nm and ~34 mm under vigorous stirring process, respectively (Wang *et al.*, 2017). However, the size of Ch-TPP under high-intensity ultrasonication process was around 300 nm with 0.53 of PDI (Tang *et al.*, 2003). Fig. 4.1C depicts the morphology of VC-GCh (a), VC-GCh-PCNC (b) and VC-GCh-TPP (c) nanocapsules, and Scheme 2 summarizes the microstructure of the nanocapsules and the chemical functionality of each component. In corroboration, TEM images described the formation of spherical and monodispersed nanocapsules. The VC-GCh mixture formed through ionic gelation possessed an amorphous structure of around 600-620 nm (Fig. 4.1Ca). Both VC-loaded VC-GCh-TPP (Fig. 4.1Cb) and VC-GCh-PCNC nanocapsules (Fig. 4.1Cc) maintained a spherical shape with an average size of 400-500 nm. The sample cross-linked using PCNC showed enhanced contrast signals compared to VC-GCh-TPP, associated with the high VC encapsulation. Additionally, this phenomenon supports our hypothesis of better cross-linking capacity and higher VC loading in the GCh-PCNC system.

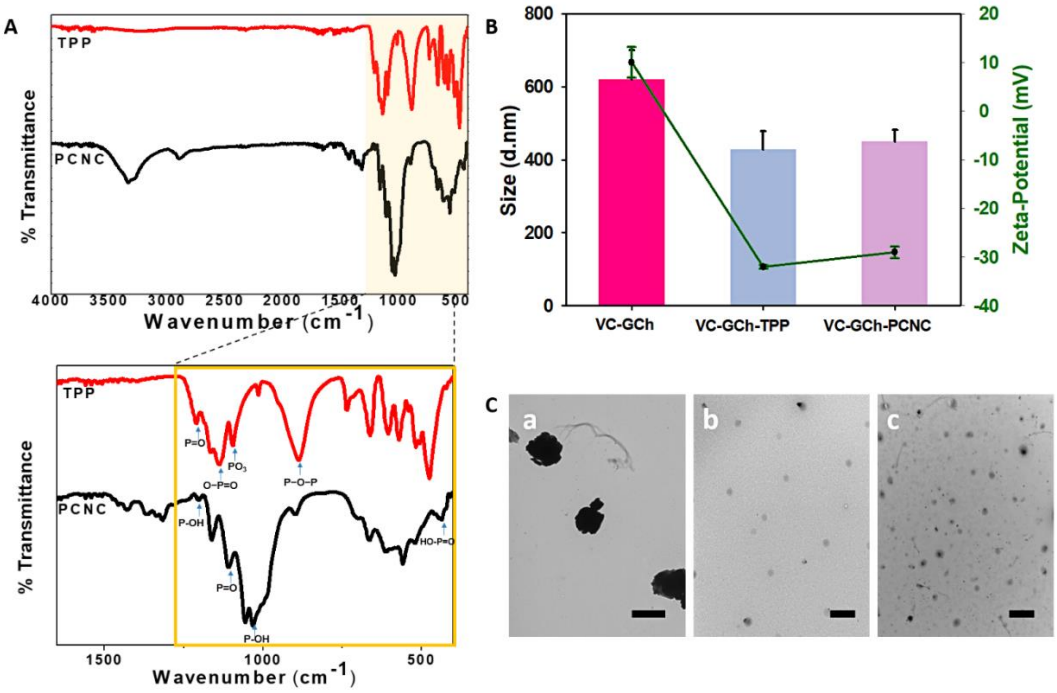

Fig. 4.1 (A) The IR spectra of TPP (upper trace) and PCNC (lower trace); (B) Zeta potential and z-average particle sizes of VC-GCh, VC-GCh-PCNC and VC-GCh-TPP nanocapsules, and **(C)** TEM images of (a): VC-GCh complex (Scale bar: 500 nm) (b): VC-GCh-TPP (Scale bar: 2μm), and (c): VC-GCh-PCNC (Scale bar: 2μm).

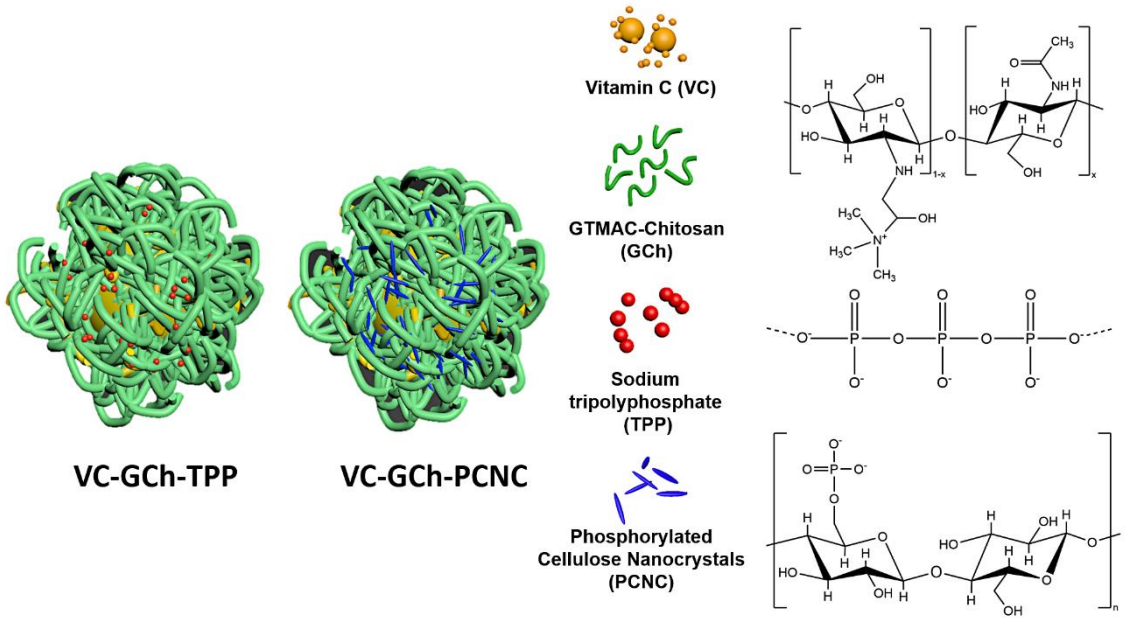

Scheme. 4.2. Schematic illustrations are describing the microstructure of the nanocapsules and the chemical functionality of each of the components.

External environmental conditions, such as light, high temperatures, low pH, and dissolved oxygen, could expedite the VC degradation (Burdurlu *et al.*, 2006; Zerdin *et al.*, 2003). Therefore, it is essential to protect the VC to yield the desired performance for a given application. Removing dissolved oxygen in a light-protected environment is an important measure to ensure no VC degradation. As shown in Fig. 4.2A, nitrogen purging brought minimal to no degradation over 5 days than the VC exposed to ambient conditions. Without nitrogen purging degraded rapidly, VC solution resulted in 86% within the first 24 h and entirely within 4 days. Moreover, a controlled environment prevents VC degradation, with the concentration maintained at almost 98% at the end of 5 days. Thus, the optimal condition

for conducting the VC release requires continuous nitrogen purging, which was being adopted for accurate VC quantifications from the prepared nanocapsules.

The encapsulation efficiency for both VC-GCh-PCNC and VC-GCh-TPP nanocapsules was measured in neutral pH. Since the pK_a of vitamin C is pH 4.2 and 11.6 (Tian *et al.*, 2009), at neutral pH, vitamin C was ionized, yielding more negative charges to interacted with GCh, leading to higher encapsulation VC. The indirect method yielded an EE of 90.3 ± 0.42% for VC-GCh-PCNC, which was 33% higher than VC-GCh-TPP (57.3 ± 0.28%) nanocapsules based on the vitamin C calibration curve. This significant difference in EE confirmed that nanocapsules prepared using GCh and PCNC possessed good encapsulation of VC and stability due to the chemical bonding compared to the weaker TPP cross-linked VC-GCh-TPP nanocapsule system. In the previous study by Desai and co-workers, the encapsulation efficiency of VC-loaded Ch-TPP capsules using different molecular weight types was in the range of 52.74–67.25% (Desai *et al.*, 2006).

An incremental release test to simulate food storage performed over 14 days under continuous nitrogen purging conditions shown in Fig. 4.2B. A burst release of more than 75% in a few hours was observed for VC only (control) than the nanocapsule systems that clearly explain the importance of encapsulation. On the other hand, the VC-GCh-TPP nanocapsules recorded a more rapid release profile of 42% within a day and approached 76% in two weeks. In contrast, VC-GCh-PCNC showed slow-release of VC to reach 18% over

the extended period of 14 days. A slow release of VC was achieved using VC-GCh-PCNC, primarily due to the PCNC that possessed a more robust and durable cross-link than TPP. PCNC may also function as a filler for the GCh matrix (Xu *et al.*, 2019), thereby improving the nanocapsules' mechanical strength that might also be contributed to the controlled release of VC from the system. Water-soluble GCh with TPP has been reported to load protein, insulin, quercetin, and Bovine Serum Albumin (BSA) (Rwei *et al.*, 2014; H.-l. Zhang *et al.*, 2009) and *In vitro* study, they demonstrated an initial burst and then slow/continuous release trends. Even though high EE% and slow-release rate of GCh were shown comparing to Ch-TPP, almost 72-80% were released within 24 h due to the weak ionization degree of GCh at pH 7.4 and fewer positively charged amine groups. However, in our study, PCNC provided function as a filler for the GCh matrix, thereby improving the nanocapsules' mechanical strength that might also be contributed to the controlled release of VC from the system (Xu *et al.*, 2019). Therefore, the VC-GCh-PCNC would be more useful for the long-term storage of active ingredients in foods, cosmetics, and personal care applications.

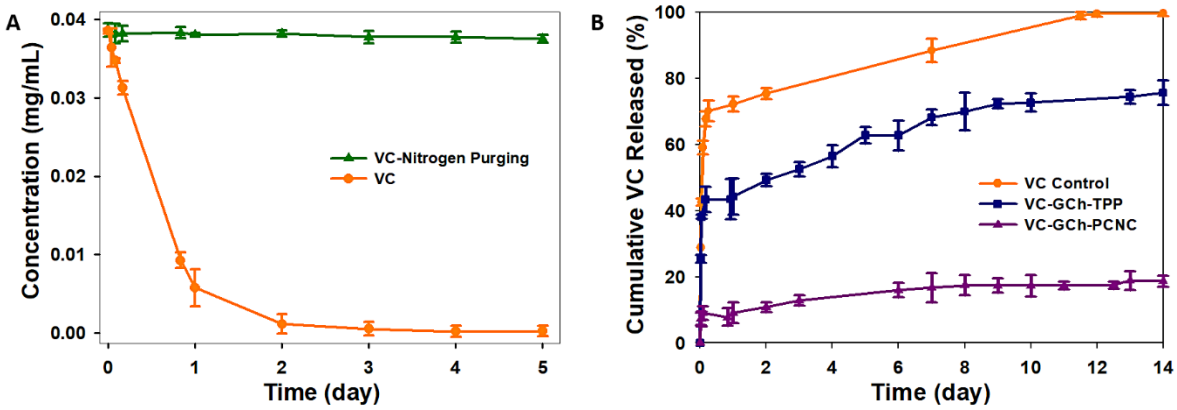

Fig. 4.2 (A) Changes in concentration concerning the time of a 0.04 mg/mL VC solution in PBS under nitrogen gas purging, limited light exposure, and constant temperature. **(B)** The cumulative release profile of VC from nanocapsules through a dialysis membrane to time.

The DPPH solution is violet in colour and has a characteristic UV-visible absorption peak at 517 nm in the non-reduced state (Fig. 4.3A). The results of the DPPH free radical scavenging activity experiments for VC, VC-GCh-TPP, and VC-GCh-PCNC nanocapsules for 30 min are shown in Fig. 4.3B. A higher scavenging activity in the filtrate (free VC) reflects a lower encapsulating capacity of the nanocapsules and vice versa. As seen in Fig. 4.3B, the filtrate of VC-GCh-PCNC possessed lower 13.5 ± 0.58% scavenging activity (%) compared to VC-GCh-TPP (44.7 ± 0.89%) and free VC (56.7 ± 0.62%) after 30 min and Fig. 4.3C shows the antioxidant power for 5 days, displaying still lower scavenging activity (%) of VC-GCh-PCNC. However, in contrast, the retained VC in GCh-PCNC nanocapsules possessed a significant free-radical scavenging activity than VC in GCh-TPP since PCNC provides a better cross-linking capacity with GCh yielding a compact nanocapsule that preserves the VC from external degradation over a long storage time.

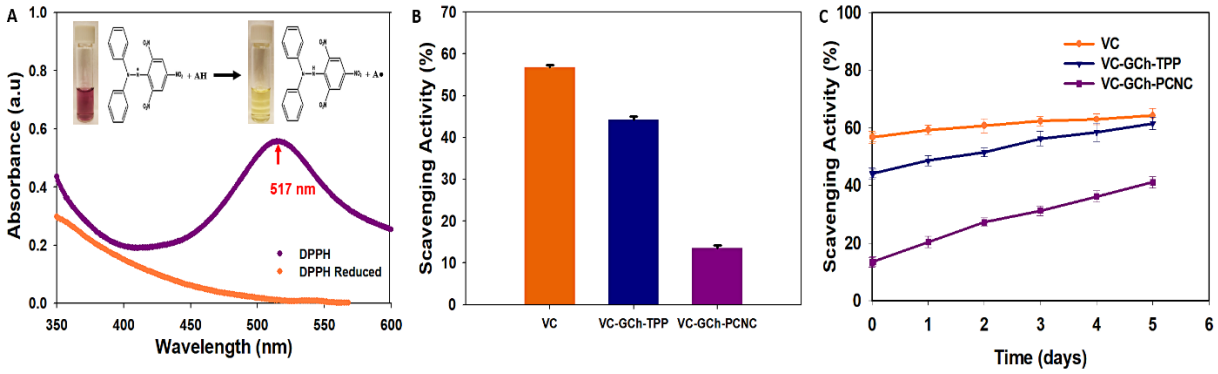

Fig. 4.3 (A) DPPH absorption spectra, (B) DPPH free radical scavenging activity from the filtrates of nanocapsule dispersions of VC- GCh-TPP and VC-GCh-PCNC for 30 min, and **(C)** DPPH free radical scavenging activity from the filtrates of nanocapsule dispersions of VC- GCh-TPP and VC-GCh-PCNC for 5 days.

The data obtained from the VC release studies from VC-GCh-PCNC and VC-GCh-TPP nanocapsules were used to elucidate the various drug release kinetic models (Zero-Order, First-Order, and Higuchi). The zero-order release corresponds to constant release with the same amount of VC release per time. The first-order model is a concentration-dependent release with the same rate of drug release per time. It is the case of sustained-release and matrix diffusion-controlled release. The Higuchi model can be used to determine the release of the drug from the matrix (Fu & Kao, 2010; Mircioiu *et al.*, 2019). Based on the equations (3-5), the best kinetic model was determined by the highest coefficients of determination (R^2). These kinetic equations will provide the VC release mechanism, delivery behaviour from nanocapsules. Besides, the rate constants (k) were obtained from the linear regressions

of these models (Table 2), and they were used to identify the fittest model for the release of VC from the nanocapsules. Both first-order and Higuchi models yielded sufficiently high correlation constants (>0.95), indicating a good fit for the kinetic data. A first-order fit suggests that the release of VC from the nanocapsules was corresponding the sustained-release and matrix diffusion-controlled release. In contrast, a Higuchi fit could represent a diffusing water-soluble drug in a matrix system, where the square root of time-dependent release is associated with the Fickian diffusion (Caccavo *et al.,* 2015; Chiarappa *et al.,* 2017). In summary, the VC release was mediated by diffusion from the GCh matrix, where the VC was electrostatically bound. The diffusion rate was attributed to the GCh-PCNC polymer matrix's strength due to cross-linking for the lowest VC release.

Table 4.2. Rate and correlation constants for both VC-GCh-PCNC and VC-GCh-TPP nanocapsules fit zero-order, first-order, and Higuchi mathematical models.

Nanocapsule	Zero-Order		First-Order		Higuchi	
	K_0 (h^{-1})	R^2	K_1 (h^{-1})	R^2	K_H ($h^{-0.5}$)	R^2
VC-GCh-PCNC	0.05	0.92	3×10^{-4}	0.97	0.77	0.96
VC-GCh-TPP	0.17	0.91	1.70×10^{-3}	0.97	2.79	0.95

* K_0 is the zero-order release constant.
* K_1 is the first-order release constant.
* K_H is the Higuchi dissolution constant.

Theoretically, as depicted in Fig. 4.4A, orally swallowed food passes through the esophagus to reach the stomach in several seconds. The food remains in the stomach and is digested by

the gastric acid and enzymes (pH 1-3, 1.5-4 h), after which it enters the duodenum, and the small intestine via peristalsis, induced by a series of muscular contractions. It is mixed with digestive juices and enzymes from the pancreas, liver, and intestine (pH 6-8, 1-2 h), where the water and nutrients are absorbed into the bloodstream. As peristalsis continues, the food and fluid movement's conveyed the undigested fractions to the large intestine (pH 5-7, 12-24 h), where the remaining water is absorbed, resulting in the solid stool (McClements, 2010). The digestion of VC occurs similarly, and after ingestion, it will be oxidized to DHA and wholly absorbed in the small intestine (Akyön, 2002). The release profiles of VC-GCh-PCNC in a simulated human digestive system at the specific pH environments and pH 7.4 (control) are shown in Fig. 4.4B. When changing the release medium pH to simulate the conditions of the digestive system, it was observed that a higher cumulative VC release over 8 h compared to the control pH. At 8 h, the digestion simulation had achieved an incremental release of approximately 27%, compared to neutral pH, where less than 10% of the VC was released. Since chitosan and CNC have mucoadhesive properties, they could attach to the mucous membrane and slowly release the VC. Cationic chitosan exhibited high mucoadhesive properties and could bind to negatively charged mucin, resulting in strong mucosal adhesion. Moreover, the high surface area could interact with mucin rather than Tempo-CNF and CNF, and hydrophobic attraction or hydrogen bonding promotes the adhesion of mucin to CNC (Lin *et al.*, 2019). After digestion, Chitosan can be degraded by enzymes, such as lysozyme and human bacterial enzymes in our body fluid, especially in our lungs and colons. Lončarević *et al.* (2017) stated that in the enzymatic digestion process, the

enzyme is first diffused to the solution and partitioned to the surface of the complex. The enzyme adsorbs in the complex initiates the catalytic reaction that resulted in the scission of the macromolecular backbone, and the bioactive substance is then released into bulk solution (Lončarević *et al.*, 2017). If the chitosan complex is porous, then the degradation would occur more rapidly. Hence with the addition of CNC, which acted as reinforcement in the chitosan complex, the degradation and burst releasing were significantly reduced. However, as there is a lack of cellulase intake by the human body, most of the CNC will be excreted, or it could be fermented by gut microflora, such as *Ruminococcus champanellensis* present in the human fecal (Zhang *et al.*, 2018). The pH sensitivity of the nanocapsules is desirable in food preparations to ensure that VC remains encapsulated and protected during storage, whereby in the digestive tract following ingestion, a controlled release is desirable.

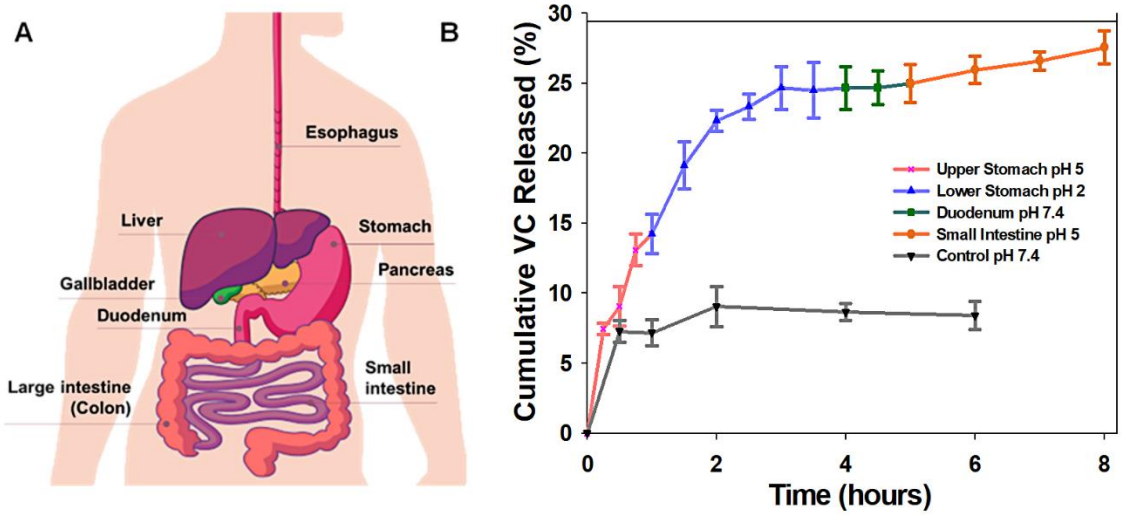

Fig. 4.4 (A): diagram of the human digestive system and (B): *In vitro* simulation of various conditions of the digestive system of VC-GCh-PCNC.

It is well-known that chitosan possesses antibacterial properties against a wide range of microorganisms. The antimicrobial characteristic of chitosan is affected by intrinsic and extrinsic factors, such as strain, pH, ionic strength, molecular weight or degree of deacetylation of chitosan etc. Chitosan loses its antimicrobial function above its pK_a due to the deprotonation of the amino groups and its low solubility in water. However, Atay (2019) claimed that chitosan has limited activity because amino groups in the chitosan backbone can only act as weak positive charge centers (Atay, 2019). Therefore, in this study, we enhanced the antibacterial property by grafting GTMAC to the chitosan backbone to introduce more cationic groups to the chitosan that will bind to the negative cell membrane and kill the bacteria. The range of antimicrobial activities of GCh against *E. coli* and *S. aureus* were both 8 to 16 µg/mL (Fig. 4.5).

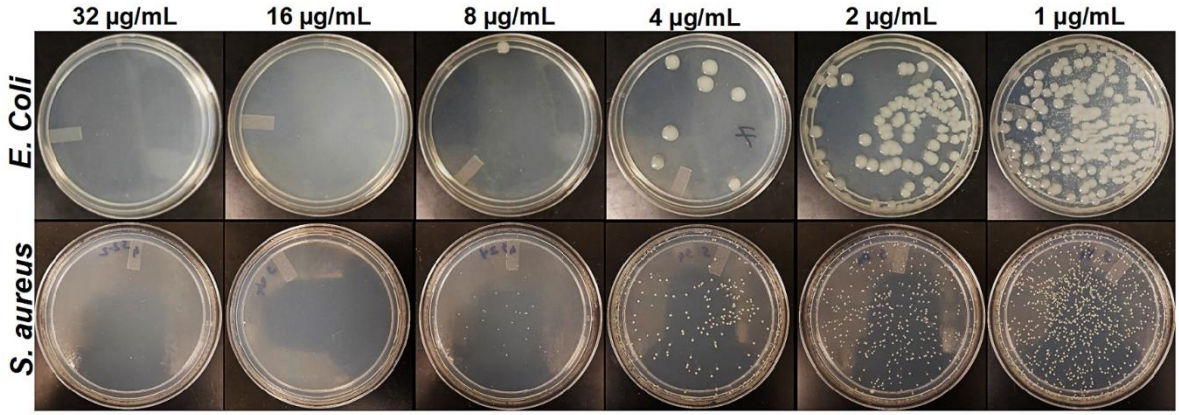

Fig. 4.5 Antimicrobial activity of VC- GCh-PCNC with *E. coli* and with *S. aureus*. (*MIC values of GTMAC-Chitosan for two types of bacteria were 32-64 µg/mL-data not shown).

Other reasons for the antimicrobial effects of the complex are VC has been shown to possess antibacterial property against *S. epidermidis, E. coli and P. aeruginosa* (Pandit *et al*., 2017), and low concentration of VC (0.15 mg/mL) inhibited the growth of *S. aureus* (Mousavi *et al*., 2019). Liping *et al.* (2020) developed water-soluble chitosan with vitamin C complex (CSVC) and confirmed its antibacterial activity against *E. coli*. Compared to the blank control, the MIC of CSVC against *E. coli* was about 5 mg/mL (Liping *et al*., 2020). In this study, due to the quaternary ammonium group and VC presence, the nanocapsule system inhibited the pathogenic bacteria population at minimal concentrations. Thus, VC-GCh-PCNC could sustain against bacteria contamination over a reasonably long period, making them a suitable antimicrobial agent for functional food systems.

4.4 Conclusions

This study examines the stabilization mechanism and effectiveness of PCNC over TPP on improving the stability, encapsulation, and VC release in the VC-GCh-PCNC nanocapsule system. PCNC could effectively stabilize the system via stronger ionic gelation compared to TPP. The stability of VC in the system is highly dependent on light, pH, and dissolved oxygen of the environment. A better kinetic release of VC has been achieved under nitrogen purge. The PCNC cross-linked nanocapsules possessed a sustained release profile, making them ideal candidates for prolonged VC storage. The kinetic release profiles were fitted to the first-order and Higuchi kinetic models (R^2 >0.95), showing a concentration-dependent release from the VC-GCh-PCNC nanocapsule system. A digestive system simulated *in vitro* release

test by varying the pHs, which showed a faster release rate at low pHs that was attributed to the degree of quaternization of GCh. The sedimented VC-GCh-PCNC possessed a higher antioxidant capacity than VC-GCh-TPP. Additionally, the MIC for *E. coli* and *S. aureus* bacterial strains were between 8 and 16 μg/mL, which suggested that the VC-GCh-PCNC nanocapsules were efficient antimicrobial agents that could extend the shelf-life of food systems. These results showed that VC's stability was enhanced in the presence of PCNC, thereby offering a strategy for the preservation of highly unstable compounds (such as VC) during long-term storage in functional food materials.

Chapter 5

Functionalized Ferulic Acid and Cellulose Nanocrystals Stabilized Smart Multiple Pickering Emulsion for Enhanced Probiotics Delivery

The material in this chapter will be comprised part of a patent application and also reformatted into a research paper to be submitted to a journal.

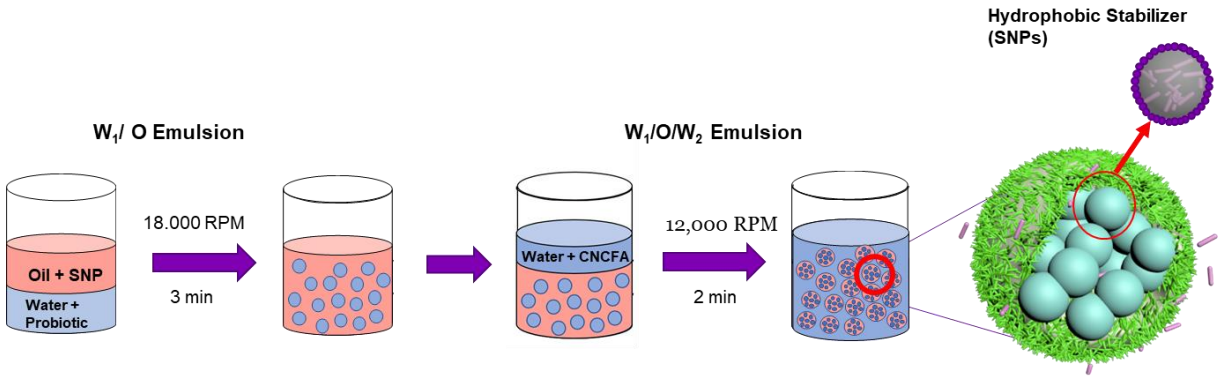

5.1 Introduction

Probiotics effectively inhibit harmful bacteria by secreting antibacterial bacteriocin, lactic acid, intestinal settlement of harmful bacteria, and enhancing immune activity (Yan & Polk, 2011). However, probiotics must survive the gastric acid secreted from the stomach, bile from the gallbladder, and various digestive enzymes from the small intestine. A relatively large amount is recommended to generate a beneficial health effect of probiotics, typically a minimum of 10^6-10^7, a total of 10^8 to 10^9 CFU/g or mL per day (Kechagia *et al.*, 2013). However, adding probiotic cells directly to foods results in a significant reduction in cell viability during storage and passage through the intestinal tract. Therefore, during storage

and digestion, these probiotics may have reduced viability below the recommended levels to achieve the desired health benefits. Thus, probiotics must be encapsulated with another protective material, where encapsulation protects probiotic cells from external environmental factors and promotes bacterial viability during processing, storage and digestion. Moreover, encapsulation may also improve probiotic efficiency by controlling the release of probiotics at the right site of action in the intestine.

Various encapsulation techniques were developed to improve the survivability of probiotics (Shima *et al.*, 2006). One particular method is a multiple emulsion system, where a water-in-oil ($W_{substance}$/O) emulsion is again emulsified in water, resulting in a water-in-oil-in-water ($W_{substance}$/O/W) emulsion. Recently, the multiple emulsion has been developed in various forms, such as O/W/O and W/O/W, depending on the applications. W/O/W type emulsions are the most preferred choice for various industries over O/W/O type emulsions due to limitations, such as solubility. Typically, W/O/W emulsions are used in drug delivery systems and food applications to encapsulate probiotics, vitamins and minerals (Muschiolik & Dickinson, 2017). W/O/W emulsions can be produced in two steps. First, a stable W/O emulsion is prepared with a hydrophobic emulsifier at higher shear forces and then re-dispersed in a hydrophilic emulsifier solution at a lower shear force. This is done because when a high shear force is applied in the second step, the coalescence of the W/O encapsulants can occur due to the merging of the internal water droplets and the rupture of the oil phase film (Ortiz *et al*., 2020; Thompson *et al*., 2015; Zou *et al*., 2013).

However, conventional surfactants, such as surface-active low molecular weight polymers, have food safety issues and high costs (Sharma, 2014). Due to these limitations, interest in the utilization of naturally derived and food-grade emulsifiers is on the rise. One example of the utilization of natural-based nanoparticles as an emulsifier is Pickering emulsions, which are stabilized by solid nanoparticles (Baek *et al.*, 2019; McClements *et al.*, 2017). These nanoparticles strongly bind and accumulate at the oil-water or water-oil interface to produce a rigid barrier that minimizes the coalescence and increasing stability when compared to conventional surfactants. Moreover, food-grade solid nanoparticles, including cellulose nanocrystals (CNCs), have no toxicity, leading to higher safety for *in vivo* applications. CNCs are produced by acid hydrolysis of cellulose fibers with lengths ranging from 100-250 nm. It is considered one of the preferred candidates for Pickering emulsion preparation due to its low cost, biocompatibility, sustainability, and adaptable surface modifications, which have been successfully manipulated in food emulsion systems (Tang *et al.*, 2016).

FA has many beneficial effects on health, and food industries have been utilizing it in their formulations (de Oliveira Silva & Batista, 2017). FA has been approved as a food preservative and natural antioxidant (Adeyemi *et al*., 2019; Mota *et al*., 2008). It is being used in Japan to preserve oranges and to prevent the autoxidation of linseed oil (Ou & Kwok, 2004). It has also been used to maintain the green colour of peas and avoid discoloration of green tea and bananas. The recommendation of daily intake is approximately 150–250 mg/day due to its low toxicity (Gohil *et al*., 2012; Lin *et al*., 2013).

Up to now, there are no data available for the use of modified FA as a Pickering emulsion stabilizer. The CNCs are highly applicable and sustainable emerging nanomaterials suitable for use as novel emulsifiers in food applications. This chapter presents a synergistic approach by combining FA and CNC to provide a better alternative to improve emulsifiers and encapsulate active probiotics within an emulsion. This modification utilizes the dissociation constant of the phenolic acid, and with the pH-sensitive deprotonation, the emulsion can be induced to break and release the probiotics in neutral or basic pH. The successful release of probiotics in a high pH environment offers a strategy to deliver appropriate treatments *in vivo* that is beneficial to intestinal health. Furthermore, these are properties that would greatly expand their applicability for food and biomedical applications.

5.2 Materials and Methods

5.2.1 Materials

Trans-Ferulic acid (FA, MW=194.18, 99%), corn starch, baker's yeast (*Saccharomyces cerevisiae*) 1,1-diphenyl-2-picryl hydrazyl (DPPH), hydrochloric acid, sodium hydroxide, and Nile red were purchased from Sigma-Aldrich (St. Louis, MO, U.S.A.). Cellulose nanocrystals (CNCs) were provided by CelluForce Inc. (Montreal, Canada). 100% reagent alcohol was purchased from Fisherbrand (HistoPrep™, Fisher, Ottawa, ON, Canada or Pittsburgh, PA), and vegetable oil was purchased from a local market in Waterloo (ON, Canada).

5.2.2 Preparation of CNCFA

To conduct the binding capacity, 1 g of CNCs and 10, 20, 40, 60, 80 and 100 mg of FA were dispersed in 0.8 mL and 2 mL of reagent alcohol, respectively. The FA solution was introduced into the CNC suspension, followed by stirring for 24 h. The suspensions were dried in the oven at 35 °C for 24 h. After drying, the CNCFA powder was re-dispersed in 200 mL of pH solutions range from pH 1-8, mixing for 24 h.

5.2.3 Preparation of SNPs

To replace synthetic emulsifiers with natural hydrophobic emulsifiers for W/O emulsion systems, the starch nanoparticles were prepared using a nanoprecipitation method, adapted and modified from the protocol described by Qin *et al*. (2016). Five grams of corn starch was dispersed in 100 mL of Milli-Q water in a round flask and heated at 90 °C to produce a gelatinized solution. After 1 h, the temperature was set to 70 °C. A hundred millilitres of ethanol was added dropwise to the gelatinized starch suspension with constant stirring (500 rpm) for 2 h. The suspensions were washed using ethanol at least 3 times by centrifugation (7000 rpm/ 7 min). The sediments were dried in the oven at 50 °C for 24 h and then ground to obtain a fine powder. The white, fine powder obtained was characterized and used as a hydrophobic emulsifier.

5.2.4 RPM test

To check the viability of yeast using the SNPs, various homogenizer speeds at 12000, 18000,

20000, and 22000 rpm were applied for 3 min using IKA T-25 high-speed homogenizer at a pH 7.5. The four Pickering emulsions prepared at the various speeds were transferred to the agar plates for serial dilutions. The detailed methods will be discussed in section 5.2.6.8.

5.2.5 Preparation of double Pickering emulsion

Multiple Pickering emulsions (W/O/W) were prepared by a two-step method, and the schematic for the process is shown in Fig. 5.1. A $W_{1,\ yeast}$/O emulsion (ratio 3:7) was first produced stabilized by a hydrophobic emulsifier (modified SNPs), using a high-speed homogenizer (UltraTurrax T25 homogenizer, IKA, Germany) at 18,000 rpm for 3 mins. In the second emulsification step, $W_{1,\ yeast}$/O/$W_{2,\ CNCFA}$ emulsions were obtained with the same high-speed homogenizer at 12,000 rpm for 2 mins. The emulsion ratio was 3:7 ($W_{1,\ yeast}$/O/$W_{2,\ CNCFA}$), and CNCFA nanoparticles were used as the hydrophilic emulsifiers. To distinguish the oil and water phase, 1 mg/mL of Nile red, a hydrophobic dye, was used to produce the fluorescence in the oil phase. The pH of the emulsions was adjusted to 2 and 7.5 to mimic the gastric and intestinal pH, and the viability of yeast was evaluated. All the samples were examined immediately using the optical microscope.

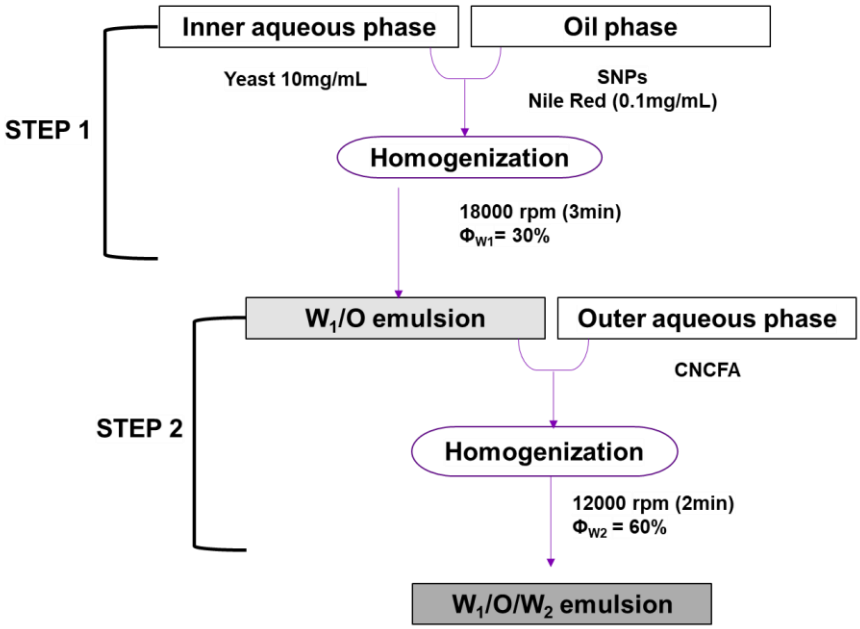

Fig. 5.1 The schematic for the process of multiple Pickering emulsion (W/O/W).

5.2.6 Characterization of the nanoparticles

5.2.6.1 Size and zeta-potential analysis

The size and surface charge of CNC, CNCFA and SNPs at different pH were performed using a Zetasizer (Malvern, Nano ZS90, UK). Each sample was diluted 10 times and measured in triplicates.

5.2.6.2 The adsorption of CNCFA

The CNCFA is formed by hydrogen bonding while both CNCs and FA components are stirred for 24 h. The instruments, UV-vis (Agilent 8453 UV-visible spectrophotometer, Santa Clara, CA, USA) was used to confirm that FA had adsorbed onto CNCs. For the UV test, all the samples were placed in quartz cuvettes (Hellma Analytics), and the spectra were recorded

over the wavelength range of 200 to 400nm. They were filtered using the 10 ml ultrafiltration cell with a 0.1 μm filter membrane to remove unbounded FA. For the measurement purposes regarding the characterization of FA, filtration was used; however, FA will not be filtered for further experiments as free FA acts as a super antioxidant.

The adsorption equilibrium capacity (q_e) was calculated according to equation (5.1) (Dávila-Guzman *et al.*, 2012):

$$q_e = \frac{(C_0 - C_e)V}{m} \quad (5.1)$$

where C_0 is the initial FA concentration and C_e is the equilibrium concentration after 24 h; V is the solution volume in L, and m is the dry weight of CNC in g.

5.2.6.3 FTIR structure analysis

In order to examine the chemical structures of CNC, FA, and CNCFA, FTIR analysis was performed using a Bruker Tensor 27 FTIR spectrometer (Bruker, Billerica, MA, USA). The spectrum of each sample was recorded as the average of 32 scans at 4 cm^{-1} resolution at 25 °C, using KBr-pellets as blank.

5.2.6.4 Free radical scavenging activity

The 2,2-diphenyl-1-picrylhydrazyl (DPPH) assay was conducted to measure the free radical scavenging activity of FA and CNCFA at pH 2 and 7.5 as a function of time. A DPPH solution (0.025mg/mL) was prepared in methanol and covered with aluminum foil to prevent light exposure. 1.5 mL of FA or CNCFA sample was added to 10 mL of the prepared DPPH

solution in an aluminum foil-covered vial, and the sample was stirred on a magnetic mixer. All the absorbances were measured at 517 nm at different times (0, 5, 10, 15, 20, 25, and 30 min) using a Cary 100 Bio UV-Vis Spectrophotometer. The scavenging activity was calculated using equation (5.2):

$$SA\% = \frac{A_{control} - A_{sample}}{A_{control}} \times 100\% \quad (5.2)$$

5.2.6.5 Transmission electron microscopy

The morphology of the modified SNPs was examined using a transmission electron microscope (TEM, Philips CM10 electron microscopy, an acceleration voltage of 60 kV). One drop of diluted suspensions was placed on a carbon-coated copper grid (200 mesh), air-dried and examined under TEM.

5.2.6.6 Contact angle

The measurement of contact angles of CNC, CNCFA, SNPs was performed using a set-up equipped with a CDD camera. All the sample powder was prepared as pellets by a KBr press. 3 μL of water was dropped on the pellets, and then the angle was determined by the CDD camera software, and the measurements were conducted in triplicate.

5.2.6.7 Optical microscope

The morphologies of the Pickering emulsions and yeast within the emulsions were observed by an optical microscope (Nikon Elipse Ti-S, Nikon Instruments Inc., USA) equipped with

a CCD camera (QImaging Retiga 2000R) and confocal microscope (Zeiss LSM 510 Meta Laser Scanning Confocal Microscope (CLSM). For the yeast test, one colony on the plate was swabbed by a sterile swab dispersed in PBS (pH 2 and 7.5).

5.2.6.8 Final yeast CFU enumeration at different pH

To prepare serial dilutions, 90 μL of PBS was placed into 10^{-1} to 10^{-8} microcentrifuge tubes, then 10 μL from the prepared W/O/W emulsions in pH 2 and 7.5 solutions were transferred to the first microcentrifuge tube. The diluted samples were vortexed to achieve a uniform mixture, and 10 μL of this mixture was transferred from the first tube to the second tube in the series. Upon the completion of serial dilution, 100 μL of samples were added to the agar plate to perform measurements in triplicate. Sterilized glass beads were used to spread the contents of the serial dilution in each plate. Upon completion of plating, each plate was incubated at 40 °C for 48 h.

5.2.6.9 Statistical analysis

All experiments were performed as three independent preparation, and the results were expressed as the average with error bars of ± standard deviations.

5.3 Results and discussion

In this study, the role of FA in the newly formed CNCFA and the interactions between FA and CNC were studied. The antioxidant property and stability of Pickering emulsion were demonstrated by adsorbing FA onto the CNC surface, forming a food-grade emulsifier.

Ferulic acid (FA), 4-hydroxy-3-methoxy benzoic acid, is abundantly present in plant cell walls and seeds of plants. It comprises a phenolic compound with a carboxyl group (-COOH), hydroxyl group (-OH) and ethylenic bond (C=C) (Srinivasan *et al*., 2007). The chemical structure of FA below and above *pKa* are shown in Fig. 5.2A. FA is subjected to protonation in an environment where the pH of the solvent is lower than the pK_a (such as a strong acid). Alternatively, the *pKa* dissociation values can describe the adsorption behaviour of the phenolic acid. When the pH of the solvent is greater than the *pKa* (between pH 4.5-4.72), the -COOH conjugated to phenol ring will deprotonate (COO^-) and dissociate into the ionized form (Al Arni *et al*., 2010). Dávila-Guzman *et al*. (2012) state that at pH <4, FA is non-ionic, where it can be better bound to an adsorbent. Moreover, at solution pH greater than 4, the ferulic acid is partially ionized and becomes an ion-ferulate, reducing the FA adsorption due to the repulsive force between the FA compound and the adsorbent (Dávila-Guzman *et al*., 2012). The UV-Vis results shown in Fig. 5.2B confirmed this behaviour, where the UV spectrum of FA over the range of 200-400 nm exhibited two peaks at 215 and 322 nm, but the hypsochromic shifting of the maximum absorption band from 322 to 280 nm is due to dissociation of the carboxyl groups (Carunchio *et al.*, 2001).

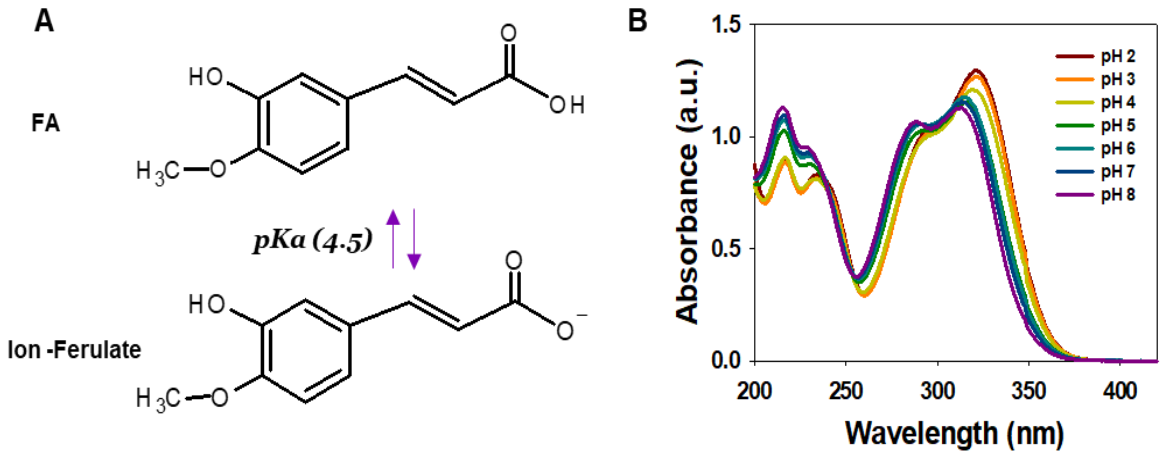

Fig. 5.2 A) The chemical structure of FA below and above *pKa* value (pH 4.5) and B) absorbance spectra of FA, the effect of pH changes from 2 to 7.5.

Using ethanol to prepare CNCFA is suitable to increase the solubility of FA and the binding interactions between CNC and FA since FA is poorly soluble in water (0.78 g/L at room temperature) (Wang *et al.*, 2021). Fig. 5.3. shows the redispersion of CNCFA powder containing different concentrations of FA in Milli-Q water (pH 4, below *pKa*). When the concentration was increased, the CNCFA dispersions became opaque, and un-bound FA or un-dissolved crystal (Das & Wong, 2020) was found floating on the edge of the bottle. To examine the use of this emulsifier in the multiple Pickering emulsion, an O/W emulsion was prepared, and the morphologies of the emulsion were observed using an optical microscope. As a result, the emulsion containing 80 and 100 mg displayed an irregular shape and size distribution. This is assumed that two different sizes (CNCFA and unbound FA crystal) stabilizers may not stabilize the emulsion, inducing coalescence of the O/W emulsion. This makes lower coverage efficiency of water droplets. (Zembyla *et al.*, 2019).

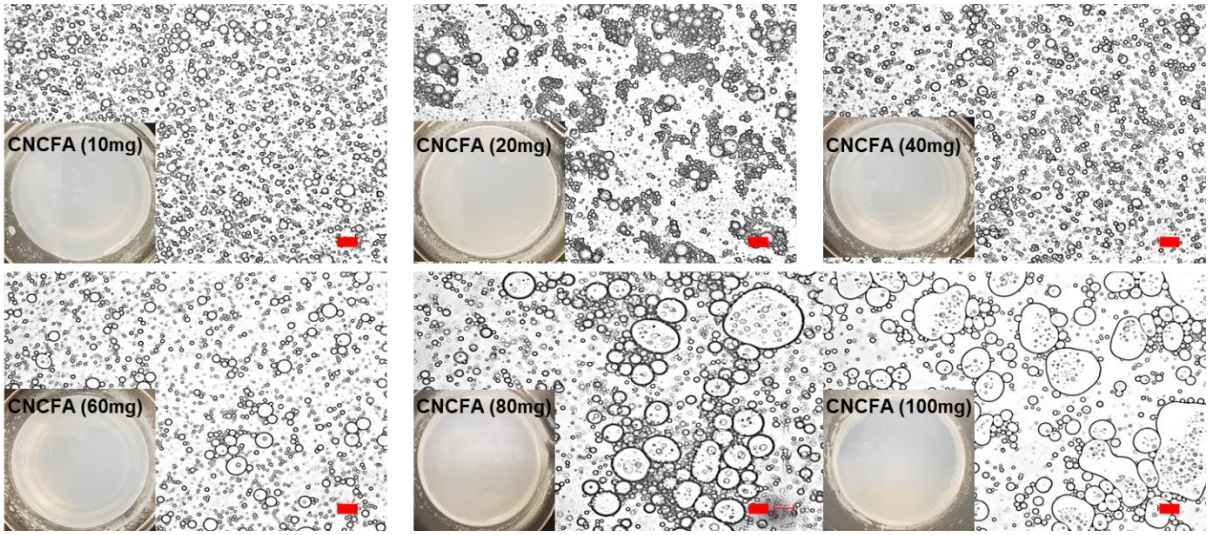

Fig. 5.3 CNCFA dispersions containing different concentrations of FA (10-100 mg) and optical microscope images of O/W Pickering emulsions (Scale bar: 20μm).

As the optimal concentration, 60 mg of CNCFA was selected because it produced a stable emulsion, and a higher CNC coating will generate a higher antioxidant effect, which will be further examined. The particle size and zeta-potential of CNC and CNCFA were conducted to elucidate the FA binding capabilities on CNC. As shown in Fig. 5.4A, the CNC at all pH ranges of 1 to 8 possessed a negative zeta-potential at all pHs due to the sulphate ester groups on the surface. At a low pH of 1, the zeta potential of the CNC suspension increased to -10 mV since the *pKa* of the sulfuric acid groups was about 1.9. Therefore, the protonation of the sulfate group reduced the net charge below its *pKa*. Interestingly, at a pH of 7, the zeta potential increased to -40 mV. Qi *et al.* (2019) explained that the electron shielding occurred with the addition of Na^+, resulting in a reduction in the zeta potential of CNC. However, at the same concentration, the effect of HCl on the zeta potential of a CNC suspension was

higher than NaOH owing to reduced crystallinity, which was less reactive to ions upon the addition of -OH (Qi *et al.*, 2019). On the other hand, in terms of the size of CNC dispersion at different pH levels, CNC aggregation yielding particle size of 900 nm was observed below the *pKa* value. The attractive force induced by hydrogen bonding between CNC and FA is greater than the repulsive force. When pH was increased from 2 to 8, the particle sizes remained constant at around 100 nm. In Fig. 5.4B, CNCFA dispersion at different pHs displayed a similar trend of size and zeta-potential as the CNC dispersion. Still, with a slight difference, it showed a slightly larger size due to the adsorption FA to CNC by hydrogen bonding, hydrophobic interaction and lower zeta-potential values below the *pKa* value of FA. Therefore, when at a condition above the *pKa* (>4.2) of CNCFA, the FA in CNCFA would detach from the CNCs surface since the CNCs possessed negative charges as a result of the sulfate groups. Therefore, the changes in the adsorption of phenolic acid may vary depending on the pH and salt concentration.

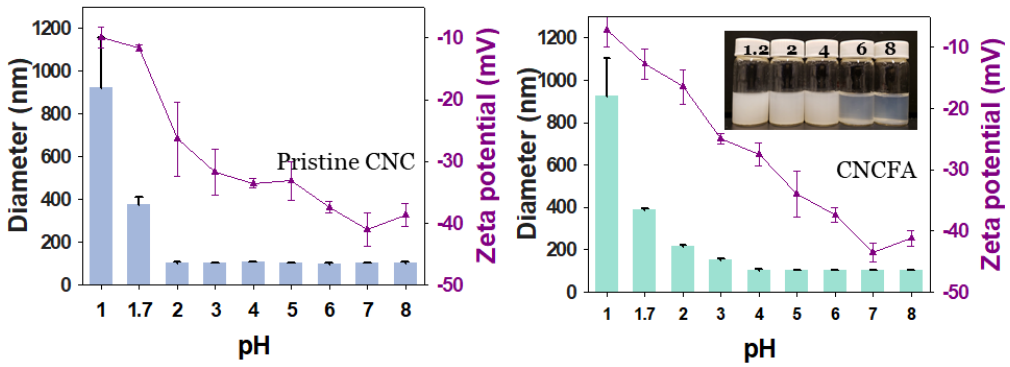

Fig. 5.4 A) Particle size and zeta-potential of CNC from pH 1-8 and B) particle size and zeta-potential of CNCFA from pH 1-8.

To understand the strengthening mechanism of CNCFA nanoparticles, the binding mechanism of FA with CNC should be elucidated. The interactions between FA and CNC are dominated by hydrogen bonding and hydrophobic interactions. Hydrogen bonding has been considered to be the main driving force towards the formation of CNCFA. It can be explained by the abundance of –OH groups on both the FA and CNC, where the –COOH groups below the *pKa* values would form hydrogen bonds with the OH groups, as shown in Figure 5.5. The hydrogen bonding between the FA facilitated the coating of FA onto CNC that yielded an apparently more hydrophobic CNCFA system below the *pKa* value. This may allow it to interact with its surroundings or surfaces via hydrophobic forces (Fig. 5.5), which could involve a benzene ring of FA and hydrophobic sites of CNC, (200) lattice plane (Bruel *et al.*, 2019). Chang *et al.* (2020) combined protein ovalbumin (OVA) and FA via hydrophobic interaction and hydrogen bonds and measured the surface hydrophobicity FA-OVA using ANS method (1-anilinonaphthalene-8-fulfonic acid), which is a fluorescent probe that could reveal the hydrophobic sites in the protein by a Fluor Spectrophotometer. When the concentration of FA was increased from 1:1 to 1:40, the hydrophobicity of surface (H_o) decreased from 693.69 to 577.65. Since unmodified OVA is hydrophobic (716.39), FA binds to the hydrophobic part of amino acid on OVA via hydrophobic interaction, resulting in the reduction of the hydrophobic site (Chang *et al.*, 2020).

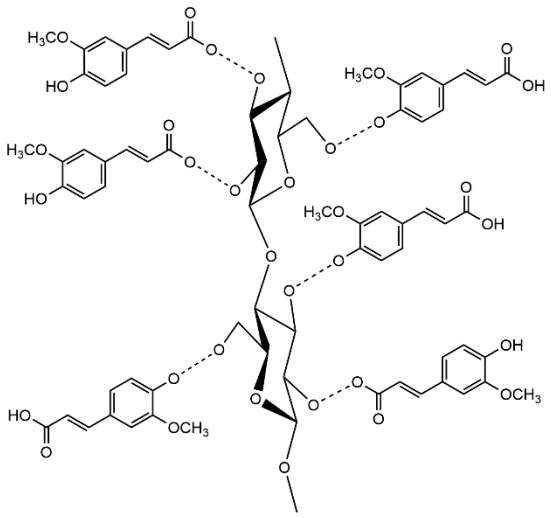

Fig. 5.5 The chemical structure of CNCFA by hydrogen bonding.

Fig. 5.6A shows the adsorption capacity for FA on CNC at various pH values. Below the *pKa*, the highest adsorption was observed, and the maximum adsorption number was 1.91 mg FA/g of CNC. On the other hand, at high pH, we observed a reduction in the adsorption capacity of FA with a value of 0.03 mg FA/g of CNC since FA became ionic due to the deprotonation of the carboxyl groups. Many researchers have reported on the adsorption capacity of ferulic acid on the different types of resin, such as zeolite (139 mg/g (Simon *et al.*, 2015) and 203.2 mg/g (Thiel *et al.*, 2013)), XAD7HP (63.6 mg/g) (Thiel *et al.*, 2013), amberlite resin XAD16 (19 mg/g (Simon *et al.*, 2015) and 133 mg/g (Dávila-Guzman *et al.*, 2012)) as an inorganic adsorbent at different pH and time. Moreover, there are few studies using dietary fibers (DFs), such as cellulose and xylan, at digestion environment at pH 2 (stomach chyme), 4.5 (arithmetic), and 7 (ileum chyme). Each DFs were prepared at different pH conditions using buffers. FA was first dissolved in ethanol and then transferred to buffers

with a 4% final ethanol concentration. The ratio of FA (100 mg/L) to DFs was 1:50. At pH of 2, the maximum adsorption was 0.529 mg/100 mg of cellulose and 0.568 mg/100 mg of xylan. However, the author claimed that the FA adsorption onto DFs displayed lower than the synthetic macroporous resin (11.7 mg/100 mg) due to the higher specific area of macroporous resins of between 400 and 1200 m^2/g, compared to a lower specific area in microcrystalline cellulose, 2.39 m^2/g (Costa *et al.*, 2015).

The contact angle of native cellulose and modified CNCFA were investigated using water contact measurements. Fig. 5.6B shows that the pristine CNC possessed a low contact angle of 32° because cellulose is interconnected by hydrogen bonding between -OH groups of CNC and water molecules, resulting in a relatively flat droplet (Trinh & Mekonnen, 2018). Whereas the contact angle of CNCFA increased to 70° with the carboxyl groups, leading to more hydrophobicity. Chartrand *et al.* (2017) developed modified microcrystalline cellulose (MCC) with FA via esterification, resulting in benzyl ring and hydroxyl groups on the hydrophilic MCC. They conducted water contact angle measurements, and MCC (45°) with FA displayed a contact angle of 67° (Chartrand *et al.*, 2017). The anticipated CNCFA at pH 2 and 7.5 is illustrated schematically in Fig. 5.6C. Based on the results of several tests, FA was bound to CNC, and it became gel-like through hydrogen bonding in acidic conditions. On the other hand, at pH 7.5, most FA was desorbed from the CNCs due to the repulsive forces.

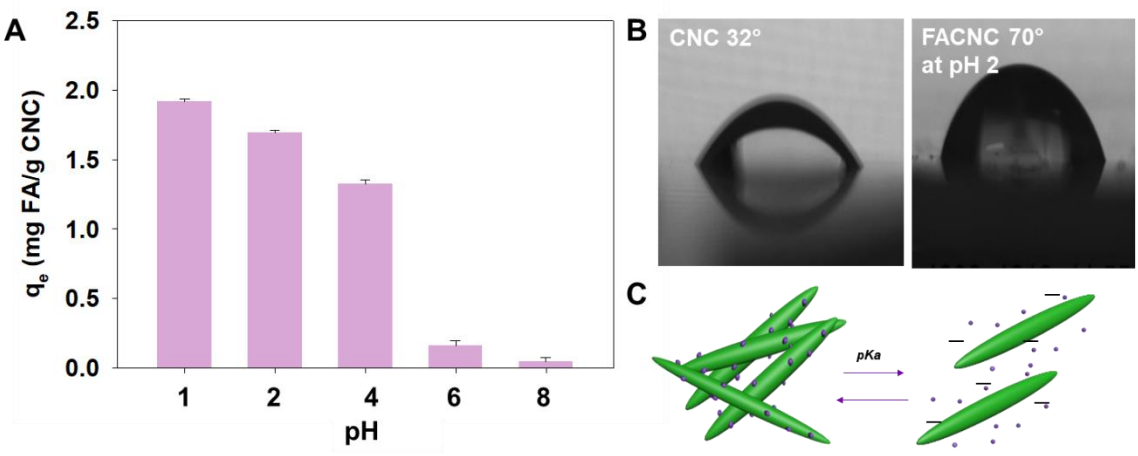

Fig. 5.6 A) Influence of pH on maximum adsorption capacity of FA on CNC, B) images of contact angles of native CNC and CNCFA, and C) schematic illustration demonstrating the *pKa* of FA.

The interaction between FA and CNC is controlled by non-covalent interactions, such as hydrogen bonding, which occurs between H-receptor sites on the CNC and the hydroxyl group/carboxyl groups of FA. Hydrophobic interactions may occur in the bonding between the phenyl ring of FA with the hydrophobic domains on CNC. To evaluate the hydrogen bonding interactions between FA and CNC, FTIR measurements were conducted (Fig. 5.7). Due to the various functional groups, the peaks for the FA before and after adsorption were clearly evident. The peaks of native FA were observed at 3,437 cm^{-1}, which is characteristic of the OH group in phenolic compounds. The broadband at the C-H stretching of the benzene ring is 2,850 cm^{-1} band. After modified CNC with FA, new peaks were observed at 3394 (-OH) and 651 (phenolic hydroxyl) cm^{-1} due to the formation of hydrogen bonding between

FA and CNC, which reduced the –OH groups of CNC, leading to the shift and narrowing of their vibration frequencies (Hu *et al.*, 2017; Panwar *et al.*, 2016).

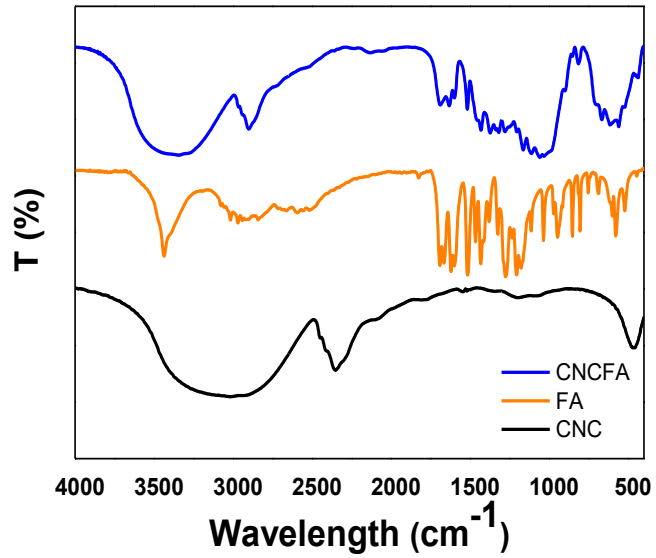

Fig. 5.7 FTIR spectra of CNC, FA, and CNCFA.

Starch is a biodegradable, renewable and natural polymer found in crops and cereals (e.g. rice, maize, wheat, corn, tapioca, potato) (Jimenez *et al.*, 2012). It is widely used in food and pharmaceuticals owing to its various functions, such as thickener, stabilizer and gelling agent (Berski *et al.*, 2011). However, according to Vanier *et al*. (2020), starch is physically weak or easily gelatinized and has limitations due to retrogradation during storage and processing (Vanier *et al.*, 2020). A higher concentration of starch (maize and wheat) is needed for beverage emulsions compared to conventional surfactants, such as Tween-20, to prepare a stable emulsion. The remaining starch in the aqueous phase was the result of emulsion instability that induced creaming and flocculation between oil droplets. Recently, it has been

reported that starch nanoparticles/nanocrystals with a small size can be a suitable *Pickering emulsion stabilizer*. To improve the hydrophobicity of starch nanoparticles for adsorption at oil-water interface, modified starches, such as octenyl succinic anhydride (OSA) has been reported (Ge *et al.*, 2017).

In this study, to confirm the morphology and mean size of the modified SNPs, TEM and Zetasizer were used. To conduct the wettability of SNPs at different pHs, a contact angle instrument was used. The results shown in Fig. 5.8A and B were consistent with the TEM images, as most particles were uniform with spherical particles at a diameter of 130 nm at a pH of 2. Moreover, the PDI value was about 0.41, indicating that the SNPs distribution was homogenous (Table 5.1).

Table 5.1 Particle size and zeta-potential of SNPs at pH 2 and 7.5.

	pH 2 (A)	pH 7.5 (B)
Size (nm)	138.6 ± 0.6	3760 ± 138
PDI	0.418	1
Zeta-potential (mV)	-8.34 ± 0.8	-12.5 ± 1.5

Theoretically, when the angle of the emulsifier is 90°, the stabilization energy of the emulsion is high; and the particle would be in contact with the two opposing phases without bias so that the surface shape of the droplet can be effectively maintained. However, some agglomeration was observed for the particles due to the high energy of ultrasonication, which could cause the modified SNP to break down and swell. On the contrary, at a pH of 7.5 and

with high alkaline treatment, no spherical particles were evident, and only a heterogeneous matrix was observed (Fig. 5.8C). This is because alkaline materials, such as urea or NaOH, destroyed the crystalline structure and increased the solubility, whereas the minimum acid solubility of starch was observed at low pH.

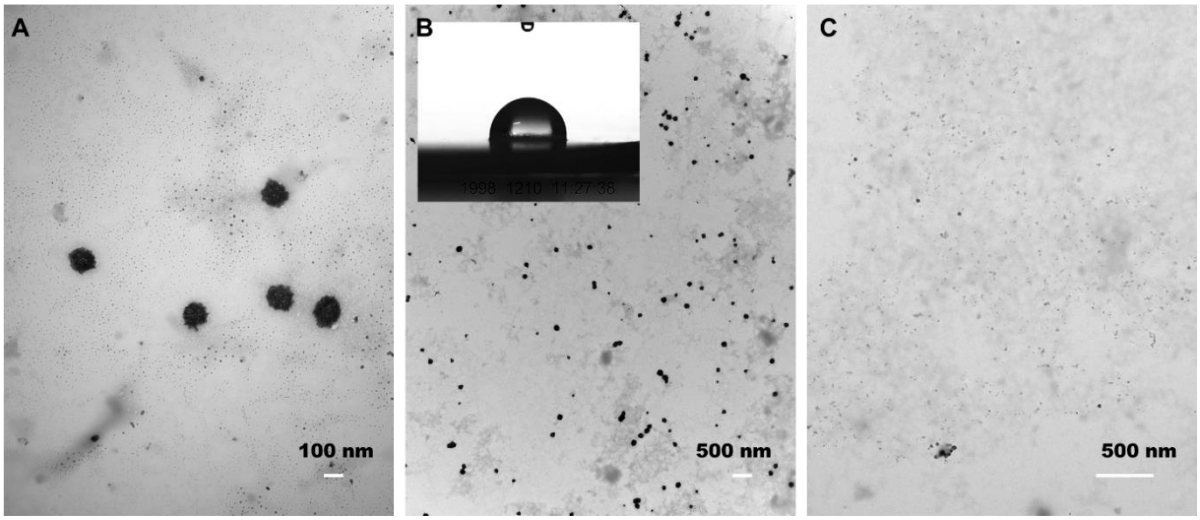

Fig. 5.8 The TEM images of SNPs at A) & B) at pH 2 and C) at pH 7.5 and contact angle of SNPs at pH 2.

DPPH (2,2-diphenyl-1-picrylhydrazyl) is a purple compound that reacts rapidly with antioxidants. Thus, to measure the DPPH radical reduction hydrogen-donating ability through a colour change from purple to yellow. The electron-donating capability was measured at 517 nm and is expressed as the antioxidant power. The results of measuring the DPPH radical scavenging activity of FA, non-filtered CNCFA at pH 2 and 7.5 and filtered CNCFA at pH 2 and 7.5 are shown in Fig. 5.9. The FA Scavenging activity (% SA) was

99.1% at 30 min, showing the highest antioxidant activity. The antioxidant activity of FA is caused by the proton transfer from the phenolic and unsaturated carboxyl groups to the DPPH radicals. Ferulic acid, which is a derivative of hydroxycinnamic acid, has higher antioxidant property than hydroxybenzoic acids, such as vanillic acid. FA is a powerful antioxidant that neutralizes free radicals and inhibits reactive oxygen species (ROS) or nitrogen to protect living organisms due to these functional groups. The phenoxy and hydroxy groups of FA donate electrons to remove the free radicals. In addition, the FA's benzene ring hinders the free radical reaction, and the carboxyl groups also attack the free radical site, preventing the premature oxidation of DNA and lipids as this group binds to the lipid bilayer (Srinivasan *et al.*, 2007). This is due to the presence of (-CH=CH-) between the phenyl ring and the carboxyl group, inducing stronger hydrogen donating capacity (Al Jitan *et al.*, 2018). As it is known that the FA has a strong antioxidant effect, displaying an excellent antioxidation effect in 1 minute and almost 94% in 30 minutes. Surprisingly, CNCFA at pH 7.5 showed a similar effect to FA, but it had a little antioxidant effect after filtration. This suggests that most of the FA were bound to the CNCs. Regarding CNCFA at pH 2, almost 60% of the results were observed in 30 min both before and after the filtration.

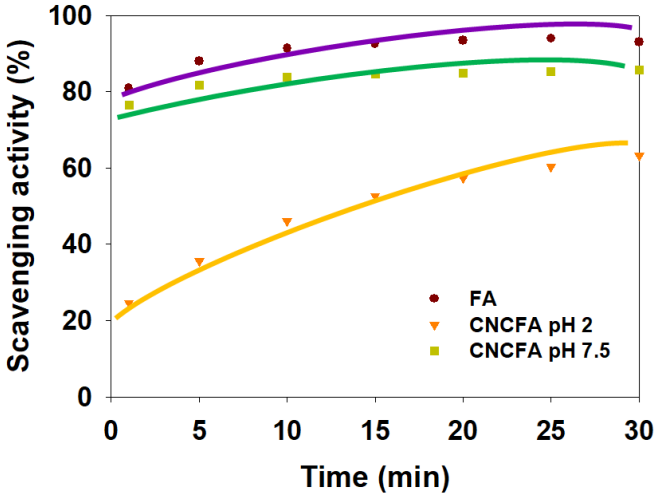

Fig. 5.9 The free-radical scavenging activity of FA and CNCFA at pH 2 and 7.5 by DPPH assay.

The multiple Pickering emulsions (W/O/W) containing yeast at different pHs were observed through an optical microscope. The main parameters examined in this study consisted of food-grade emulsifiers, CNCFA and SNPs, where they absorbed rapidly at the oil-water interface and reduced the interfacial tension. The release of bioactive compounds (e.g., probiotics) can be achieved by destabilizing the emulsions at neutral to basic pH found in the intestine, which caused the deprotonation of the carboxyl groups of FA and destabilized the emulsion droplets. Besides, another critical factor of the multiple emulsion in the preparation step is to find the optimal speed of the high-speed homogenizer. The higher driving force caused the breakage of emulsion, followed by the release of active substances and induced the coalescence of the droplets that resulted in phase separation. The purpose of this study is to enable the probiotics to safely pass through the stomach with strong gastric acid as the

emulsions remained stable in low pH conditions. However, the insufficient mixing speed induced the emulsion phase to separate within a short period of time during processing and storage, which reduced the viability of the probiotics. As shown in Fig. 5.10A and B, the highest viabilities were observed at 12,000 and 18,000, which yielded 2.23 x 10^7 CFU/mL and 2.12 x 10^7 CFU/mL, respectively. Ding and Shah (2009) investigated the homogenization technique using two different homogenization machines, a high-speed homogenizer and a Microfluidics microfluidizer, to reduce the size of calcium alginate beads. Various settings were used in the homogenization study, such as speed (rpm), duration (min), and pressure (psi). Both homogenization techniques reduced the microcapsule size, but the higher speed and longer time significantly reduced the viability of the probiotics. This is because the probiotics are susceptible to high mechanical shearing stress and sensitive to external stress, such as heat and oxygen, during the homogenization (Capela *et al.*, 2007; Ding & Shah, 2009). Therefore, optimal condition tests are required to maintain the viability of the probiotic, which depends on the machine time and species of probiotic microorganisms.

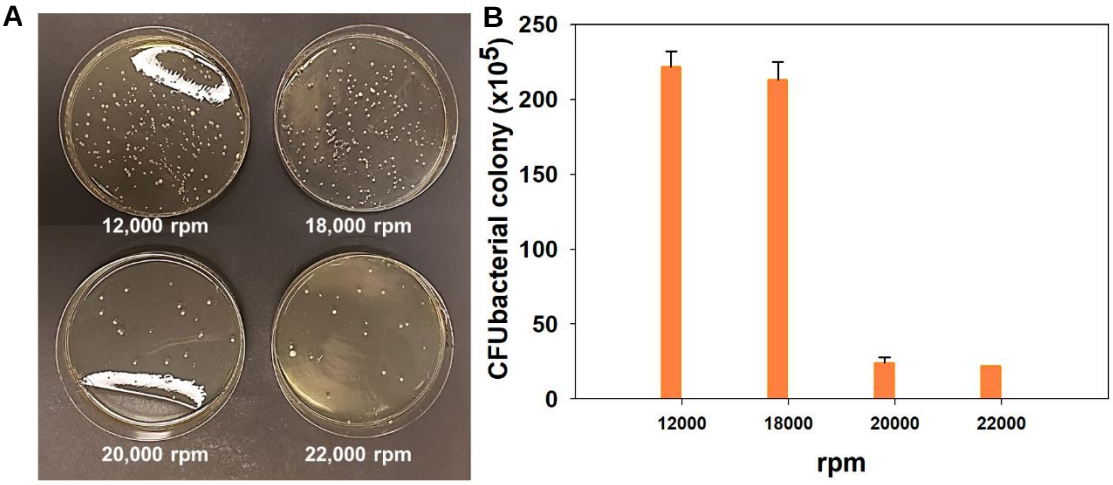

Fig. 5.10 Effect of homogenization time with a high-speed homogenizer at various speeds.

The freshly made W/O/W emulsions were transferred to each solution maintained at a pH of 2 and 7.5, and changes in the morphologies were examined (Fig.5.11). The changes of oil droplets of W/O/W Pickering emulsions at different pHs are shown in Fig. 5.11A-D. These results were recorded using an optical microscope based on bright-field microscopy. By comparing the results with the original W/O/W Pickering emulsion (Fig. 5.11B), it was confirmed that the aggregation was enhanced at a pH of 2 (Fig 5.11C). Simultaneously, the oil droplets coalesced, burst, and disappeared when the pH was increased beyond the *pKa* of FA up to a pH of 7.5 (Fig. 5.11D1-D3, time flow observation). It seems that this change is related to the zeta potential value between CNCs and FA. When CNCFA was adsorbed on the oil droplets, the electrostatic repulsive force was reduced at low pH, resulting in aggregation; however, when the pH was increased to 7.5, the electrostatic repulsion also increased causing the emulsion to become unstable due to the detachment of FA.

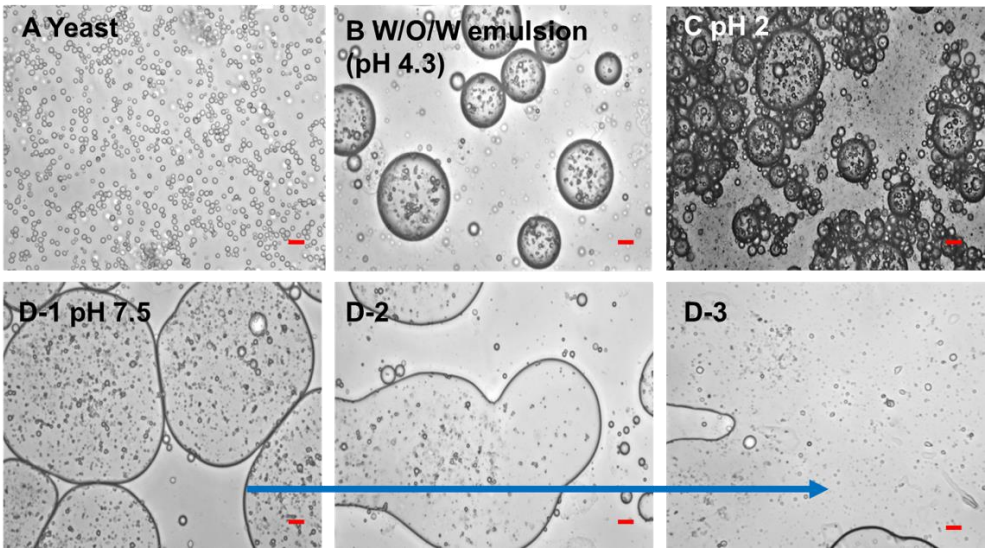

Fig. 5.11 The optical microscope images of A) yeast, B) W/O/W Pickering emulsion at pH 4.3, C) W/O/W Pickering emulsion at pH 2, D-1 to D-3) change in the morphologies of W/O/W Pickering emulsion at 7.5 (scale bar: 20 μm).

The 2-weeks stability test of the multiple Pickering emulsion at pH 2 and 7.5 was conducted, and the results are shown in Fig. 5.12. The emulsion was stable at pH 2 without phase separation. However, separation started when the emulsion was transferred to a high pH solution. The optical microscope images of the Pickering emulsions at pH 2 confirmed that the particles of the emulsion after 2 weeks were still stable. The high stiffness and numerous hydroxyl groups on the CNC acted as a nano-reinforcement and participated in the crosslinking of the hydrogen-bonded structure. Recently, there are many studies on phenolic or polyphenol-based emulsifiers for Pickering emulsions because they not only increased the antioxidant property, but they improved the stability of the emulsion, which was also reported

for gallic acid (GA) or tannic acid in zein nanoparticles. Interestingly, the phenolic nucleus of the polyphenols could be used as Pickering stabilizers for the water-oil interface. A complex consisting of polyphenol and whey protein demonstrated a significant improvement in the stability of the emulsion. Complex formation mechanisms could be associated with hydrogen bonding, hydrophobic or electrostatic attraction between the protein at the interface with the polyphenol particles with opposite charges. Confocal images of the Pickering emulsion stabilized by polyphenol particles and whey protein confirmed the location of the complex at the oil-water interface. The emulsion showed high stability at pH 3 rather than at pH 7 due to the chemical decomposition of polyphenols at alkaline pH, resulting in a weaker complex (Zembyla *et al.*, 2019).

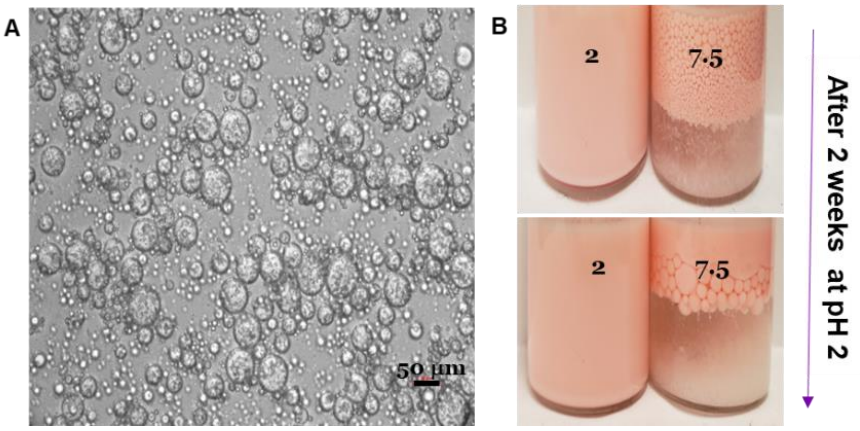

Fig. 5.12 A) Optical microscope images of Pickering emulsions at pH 2 after 2 weeks and B) actual pictures of the Pickering emulsions before and after 2 weeks (scale bar: 50 μm).

Table 5.2 shows the total number of yeasts in the pH-conditioned Pickering emulsions calculated from the standard broth dilution methods. The initial number of utilized yeasts

was 10^8, and the population of 5.7 x 10^6 and 3.14 x 10^7 CFU mg/mL were observed for pH 2 and pH 7.5, respectively. The reduced yeast number obtained at the lower pH value was interestingly different when viewed under the microscope.

Table 5.2 The total number and survivability of yeasts in pH-treated Pickering emulsions.

Initial	pH 2 (10^{-4})	pH 7.5 (10^{-4})
10^8	5.7 x 10^6	3.14 x 10^7
Survivability (%)	84.5 %	93.71 %

After the incubation period, one colony was removed by rolling the swab and transferred to the glass slide to examine the morphologies of the emulsion. Surprisingly, the microscopic observation clearly showed that at pH 2 (Fig. 5.13A-1 and 5.13A-2), the yeast was protected inside the oil droplets, which corresponded to a lower population on the plates. Whereas at the pH of 7.5, more yeast was observed (Fig. 5.13B) with no encapsulating layer because the emulsion droplets broke and released the yeasts at alkaline pH, thus resulting in a higher population on plates.

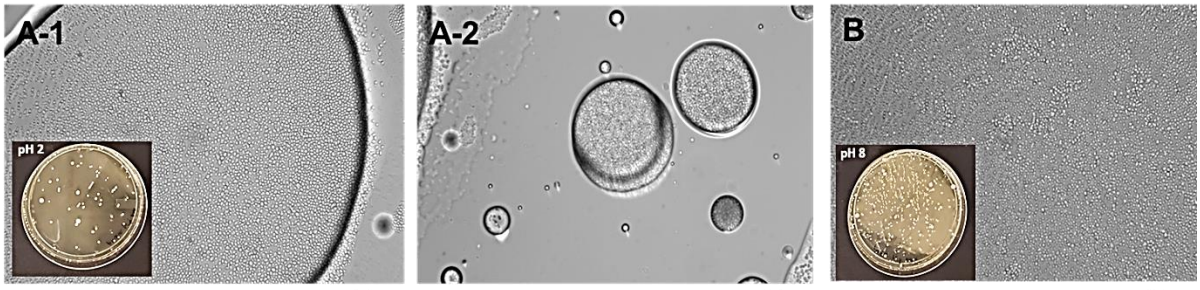

Fig. 5.13 The optical microscope images after swabbing of (A-1 and A-2) yeast at pH 2 and (B) at pH 7.5.

5.4 Conclusions

In this study, functional material ferulic acid, coated on CNC, could function as a stable emulsifier at the oil and water interface. The ferulic acid (FA) functionalized cellulose nanocrystals (CNCs) (CNCFA) was used, where FA acts as an antioxidant and pH-responsive compound to prepare "smart," multiple Pickering emulsion containing yeast with a modified plant-based emulsifier. This modification was adopted such that the dissociation constant of the phenolic acid would induce the deprotonation of the carboxyl groups, causing the emulsion to burst and releasing the probiotics. The viability of yeast during the emulsification process, storage, and intestinal delivery was demonstrated with higher survivability against severe acidic conditions in the stomach (pH 1.5-2.5). The results from this study can be used to prepare various healthy microflora deliverable as a prophylactic or treatment towards inflammation and infection of the intestine. Moreover, the successful release of probiotics in a high pH environment can be safely used to deliver appropriate treatments i*n vivo* to benefit intestinal health.

Chapter 6

A New Approach for the Encapsulation of Probiotics using Shellac and Cellulose Nanocrystals

The material in this chapter will be comprised part of a patent application and also reformatted into a research paper to be submitted to a journal

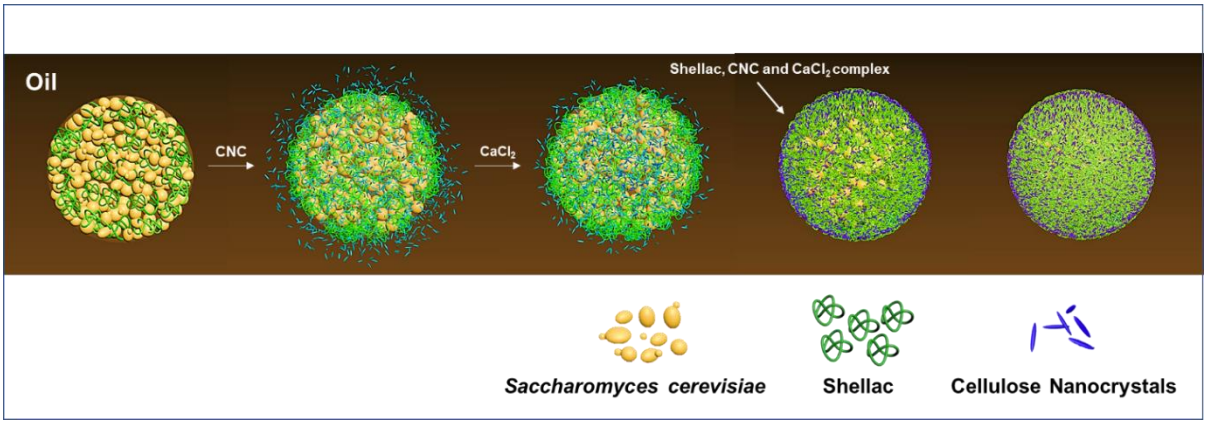

6.1 Introduction

Sustainable coating materials, including polysaccharides, have been widely used in food, pharmaceutical, and agricultural industries for encapsulating active ingredients and molecules (Hategekimana *et al.*, 2015; Jung *et al.*, 2015; Pu *et al.*, 2011). However, these high molecular weight coating materials suffer from a limited dissociation rate due to the polymer chain interactions, resulting in a longer release time. These systems are rendered less desirable due to their high cost, poor barrier performance, and high moisture sensitivity compared to conventional materials, such as petroleum-based polymers. A suitable coating

material should possess self-assembly characteristics with strong interactions and is compatible with the encapsulating materials. It should also function as an amphiphilic material to form microcapsules with the hydrophobic active compounds. Previously, Gemini amphiphiles with lower critical micelle concentrations (CMCs) were synthesized and utilized to prepare microparticles (Song *et al.*, 2013). However, these compounds failed to form a stable encapsulating system due to the lack of intra-molecular polar groups.

Shellac is a natural resin that is approved as a food-safe additive by the U.S Food and Drug Administration (Luangtana-Anan *et al.*, 2010). This alkaline or alcohol soluble *lac* insect resin is hydrophobic, biodegradable, and renewable, making it a suitable candidate for commercial applications (Hamad *et al.*, 2012). The resin's unique chemical structure comprises hydrophilic aleuritic acid and hydrophobic cyclic terpenic acids, connected through ester bonds. Hence it is considered as an amphiphile. Additionally, this resin consists of other functional groups (-CHO, -OH, -COOH), where they can interact with various polymers or chemical components through electrostatic or hydrogen bonding to form a functional biomaterial (Soradech *et al.*, 2012; Tang *et al.*, 2019). Thus, shellac is considered a suitable candidate as a coating material for functional food systems.

Cellulose nanocrystals (CNC) are natural materials with emerging biomedical applications due to their excellent physical, chemical, and biological properties, including biocompatibility and biodegradability (Du *et al.*, 2019; Kim *et al.*, 2019). Cellulose esters-

based adhesive films can strongly interact with drugs through hydrogen bonding. The films' capillary systems expand in the presence of moisture, which weakens the hydrogen bonding network, facilitating the release of the drug or active compounds. Although cellulose polymers have good adhesion characteristics, they are limited by their brittleness, rigid-like structure, hydrophilic character, and weak barrier against water (Hult *et al.*, 2010). These shortcomings can be addressed by utilizing a suitable film-forming material that enhances the composite film formation, structure and permeability. In this study, CNC is used as a suitable film-forming material.

Probiotics are mixed cultures of microorganisms that benefit the host by improving indigenous microflora's wellness, and they are capable of preventing and treating pathological disorders (Gupta & Garg, 2009). The beneficial effects of probiotics are highly dependent on their survival in harsh acidic gastric conditions (pH 1.5-3) and their delivery in the intestinal environment (pH 7-8) (Fioramonti *et al.*, 2003). Additionally, probiotics suffer from detrimental food processing techniques and storage conditions (Tripathi & Giri, 2014). Appropriate encapsulation of probiotics is paramount to provide a suitable physical barrier from harmful conditions that could hinder their maximum viability during the delivery.

Current microencapsulation techniques used for probiotic loading include freeze-drying, spray-drying, electrospinning, emulsification, and extrusion. However, these methods are prone to induce cell lysis due to their high processing temperatures, oxidative stress, organic

or alkaline solvents, and multi-step processes (Cheow & Hadinoto, 2013; Peighambardoust *et al.*, 2011). For example, produced dry probiotics are prone to moisture absorption during storage. The altered glass transition temperature of the coating resulting from this leads to a significant acceleration of inactivation of probiotic bacteria (Passot *et al.*, 2012). Hence, to address these challenges, it is vital to design microcapsules capable of storing the probiotic in a liquid medium, preferably oil, which could preserve the cells throughout the gastrointestinal tract and trigger the release in the intestinal environment.

For the first time, we describe the preparation of novel composite shellac-cellulose nanocrystal microcapsules capable of encapsulating and preserving probiotics from harsh environments. Additionally, a triggered disintegration mechanism of cell release from the microcapsules is realized at intestinal pH conditions and is presented as a proof-of-concept.

6.2 Experimental section

6.2.1 Materials

Shellac (Dewaxed Orange) was ordered from Inoxia Ltd (Cranleigh, United Kingdom). Baker's yeast (*Saccharomyces cerevisiae*), calcium chloride, calcofluor white stain, mucin, pancreatin, pepsin, Nile red and methylene blue (MB) were purchased from Sigma-Aldrich (St. Louis, MO, U.S.A.). Cellulose nanocrystals were provided by CelluForce Inc. (Montreal, Canada). Absolute ethanol and 100% denatured alcohol (with 5% isopropyl alcohol, 5% methyl alcohol, and $\leq$ 0.03% water) were purchased from Fisherbrand HistoPrepTM (Fisher,

Ottawa, ON, Canada or Pittsburgh, PA). Vegetable oil was purchased from a local market in Waterloo (ON, Canada).

6.2.2 Preparation of Shellac dispersion

Four concentrations (2.5, 5, 7.5, and 10 mg/mL) were dissolved in 10 mL of denatured alcohol and redispersed in 190 mL of Milli-Q water to achieve the desired concentration. ShCNC was prepared with 3 mL of shellac dispersion (5 mg/mL in 5% ethanol) and 2% CNC dispersion, and 0.8% $CaCl_2$ solution was added to ShCNC to produce ShCNCCa, which was used for future testing.

6.2.3 CO_2 test

S. cerevisiae produces CO_2 and ethanol as anaerobic by-products in the fermentation when incubated with sugar at the optimum temperature and pH. We developed and utilized a method to assess the yeast activity by recording the CO_2 release using an in-house assembled apparatus (Fig. 6.1). The hot plate was set to 40 °C to promote the metabolism of yeast in the presence of glucose at 400 rpm. It was conducted at four pHs (2, 5, 7.5, 8 and 9.3) to measure the CO_2 production in order to assess the viability of the yeast. The test was performed by incubating 50 mg of Baker's yeast with 50 mg D-glucose in 5 mL Milli-Q water. Three trials were performed at each pH value, and an averaged value was recorded.

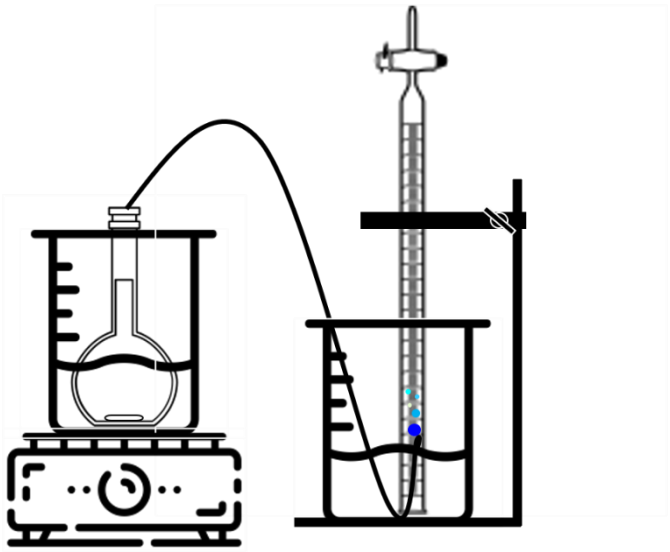

Fig. 6.1 The scheme of self-assembled apparatus for CO_2 test.

6.2.4 Determination of the antisolvent effect

To confirm the anti-solvent precipitation process, slight changes to the previous methodology were implemented (Chen *et al.*, 2018; Doost *et al.*, 2019). Shellac was grounded to a fine powder and dissolved in 5 mL of 100% denatured alcohol solution. Shellac solution was used as the solvent, while Milli-Q water and oil were used as the anti-solvent. The 5 mL shellac solution was added to 15 mL Milli-Q water solution to achieve a volumetric ratio of ethanol to the aqueous phase of 1:3. The ethanol in the solution mixture was evaporated in a water bath at 50 °C at a stirring speed of 750 rpm. Samples of the mixed dispersion were removed to determine the size at predetermined timed intervals (1 min – 30 min).

6.2.5 Preparation of Pickering emulsion

A W/O emulsion (ratio 4:6) was prepared using the Pickering emulsification technique. Specifically, 30 mg yeast was dispersed in water to hydrate, and 100 µL methylene blue (10 mg/mL) was added. The excess dye was removed using a centrifuge at 3,000 rpm for 2 min. Then, 3 mL of 5% shellac dispersion was added to the dyed yeast and mixed with vegetable oil using a high-speed homogenizer (Ultra Turrax T25 homogenizer, IKA, Germany) at 9,500 rpm for 3 min, followed by the addition of 2% calcofluor white dyed CNC (CNC-CW) and 0.8% $CaCl_2$ solution to improve the emulsion stability. To distinguish between the oil and water phase, 1 mg/mL of hydrophobic Nile red and 10 mg/mL of hydrophilic CW were used. To precisely detect the CNC-CW, unbound CW was removed by ultrafiltration with a 0.1µm filter. The emulsions' pHs were adjusted to 2 or 7.5 to mimic the gastric and intestinal pH conditions, and the yeast viability was assessed.

6.2.6 Preparation of simulated gastric (SGF) and intestinal fluid (SIF)

The modified methodologies of SGF and SIF were utilized (Annunziata *et al.*, 2019). 500 mg of pepsin was dissolved in 25 mL of 0.1 N HCl. The final pH was adjusted to pH 2 using 1 N HCl. The solution was then incubated at 37 °C under continuous stirring at 250 rpm for 2 h. For SIF, the pH of the 15 mL water was adjusted to 6.5 using 0.5 N $CaCl_2$. 5 mL of 1:1 pancreatin (v/v) and bile salt solution was made with 40 mg (8 mg/mL) pancreatin and 200 mg bile salt (50 mg/mL). 15 mL water and 5 mL solution were mixed and incubated at 37 °C under continuous stirring at 250 rpm for 2 h.

6.2.7 Material characterization

6.2.7.1 Size and zeta-potential analysis

The hydrodynamic particle size and surface charge of the yeast, shellac, ShCNCCa at different pHs ranging from 2 to 9 were determined by the Zetasizer Nano ZS instrument (Nanosizer ZS, Malvern, UK). Shellac (5 mg/mL) was dissolved in ethanol, and the volume was adjusted with Milli-Q water to reach an ethanol concentration of 5%. For the size distribution of the ShCNCCa complex, 5 mg/mL of shellac in 5% ethanol was mixed with 2% CNC and 0.8% $CaCl_2$ through high-speed homogenization at 12000 rpm for 5 minutes, using the high-speed homogenizer (Ultra Turrax T25 homogenizer, IKA, Germany). Aliquots of each sample were adjusted to their desired pH with concentrated HCl and NaOH. Each sample was measured three times, and the mean ± standard deviation of the data was calculated.

6.2.7.2 Fourier transform infrared (FTIR) spectroscopy

CNC, Shellac, ShCNC, and ShCNCCa were analyzed using the FTIR spectrophotometer (Bruker Tensor 27 FTIR spectrometer, Billerica, MA, USA). Dried samples were grounded in a mortar and compressed with potassium bromide (KBr) to form pellets. The FTIR spectra of each sample were recorded between 4000 cm^{-1} and 400 cm^{-1}, with a resolution of 4 cm^{-1} and 32 scans.

6.2.7.3 Microstructural investigation

The morphologies of the yeast, ShCNC, ShCNCCa complex and yeast encapsulated Pickering emulsions at pH 2 and 7.5 were analyzed using a transmission electron microscope, Philips CM10 (TEM), Environmental scanning electron microscope, (*Quanta FEG-250*, Republic of Czech (ESEM)), optical, fluorescence (Nikon Eclipse Ti-S, Nikon Instruments Inc., USA), and confocal microscope (Zeiss LSM 510 Meta Laser Scanning Confocal Microscope (CLSM). For the sample preparation of ESEM, after fixing the carbon tape to the aluminum stub, the emulsion sample is loaded onto the carbon tape surface. A TEM at an acceleration voltage of 60 kV. One drop of each diluted suspension was placed on a carbon-coated copper grid (200 mesh) under filter paper, air-dried and examined under the machine. Also, fresh samples of encapsulated yeast Pickering emulsions with the ShCNC and ShCNCCa at pH 2 and 7.5 were observed by an optical and fluorescence microscope equipped with a CCD camera (QImaging Retiga 2000R). Afterwards, a confocal microscope was used to detect the interaction of the shellac nanoparticle dispersion with oil for figuring out the anti-solvent effect. The dispersion sample was smeared with oil to make contact with each other. Also, we have checked the distribution and position of the Shellac and CNC in the Pickering emulsion. The observation magnification was 63x/1.4 Oil DIC, and an immersion objective lens was used, with the immersion medium being oil. Images were taken under DAPI's 405, argon 514 and 543 nm laser conditions. The measured image was shaped into a 3D image using ZEN 2009 analysis software. To calculate the retention of yeast in different microcapsules, the number of yeast particles was analyzed using the ImageJ, and the average of all counts was determined from the optical micrographs.

6.2.7.4 Mucoadhesive test

The assessment of mucoadhesion for the ShCNCCa was conducted using the viscosity method based on a previous study by Lin *et al*. (2019), where the synergism between ShCNCCa and mucin was characterized by an increase in the system's viscosity. Modifications to this method were made for the assessment of the ShCNCCa system. SIF set at pH 7.5 was prepared 24 h in advance and stirred. Shellac flakes were grounded to a fine powder, and 1% of shellac along with 4% CNC were added to the SIF sample. Another SIF was added with 10% porcine gastric mucin. Both samples were completely dispersed in their aqueous medium via ultrasonication at room temperature. 1:1 ratios of both mixtures were incorporated and placed on a magnetic stirrer to yield a homogenized mixture comprising 5% mucin, 0.5% shellac, and 2% CNC. In an alternate trial, 10 mg/mL of yeast was added to the ShCNCCa-mucin-in-SIF prior to preparing the solution mixture. The enhancement in the viscosity was measured using the Kinexus Ultra+ Rheometer. The cylindrical fixture was used, with a cup (DO25 C0107 AL) and bob (DG25 L0381 SS) geometry, and the sample was heated to 37°C. The shear rate was set to a range from 0.1 to 50 s^{-1}. The enhancement and relative enhancement were calculated at shear rates of 3.98 and 10.00 1/s using equations Eq 6.1 and 6.2 provided from a previous study by (Lin *et al.*, 2019):

$$\eta_{enhancement} = [\eta_{mixture} - (\eta_{nanocellulose} + \eta_{mucin})] \times 1000 \quad (6.1)$$

$$\eta_{relative} = [\eta_{mixture} \div (\eta_{nanocellulose} + \eta_{mucin})] \quad (6.2)$$

6.2.8 Statistical analysis

All experiments were performed as three independent preparation, and the results are expressed as means with error bars of ± standard deviations.

6.3 Results and discussion

Shellac is known to be insoluble in water because of its many carboxyl groups (Penning, 1996). The protons of these carboxylic acids can be removed by dissolving shellac in alkaline solvents, such as sodium hydroxide and ammonia (Shellac has a pK_a of 6.9–7.5) (Al-Obaidy *et al.*, 2019). Additionally, shellac is completely soluble in methanol, ethanol and partially soluble in ethyl acetate, chloroform and ether (Cagil, 2020). Since this study concerns the development of microcapsules for food applications, low concentrations of ethanol, which is harmless to humans was used. In addition to the solubility consideration, another crucial factor in selecting a low concentration of ethanol is to ensure the viability of the probiotics or yeast used in the study. The 5% ethanol was used as the optimum concentration to produce shellac dispersions via the anti-solvent precipitation process, and different shellac concentrations (2.5, 5, 7.5, and 10 mg/mL) were studied. As shown in Fig. 6.2A, after diluting to prepare 2.5 and 5 mg/mL shellac dispersion, a homogenized light brown dispersion with no sediment was observed. In contrast, significant particle aggregations leading to dark and sticky sedimentations at the bottom of the vial occurred at a shellac concentration of 7.5 and 10 mg/mL. The hydrodynamic size and zeta potential were measured and shown in Fig. 6.2B. The mean particle size increased with increasing shellac

concentration, which changed from nano to micron size range (> 1 μm in diameter), which corresponded to particle aggregation as shown in Fig. 6.2A. At 2.5 and 5 mg/mL, the particles were narrowly dispersed and within the size range of 130 and 250 nm. However, at 7.5 and 10 mg, micron-size particles were observed with a significant scattering. Smaller nanoparticles are desirable since they can readily adsorb at the oil-water interface due to high diffusivity compared to larger particles (Iyer *et al.*, 2015).

On the other hand, the zeta potential changed from -30 to -16 mV when the shellac concentration was increased, which is most likely caused by particle agglomeration that shielded the surface charges. Fig. 6.2C shows the zeta-potential trend of shellac dispersion (5 mg/ml in 5% denatured alcohol) from pH 2 to 9. At basic pH (above *pKa*), shellac was fully solubilized in solution, as indicated by the maroon colour and clear dispersion (Fig. 6.3). As the pH approached the acidic condition, the zeta-potential became less negative due to the presence of H^+ ions. The influence of pH on the zeta-potential became more significant when the pH transitioned from 4 to 2. The protonation of the carboxylic groups of the aleuritic and terpenic acids on the shellac resulted in the zeta-potential approaching the isoelectric point (*pI*) of 3, which destabilized the shellac system (Spasojević *et al.*, 2020), resulting in the precipitation and sedimentation of shellac particles. Likewise, the sedimentation was also observed at pH 2. In Fig. 6.2D, the size distribution of the ShCNCCa complex between the pH of 2 to 9 correlated with the results depicted in Fig. 6.2C. At basic pH (above *pKa*), shellac was more dispersible, as indicated by the reduction in the particle size and the light

purple colour of the dispersion (Fig. 6.4). As the pH approached the acidic condition, the size of the ShCNCCa increased, reaching a maximum at pH 3, which correlated with the *pI* of the shellac dispersion shown in Fig. 6.2C. Shellac, being most unstable at this pH condition, would lead to the largest size of the complex, causing an increase in overall particle size. Despite this, there is no complete destabilization of the complex due to deprotonated -OH groups from the CNC.

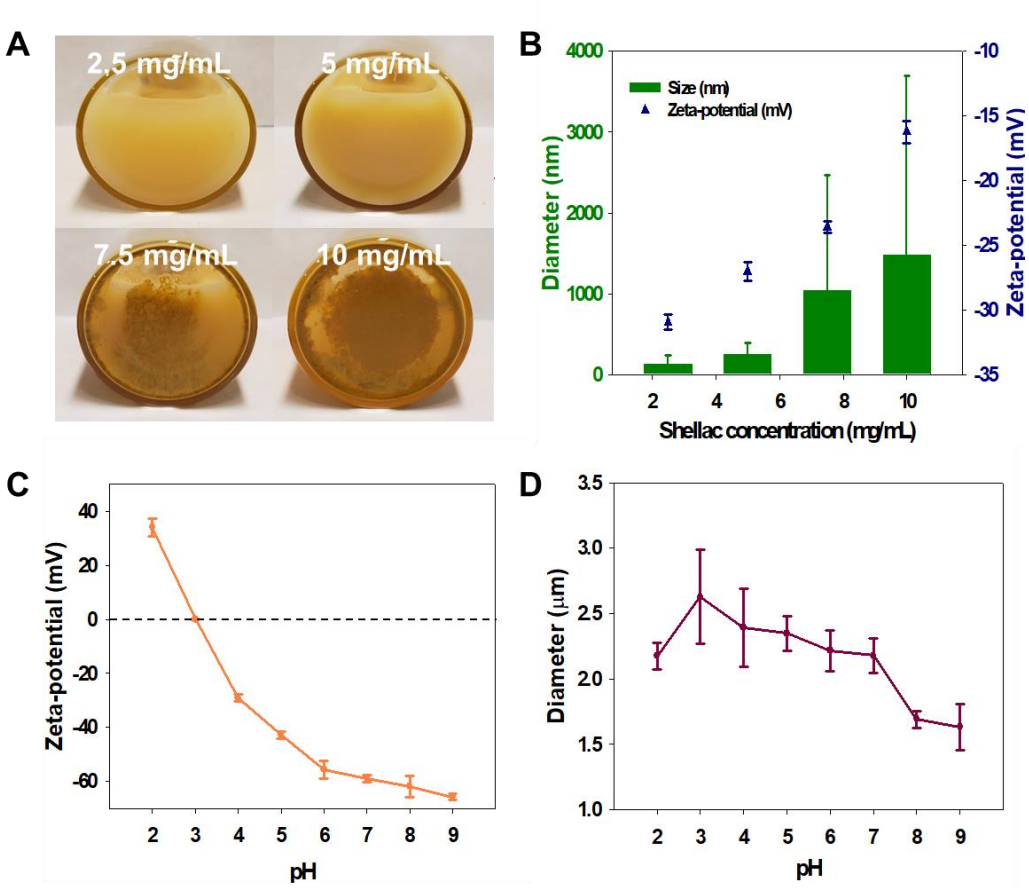

Fig. 6.2 A) Shellac dispersion in 5% DA at different concentrations (2.5, 5, 7.5, and 10 mg/mL), B) size and zeta-potential of 4 concentrations of shellac dispersion in 5% DA, C) zeta-potential of shellac dispersion (5 mg/mL) at various pH (2-9), and D) diameter of ShCNCCa at various pHs (2-9).

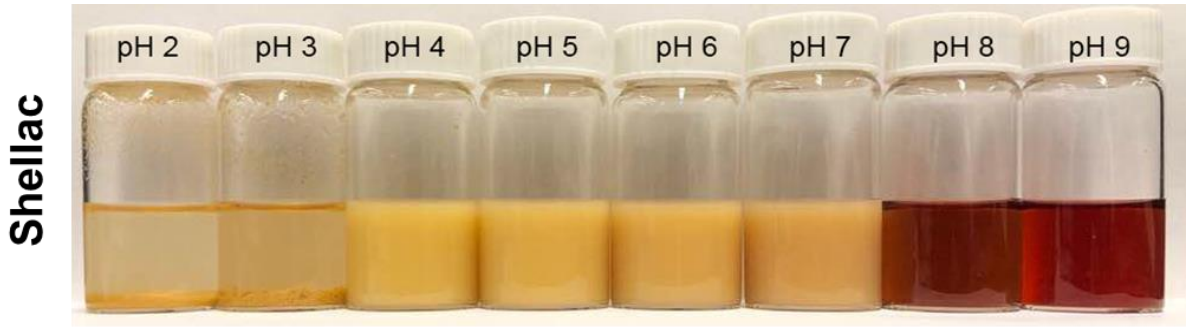

Fig. 6.3 Photographs of Shellac solutions at different pH (2-9).

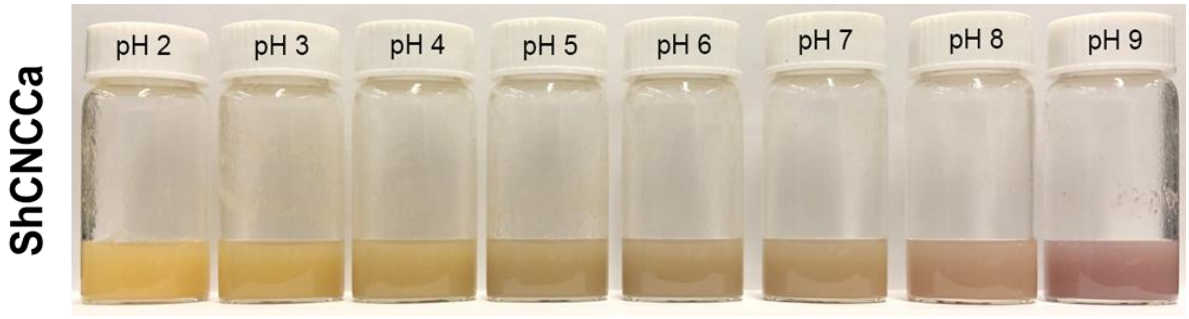

Fig. 6.4 Photographs of ShCNCCa complex at different pH (2-9).

The schematic for the formation of the ShCNCCa complex is shown in Fig. 6.5, and the qualitative verification of functional groups between CNC, shellac, $CaCl_2$ was obtained by FT-IR, as presented in Fig. 6.6.

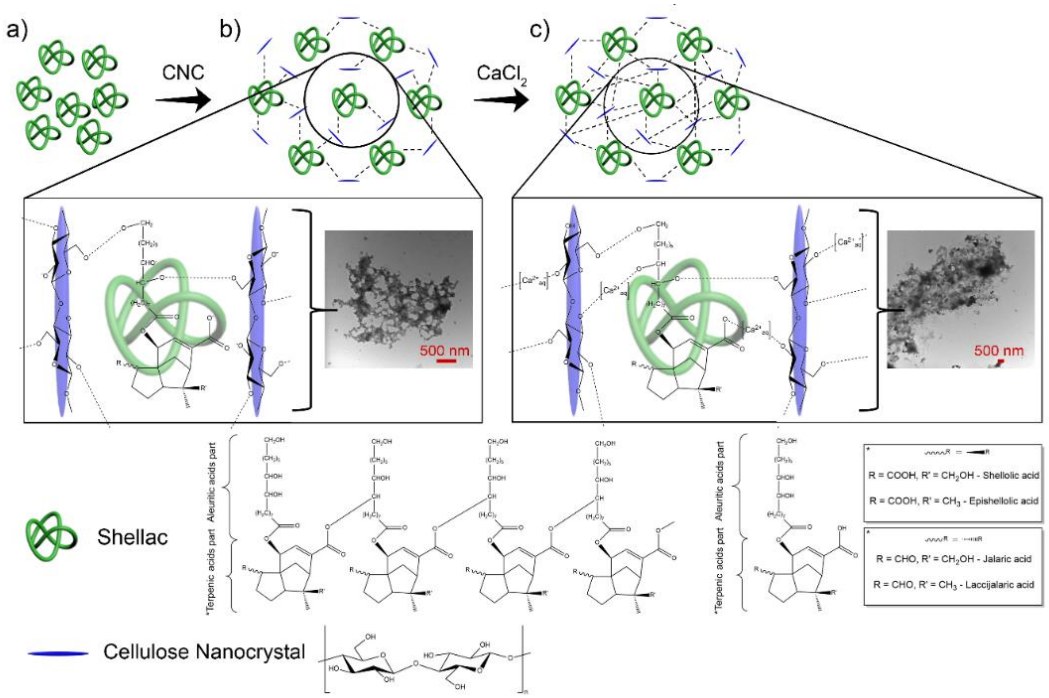

Fig. 6.5 Schematic of the formation of ShCNCCa complex.

FTIR was conducted to evaluate and confirm the interaction of CNC with Shellac and $CaCl_2$. Fig. 6.6 shows the FTIR spectra of Shellac, ShCNC and ShCNCCa. Key peaks present in the Shellac are broad -OH stretching vibration band, terpenic acids carbonyl stretching vibration band and C-O stretching band at 3427 cm^{-1}, 1738 cm^{-1} and 1265 cm^{-1}, respectively. Upon the addition of CNC, there was no significant peak intensity observed for the broad -OH stretching vibration band, signifying the hydrogen-bonding interaction between shellac and the CNC. According to ShCNCCa peak, there was no peak for the carbonyl stretching vibration band, possibly indication the bonding interactions between Ca^{2+} and C=O since shellac would interact with Ca^{2+}.

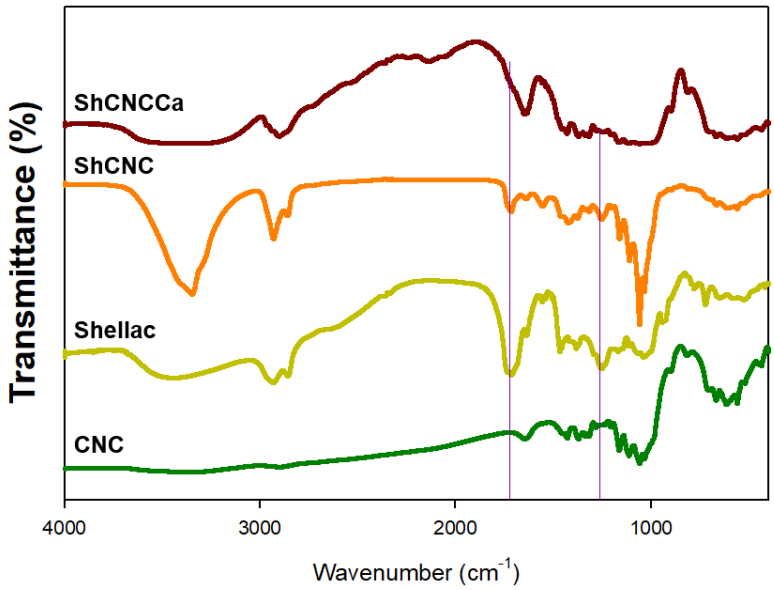

Fig. 6.6 FT-IR data of CNC, Shellac, ShCNC, and ShCNCCa.

The anti-solvent precipitation method was used to confirm that the size of the nanoparticles increased with the mixing time of the solvent and anti-solvent solution. Furthermore, it was also used to analyze the interactions between shellac and water or oil in the formation of the nanoparticles. Fig. 6.7A depicts a 3D model of the anti-solvent process that describes the different stages of nanoparticle growth: supersaturation, nucleation, particle growth by condensation and coagulation. After adding the solvent to the anti-solvent, the mixture's solvent power was reduced, leading to supersaturation. When the mixture exceeds the critical supersaturation concentration, nucleation occurs, inducing the shellac nanoparticles to precipitate. As the concentration of pure solute decreases, the mixture passes the critical supersaturation concentration where nucleation ceases, and the number of nuclei remains constant. The remaining nuclei continue to grow through condensation and coagulation.

Particle growth through condensation will occur as single molecules are added to the particle surface. Condensation will cease when the concentration of the free solute is reduced below the equilibrium saturation concentration. Particle growth through coagulation occurs when the solute concentration is lower than the equilibrium saturation concentration and when the attractive interactions exceed the repulsive interactions (Joye & McClements, 2013).

The size distribution of shellac nanoparticles using the anti-solvent precipitation method was analyzed using a dynamic light scattering instrument (DLS). Figs. 6.7B and 6.7C show a positive correlation between the mixing time of the anti-solvent (water) and particle size. When the samples were mixed for an extended period, the size and scattering intensities increased due to the formation of larger particles. At lower mixing times, the rapid attainment of the homogenous supersaturation resulted in the rapid nucleation of the particles. Thus less time was needed for the particle growth by condensation and coagulation. This relationship is shown in Fig. 6.7C, where there is an overall increase in the particle size as a function of mixing time. At mixing times of between 1 to 5 minutes, nucleation with low particle growth by condensation was dominant, and when it was increased to between 5 to 10 minutes, more particle growth occurred via condensation, resulting in the dramatic increase in the particle size. However, when the mixing time exceeded 10 minutes, the particle size plateaued and condensation ceased, as the concentration of free solute was now below the equilibrium saturation concentration. Furthermore, coagulation was reduced with continuous stirring as aggregated particles could be dissociated through mechanical mixing (Joye & McClements,

2013). Fig. 6.7D shows the 3D image of the microcapsules, and Fig. 6.7E shows the cross-sectional intensity of a microcapsule acquired with the confocal laser scanning microscope. The intensity profiles provide insights into the interactions between the shellac dispersion and oil (anti-solvent). The low intensity in the middle of the microcapsule indicated that the shellac had precipitated and migrated to the oil-water interface. The high intensity of shellac measured at the microcapsule outer shell suggested that the anti-solvent effect drove the shellac to the oil-water interface to form a shell.

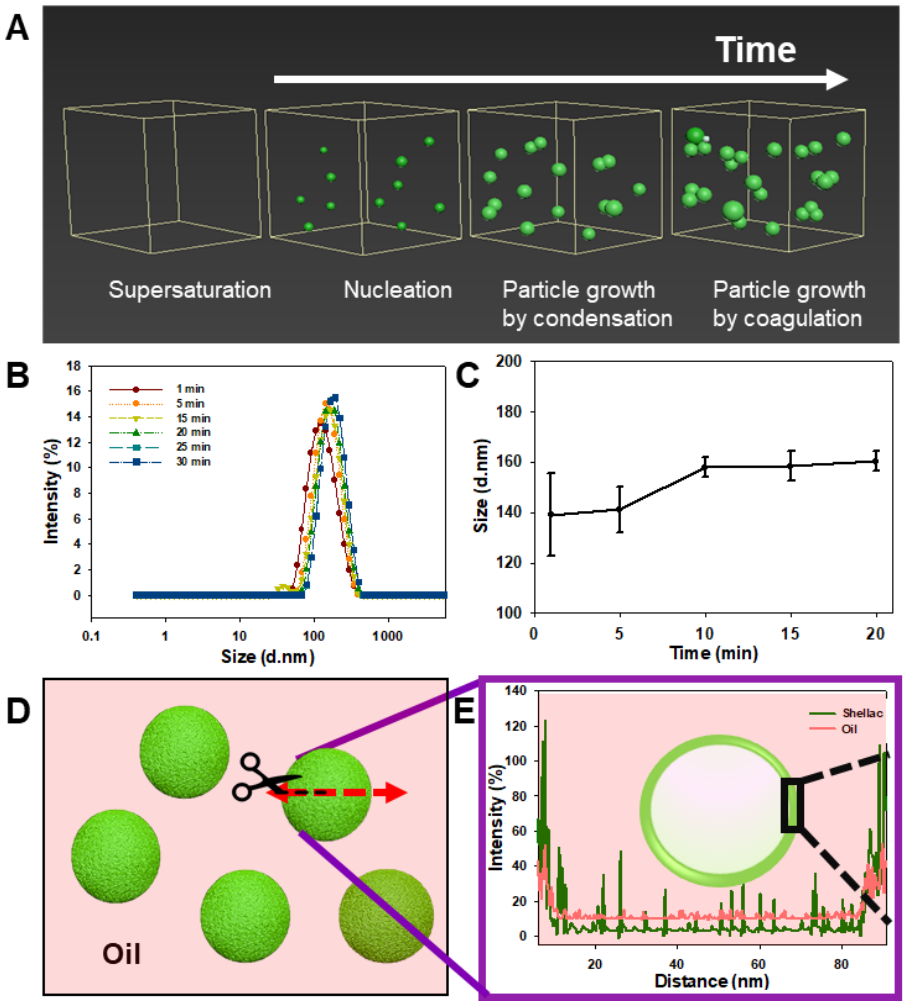

Fig. 6.7 A) Proposed 3D model of the growth of particle size during anti-solvent precipitation process, B) Intensity size distribution of shellac nanoparticles in water versus particle diameter. The different colours represent the measurements at different mixing times, C) Particle size change of shellac nanoparticles in water as a function of mixing time, and D and E) 3D images of W/O emulsion and the corresponding fluorescence intensity profiles of shellac (green) and oil (pink).

In order to evaluate the pH effect on the probiotics, we conducted the pH-controlled studies on the yeast by monitoring the CO_2 release as a function of time (Fig. 6.8A). At pH 2, the amounts of CO_2 released were 0.6 ml, indicating that the yeast cells had lysed. At pH of 5, 7.5, the CO_2 release was fairly similar. However, at a pH of 8, the CO_2 release was lower, and it reduced further at pH 9.3. Thus, we concluded that the condition for the viability of the yeast was between the pH of 5 to 7.5 (Reethu Narayanan & Ch, 2012). Yeast viability was lower in an extremely acidic and basic environment. Additionally, the yeast was dyed with methylene blue to allow us to check its viability under the microscope and compare it with CO_2 release tests. $CaCl_2$ was added to the yeast dispersion to improve its stability, and Ca^{2+} ions are known to promote yeast growth (Cui *et al.*, 2009), and they did not inhibit the viability of yeast, as shown in Fig. 6.8B. Thus, the CO_2 test was conducted to examine the impact of the encapsulation strategy on the viability of yeast cells. Kwolek-Mirek and Zadrag-Tecza (2014) stated that living cells enzymatically reduce the dye by pumping the methylene blue out of the cell. Hence live yeast cells do not stain (Fig. 6.8C), while dead cells are stained blue (Kwolek-Mirek & Zadrag-Tecza, 2014). Therefore, the live and dead yeast could be clearly distinguished under different pH conditions. Moreover, dead cells that are stained with methylene blue emit red fluorescence under a fluorescence microscope.

From the magnified image of Fig. 6.8C, many dead yeast cells were evident when they were incubated at a pH of 2. However, once ShCNCCa was added to the yeast, partial coverage on yeast occurred (Fig. 6.8D) as indicated by the green-fluorescent shellac and red-

fluorescent methylene blue-dyed shellac coated yeast from the fluorescence images. Identification of the shellac in the emulsion droplets was possible due to shellac's auto-fluorescence characteristics (Bellan *et al.*, 2012). Fig. 6.4E shows the zeta-potential distribution of yeast in the presence of 0 and 0.8wt% $CaCl_2$. At pH 2 and 3, the dispersed yeast in 0 and 0.8wt% $CaCl_2$ possessed a positive zeta potential. As the pH increased, the zeta-potential of both yeast dispersions became negative, reaching -28.33 mV and -16.37 mV at pH 9 for the 0 and 0.8wt% $CaCl_2$, respectively. In the presence of divalent cations, the *pI* remained relatively unchanged, which is consistent with the findings of Narong and James, where they reported a *pI* of pH 3.6 in the presence and absence of monovalent sodium ions (Narong & James, 2006). The same behaviour of yeast in Ca^{2+} solutions suggested that the addition of these ions compressed the electrical double layer of the yeast particles. While comparing the CO_2 release tests (Fig. 6.8F) of the control, ShCNC and ShCNCCa at pH 2, approximately 5 times more CO_2 was released due to the coating of ShCNCCa on the yeast cells that preserved the yeasts in unfavourable pH conditions. The partial coverage of yeast was possible because of; (1) CNC acting as a reinforcement in the polymer matrix (Obradovic *et al.*, 2017) and Ca^{2+} as a bridging ion (Luo *et al.*, 2016) to cross-link the carboxyl groups of shellac (2) zeta-potential of yeast at pH 2 was positive as it was below the *pI* (pH 3.1) of the yeast cell wall protein (Narong & James, 2006); hence it could interact with the negative charges via electrostatic interaction to form the shellac complex (Rogowska *et al.*, 2018).

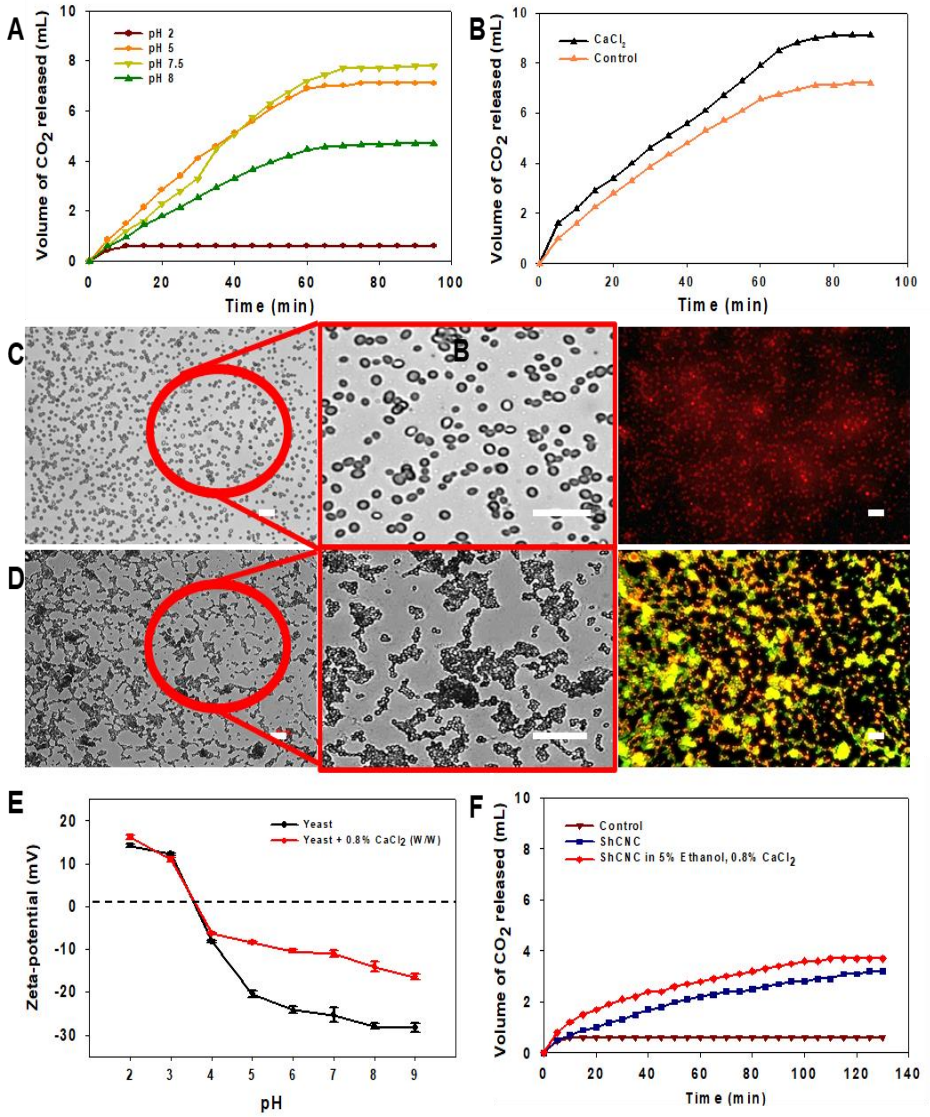

Fig. 6.8 A) Control CO_2 release of yeast in varying pHs B) CO_2 release by yeast at pH 5 with and without $CaCl_2$, C) Optical and fluorescence microscopy of yeast dyed with methylene blue to determine the viability at pH 2 (Scale bar: 50 μm), D) Optical and fluorescence microscopy of the partial coverage of yeast by ShCNCCa (dyed in methylene blue) to determine the viability at pH 2 (Scale bar: 50 μm), E) Zeta-potential of yeast and yeast with 0.8% $CaCl_2$ at various pH (2-9), and F) CO_2 release of yeast at various conditions at pH 2.

The morphologies of the Pickering emulsions at pH 2 and 7.5 were observed by optical, confocal microscopy, TEM, and ESEM. In the initial stage, various Pickering emulsions were prepared with shellac, ShCa, ShCNC and ShCNCCa to compare their emulsifying properties. As shown in Fig. 6.9A, when the only shellac was used, the emulsion droplets were larger and were irregular in shapes due to agglomeration and coalescence, and the yeast loading was low. When $CaCl_2$ was added to the shellac, a drastic reduction in the droplet size was observed. However, as shown in Fig. 6.9B, the droplets were irregular in shape due to the unstable oil-water interface. Pickering emulsions produced using ShCNC yielded spherical emulsion droplets (Fig. 6.9C). However, coalescence occurred after a short time which is possibly due to the porous nature of the ShCNC shell. The shellac and CNC complexation were facilitated by the hydrogen bonding between the carboxyl and hydroxyl groups present on shellac and CNC (Obradovic *et al*., 2017). However, the nanocomplex formed did not yield a strong, stable continuous network, as shown in the TEM micrograph (Fig. 6.9D). However, when $CaCl_2$ was incorporated in the emulsion prepared with ShCNC, uniform spherical particles were observed with a significant increase in the encapsulated yeasts (Fig. 6.9E). This demonstrated that calcium ions play a major role in the formation of a strong cross-linking and stable network between shellac and CNC (Fig. 6.9F). Moreover, the CNC was intercalated with the shellac and calcium ions at the oil-water interface forming an "impermeable" membrane resulting in a stable and spherical microcapsule. This resulted in the improved retention of yeast cells, as shown by the average number of yeast particles encapsulated per droplet. With only the shellac complex, the average number of yeasts

particles recorded per droplet was 20.86. With calcium ions to screen the charge and CNC for hydrogen bonding interaction with shellac, robust microcapsules cannot be formed to encapsulate and preserve the high number of yeast particles. However, with the ShCNCCa complex, where the additional interactions from CNC and calcium ions produce robust microcapsules, where the average number of yeast particles encapsulated per droplet increased to 125.65, representing a 602.35% increase in yeast retention.

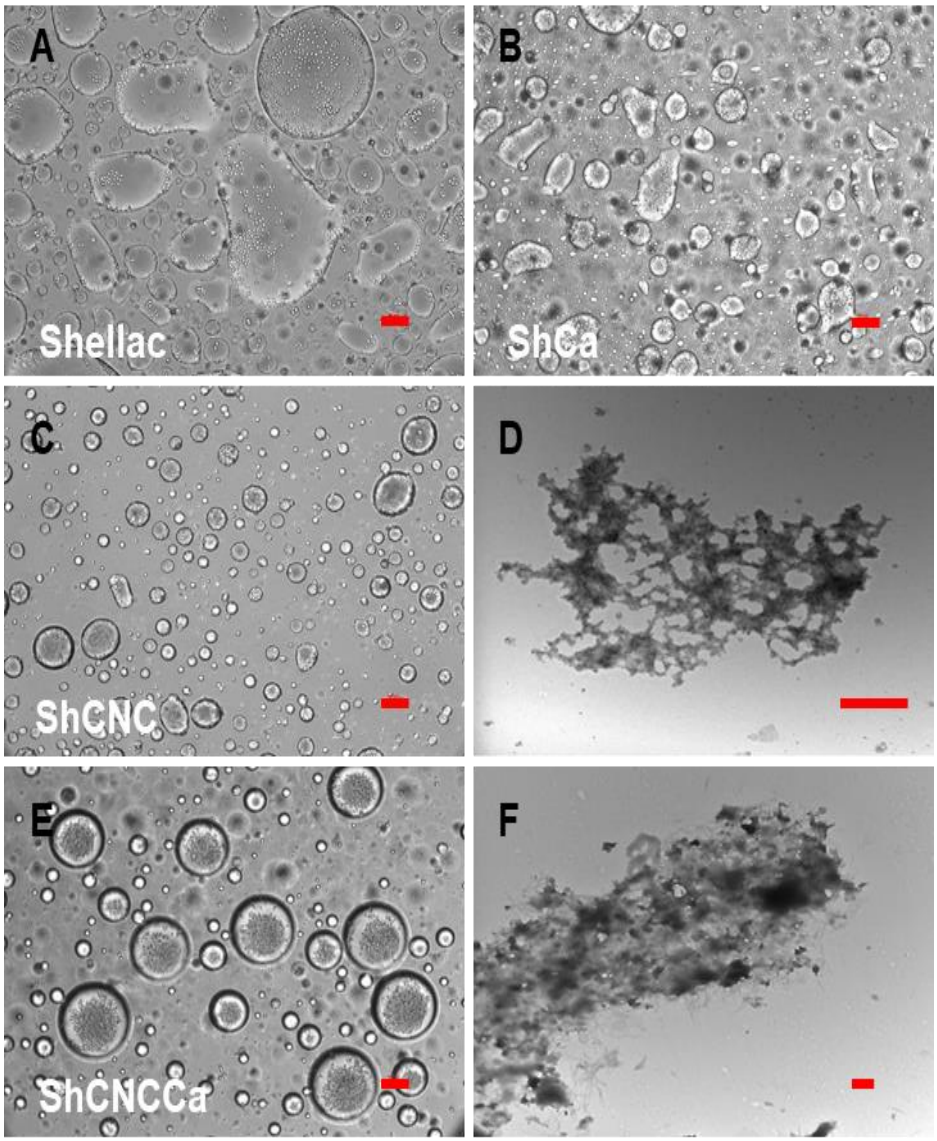

Fig. 6.9 Optical and fluorescence micrographs of encapsulation of yeast with A) Shellac B) ShCa, C) ShCNC, and E) ShCNCCa. TEM Micrographs of D) ShCa and F) ShCNCCa. Scale bar; A, B, C, and E: 50 μm, D and F: 500 nm.

To confirm the ShCNCCa complex formation in the Pickering emulsion, CNC and oil were stained using a Calcofluor white and Nile Red, respectively, while shellac possessed a natural

auto-fluorescence**.** The confocal 3D stacked images obtained using the CLSM provided information on the distribution of the CNC, shellac and oil in the Pickering emulsion. Fig. 6.10A shows the 2D image that confirmed that both CNC and shellac formed complexes at the oil-water interface. Fig. 6.10B shows the cross-section of the emulsion droplet, where the oil phase segregated from the water phase, and the ShCNCCa complex was located at the oil-water interface. The ShCNCCa complex lowered the interfacial tension of the oil-water that yielded an emulsion that was stabilized against flocculation and coalescence (Fig. 6.11). A 2.5-dimensional image of emulsion droplet revealed both blue and green fluorescence at the oil-water interface, confirming the complexation of CNC and shellac (Fig. 6.12).

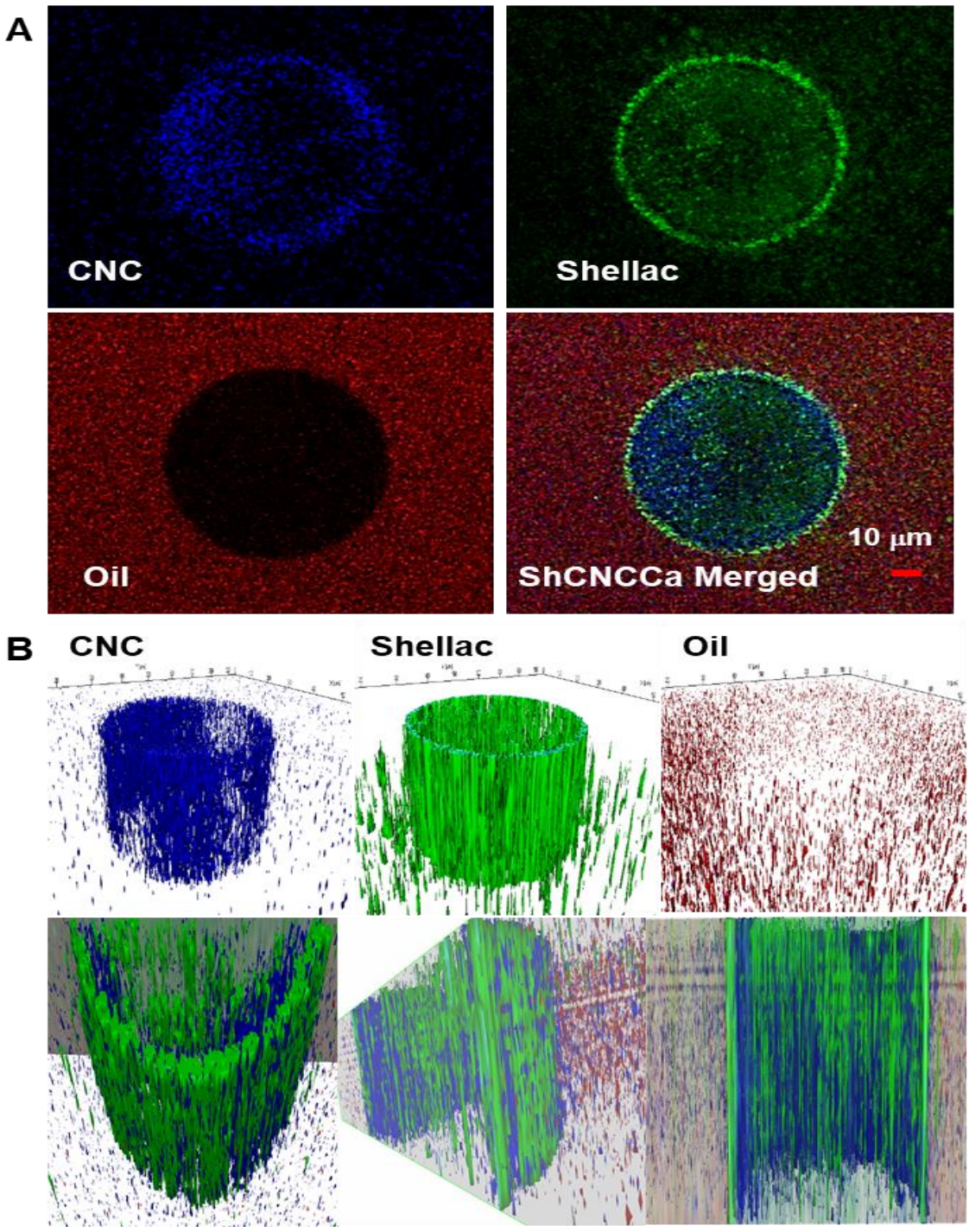

Fig. 6.10 A) Confocal images of isolating the materials that compose the surface of the encapsulation; CNC, Shellac, oil, and merges capsule and B) Z-sequences of optical slices (*3D* image stacks).

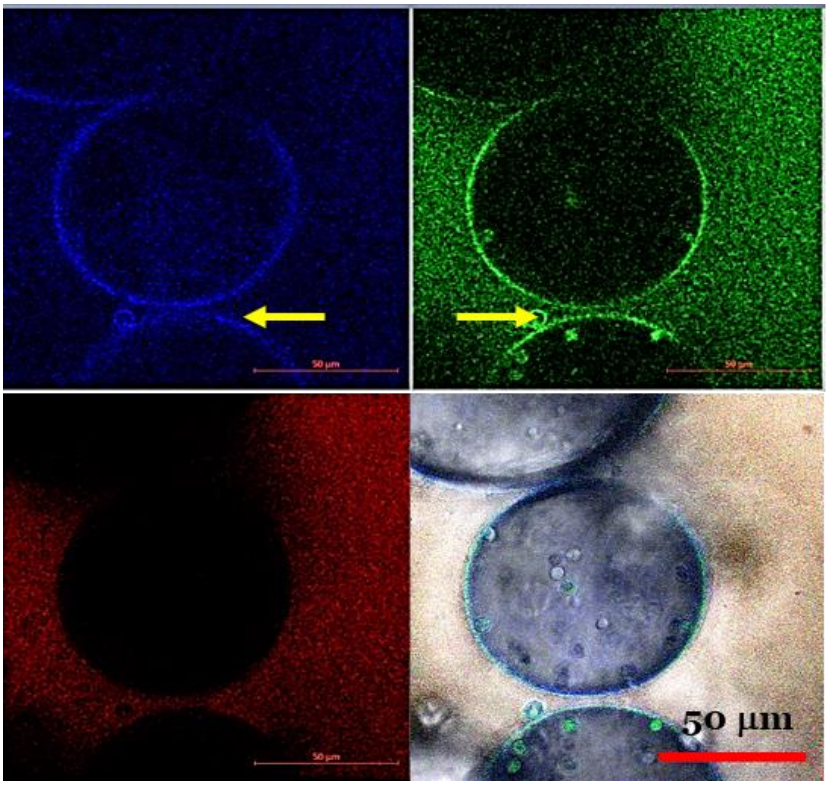

Fig. 6.11 Confocal microscope images of W_{yeast}/O emulsion with ShCNCCa complex in pH 2 (pepsin) shows preventing coalescence effect (Blue; CNCCW, green; Shellac, and red; oil).

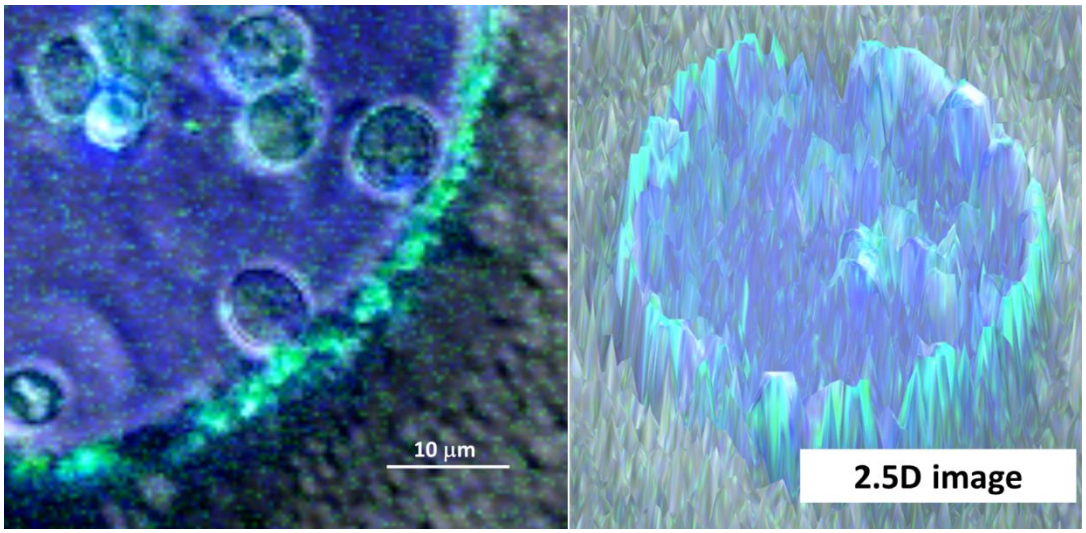

Fig. 6.12 2.5-dimensional image of emulsion, displaying both blue and green at the outer surface, implying that CNC and Shellac are present.

To provide further evidence on the structure of the microcapsule, the sample was scanned using the imaging software in two configurations, and the direction of the scan is indicated by the arrow in Fig. 6.13A and 6.13B; (1) transverse scan through the microcapsule and (2) secant scan along the circumference of the microcapsule. In Fig. 6.13A, the three distinct phases within the microcapsule could be determined, where the water phase within the capsule (between 0-2300nm), coating (2300-3600nm), and the oil phase (>3600nm) was identified. In the water phase, the intensity of the fluorescence from the oil was close to zero, while there was detectable fluorescence from both the CNC and shellac. The intensity of the coating layer consisted mainly of CNC and shellac, suggesting that it comprised mainly of these two major components. Both the green and blue fluorescence intensities were detectable in the water phase, confirming that the shellac precipitated when the denatured methanol evaporated, and the precipitated shellac then complexed with the CNC and calcium at the oil-water interface. However, near the coating layer, the green and blue peaks were significantly larger, indicating the presence of both higher amounts of shellac and CNC. The coating thickness was estimated to be about 1- 1.3 microns using the software. In the oil phase region of the coating, the intensity of CNC and shellac began to decrease, and the intensity from the oil peak began to rise. In Fig. 6.13B, a secant scan was conducted along with the circumference/surface of the microcapsule as indicated by the red arrow. Green and blue peaks appeared together, while the red intensities were close to zero, indicating that the oil was absent at the surface of the coating. The evidence from confocal microscope analyses suggested that the emulsion surface was composed of shellac, CNC and $CaCl_2$.

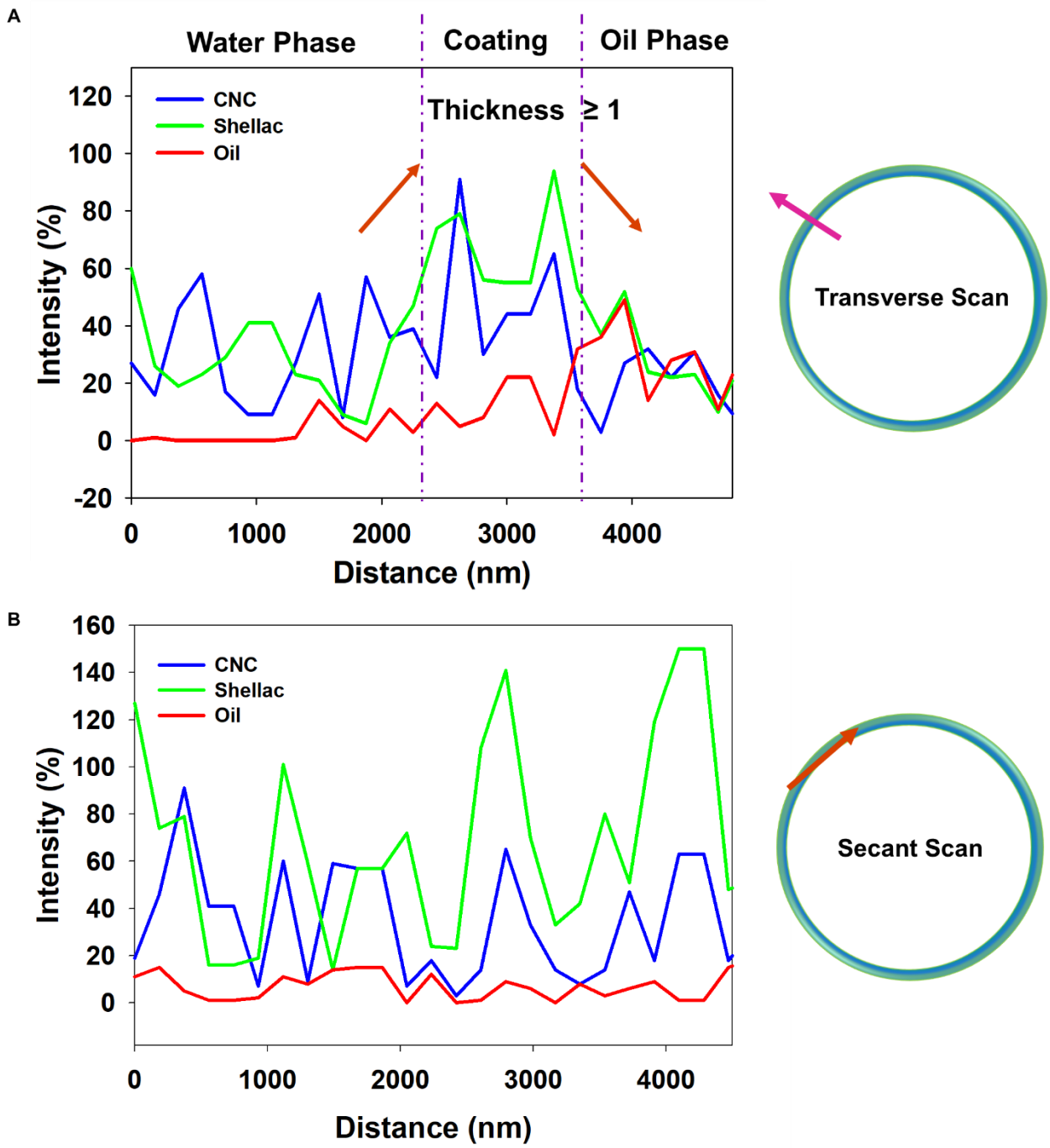

Fig. 6.13 A) determination of complex intensity through transverse scan and thickness of the coating and B) secant along with the ark of the emulsion.

TEM (without yeast) and ESEM (with yeast) tests were conducted to examine how the evolution of the shellac capsules with the pH of the solution. Fig. 6.14 shows a rigid ShCNCCa capsule in a low pH environment of 2. However, at pH 7.5, TEM images show only the presence of CNC. As expected, shellac had dissolved at alkaline pH because of its good solubility. Furthermore, the repulsion that occurred between negatively charged shellac (solubilized form) and CNC from the deprotonated carboxyl groups caused the Shellac/CNC complex to disintegrate, and only the CNCs were present.

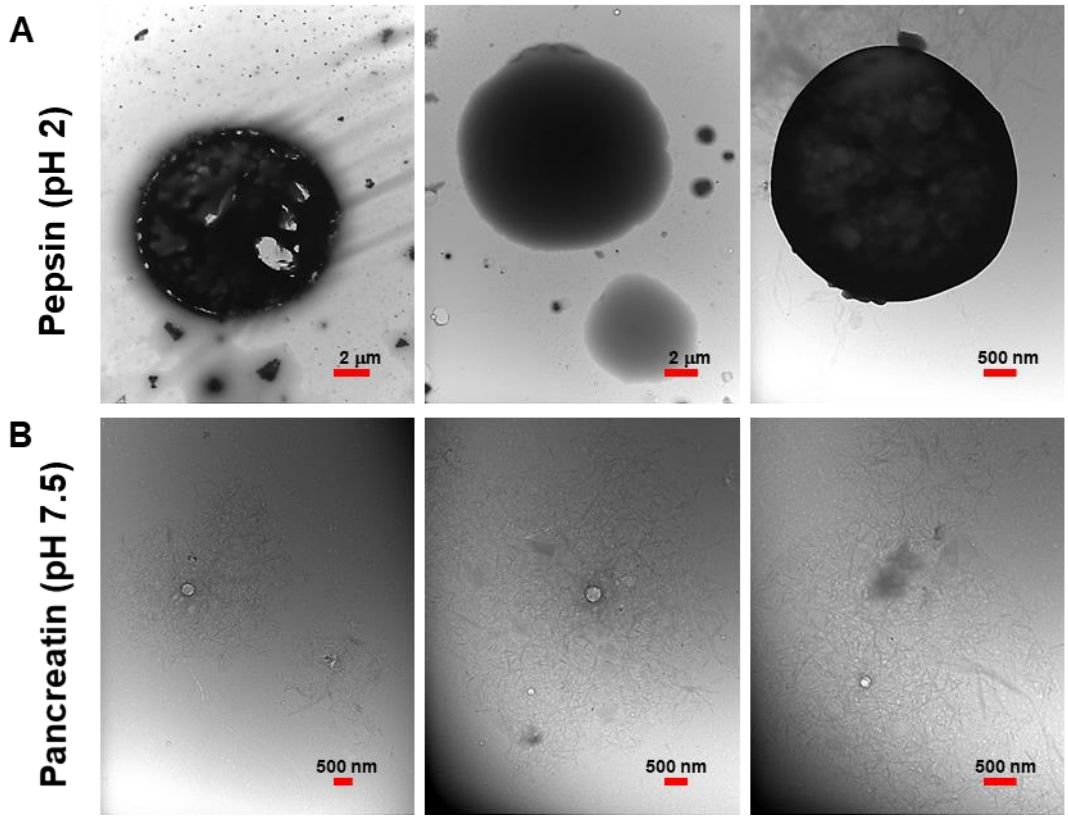

Fig. 6.14 TEM images of W/O emulsion with ShCNCCa complex in (A) pH 2 (pepsin) and (B) pH 7.5 (pancreatin).

At pH 7.5, the microcapsule dissociated as revealed by the ESEM images in Fig. 6.15, which was corroborated by the TEM results. The encapsulated yeast with tight integration was released from the microcapsules and spilled into the continuous phase in the intestinal medium, pancreatin.

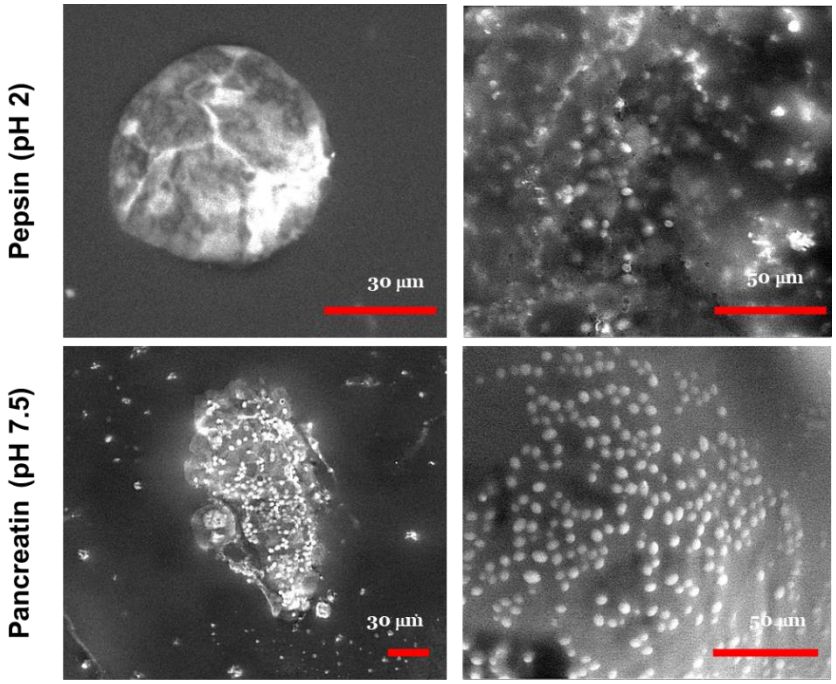

Fig. 6.15 SEM images of W_{yeast}/O emulsion with ShCNCCa complex in (A) pH 2 (pepsin) and (B) pH 7.5 (pancreatin).

To examine the viability of yeast in the W/O emulsion, Shellac, CNC and $CaCl_2$ were introduced to the yeast dispersion. At pH 2, shellac precipitated when the carboxyl groups were protonated and complexed with CNC and $CaCl_2$ to form a shell coating that protected the yeast from the acidic environment (Fig. 6.16). Figs. 6.14, 6.15 and 6.16 displayed similar results demonstrating the promising encapsulation and release of probiotics at the pH

condition of the gastrointestinal tract. In addition, a significant amount of CO_2 release was observed, as shown in Fig. 6.17. A slightly lower CO_2 production was observed for the microcapsules at pH 2 despite ShCNCCa complexes (Fig. 6.8E), signifying an effective encapsulation of yeast. On the other hand, at high pH, a larger amount of CO_2 was produced due to the broken capsule that released the encapsulated yeast, which was free to produce the CO_2 gas. Hence, the proposed enteric coating system could be translated into real food applications for delivering probiotics or active substances to the intestine.

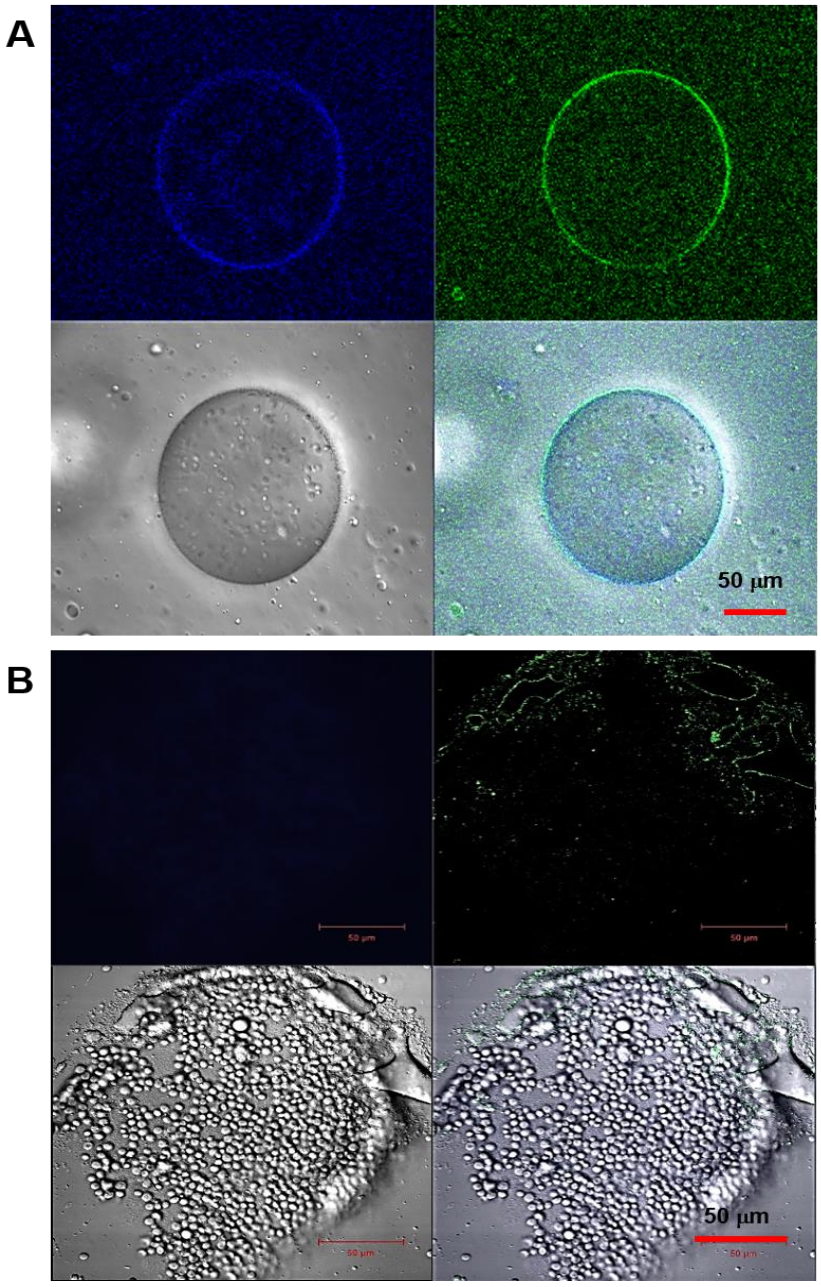

Fig. 6.16 Confocal images of droplets with ShCNCCa at (A) pH 2 and (B) pH 7.5.

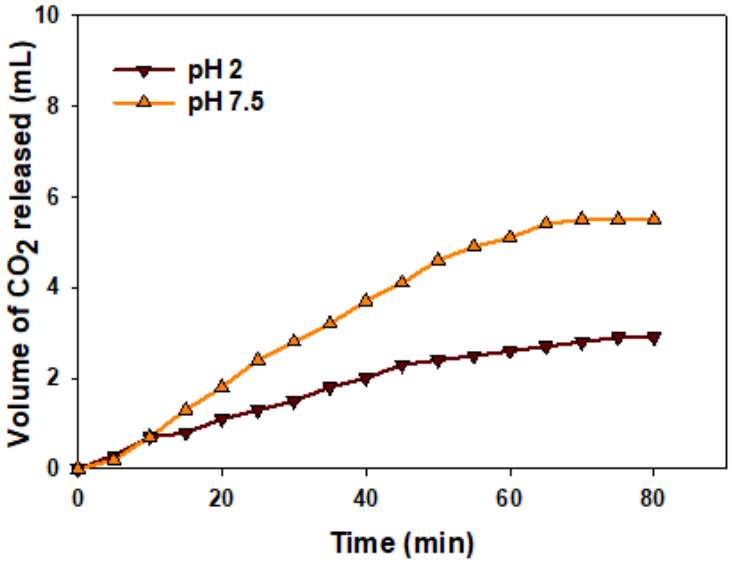

Fig. 6.17 CO_2 release of yeast in varying pH levels in Pickering emulsions.

The viscometric analysis provides insights into the interactions of microcapsules and mucins found on the intestinal walls (Hassan & Gallo, 1990; Lin *et al.*, 2019). The mucoadhesion characteristics of the formulations were examined by conducting viscometric measurements. Fig. 6.18 summarizes the results on the interaction between the ShCNCCa-mucin and ShCNCCa-mucin containing yeast, which was kept in the intestinal-mucosal environment using a simulated intestinal fluid (SIF). According to Lin *et al.* (2019), the presence of bile salts in SIF impact the shear-thinning characteristics since the pH and ionic strength of SIF (consistent with the intestinal conditions) alter the fluid behaviour of the system, which is further impacted by the presence of CNC and shellac (Lin *et al.*, 2019). Fig. 6.18A compares the viscosities of mucin, ShCNC and ShCNCCa-mucin, where the highest enhancement in viscosity was observed in the presence of ShCNCCa. All the samples displayed a shear-thinning profile. The addition of yeast to the ShCNCCa complex resulted in a marginal

enhancement in the viscosity (Fig. 6.18B), and the viscosity profiles were similar to those without yeasts.

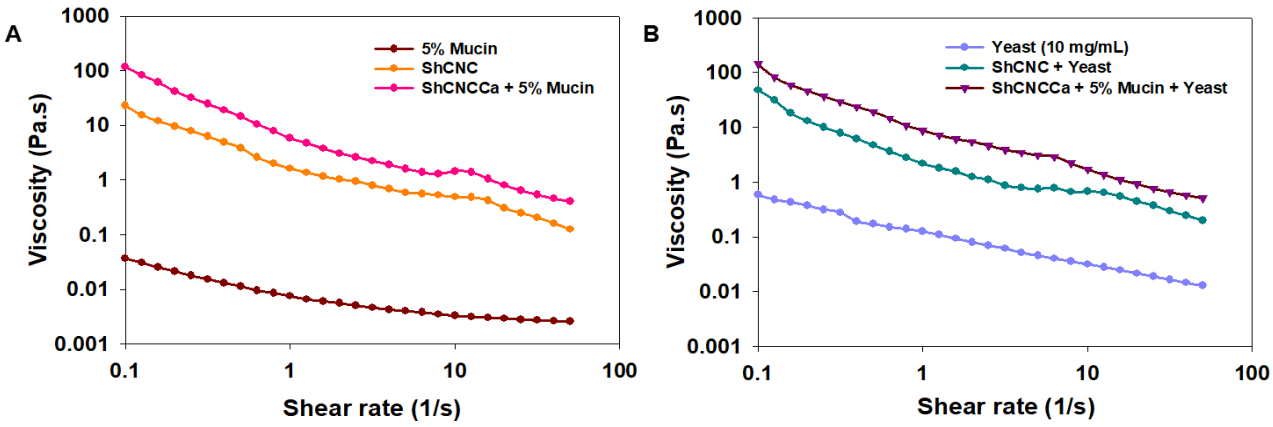

Fig. 6.18 shows the viscosity versus the shear rate of (A) mucin, ShCNC, and ShCNCCa-mucin B) the same composition, but with added yeast. Each sample was subjected to a shear rate of 0.1 to 50 1/s. Rheometric data was measured using a Kinexus Ultra + rheometer via a cup (DO25 C0107 AL) and bob (DG25 L0381 SS) at 37°C.

The data in Fig. 6.18 were analyzed and summarized in Table 6.1, where the relative viscosity of the mixture at the shear rates of 3.98 and 10.00 1/s confirmed the expected enhancement in the presence of mucin (De Loubens *et al.*, 2013; Lin *et al.*, 2019). Fig. 6.18A portrays the significant enhancement within the SIF environment; the viscosity of both ShCNCCa-mucin and ShCNCCa-mucin with yeast (10 mg/mL) mixtures increased in viscosity when compared to the 5% mucin matrix. The ShCNCCa-mucin mixtures demonstrated enhancement, whereby the viscosity at the shear rates of 3.98 and 10.00 1/s was 2613.4 and 905.9 mPa.s, respectively; these values were significantly higher than the viscosity of 5wt% mucin. A

similar observation was recorded for the ShCNCCa-mucin with the yeast mixture, where the viscosity was found to be 2660.9 and 990.1 mPa.s at the shear rates of 3.98 and 10.00 1/s, respectively. These viscosities were, however, significantly larger than the viscosity of 5wt% mucin.-The concentration of CNC and shellac would likely impact the viscosity, and this was reported previously for other variants of nanocellulose (Lin *et al.*, 2019). A 1 wt% cellulose nanofibril (CNF) in such a mixture displayed a higher viscosity enhancement compared to a 0.1wt% CNF mixture.

The relative viscosity was used to assess the degree of enhancement and values greater than 1 indicate a stronger interaction between the polymers and mucin (Lin *et al.*, 2019). The relative enhancement did not seem to be affected by the addition of yeast. Mucoadhesion between the polymers and mucous decreased the mucous's fluidity (King, 2006); hence our results suggested that systems with ShCNCCa displayed favourable mucoadhesion within the intestinal environment. This will improve the delivery of active compounds using the proposed encapsulation system with the rationale that the ShCNCCa complex will exhibit enhanced mucoadhesion within the SIF environment of the human intestine; the ShCNCCa delivery system could harness this enhanced mucoadhesion to ensure that the active compounds can be released upon coalescence of the delivery system. This further ensures that the delivery of the active compound would not be negated by the passage through the GIT.

Table 6.1 Viscosities of 2% CNC + 0.55% Shellac + 5% Mucin and 2% CNC + 0.5% Shellac + 5% Mucin + Yeast (10 mg/mL).

	SIF – pH 7.5	
Shear Rate (1/s)	3.98	10.00
ShCNCCa-mucin		
$\eta_{enhancement}$ (mPa. s)	2613.4	905.9
$\eta_{relative}$	4.65	2.66
ShCNCCa-mucin with yeast (10 mg/mL)		
$\eta_{enhancement}$ (mPa. s)	2660.9	990.1
$\eta_{relative}$	4.26	2.37

$$\eta_{enhancement} = [\eta_{mixture} - (\eta_{nanocellulose} + \eta_{mucin})] \times 1000 \quad (6.1)$$

$$\eta_{relative} = [\eta_{mixture} \div (\eta_{nanocellulose} + \eta_{mucin})] \quad (6.2)$$

6.4 Conclusions

A uniform, probiotic-containing microcapsules were produced with shellac and CNC using the Pickering emulsion approach. Through theoretical and various microscopic techniques, the formation of the protective shellac layer and yeast encapsulation was achieved. Probiotic release and CO_2 production indicated that the microcapsule dissolution was pH-dependent and occurred in a basic pH environment that was greater than the *pKa* of shellac. Shellac microcapsules could maintain the survivability of *S. cerevisiae* during exposure to simulated gastric and intestinal environments. The incorporation of CNC improved yeast survival in

gastric conditions. When the CO_2 release was measured, coating with shellac complex reduced the gas release compared to the control due to the slower dissolution of shellac in the intestinal fluid. The probiotic-microcapsule formation was examined using confocal laser scanning microscopy that confirmed the formation of the shellac network with CNC and $CaCl_2$. This method could be effective in preparing to encapsulate systems for probiotic delivery suitable for the biomedical, food and cosmetic industries.

Chapter 7

Conclusions and recommendation for future studies

7.1 Conclusions and Contributions

Emulsions are one of the common technologies in the food, cosmetic and pharmaceutical industries. In the food industry, synthetic surfactants are widely used, as evident from the ingredient lists of unfamiliar food additives (emulsifiers) shown on the back of the food packaging. However, many of today's consumers seek healthy foods that provide functional benefits for their health.

Therefore, Pickering Emulsion has recently emerged as an excellent strategy to stabilize emulsion systems in functional foods. Unlike conventional emulsions, the Pickering emulsion is attractive in food research since it is surfactant-free and can irreversibly absorb to the oil-water interface to produce safe, stable and environmentally friendly food systems.

The Ph.D. research seeks to develop nano- and micro-capsules using an emulsification technique to protect active substances, such as vitamin C and probiotics, that are easily oxidized under various conditions. Using this approach, stable, rigid capsules that offer long-term storage were produced.

Chitosan, a natural polymer, was ionically cross-linked with negatively charged polyanions and used as a Pickering emulsifier described in chapter 3. By modifying chitosan with

GTMAC, the modified chitosan was water-soluble at all pHs, and it was complexed with PCNC to prepare nanocomplexes for functional food applications. The complexation of GCh and PCNC resulted in the formation of nanoscale complexes with an average diameter of 300–350 nm and a hard-sphere morphology. The GCh-PCNC complexes yielded very stable Pickering emulsions compared to emulsion prepared from the GCh-TPP system. These novel nanostructures provide a new approach to stabilize emulsion for functional food formulation.

Chapter 4 examines the stabilization mechanism and effectiveness of PCNC over TPP to improve the stability. The encapsulation and VC release of the VC-GCh-PCNC nanocapsule system were examined. PCNC could effectively stabilize the system via stronger ionic gelation compared to TPP. The stability of VC in the system is highly dependent on light, pH, and dissolved oxygen of the environment. A better kinetic release of VC was achieved under a nitrogen purge. The PCNC cross-linked nanocapsules possessed a sustained release profile, making them ideal candidates for prolonged VC storage. The kinetic release profiles were fitted to first-order and Higuchi kinetic models (R^2 >0.95), confirming the concentration-dependent release of VC from the VC-GCh-PCNC nanocapsule system. A simulated digestive system for in vitro release test at varying pHs showed faster release rates at low pHs that were attributed to the degree of quaternization of GCh in the system. The sedimented VC-GCh-PCNC possessed a higher antioxidant capacity than VC-GCh-TPP. Additionally, the MIC for *E. coli* and *S. aureus* bacterial strains were between 8 to 16 μg/mL, which suggested that the VC-GCh-PCNC complexes were efficient antimicrobial agents that

could extend the shelf-life of the food system. These results showed that VC's stability was enhanced in the presence of PCNC, thereby offering a strategy for the preservation of highly unstable compounds (such as VC) during long-term storage in functional food materials.

In Chapters 5 and 6, functional materials (e.g., ferulic acid and shellac) coated on CNC could function as a stable emulsifier at the W/O interface. The ferulic acid (FA) functionalized cellulose nanocrystals (CNCs) (CNCFA) was used, where FA acts as an antioxidant and pH-responsive compound for the preparation of "smart," multiple Pickering emulsion containing yeast with a modified plant-based emulsifier. The viability of yeast during the emulsification process, storage, and intestinal delivery was demonstrated with higher survivability against severe acidic conditions in the stomach (pH 1.5-2.5). Hence, the multiple Pickering emulsion could be delivered to the intestine, where the encapsulated probiotics could be released due to the pH responsivity of intestinal conditions. This system can be applied and scaled for food applications.

The W/O Pickering emulsion using natural-based nanoparticles, CNC, and Shellac was developed as a new approach for the systematic delivery of probiotics. Shellac is a suitable enteric coating material that protects probiotics in the stomach, followed by a triggered release in the intestine to confer health benefits in the human body. By adding $CaCl_2$ to the system, the network experiences increased emulsion stability. Therefore, it would be expected that the ShCNCCa network would be utilized in various food, personal and biomedical applications.

7.2 Recommendation for future studies

In chapter 3, based on the research activities on functional nanomaterials, we noted that modified cellulose nanocrystals would significantly improve the emulsion stability. In this study, lignin and hemicellulose were removed from the pulp by alkali treatment, and the CNC was extracted from cellulose by acid hydrolysis with phosphoric acid. For food research and development, post-harvesting of plant residue (peels and seeds) could be conducted to reduce the environmental concerns of food wastes. Thus, future studies could explore the extraction of cellulose nanomaterials from these sources, contributing to the reduction of carbon dioxide and methane emissions.

As reported in chapter 4, the concept of 3 in 1 system consisting of (1) encapsulation functional material to prevent harsh conditions and control release, (2) food-grade emulsifier for stability emulsion and (3) antibacterial property to resist bacterial growth should be explored and examined further. This smart emulsifier could be applied to products that could be stored for a long time, for example, vitamin C beverages (e.g., orange juice, fruit juice), cereal, even short shelf-life breakfast foods (e.g., ready meal). Therefore, a more reliable test for long-term storage stability, release profiles, and product degradation should be further examined.

The novel nanoparticles CNCFA and complex form of ShCNCCa, as described in chapter 5 and 6, could be used for enteric coating because both FA and Sh consisting of COOH groups

that possessed a pH-dependent solubility above the *pKa* value. However, other than the enteric-coated application, food packaging/coating could be explored since FA is approved as a food preservative and natural antioxidant. It also has a strong UV blocking function. In addition, Sh can prevent the growth of aerobic bacteria and the evaporation of contents within the food.

Food packaging/coating is one of the most important processes in maintaining shelf life and quality. Moisture and air are factors that contributed to the safety concerns associated with contamination and degradation of food quality. Therefore, food packaging or coating on food with CNCFA and ShCNCCa could be applied to alleviate current packaging concerns and improve the robustness of the packaging systems.

References

Abitbol, T., Kloser, E., & Gray, D. G. (2013). Estimation of the surface sulfur content of cellulose nanocrystals prepared by sulfuric acid hydrolysis. Cellulose, 20(2), 785-794.

Adeyemi, O. S., Awakan, O. J., Atolani, O., Iyeye, C. O., Oweibo, O. O., Adejumo, O. J., Ibrahim, A., Batiha, G. E.-s. (2019). New Ferulic Acid Derivatives Protect Against Carbon Tetrachloride-Induced Liver Injury in Rats. The Open Biochemistry Journal, 13(1), 13-22.

Ahmed, F., & Mondal, MdIH. (2017) Preparation and characterization of functionalized chitosan derivatives from prawn waste for cellulose fibre modification to enhance textile properties. Journal of Textile Science & Engineering, 7(5), 318-327.

Akash, B. (2015). Thermochemical depolymerization of biomass. Procedia Computer Science, 52, 827-834.

Akhlaghi, S. P., Berry, R. M., & Tam, K. C. (2015). Modified cellulose nanocrystal for vitamin C delivery. Aaps Pharmscitech, 16(2), 306-314.

Akyön, Y. (2002). Effect of antioxidants on the immune response of Helicobacter pylori. Clinical Microbiology and Infection, 8(7), 438-441.

Al Arni, S., Drake, A. F., Del Borghi, M., & Converti, A. (2010). Study of aromatic compounds derived from sugarcane bagasse. Part I: effect of pH. Chemical Engineering & Technology: Industrial Chemistry-Plant Equipment-Process Engineering-Biotechnology, 33(6), 895-901.

Al Jitan, S., Alkhoori, S. A., & Yousef, L. F. (2018). Phenolic acids from plants: extraction and application to human health. Studies in Natural Products Chemistry, 58, 389-417.

Albert, C., Beladjine, M., Tsapis, N., Fattal, E., Agnely, F., & Huang, N. (2019). Pickering emulsions: Preparation processes, key parameters governing their properties and potential for pharmaceutical applications. Journal of Controlled Release, 309, 302-332.

Al-Gousous, J., Penning, M., & Langguth, P. (2015). Molecular insights into shellac film coats from different aqueous shellac salt solutions and their effect on the disintegration of enteric-coated soft gelatin capsules. International journal of pharmaceutics, 484(1-2), 283-291.

Alipour, S. M., Nouri, M., Mokhtari, J., & Bahrami, S. H. (2009). Electrospinning of poly (vinyl alcohol)–water-soluble quaternized chitosan derivative blend. Carbohydrate research, 344(18), 2496-2501.

Alishahi, A., Mirvaghefi, A., Tehrani, M. R., Farahmand, H., Shojaosadati, S. A., Dorkoosh, F. A., & Elsabee, M. Z. (2011). Shelf life and delivery enhancement of vitamin C using chitosan nanoparticles. Food Chemistry, 126(3), 935-940.

Al-Obaidy, S. S., Greenway, G. M., & Paunov, V. N. (2019). Dual-functionalised shellac nanocarriers give a super-boost of the antimicrobial action of berberine. Nanoscale Advances, 1(2), 858-872.

Annunziata, G., Maisto, M., Schisano, C., Ciampaglia, R., Narciso, V., Tenore, G. C., & Novellino, E. (2019). Effects of grape pomace polyphenolic extract (Taurisolo®) in reducing TMAO serum levels in humans: preliminary results from a randomized, placebo-controlled, cross-over study. Nutrients, 11(1), 139-150.

Ashori, A. (2006). Nonwood fibers—A potential source of raw material in papermaking. Polymer-Plastics Technology and Engineering, 45(10), 1133-1136.

Ashrafizadeh, M., Tam, K. C., Javadi, A., Abdollahi, M., Sadeghnejad, S., & Bahramian, A. (2020). Dual physically and chemically cross-linked polyelectrolyte nanohydrogels: Compositional and pH-dependent behavior studies. European Polymer Journal, 122, 109398.

Atay, H. Y. (2019). Antibacterial activity of chitosan-based systems. In Functional chitosan. Springer, Singapore, 457-489.

Azevedo, M. A., Bourbon, A. I., Vicente, A. A., & Cerqueira, M. A. (2014). Alginate/chitosan nanoparticles for encapsulation and controlled release of vitamin B2. International Journal of Biological Macromolecules, 71, 141-146.

Baek, J., Wahid-Pedro, F., Kim, K., Kim, K., & Tam, K. C. (2019). Phosphorylated-CNC/modified-chitosan nanocomplexes for the stabilization of Pickering emulsions. Carbohydrate polymers, 206, 520-527.

Bai, L., Huan, S., Li, Z., & McClements, D. J. (2017). Comparison of emulsifying properties of food-grade polysaccharides in oil-in-water emulsions: Gum arabic, beet pectin, and corn fiber gum. Food Hydrocolloids, 66, 144-153.

Bar, H., & Bianco-Peled, H. (2020). Modification of shellac coating using Jeffamine® for enhanced mechanical properties and stability. Progress in Organic Coatings, 141, 105559.

Barthel, M. J., Rinkenauer, A. C., Wagner, M., Mansfeld, U., Hoeppener, S., Czaplewska, J. A., & Schubert, U. S. (2014). Small but powerful: co-assembly of polyether-based triblock terpolymers into sub-30 nm micelles and synergistic effects on cellular interactions. Biomacromolecules, 15, 2426-2439.

Bayat, A., Dorkoosh, F. A., Dehpour, A. R., Moezi, L., Larijani, B., Junginger, H. E., & Rafiee-Tehrani, M. (2008). Nanoparticles of quaternized chitosan derivatives as a carrier for colon delivery of insulin: ex vivo and in vivo studies. International Journal of Pharmaceutics, 356(1-2), 259-266.

Bellan, L. M., Pearsall, M., Cropek, D. M., & Langer, R. (2012). A 3D interconnected microchannel network formed in gelatin by sacrificial shellac microfibers. Advanced Materials, 24(38), 5187-5191.

Bendich, A., Machlin, L., Scandurra, O., Burton, G., & Wayner, D. (1986). The antioxidant role of vitamin C. Advances in Free Radical Biology & Medicine, 2(2), 419-444.

Berski, W., Ptaszek, A., Ptaszek, P., Ziobro, R., Kowalski, G., Grzesik, M., & Achremowicz, B. (2011). Pasting and rheological properties of oat starch and its derivatives. Carbohydrate Polymers, 83(2), 665-671.

Binks, B. P. (2002). Particles as surfactants—similarities and differences. Current Opinion in Colloid & Interface Science, 7(1-2), 21-41.

Binks, B., & Fletcher, P. (2001). Particles adsorbed at the oil− water interface: A theoretical comparison between spheres of uniform wettability and “Janus” particles. Langmuir, 17(16), 4708-4710.

Bodannes, R. S., & Chan, P. C. (1979). Ascorbic-Acid as a Scavenger of Singlet Oxygen. Febs Letters, 105(2), 195-196.

Bondeson, D., Mathew, A., & Oksman, K. (2006). Optimization of the isolation of nanocrystals from microcrystalline cellulose by acid hydrolysis. Cellulose, 13(2), 171-180.

Brinchi, L., Cotana, F., Fortunati, E., & Kenny, J. (2013). Production of nanocrystalline cellulose from lignocellulosic biomass: technology and applications. Carbohydrate polymers, 94(1), 154-169.

Brinker, C. J., & Scherer, G. W. (2013). Sol-gel science: the physics and chemistry of sol-gel processing. Academic press.

Bruel, C., Tavares, J. R., Carreau, P. J., & Heuzey, M.-C. (2019). The structural amphiphilicity of cellulose nanocrystals characterized from their cohesion parameters. Carbohydrate Polymers, 205, 184-191.

Burdock, G. A., Carabin, I. G., & Griffiths, J. C. (2006). The importance of GRAS to the functional food and nutraceutical industries. Toxicology, 221(1), 17-27.

Burdurlu, H. S., Koca, N., & Karadeniz, F. (2006). Degradation of vitamin C in citrus juice concentrates during storage. Journal of Food Engineering, 74(2), 211-216.

Caccavo, D., Cascone, S., Lamberti, G., & Barba, A. A. (2015). Controlled drug release from hydrogel-based matrices: Experiments and modeling. International Journal of Pharmaceutics, 486(1-2), 144-152.

Cagil, E. M. (2020). Production and characterization of a new pH-responsive shellac system for controlled drug release. Journal of Molecular Structure, 1217, 128382.

Camarero Espinosa, S., Kuhnt, T., Foster, E. J., & Weder, C. (2013). Isolation of thermally stable cellulose nanocrystals by phosphoric acid hydrolysis. Biomacromolecules, 14, 1223-1230.

Canada Functional Foods & Natural Health Products Market Size, Share & Trends Analysis Report By Product (Functional Foods (Dairy, Fats & Oil), Natural Health (Vitamins, Carotenoids)), By Form, And Segment Forecasts, 2019 – 2025. https://www.grandviewresearch.com/industry-analysis/canada-functional-foods-natural-health-products-market.

Cao, X., Chen, Y., Chang, P. R., Muir, A. D., & Falk, G. (2008). Starch-based nanocomposites reinforced with flax cellulose nanocrystals. Express Polym Lett, 2(7), 502-510.

Capela, P., Hay, T., & Shah, N. (2007). Effect of homogenisation on bead size and survival of encapsulated probiotic bacteria. Food Research International, 40(10), 1261-1269.

Carunchio, F., Crescenzi, C., Girelli, A. M., Messina, A., & Tarola, A. M. (2001). Oxidation of ferulic acid by laccase: identification of the products and inhibitory effects of some dipeptides. Talanta, 55(1), 189-200.

Cha, J. U., Lee, S. W., Hong, J. K., Cha, J. H., & Ko, W. H. (2016). Enteric coating composition, enteric coating film, and food formulation. In: Google Patents.

Chang, K., Liu, J., Jiang, W., Zhang, R., Zhang, T., & Liu, B. (2020). Ferulic acid-ovalbumin protein nanoparticles: Structure and foaming behavior. Food Research International, 136, 109311.

Chappat, M. (1994). Some applications of emulsions. Colloids and Surfaces A: Physicochemical and Engineering Aspects, 91, 57-77.

Chartrand, A., Lavoie, J. M., & Huneault, M. A. (2017). Surface modification of microcrystalline cellulose (MCC) and its application in LDPE-based composites. Journal of Applied Polymer Science, 134(1), 44343.

Chassaing, B., Koren, O., Goodrich, J. K., Poole, A. C., Srinivasan, S., Ley, R. E., & Gewirtz, A. T. (2015). Dietary emulsifiers impact the mouse gut microbiota promoting colitis and metabolic syndrome. Nature, 519(7541), 92-96.

Chauhan, O., Nanjappa, C., Ashok, N., Ravi, N., Roopa, N., & Raju, P. (2015). Shellac and Aloe vera gel based surface coating for shelf life extension of tomatoes. Journal of food science and technology, 52(2), 1200-1205.

Chen, L., Ao, F., Ge, X., & Shen, W. (2020). Food-Grade Pickering Emulsions: Preparation, Stabilization and Applications. Molecules, 25(14), 3202.

Chen, S., Xu, C., Mao, L., Liu, F., Sun, C., Dai, L., & Gao, Y. (2018). Fabrication and characterization of binary composite nanoparticles between zein and shellac by anti-solvent co-precipitation. Food and Bioproducts Processing, 107, 88-96.

Chen, Y. W., Tan, T. H., Lee, H. V., & Abd Hamid, S. B. (2017). Easy fabrication of highly thermal-stable cellulose nanocrystals using Cr (NO3) 3 catalytic hydrolysis system: A feasibility study from macro-to nano-dimensions. Materials, 10(1), 42.

Cheng, C., Guo, R., Lan, J., & Jiang, S. (2017). Extraction of lotus fibres from lotus stems under microwave irradiation. Royal Society open science, 4, 170747.

Cheow, W. S., & Hadinoto, K. (2013). Biofilm-like Lactobacillus rhamnosus probiotics encapsulated in alginate and carrageenan microcapsules exhibiting enhanced thermotolerance and freeze-drying resistance. Biomacromolecules, 14(9), 3214-3222.

Chesner, L. (1963). Some Bleaching Problems and Developments associated with Hydrogen Peroxide, Peracetic Acid, and Sodium Chlorite. Coloration Technology, 79(4), 139-146.

Chiarappa, G., Abrami, M., Dapas, B., Farra, R., Trebez, F., Musiani, F., Grassi, G., Grassi, M. (2017). Mathematical Modeling of Drug Release from Natural Polysaccharides Based Matrices. Natural Product Communications, 12(6), 873-880.

Cho, J., Grant, J., Piquette-Miller, M., & Allen, C. (2006). Synthesis and physicochemical and dynamic mechanical properties of a water-soluble chitosan derivative as a biomaterial. Biomacromolecules, 7, 2845-2855.

Costa, T. d. S., Rogez, H., & Pena, R. d. S. (2015). Adsorption capacity of phenolic compounds onto cellulose and xylan. Food Science and Technology, 35(2), 314-320.

Credou, J., & Berthelot, T. (2014). Cellulose: from biocompatible to bioactive material. Journal of Materials Chemistry B, 2, 4767-4788.

Crofton, A. R., Hudson, S. M., Howard, K., Pender, T., Abdelgawad, A., Wolski, D., & Kirsch, W. M. (2016). Formulation and characterization of a plasma sterilized, pharmaceutical grade chitosan powder. Carbohydrate polymers, 146, 420-426.

Cui, J., Kaandorp, J. A., Sloot, P. M., Lloyd, C. M., & Filatov, M. V. (2009). Calcium homeostasis and signaling in yeast cells and cardiac myocytes. FEMS yeast research, 9(8), 1137-1147.

Dagnon, K. L., Way, A. E., Carson, S. O., Silva, J., Maia, J., & Rowan, S. J. (2013). Controlling the rate of water-induced switching in mechanically dynamic cellulose nanocrystal composites. Macromolecules, 46, 8203-8212.

Das, S., & Jacob, S. E. (2011). Shellac. Dermatitis, 22(4), 220-222.

Das, S., & Wong, A. B. (2020). Stabilization of ferulic acid in topical gel formulation via nanoencapsulation and pH optimization. Scientific reports, 10(1), 1-18.

Dávila-Guzman, N., Cerino-Córdova, F., Diaz-Flores, P., Rangel-Mendez, J., Sánchez-González, M., & Soto-Regalado, E. (2012). Equilibrium and kinetic studies of ferulic acid adsorption by Amberlite XAD-16. Chemical Engineering Journal, 183, 112-116.

de Britto, D., de Moura, M. R., Aouada, F. A., Mattoso, L. H., & Assis, O. B. (2012). N, N, N-trimethyl chitosan nanoparticles as a vitamin carrier system. Food Hydrocolloids, 27(2), 487-493.

De Loubens, C., Lentle, R. G., Love, R. J., Hulls, C., & Janssen, P. W. (2013). Fluid mechanical consequences of pendular activity, segmentation and pyloric outflow in the proximal duodenum of the rat and the guinea pig. Journal of the Royal Society Interface, 10(83), 1-12.

de Oliveira Silva, E., & Batista, R. (2017). Ferulic acid and naturally occurring compounds bearing a feruloyl moiety: a review on their structures, occurrence, and potential health benefits. Comprehensive Reviews in Food Science and Food Safety, 16(4), 580-616.

de Paz, L. E. C., Resin, A., Howard, K. A., Sutherland, D. S., & Wejse, P. L. (2011). Antimicrobial effect of chitosan nanoparticles on Streptococcus mutans biofilms. Applied and environmental microbiology, 77(11), 3892-3895.

Decarlo, A. A., Ellis, A., Dooley, T. P., & Belousova, M. (2014). Composition, preparation, and use of dense chitosan membrane materials. In: Google Patents.

Desai, K., & Park, H. J. (2005). Encapsulation of vitamin C in tripolyphosphate cross-linked chitosan microspheres by spray drying. J. Microencapsul., 22(2), 179-192.

Desai, K., Liu, C., & Park, H. J. (2006). Characteristics of vitamin C encapsulated tripolyphosphate-chitosan microspheres as affected by chitosan molecular weight. Journal of microencapsulation, 23(1), 79-90.

Deshpande, S. S. (2002). Handbook of food toxicology. Marcel Dekker, Inc., New York, NY, USA, 262

Ding, W., & Shah, N. P. (2009). Effect of homogenization techniques on reducing the size of microcapsules and the survival of probiotic bacteria therein. Journal of food science, 74(6), M231-M236.

Doost, A. S., Kassozi, V., Grootaert, C., Claeys, M., Dewettinck, K., Van Camp, J., & Van der Meeren, P. (2019). Self-assembly, functionality, and in-vitro properties of quercetin loaded nanoparticles based on shellac-almond gum biological macromolecules. International journal of biological macromolecules, 129, 1024-1033.

Dos Santos, Z. M., Caroni, A. L. P. F., Pereira, M. R., Da Silva, D. R., & Fonseca, J. L. C. (2009). Determination of deacetylation degree of chitosan: a comparison between conductometric titration and CHN elemental analysis. Carbohydrate Research, 344, 2591-2595.

Du, H., Liu, W., Zhang, M., Si, C., Zhang, X., & Li, B. (2019). Cellulose nanocrystals and cellulose nanofibrils based hydrogels for biomedical applications. Carbohydrate Polymers, 209, 130-144.

Eyley, S., & Thielemans, W. (2014). Surface modification of cellulose nanocrystals. Nanoscale, 6(14), 7764-7779.

Falkehag, S. I., Marton, J., & Adler, E. (1966). Chromophores in kraft lignin. Adv. Chem. Ser, 59, 75-89.

Farag, Y., & Leopold, C. (2009). Physicochemical properties of various shellac types. Dissolut. Technol, 16, 33-39.

Farag, Y., & Leopold, C. S. (2011). Development of shellac-coated sustained release pellet formulations. European journal of pharmaceutical sciences, 42(4), 400-405.

Fioramonti, J., Theodorou, V., & Bueno, L. (2003). Probiotics: what are they? What are their effects on gut physiology? Best Practice & Research Clinical Gastroenterology, 17(5), 711-724.

Food and Agricultural Organization of the United Nations and World Health Organization. Joint FAO/WHO working group report on drafting guidelines for the evaluation of probiotics in food. Food and Agricultural Organization of the United Nations [online], ftp://ftp.fao.org/es/ esn/food/wgreport2.pdf (2002).

Fortunati, E., Peltzer, M., Armentano, I., Torre, L., Jiménez, A., & Kenny, J. (2012). Effects of modified cellulose nanocrystals on the barrier and migration properties of PLA nano-biocomposites. Carbohydrate polymers, 90(2), 948-956.

Fu, Y., & Kao, W. J. (2010). Drug release kinetics and transport mechanisms of non-degradable and degradable polymeric delivery systems. Expert opinion on drug delivery, 7(4), 429-444.

Fude, C., Lei, Y., Jie, J., Hongze, P., Wenhui, L., & Dongmei, C. (2007). Preparation and in vitro evaluation of pH, time-based and enzyme-degradable pellets for colonic drug delivery. Drug development and industrial pharmacy, 33(9), 999-1007.

Fujisawa, S., Togawa, E., & Kuroda, K. (2017). Nanocellulose-stabilized Pickering emulsions and their applications. Science and Technology of Advanced Materials, 18, 959-971.

Functional Foods Market Size, Share & Trends Analysis Report by Ingredient (Carotenoids, Prebiotics & Probiotics, Fatty Acids, Dietary Fibers), By Product, By Application, And Segment Forecasts, 2019 – 2025.
https://www.grandviewresearch.com/industry-analysis/functional-food-market

Gao, J., Li, K., Xu, J., Zhang, W., Ma, J., Liu, L., Sun. Y., Zhang, H., Li, K. (2018). Unexpected Rheological Behavior of a Hydrophobic Associative Shellac-Based Oligomeric Food Thickener. Journal of Agricultural and Food chemistry, 66(26), 6799-6805.

Gately, N. M., & Kennedy, J. E. (2017). The development of a melt-extruded shellac carrier for the targeted delivery of probiotics to the colon. Pharmaceutics, 9(4), 38.

Ge, S., Xiong, L., Li, M., Liu, J., Yang, J., Chang, R., Liang, C., Sun, Q. (2017). Characterizations of Pickering emulsions stabilized by starch nanoparticles: Influence of starch variety and particle size. Food chemistry, 234, 339-347.

Geng, C.-z., Hu, X., Yang, G.-h., Zhang, Q., Chen, F., & Fu, Q. (2015). Mechanically reinforced chitosan/cellulose nanocrystals composites with good transparency and biocompatibility. Chinese Journal of Polymer Science, 33(1), 61-69.

Ghalia, M. A., & Dahman, Y. (2017). Synthesis and utilization of natural fiber-reinforced poly (lactic acid) bionanocomposites. In Lignocellulosic Fibre and Biomass-Based Composite Materials Woodhead Publishing, 313-345.

Ghasemi, H., Darjani, S., Mazloomi, H., & Mozaffari, S. (2020). Preparation of stable multiple emulsions using food-grade emulsifiers: Evaluating the effects of emulsifier concentration, W/O phase ratio, and emulsification process. SN Applied Sciences, 2(12), 1-9.

Ghube, K., Khade, P., & Bhosale, A. (2020). A Review on Enteric Coating. Journal of Current Pharma Research, 10(4), 3848-3862.

Gohil, K. J., Kshirsagar, S. B., & Sahane, R. S. (2012). Ferulic acid-A comprehensive pharmacology of an important bioflavonoid. Int J Pharm Sci Res, 3, 700-710.

Grishkewich, N., Mohammed, N., Tang, J., & Tam, K. C. (2017). Recent advances in the application of cellulose nanocrystals. Current Opinion in Colloid & Interface Science, 29, 32-45.

Gupta, V., & Garg, R. (2009). Probiotics. Indian journal of medical microbiology, 27(3), 202.

Habibi, Y., & Dufresne, A. (2008). Highly filled bionanocomposites from functionalized polysaccharide nanocrystals. Biomacromolecules, 9(7), 1974-1980.

Habibi, Y., Lucia, L. A., & Rojas, O. J. (2010). Cellulose nanocrystals: chemistry, self-assembly, and applications. Chemical reviews, 110, 3479-3500.

Hagenmaier, R. D., & Shaw, P. E. (1991). Permeability of shellac coatings to gases and water vapor. Journal of Agricultural and Food chemistry, 39(5), 825-829.

Hamad, S. A., Stoyanov, S. D., & Paunov, V. N. (2012). Triggered cell release from shellac–cell composite microcapsules. Soft Matter, 8(18), 5069-5077.

Hamed, I., Özogul, F., & Regenstein, J. M. (2016). Industrial applications of crustacean by-products (chitin, chitosan, and chitooligosaccharides): A review. Trends in Food Science & Technology, 48, 40-50.

Hansuld, E. M., Briens, L., McCann, J. A., & Sayani, A. (2009). Audible acoustics in high-shear wet granulation: Application of frequency filtering. International journal of pharmaceutics, 378(1-2), 37-44.

Hasler, C. M. (2002). Functional foods: benefits, concerns and challenges—a position paper from the American Council on Science and Health. The Journal of nutrition, 132(12), 3772-3781.

Hassan, E. E., & Gallo, J. M. (1990). A simple rheological method for the in vitro assessment of mucin-polymer bioadhesive bond strength. Pharmaceutical research, 7(5), 491-495.

Hategekimana, J., Masamba, K. G., Ma, J., & Zhong, F. (2015). Encapsulation of vitamin E: effect of physicochemical properties of wall material on retention and stability. Carbohydrate Polymers, 124, 172-179.

He, G., Kong, Y., Zheng, H., Ke, W., Chen, X., Yin, Y., & Yi, Y. (2018). Preparation and properties of poly (amidoamine) dendrimer/quaternary ammonium chitosan hydrogels. Journal of Wuhan University of Technology-Mater. Sci. Ed., 33(3), 736-743.

Hebishy, E., Buffa, M., Guamis, B., Blasco-Moreno, A., & Trujillo, A.-J. (2015). Physical and oxidative stability of whey protein oil-in-water emulsions produced by conventional and ultra-high-pressure homogenization: Effects of pressure and protein concentration on emulsion characteristics. Innovative Food Science & Emerging Technologies, 32, 79-90.

HeK, G. (1982). Their Effect on the Flow of Dough'. Cereal Chem, 59(4), 291-296.

Hu, Z., Berry, R. M., Pelton, R., & Cranston, E. D. (2017). One-pot water-based hydrophobic surface modification of cellulose nanocrystals using plant polyphenols. ACS Sustainable Chemistry & Engineering, 5(6), 5018-5026.

Hult, E.-L., Iotti, M., & Lenes, M. (2010). Efficient approach to high barrier packaging using microfibrillar cellulose and shellac. Cellulose, 17(3), 575-586.

Hunter, R. J. (2001). Foundations of colloid science: Oxford university press.

Ifuku, S., Nogi, M., Abe, K., Handa, K., Nakatsubo, F., & Yano, H. (2007). Surface modification of bacterial cellulose nanofibers for property enhancement of optically transparent composites: dependence on acetyl-group DS. Biomacromolecules, 8(6), 1973-1978.

Ilyas, R. A., Sapuan, S. M., Ishak, M. R., & Zainudin, E. S. (2017). Effect of delignification on the physical, thermal, chemical, and structural properties of sugar palm fibre. BioResources, 12, 8734-8754.

Iravani, S., Korbekandi, H., & Mirmohammadi, S. V. (2015). Technology and potential applications of probiotic encapsulation in fermented milk products. Journal of food science and technology, 52(8), 4679-4696.

Ito, T., Tsuji, Y., Aramaki, K., & Tonooka, N. (2012). Two-step emulsification process for water-in-oil-in-water multiple emulsions stabilized by lamellar liquid crystals. Journal of oleo science, 61(8), 413-420.

Jiang, F., & Hsieh, Y.-L. (2015). Cellulose nanocrystal isolation from tomato peels and assembled nanofibers. Carbohydrate polymers, 122, 60-68.

Jiao, Z., Wang, X., Yin, Y., Xia, J., & Mei, Y. (2018). Preparation and evaluation of a chitosan-coated antioxidant liposome containing vitamin C and folic acid. Journal of microencapsulation, 35(3), 272-280.

Jimenez, A., Fabra, M. J., Talens, P., & Chiralt, A. (2012). Edible and biodegradable starch films: a review. Food and Bioprocess Technology, 5(6), 2058-2076.

Jiménez-Fernández, E., Ruyra, A., Roher, N., Zuasti, E., Infante, C., & Fernández-Díaz, C. (2014). Nanoparticles as a novel delivery system for vitamin C administration in aquaculture. Aquaculture, 432, 426-433.

Jonassen, H., Kjøniksen, A. L., & Hiorth, M. (2012). Stability of chitosan nanoparticles cross-linked with tripolyphosphate. Biomacromolecules, 13, 3747-3756.

Joye, I. J., & McClements, D. J. (2013). Production of nanoparticles by anti-solvent precipitation for use in food systems. Trends in Food Science & Technology, 34(2), 109-123.

Julius, W. J., Eline, M., Sonja, I. R., Kira, E., Albert, P., & Willem, K. (2014). Particle shape anisotropy in Pickering emulsions: cubes and peanuts. Langmuir, 30, 955-964.

Jung, J., Cavender, G., Simonsen, J., & Zhao, Y. (2015). Investigation of the mechanisms of using metal complexation and cellulose nanofiber/sodium alginate layer-by-layer coating for retaining anthocyanin pigments in thermally processed blueberries in aqueous media. Journal of agricultural and food chemistry, 63(11), 3031-3038.

Jungnikl, K., Paris, O., Fratzl, P., & Burgert, I. (2008). The implication of chemical extraction treatments on the cell wall nanostructure of softwood. Cellulose, 15, 407-418.

Karbstein, H., & Schubert, H. (1995). Developments in the continuous mechanical production of oil-in-water macro-emulsions. Chemical Engineering and Processing: Process Intensification, 34(3), 205-211.

Karimi, M., Avci, P., Ahi, M., Gazori, T., Hamblin, M. R., & Naderi-Manesh, H. (2013). Evaluation of chitosan-tripolyphosphate nanoparticles as a p-shRNA delivery vector: formulation, optimization and cellular uptake study. Journal of nanopharmaceutics and drug delivery, 1(3), 266-278.

Katouzian, I., & Jafari, S. M. (2016). Nano-encapsulation as a promising approach for targeted delivery and controlled release of vitamins. Trends in Food Science & Technology, 53, 34-48.

Kechagia, M., Basoulis, D., Konstantopoulou, S., Dimitriadi, D., Gyftopoulou, K., Skarmoutsou, N., & Fakiri, E. M. (2013). Health benefits of probiotics: a review. International Scholarly Research Notices, 2013.

Kim, D., Islam, M. S., & Tam, M. K. (2019). The use of nano-polysaccharides in biomedical applications. In Advanced Functional Materials from Nanopolysaccharides. Springer, 171-219.

King, M. (2006). Physiology of mucus clearance. Paediatric respiratory reviews, 7, S212-S214.

Kokol, V., Božič, M., Vogrinčič, R., & Mathew, A. P. (2015). Characterisation and properties of homo-and heterogenously phosphorylated nanocellulose. Carbohydrate polymers, 125, 301-313.

Kong, L., Amstad, E., Hai, M., Ke, X., Chen, D., Zhao, C.-X., & Weitz, D. A. (2017). Biocompatible microcapsules with a water core templated from single emulsions. Chinese Chemical Letters, 28(9), 1897-1900.

Krasaekoopt, W., Bhandari, B., & Deeth, H. (2003). Evaluation of encapsulation techniques of probiotics for yoghurt. International dairy journal, 13(1), 3-13.

Krause, K., & Müller, R. (2001). Production of aqueous shellac dispersions by high pressure homogenisation. International journal of pharmaceutics, 223(1-2), 89-92.

Kumar, M. N. V. R. (2000). A review of chitin and chitosan applications. Reactive & Functional Polymers, 46(1), 1-27.

Kumar, P., Barrett, D. M., Delwiche, M. J., & Stroeve, P. (2009). Methods for pretreatment of lignocellulosic biomass for efficient hydrolysis and biofuel production. Industrial & engineering chemistry research, 48(8), 3713-3729.

Kwolek-Mirek, M., & Zadrag-Tecza, R. (2014). Comparison of methods used for assessing the viability and vitality of yeast cells. FEMS yeast research, 14(7), 1068-1079.

Lad, V. N., & Murthy, Z. V. P. (2012). Enhancing the stability of oil-in-water emulsions emulsified by coconut milk protein with the application of acoustic cavitation. Industrial & engineering chemistry research, 51(11), 4222-4229.

Larsen, S. W., Ostergaard, J., Yaghmur, A., Jensen, H., & Larsen, C. (2013). Use of in vitro release models in the design of sustained and localized drug delivery systems for subcutaneous and intra-articular administration. Journal of Drug Delivery Science and Technology, 23(4), 315-324.

Lazaridou , M., Christodoulou, E., Nerantzaki, M., Kostoglou, M., Lambropoulou, D. A., Katsarou, A., Pantopoulos, K., Bikiaris, D. N. (2020). Formulation and in-vitro characterization of chitosan-nanoparticles loaded with the iron chelator deferoxamine mesylate (DFO). Pharmaceutics, 12(3), 238.

Li, C., Yu, W., Wu, P., & Chen, X. D. (2020). Current in vitro digestion systems for understanding food digestion in human upper gastrointestinal tract. Trends in Food Science & Technology, 96, 114-126.

Li, H., Du, Y., Wu, X., & Zhan, H. (2004). Effect of molecular weight and degree of substitution of quaternary chitosan on its adsorption and flocculation properties for potential retention-aids in alkaline papermaking. Colloids and Surfaces A: Physicochemical and Engineering Aspects, 242, 1-8.

Lim, S. H., & Hudson, S. M. (2004). Synthesis and antimicrobial activity of a water-soluble chitosan derivative with a fiber-reactive group. Carbohydrate research, 339(2), 313-319.

Lim, S.-H., & Hudson, S. M. (2003). Review of chitosan and its derivatives as antimicrobial agents and their uses as textile chemicals. Journal of macromolecular science, part C: Polymer reviews, 43(2), 223-269.

Limmatvapirat, S., Limmatvapirat, C., Luangtana-anan, M., Nunthanid, J., Oguchi, T., Tozuka, Y., Yamamoto, K., Puttipipatkhachorn, S. (2004). Modification of physicochemical and mechanical properties of shellac by partial hydrolysis. International journal of pharmaceutics, 278(1), 41-49.

Limmatvapirat, S., Limmatvapirat, C., Puttipipatkhachorn, S., Nuntanid, J., & Luangtana-anan, M. (2007). Enhanced enteric properties and stability of shellac films through composite salts formation. European Journal of Pharmaceutics and Biopharmaceutics, 67(3), 690-698.

Limmatvapirat, S., Nunthanid, J., Puttipipatkhachorn, S., & Luangtana-anan, M. (2005). Effect of alkali treatment on properties of native shellac and stability of hydrolyzed shellac. Pharmaceutical development and technology, 10(1), 41-46.

Lin, N., Gèze, A., Wouessidjewe, D., Huang, J., & Dufresne, A. (2016). Biocompatible double-membrane hydrogels from cationic cellulose nanocrystals and anionic alginate as complexing drugs codelivery. ACS applied materials & interfaces, 8(11), 6880-6889.

Lin, T. Y., Lu, C. W., Huang, S.-K., & Wang, S.-J. (2013). Ferulic acid suppresses glutamate release through inhibition of voltage-dependent calcium entry in rat cerebrocortical nerve terminals. Journal of Medicinal Food, 16(2), 112-119.

Lin, Y.-J., Shatkin, J. A., & Kong, F. (2019). Evaluating mucoadhesion properties of three types of nanocellulose in the gastrointestinal tract in vitro and ex vivo. Carbohydrate Polymers, 210, 157-166.

Lin, Y.-J., Shatkin, J. A., & Kong, F. (2019). Evaluating mucoadhesion properties of three types of nanocellulose in the gastrointestinal tract in vitro and ex vivo. Carbohydrate polymers, 210, 157-166.

Liping, L., Kexin, L., Huipu, D., Jia, L., & Jie, Z. (2020). Study on Preparation of a Chitosan/Vitamin C Complex and Its Properties in Cosmetics. Natural Product Communications, 15(10), 1-9.

Liu, B., Wang, X., Pang, C., Luo, J., Luo, Y., & Sun, R. (2013). Preparation and antimicrobial property of chitosan oligosaccharide derivative/rectorite nanocomposite. Carbohydrate polymers, 92(2), 1078-1085.

Liu, J., Li, H., Chen, D., Jin, X., Zhao, X., Zhang, C., & Ping, Q. (2011). In vivo evaluation of novel chitosan graft polymeric micelles for delivery of paclitaxel. Drug delivery, 18(3), 181-189.

Liu, W., Tian, M., Kong, Y., Lu, J., Li, N., & Han, J. (2017). Multilayered vitamin C nanoliposomes by self-assembly of alginate and chitosan: Long-term stability and feasibility application in mandarin juice. LWT, 75, 608-615.

Lončarević, A., Ivanković, M., & Rogina, A. (2017). Lysozyme-induced degradation of chitosan: the characterisation of degraded chitosan scaffolds. Journal of Tissue Repair and Regeneration, 1(1), 12-22.

Loutfy, S. A., El-Din, H. M. A., Elberry, M. H., Allam, N. G., Hasanin, M., & Abdellah, A. M. (2016). Synthesis, characterization and cytotoxic evaluation of chitosan nanoparticles: in

vitro liver cancer model. Advances in Natural Sciences: Nanoscience and Nanotechnology, 7(3), 035008.

Luangtana-anan, M., Nunthanid, J., & Limmatvapirat, S. (2010). Effect of molecular weight and concentration of polyethylene glycol on physicochemical properties and stability of shellac film. Journal of agricultural and food chemistry, 58(24), 12934-12940.

Luo, Q., Li, K., Xu, J., Li, K., Zheng, H., Liu, L., Zhang, H., Sun, Y. (2016). Novel biobased sodium shellac for wrapping disperse multiscale emulsion particles. Journal of Agricultural and Food chemistry, 64(49), 9374-9380.

Manoharan, C., Basarkar, A., & Singh, J. (2010). Various pharmaceuticals disperse systems. In Pharmaceutical suspensions. Springer, 1-37.

Martins, A. F., de Oliveira, D. M., Pereira, A. G., Rubira, A. F., & Muniz, E. C. (2012). Chitosan/TPP microparticles obtained by microemulsion method applied in controlled release of heparin. International journal of biological macromolecules, 51(5), 1127-1133.

McClements, D. J., & Li, Y. (2010). Structured emulsion-based delivery systems: controlling the digestion and release of lipophilic food components. Advances in Colloid and Interface Science, 159(2), 213-228.

McClements, D. J., Bai, L., & Chung, C. (2017). Recent Advances in the Utilization of Natural Emulsifiers to Form and Stabilize Emulsions. Annual Review of Food Science and Technology, 8, 205-236.

McGuire, R. G., & Hagenmaier, R. D. (1996). Shellac Coatings for Grapefruits that Favor Biological Control ofPenicillium digitatumbyCandida oleophila. Biological Control, 7(1), 100-106.

Mircioiu, C., Voicu, V., Anuta, V., Tudose, A., Celia, C., Paolino, D., Fresta, M., Sandulovici, R., Mircioiu, I. (2019). Mathematical modeling of release kinetics from supramolecular drug delivery systems. Pharmaceutics, 11(3), 140.

Mivehi, L., Hajir Bahrami, S., & Malek, R. M. (2008). Properties of polyacrylonitrile-N-(2-hydroxy) propyl-3-trimethylammonium chitosan chloride blend films and fibers. Journal of applied polymer science, 109(1), 545-554.

Mollet, H., & Grubenmann, A. (2008). Formulation technology: emulsions, suspensions, solid forms. John Wiley & Sons.

Monteagudo-Mera, A., Rastall, R. A., Gibson, G. R., Charalampopoulos, D., & Chatzifragkou, A. (2019). Adhesion mechanisms mediated by probiotics and prebiotics and their potential impact on human health. Applied microbiology and biotechnology, 103(16), 6463-6472.

Morais, J. M., Rocha-Filho, P. A., & Burgess, D. J. (2010). Relationship between rheological properties and one-step W/O/W multiple emulsion formation. Langmuir, 26(23), 17874-17881.

Mota, F. L., Queimada, A. J., Pinho, S. P., & Macedo, E. A. (2008). Aqueous solubility of some natural phenolic compounds. Industrial & Engineering Chemistry Research, 47(15), 5182-5189.

Mousavi, S., Bereswill, S., & Heimesaat, M. M. (2019). Immunomodulatory and antimicrobial effects of vitamin C. European Journal of Microbiology and Immunology, 9(3), 73-79.

Moxley, G., & Zhang, Y.-H. P. (2007). More accurate determination of acid-labile carbohydrates in lignocellulose by modified quantitative saccharification. Energy & Fuels, 21(6), 3684-3688.

Mtibe, A., Linganiso, L. Z., Mathew, A. P., Oksman, K., John, M. J., & Anandjiwala, R. D. (2015). A comparative study on properties of micro and nanopapers produced from cellulose and cellulose nanofibres. Carbohydrate Polymers, 118, 1-8.

Muhammad, D. R. A., Doost, A. S., Gupta, V., bin Sintang, M. D., Van de Walle, D., Van der Meeren, P., & Dewettinck, K. (2020). Stability and functionality of xanthan gum–shellac

nanoparticles for the encapsulation of cinnamon bark extract. Food Hydrocolloids, 100, 105377.

Muschiolik, G., & Dickinson, E. (2017). Double emulsions relevant to food systems: preparation, stability, and applications. Comprehensive Reviews in Food Science and Food Safety, 16(3), 532-555.

Naidu, K. A. (2003). Vitamin C in human health and disease is still a mystery? An overview. Nutrition journal, 2(1), 1-10.

Narong, P., & James, A. (2006). Effect of pH on the ζ-potential and turbidity of yeast suspensions. Colloids and Surfaces A: Physicochemical and Engineering Aspects, 274(1-3), 130-137.

Nemet, I., & Monnier, V. M. (2011). Vitamin C degradation products and pathways in the human lens. Journal of Biological Chemistry, 286(43), 37128-37136.

Niu, A., Li, C., Zhao, Y., He, J., Yang, Y., & Wu, C. (2001). Thermal decomposition kinetics and structure of novel polystyrene clusters with mtempo as a branching agent. Macromolecules, 34, 460-464.

Nyman, P. J., Diachenko, G. W., Perfetti, G. A., McNeal, T. P., Hiatt, M. H., & Morehouse, K. M. (2007). Survey results of benzene in soft drinks and other beverages by headspace gas chromatography/mass spectrometry. Journal of agricultural and food chemistry, 56(2), 571-576.

Obradovic, J., Petibon, F., & Fardim, P. (2017). Preparation and characterisation of cellulose-shellac biocomposites. BioResources, 12(1), 1943-1959.

Ortiz, D. G., Pochat-Bohatier, C., Cambedouzou, J., Bechelany, M., & Miele, P. (2020). Current Trends in Pickering Emulsions: Particle Morphology and Applications. Engineering, 6(4), 468-482.

Ou, S., & Kwok, K. C. (2004). Ferulic acid: pharmaceutical functions, preparation and applications in foods. Journal of the Science of Food and Agriculture, 84(11), 1261-1269.

Pandit, S., Ravikumar, V., Abdel-Haleem, A. M., Derouiche, A., Mokkapati, V., Sihlbom, C., Mineta, K., Gojobori, T., Gao, X., Westerlund, F., Mijakovic, I. (2017). Low concentrations of vitamin C reduce the synthesis of extracellular polymers and destabilize bacterial biofilms. Frontiers in microbiology, 8, 2599.

Panwar, R., Sharma, A. K., Kaloti, M., Dutt, D., & Pruthi, V. (2016). Characterization and anticancer potential of ferulic acid-loaded chitosan nanoparticles against ME-180 human cervical cancer cell lines. Applied Nanoscience, 6(6), 803-813.

Park, H. M., Misra, M., Drzal, L. T., & Mohanty, A. K. (2004). "Green" nanocomposites from cellulose acetate bioplastic and clay: effect of eco-friendly triethyl citrate plasticizer. Biomacromolecules, 5, 2281-2288.

Passot, S., Cenard, S., Douania, I., Tréléa, I. C., & Fonseca, F. (2012). Critical water activity and amorphous state for optimal preservation of lyophilised lactic acid bacteria. Food Chemistry, 132(4), 1699-1705.

Pearnchob, N., Siepmann, J., & Bodmeier, R. (2003). Pharmaceutical applications of shellac: moisture-protective and taste-masking coatings and extended-release matrix tablets. Drug development and industrial pharmacy, 29(8), 925-938.

Peighambardoust, S., Tafti, A. G., & Hesari, J. (2011). Application of spray drying for preservation of lactic acid starter cultures: a review. Trends in Food Science & Technology, 22(5), 215-224.

Peng, B. L., Dhar, N., Liu, H. L., & Tam, K. C. (2011). Chemistry and applications of nanocrystalline cellulose and its derivatives: a nanotechnology perspective. The Canadian Journal of Chemical Engineering, 89(5), 1191-1206.

Peng, H., Chen, S., Luo, M., Ning, F., Zhu, X., & Xiong, H. (2016). Preparation and Self-Assembly Mechanism of Bovine Serum Albumin–Citrus Peel Pectin Conjugated Hydrogel: A Potential Delivery System for Vitamin C. Journal of Agricultural and Food Chemistry, 64(39), 7377-7384.

Penning, M. (1996). Aqueous shellac solutions for controlled release coatings. Chemical aspects of drug delivery systems, 178.

Pérez, J., Munoz-Dorado, J., de la Rubia, T. D. L. R., & Martinez, J. (2002). Biodegradation and biological treatments of cellulose, hemicellulose and lignin: an overview. International Microbiology, 5(2), 53-63.

Pu, H., Chen, L., Li, X., Xie, F., Yu, L., & Li, L. (2011). An oral colon-targeting controlled release system based on resistant starch acetate: synthetization, characterization, and preparation of film-coating pellets. Journal of agricultural and food chemistry, 59(10), 5738-5745.

Qi, W., Yu, J., Zhang, Z., & Xu, H.-N. (2019). Effect of pH on the aggregation behavior of cellulose nanocrystals in aqueous medium. Materials Research Express, 6(12), 125078.

Qin, C., Xiao, Q., Li, H., Fang, M., Liu, Y., Chen, X., & Li, Q. (2004). Calorimetric studies of the action of chitosan-N-2-hydroxypropyl trimethyl ammonium chloride on the growth of microorganisms. International journal of biological macromolecules, 34, 121-126.

Qin, Y., Liu, C., Jiang, S., Xiong, L., & Sun, Q. (2016). Characterization of starch nanoparticles prepared by nanoprecipitation: Influence of amylose content and starch type. Industrial Crops and Products, 87, 182-190.

Qussi, B., & Suess, W. G. (2005). Investigation of the effect of various shellac coating compositions containing different water-soluble polymers on in vitro drug release. Drug development and industrial pharmacy, 31(1), 99-108.

Radtchenko, I. L., Sukhorukov, G. B., & Möhwald, H. (2002). Incorporation of macromolecules into polyelectrolyte micro-and nanocapsules via surface controlled precipitation on colloidal particles. Colloids and Surfaces A: Physicochemical and Engineering Aspects, 202(2-3), 127-133.

Rambabu, N., PAnthapulakkal, S., Sain, M., & Dalai, A. (2016). Production of nanocellulose fibers from pinecone biomass: evaluation and optimization of chemical and mechanical

treatment conditions on mechanical properties of nanocellulose films. Industrial Crops and Products, 83, 746-754.

Raymond, L., Morin, F. G., & Marchessault, R. H. (1993). Degree of deacetylation of chitosan using conductometric titration and solid-state NMR. Carbohydrate Research, 246, 331-336.

Rayner, M., Marku, D., Eriksson, M., Sjöö, M., Dejmek, P., & Wahlgren, M. (2014). Biomass-based particles for the formulation of Pickering type emulsions in food and topical applications. Colloids and Surfaces A: Physicochemical and Engineering Aspects, 458, 48-62.

Reddy, K. O., Maheswari, C. U., Shukla, M., & Rajulu, A. V. (2012). Chemical composition and structural characterization of Napier grass fibers. Materials letters, 67, 35-38.

Reethu Narayanan, N. R. K., & Ch, P. J. (2012). Evaluation of probiotic potential of stress tolerant Saccharomyces cerevisiae and development of economically viable media for maximum growth. J Food Process Technol, 3(178), 1-6.

Rinaudo, M. (2006). Chitin and chitosan: Properties and applications. Progress in Polymer Science, 31(7), 603-632.

Rodrıguez-Chong, A., Ramírez, J. A., Garrote, G., & Vázquez, M. (2004). Hydrolysis of sugar cane bagasse using nitric acid: a kinetic assessment. Journal of food engineering, 61(2), 143-152.

Rogowska, A., Pomastowski, P., Złoch, M., Railean-Plugaru, V., Król, A., Rafińska, K., Szultka-Młyńska, M., Buszewski, B. (2018). The influence of different pH on the electrophoretic behaviour of Saccharomyces cerevisiae modified by calcium ions. Scientific reports, 8(1), 1-10.

Rokka, S., & Rantamäki, P. (2010). Protecting probiotic bacteria by microencapsulation: challenges for industrial applications. European Food Research and Technology, 231(1), 1-12.

Rosenzweig, O., Lavy, E., Gati, I., Kohen, R., & Friedman, M. (2013). Development and in vitro characterization of floating sustained-release drug delivery systems of polyphenols. Drug Delivery, 20(3-4), 180-189.

Rosli, N. A., Ahmad, I., & Abdullah, I. (2013). Isolation and characterization of cellulose nanocrystals from Agave angustifolia fibre. BioResources, 8, 1893-1908.

Rwei, S.-P., Chen, Y.-M., Lin, W.-Y., & Chiang, W.-Y. (2014). Synthesis and rheological characterization of water-soluble glycidyltrimethylammonium-chitosan. Marine drugs, 12(11), 5547-5562.

Saengsod, S., Limmatvapirat, S., & Luangtana-anan, M. (2019). Optimum condition of conventional bleaching process for bleached shellac. Journal of Food Process Engineering, 42(8), e13291.

Sampath, U. T. M., Ching, Y. C., Chuah, C. H., Singh, R., & Lin, P.-C. (2017). Preparation and characterization of nanocellulose reinforced semi-interpenetrating polymer network of chitosan hydrogel. Cellulose, 24(5), 2215-2228.

Sanchez-Dominguez, M., & Rodriguez-Abreu, C. (2016). Nanocolloids: A meeting point for scientists and technologists: Elsevier.

Sapei, L., Naqvi, M. A., & Rousseau, D. (2012). Stability and release properties of double emulsions for food applications. Food hydrocolloids, 27(2), 316-323.

Sauberlich, H. E. (1994). Pharmacology of vitamin C. Annual review of nutrition, 14(1), 371-391.

Schell, D., & Beermann, C. (2014). Fluidized bed microencapsulation of Lactobacillus reuteri with sweet whey and shellac for improved acid resistance and in-vitro gastro-intestinal survival. Food Research International, 62, 308-314.

Shahzad, A. (2012). Effects of alkalization on tensile, impact, and fatigue properties of hemp fiber composites. Polymer Composites, 33, 1129-1140.

Shanmugam, A. K., Steele, M., Benavente-Garcıa, O., Castillo, J., & Munch, G. (2010). Novel neuroprotective therapies for alzheimer's and Parkinsons's disease. Frontiers in Medicinal Chemistry, 4, 15-57.

Sharma, R. K. (2014). Surfactants: basics and versatility in food industries. PharmaTutor, 2(3), 17-29.

Shi, Z. Q., Tang, J. T., Chen, L., Yan, C. R., Tanvir, S., Anderson, W. A., Berry, R. M., Tam, K. C. (2015). Enhanced colloidal stability and antibacterial performance of silver nanoparticles/cellulose nanocrystal hybrids. Journal of Materials Chemistry B, 3(4), 603-611.

Shima, M., Morita, Y., Yamashita, M., & Adachi, S. (2006). Protection of Lactobacillus acidophilus from the low pH of a model gastric juice by incorporation in a W/O/W emulsion. Food hydrocolloids, 20(8), 1164-1169.

Siepmann, J., & Siepmann, F. (2013). Mathematical modeling of drug dissolution. International Journal of Pharmaceutics, 453(1), 12-24.

Simon, V., Thuret, A., Candy, L., Bassil, S., Duthen, S., Raynaud, C., & Masseron, A. (2015). Recovery of hydroxycinnamic acids from renewable resources by adsorption on zeolites. Chemical Engineering Journal, 280, 748-754.

Simpson, G. L. W., & Ortwerth, B. J. (2000). The non-oxidative degradation of ascorbic acid at physiological conditions. Biochimica Et Biophysica Acta-Molecular Basis of Disease, 1501(1), 12-24.

Song, Y., Li, Q., Li, Y., & Zhi, L. (2013). Surface and aggregation properties of heterogemini surfactants containing quaternary ammonium and guanidine moiety. Colloids and Surfaces A: Physicochemical and Engineering Aspects, 417, 236-242.

Soradech, S., Nunthanid, J., Limmatvapirat, S., & Luangtana-Anan, M. (2012). An approach for the enhancement of the mechanical properties and film coating efficiency of shellac by the formation of composite films based on shellac and gelatin. Journal of Food Engineering, 108(1), 94-102.

Spasojević, L., Katona, J., Bučko, S., Petrović, L., Budinčić, J. M., Fraj, J., Sharipova, A., Aidarova, S. (2020). Preparation of composite zein/natural resin nanoparticles. Journal of the Serbian Chemical Society, 85(3), 369-380. Srivastava, A., Liu, C., Lv, J., & Qiao, W. (2018). Enhanced intercellular release of anticancer drug by using nano-sized catanionic vesicles of doxorubicin hydrochloride and gemini surfactants. Journal of Molecular Liquids, 259, 398-410.

Srinivasan, M., Sudheer, A. R., & Menon, V. P. (2007). Ferulic acid: therapeutic potential through its antioxidant property. Journal of clinical biochemistry and nutrition, 40(2), 92-100.

Starychova, L., Zabka, M., Spaglova, M., Cuchorova, M., Vitkova, M., Cierna, M., Bartoníková, K., Gardavska, K. (2014). In Vitro Liberation of Indomethacin from Chitosan Gels Containing Microemulsion in Different Dissolution Mediums. Journal of Pharmaceutical Sciences, 103(12), 3977-3984.

Strassberger, Z., Tanase, S., & Rothenberg, G. (2014). The pros and cons of lignin valorisation in an integrated biorefinery. Rsc Advances, 4(48), 25310-25318

Stummer, S., Salar-Behzadi, S., Unger, F. M., Oelzant, S., Penning, M., & Viernstein, H. (2010). Application of shellac for the development of probiotic formulations. Food Research International, 43(5), 1312-1320.

Sun, C., Xu, C., Mao, L., Wang, D., Yang, J., & Gao, Y. (2017). Preparation, characterization and stability of curcumin-loaded zein-shellac composite colloidal particles. Food chemistry, 228, 656-667.

Sun, X. F., Sun, R., Fowler, P., & Baird, M. S. (2005). Extraction and characterization of original lignin and hemicelluloses from wheat straw. Journal of Agricultural and Food Chemistry, 53(4), 860-870.

Sun, X., & Hou, Q. (2018). Iso-concentration hydrogen peroxide bleaching of poplar chemi-thermomechanical pulp. Journal of Bioresources and Bioproducts, 3, 35-39.

Tang, E., Huang, M., & Lim, L. Y. (2003). Ultrasonication of chitosan and chitosan nanoparticles. International Journal of Pharmaceutics, 265(1-2), 103-114.

Tang, J., Berry, R. M., & Tam, K. C. (2016). Stimuli-responsive cellulose nanocrystals for surfactant-free oil harvesting. Biomacromolecules, 17(5), 1748-1756.

Tang, L., Hong, B., Li, T., & Huang, B. (2019). Development of bilayer films based on shellac and esterified cellulose nanocrystals for buccal drug delivery. Cellulose, 26(2), 1157-1167.

Teoh, P. L., Mirhosseini, H., Mustafa, S., Hussin, A. S. M., & Abdul Manap, M. Y. (2011). Recent approaches in the development of encapsulated delivery systems for probiotics. Food biotechnology, 25(1), 77-101.

Thakur, R. K., Villette, C., Aubry, J., & Delaplace, G. (2008). Dynamic emulsification and catastrophic phase inversion of lecithin-based emulsions. Colloids and Surfaces A: Physicochemical and Engineering Aspects, 315(1-3), 285-293.

Thiel, A., Tippkötter, N., Suck, K., Sohling, U., Ruf, F., & Ulber, R. (2013). New zeolite adsorbents for downstream processing of polyphenols from renewable resources. Engineering in Life Sciences, 13(3), 239-246.

Thompson, K. L., Mable, C. J., Lane, J. A., Derry, M. J., Fielding, L. A., & Armes, S. P. (2015). Preparation of Pickering double emulsions using block copolymer worms. Langmuir, 31(14), 4137-4144.

Tian, X., Tian, D., Wang, Z., & Mo, F. (2009). Synthesis and evaluation of chitosan-vitamin C complex. Indian journal of pharmaceutical sciences, 71(4), 371-376.

Torok, B., & Dransfield, T. (2017). Green chemistry: an inclusive approach: Elsevier.

Trinh, B. M., & Mekonnen, T. (2018). Hydrophobic esterification of cellulose nanocrystals for epoxy reinforcement. Polymer, 155, 64-74.

Tripathi, M. K., & Giri, S. K. (2014). Probiotic functional foods: Survival of probiotics during processing and storage. Journal of functional foods, 9, 225-241.

Uluata, S., McClements, D. J., & Decker, E. A. (2015). How the multiple antioxidant properties of ascorbic acid affect lipid oxidation in oil-in-water emulsions. Journal of Agricultural and Food Chemistry, 63(6), 1819-1824.

Urban, K., Wagner, G., Schaffner, D., Röglin, D., & Ulrich, J. (2006). Rotor-Stator and Disc Systems for Emulsification Processes. Chemical engineering & technology, 29(1), 24-31.

Ushikubo, F. Y., & Cunha, R. L. (2014). Stability mechanisms of liquid water-in-oil emulsions. Food Hydrocolloids, 34, 145-153.

Vanderfleet, O. M., Osorio, D. A., & Cranston, E. D. (2018). Optimization of cellulose nanocrystal length and surface charge density through phosphoric acid hydrolysis. Philosophical Transactions of the Royal Society a-Mathematical Physical and Engineering Sciences, 376(2112), 1-7.

Vanier, N. L., Pozzada dos Santos, J., Pinheiro Bruni, G., & Zavareze, E. d. R. (2020). Starches in Foods and Beverages. Handbook of Eating and Drinking: Interdisciplinary Perspectives, 897-913.

Verbeyst, L., Bogaerts, R., Van der Plancken, I., Hendrickx, M., & Van Loey, A. (2013). Modelling of vitamin C degradation during thermal and high-pressure treatments of red fruit. Food and Bioprocess Technology, 6(4), 1015-1023.

Vishtal, A. G., & Kraslawski, A. (2011). Challenges in industrial applications of technical lignins. BioResources, 6(3), 3547-3568.

Wang, W., Jung, J., & Zhao, Y. (2017). Chitosan-cellulose nanocrystal microencapsulation to improve encapsulation efficiency and stability of entrapped fruit anthocyanins. Carbohydrate polymers, 157, 1246-1253.

Wang, X., Zhang, S., Zhao, H., Wang, Q., Zhang, Y., Xu, H., Xia, X., Han, S. (2021). Spectroscopic Investigation into the Binding of Ferulic Acid with Sodium Deoxycholate: Hydrophobic Force Versus Hydrogen Bonding. Langmuir, 37(4), 1420-1428.

Wei, Y., Huang, Y.-H., Cheng, K.-C., & Song, Y.-L. (2020). Investigations of the influences of processing conditions on the properties of spray dried chitosan-tripolyphosphate particles loaded with theophylline. Scientific reports, 10(1), 1-12.

Xiong, K., Zhou, L., Wang, J., Ma, A., Fang, D., Xiong, L., & Sun, Q. (2020). Construction of food-grade pH-sensitive nanoparticles for delivering functional food ingredients. Trends in Food Science & Technology, 96, 102-113.

Xu, Q., Ji, Y., Sun, Q., Fu, Y., Xu, Y., & Jin, L. (2019). Fabrication of cellulose nanocrystal/chitosan hydrogel for controlled drug release. Nanomaterials, 9(2), 253.

Xu, X., Liu, Y., Fu, W., Yao, M., Ding, Z., Xuan, J., Li, D., Wang, S., Xia, Y., Cao, M. (2020). Poly (N-isopropylacrylamide)-based thermoresponsive composite hydrogels for biomedical applications. Polymers, 12(3), 580.

Yan, F., & Polk, D. (2011). Probiotics and immune health. Current opinion in gastroenterology, 27(6), 496-501.

Yan, X., Ma, C., Cui, F., McClements, D. J., Liu, X., & Liu, F. (2020). Protein-stabilized pickering emulsions: Formation, stability, properties, and applications in foods. Trends in Food Science & Technology, 103(2020), 293-303.

Yılmaz, E., Uslu, E. K., & Toksöz, B. (2020). Structure, Rheological and Sensory Properties of Some Animal Wax Based Oleogels. Journal of Oleo Science, 69(10), 1317-1329.

Yin, Y., Dang, C., Zheng, X., & Pu, J. (2017). Synthesis of 2-hydroxypropyl trimethylammonium chloride chitosan and its application in bamboo fiber paper. BioResources, 12, 2899-2911.

Younes, I., & Rinaudo, M. (2015). Chitin and chitosan preparation from marine sources. Structure, properties and applications. Marine drugs, 13(3), 1133-1174.

Zafeiri, I., Horridge, C., Tripodi, E., & Spyropoulos, F. (2017). Emulsions co-stabilised by edible pickering particles and surfactants: the effect of HLB value. Colloids and interface science communications, 100(17), 5-9.

Zandi, M. (2017). Evaluation of the Kinetics of Ascorbic Acid (Aa) Release from Alginate-Whey Protein Concentrates (Al-Wpc) Microspheres at the Simulated Gastrointestinal Condition. Journal of Food Process Engineering, 40(1).

Zanjani, M. A. K., Tarzi, B. G., Sharifan, A., & Mohammadi, N. (2014). Microencapsulation of probiotics by calcium alginate-gelatinized starch with chitosan coating and evaluation of survival in simulated human gastro-intestinal condition. Iranian journal of pharmaceutical research: IJPR, 13(3), 843-852.

Zembyla, M., Murray, B. S., Radford, S. J., & Sarkar, A. (2019). Water-in-oil Pickering emulsions stabilized by an interfacial complex of water-insoluble polyphenol crystals and protein. Journal of colloid and interface science, 548, 88-99.

Zerdin, K., Rooney, M. L., & Vermue, J. (2003). The vitamin C content of orange juice packed in an oxygen scavenger material. Food Chemistry, 82(3), 387-395.

Zhang, G., Liu, L., Zhao, Y., Ning, F., Jiang, M., & Wu, C. (2000). Self-Assembly of Carboxylated Poly (styrene-b-ethylene-co-butylene-b-styrene) Triblock Copolymer Chains in Water via a Microphase Inversion. Macromolecules, 33, 6340-6343.

Zhang, H.-l., Wu, S.-h., Tao, Y., Zang, L.-q., & Su, Z.-q. (2009). Preparation and characterization of water-soluble chitosan nanoparticles as protein delivery system. Journal of Nanomaterials, 2010 (2010). 1-5.

Zhang, S. Y., Wang, C. G., Fei, B. H., Yu, Y., Cheng, H. T., & Tian, G. L. (2013). Mechanical function of lignin and hemicelluloses in wood cell wall revealed with microtension of single wood fiber. Bioresources, 8, 2376-2385.

Zhang, T., Yang, Y., Liang, Y., Jiao, X., & Zhao, C. (2018). Beneficial effect of intestinal fermentation of natural polysaccharides. Nutrients, 10(8), 1055-1076.

Zhou, W., Liu, W., Zou, L., Liu, W., Liu, C., Liang, R., & Chen, J. (2014). Storage stability and skin permeation of vitamin C liposomes improved by pectin coating. Colloids and surfaces B: Biointerfaces, 117, 330-337.

Zhu, Y., Sun, J., Yi, C., Wei, W., & Liu, X. (2016). One-step formation of multiple Pickering emulsions stabilized by self-assembled poly (dodecyl acrylate-co-acrylic acid) nanoparticles. Soft Matter, 12(36), 7577-7584.

Zou, P., Yang, X., Wang, J., Li, Y., Yu, H., Zhang, Y., & Liu, G. (2016). Advances in characterisation and biological activities of chitosan and chitosan oligosaccharides. Food chemistry, 190, 1174-1181.

Zou, S., Wang, C., Gao, Q., & Tong, Z. (2013). Surfactant-free multiple pickering emulsions stabilized by combining hydrophobic and hydrophilic nanoparticles. Journal of dispersion science and technology, 34(2), 173-181.

Zou, X., Zhao, X., & Ye, L. (2015). Synthesis of cationic chitosan hydrogel and its controlled glucose-responsive drug release behavior. Chemical Engineering Journal, 273, 92-100.